Three-dimensional digital geometry design of soft tissue implants for patients with Poland's syndrome using Magics and Freeform® Modeling™

by

Izél van Heerden

Dissertation submitted in fulfilment of the requirements for the degree

Magister Technologiae: Design,

Department of Design and Studio Art,

Faculty of Humanities,

Central University of Technology, Free State,

Bloemfontein

Supervisor: Prof Annabel Fossey

Co-supervisor: Mr Gerrie Booysen

FEBRUARY 2016

Declaration

I, Izél van Heerden (student number [redacted]) hereby declare that this research project submitted to the Central University of Technology, Free State, for the degree Magister Technologiae: Design is my own independent work. This work or, any part thereof, has not previously been submitted by me or anyone else to any other institution in order to obtain a degree. This research project was conducted at the Central University of Technology, Free State, under the supervision of Professor Annabel Fossey and co-supervisor Mr Gerrie Booysen.

16 February 2016

.....

SIGNATURE

.....

DATE

Izél van Heerden

I certify that this statement is correct:

16 February 2016

.....

SIGNATURE OF SUPERVISOR

.....

DATE

Professor Annabel Fossey

Acknowledgements

Abba Vader, ek staan aan die einde van ‘n ongelooflike harde-klippekou tog fantastiese vervullende-moeitewerd pad van studie-sukses. Ontelbare-opgee-oomblikke het aan my persoonlikheids-deur kom klop, maar U het aan my bonatuurlike-veggees-krag gegee, Rots van Sion, en het U my geestelik-sterk-staande gehou. Daarom staan ek met ‘n dankbare-liefdehart voor U, Allerhoogste, dankbaar vir al die oorvloedige-genade-geleenthede, dankbaar vir sterkmaak-struikelblokke en dankbaar vir genade-seën-oomblikke wat omstandighede in my guns gedraai het. Baie dankie vir al die engele wat U langs my geplaas het, my dierbare-vol-liefde gesin en Ettienne my hartedief wat my so onvoorwaardelik-sonder-moeite-liefhet en getrou-ondersteun het. Dankie vir die dapper-ingryp-engel wat my vuurtoring-leiding gegee het en soveel van haar super-brein-kennis aan my oorgedra het. Dankie Here-Jesus vir U dekmantel van oorvloedige guns, liefde, seën en genade waarmee U my so sorgvuldig toevou en beskerm. Ek is gereed vir die lewe van in-U-diens-dissipelskap wat U vir my uitgelê en beplan het, ek koester U in my hart. Amen

Pappa Philip, Mamma Elené en boetie Attie, dankie vir al jul ondersteunende-moed-inpraat-liefde wat julle oorloop-harte gratis gee, die strome-pleit-gebede, al die naelbyt-inspring-en-help oomblikke, geduldige-ore en planmaak-aanhuts-vegterskap, waarmee jul my na menslike-wedloop-sukses gedryf het. Ek sou dit nooit sonder julle aan my sy kon aanpak en afhandel nie, ek is oneidig lief vir julle!

Ettienne-liefie, dankie vir die geduldige-moedhou-jare en breëskouer-troosgeaardheid waarop ek kon steun wanneer ek moedeloos-en-uitgeput was, asook die oorborrel-vreugdes wat jy saam met my gedeel het. Jy is my liefde, my vriend en my lewe, lief jou met hart en siel.

Professor Annabel Fossey (proffie) hoe kan ek begin om dankie te sê? Nog nooit het ek iemand met soveel raakvat-vegtersgees ontmoet nie, u het my gou onder u moederhen-vlerk ingeneem en stap

vir stap met geduldige-hartsliefde opgebou en aangemoedig om my beste te gee. Ek het soveel by prof geleer, prof se leiding was van top-gehalte.

Gerrie dankie vir jou planmaak-leiding, die nooit-ophou-in-my-glo gesindheid, en die ondersteunings-pad wat jy saam met my gestap het dit beteken vir my baie.

Danielle jy is my gees-sussie wat my met jou Jesus-boodskappe en sterkmaak-liefde aanmekaar gehou het, jy is 'n vriendin na aan my hart.

I would like to acknowledge the financial support provided by the National Research Foundation (NRF), the Central University of Technology, FS, and the Centre for Rapid Prototyping and Manufacturing (CRPM).

Lewenslesse vir my lewensreis: glo altyd in jouself: moet nooit in God se ingryp-liefde twyfel nie. Hy is Almagtig: streef harts-drome na en moet nooit moed verloor nie.

Table of Contents

List of Tables

List of Figures

List of Abbreviations, Copyright and Trademarks

Abbreviation	
2D	Two-dimensional.
3D	Three-dimensional.
3D-DG	Three-dimensional digital geometries.
AM	Additive manufacturing (ASTM International 2012).
Boolean	Boolean operations was first introduced in 1847 by George Boole in his book, *The Mathematical Analysis of Logic*. Boolean operations; namely, union, intersect, difference and symmetric difference, are used in geometric modelling to manipulate solid models using mathematical algorithms to construct new geometries.
CAD	Computer-aided design.
CAM	Computer-aided manufacturing.
CRPM	Centre for Rapid Prototyping and Manufacturing.
CT	Computer tomography - Medical imaging technology. These scanners works by focusing x-rays through the body and by detecting the signal on the opposite side of the body, producing images of the anatomy in a series of slices.
CUT	Central University of Technology, Free State.
DICOM	Digital Imaging and Communications in Medicine is the file format used by medical imaging technologies, such as MRI and CT.
Haptic device	The PHANTOM® Omni™ haptic device (now referred to as the Geomagic® Touch™) allows the users to touch and manipulate 3D virtual forms in virtual reality. This haptic device provides precision positioning input and high fidelity force-feedback output.
MRI	Magnetic resonance imaging - Medical imaging technology. These scanners works by aligning atoms in the body using magnetic fields to temporarily disrupt the atom alignment and timing how long it takes the

	atoms to return to their aligned state, all atoms have a magnetic field that can be altered by radio waves.
Prosthetic implants	Is an artificial device that replaces a missing body part, which may be lost through trauma, disease, or congenital conditions such as a leg, a heart, or a breast implant. (https://en.wikipedia.org/wiki/Prosthesis)
	Prosthesis as a corrective device consisting of a replacement for a part of the body, for example implant prosthesis placed permanently in tissue. (http://www.thefreedictionary.com/implant+prosthesis)
	Prosthetic implants can form part of the body (*prosthetic breast*) or may be removable, as in the case of most prosthetic legs. (http://www.medicinenet.com/script/main/art.asp?articlekey=15985)
RM	Rapid manufacturing (ASTM International 2012).
ROI	Region of interest.
RP	Rapid prototyping (ASTM International 2012).
STL	Stereolithography file format. An STL file is a standard interface for additive manufacturing technologies and uses triangular facets to approximate the shape of an object in binary and ASCII (ASTM International 2012).

Copyright and trademarks

Copyright and trademarks for the different software programs are indicated in this dissertation according to the copyright and trademark specifications of the respective developers.

3D Doctor™	Developed by Able Software Corp®
BioBuild™	Developed by Anatomics® Pty. Ltd.
Freeform® Modeling™	Developed by 3D Systems®
Magics	Developed by Materialise®
Mimics®	Developed by Materialise®

Abstract

Poland's syndrome is a unilateral congenital defect displaying deformities of mostly the soft tissues and the skeleton. The syndrome commonly affects the right side of the thorax and is more often found in males. Many Poland's syndrome patients display the absence of the pectoralis major muscle, although other muscles such as the pectoralis minor may also be affected. Poland's syndrome is also associated with hand deformities. Poland's syndrome patients usually seek medical intervention to improve their aesthetic appearance. Most of the interventions are traumatic, invasive, surgical procedures. Less invasive and traumatic approaches are constantly being developed. Therefore, the main aim of this study was to design three-dimensional digital geometries of soft tissues for two Poland's syndrome patients that can be used for the production of soft tissue implants in the manufacturing process. A female (Case Study 1) and a male (Case Study 2) Poland's syndrome patient were included as two case studies.

CT scanned digital imaging data sets were acquired of the two Poland's syndrome patients and were processed in Mimics® software to create 3D digital geometries in STL file format. A number of manipulations and pixel-by-pixel editing steps were applied to isolate the regions of interest which were then imported into the programs Magics and Freeform® Modeling™.

The program Freeform® Modeling™ was used to describe the extent of the aesthetic presentation of the deformity by determining the difference between the healthy and affected sides of the thorax in both patients. The angles between the vertical and oblique planes for both sides of the thorax were measured and the difference between these angles calculated. For the female the difference was 6.5º, while for the male it was 14º.

The design phase followed two design routes to design soft tissue 3D digital geometries of the pectoralis muscle for each patient using the programs Magics and Freeform® Modeling™. The one

route involved using a mirror image of the whole thorax (Technique A), while the other route involved firstly the isolation of the pectoralis muscle from the healthy side of the thorax and thereafter producing a mirror image (Technique B). Four different soft tissue 3D digital geometries of the pectoralis muscle resulted for each patient from these design routes.

Three different analyses were performed to compare the outcomes of the different design routes and software programs. A deviation analysis was performed using Geomagic® Control™ to calculate the deviation between the design route outcomes and constructed digital test models. Most of the deviation test points for all techniques fell within the nominated tolerance region of ≥-5 and ≤+5 mm (more than 70% for the female more than 80% for the male). An implant mass property analysis using Freeform® Modeling™ revealed that the 3D digital geometries produced using Freeform® Modeling™ Technique A presented with surface areas and volumes closest to original healthy pectoralis muscle in the female, while for the male it was Freeform® Modeling™ Technique B. A body conformation analysis was performed to ascertain to what extent the different techniques used to produce the 3D digital geometries had the potential to reconstruct the soft tissue deformities, thus the resultant 3D digital geometries were compared with an original body conformation, as well as with an ideal body conformation. For both patients the four 3D digital geometries were relatively close to the ideal body conformation dimensions.

In an attempt to compare the performance of Magics and Freeform® Modeling™, they were assessed, where possible, in terms of software functionality, hardware possibilities, and geometry development time and software/hardware costs. It could be concluded that, in this study, Freeform® Modeling™ appeared to be the better suited software program for the designing of 3D digital geometries of soft tissue implants.

Chapter 1:
Introduction to the Study

1.1 Introduction

Poland's syndrome is a rare birth defect in which affected people are born with soft tissue and skeletal deformities on one side of the chest wall. Many people with Poland's syndrome are missing the major chest muscle called the pectoralis major, or part of the underlying pectoralis minor muscle. The right side of the body is more commonly affected (Urschel 2009; Stylianos et al. 2012). Most affected people also demonstrate hand abnormalities which include shortened fingers, partial fusion of the fingers, or both (Ram & Chung 2009). The incidence of Poland's syndrome ranges from 1 in 7,000 to 1 in 100,000 live births, with a higher percentage of males affected by the syndrome than females (Mathes et al. 2005; Fokin et al. 2009; Lieber et al. 2012). Individuals affected by Poland's syndrome seek medical intervention to improve their aesthetic appearance (Mathes et al. 2005; Pereira et al. 2008).

Various reconstructive techniques have been introduced for the correction of Poland's syndrome. The approaches to reconstruction depend on the severity of the disease, gender and age of the patient (Da Silva Freitas et al. 2007; Lieber et al. 2012). None of these procedures provide simultaneous and complete satisfactory correction for both structural and cosmetic deformities (Urschel 2009; Delay et al. 2010). Most techniques and procedures require major surgery with lengthy operative durations accompanied by extended recovery times and numerous post-operative procedures. These procedures may leave scarring and/or additional deformities, often with relatively poor aesthetic results (Costa et al. 2010a; Delay et al. 2010).

Designing and developing custom-made prosthetic implants for the reconstruction of chest wall and soft tissue deformities of Poland's syndrome is an attractive alternative to invasive surgery. This

alternative approach is less invasive and requires less extensive recovery times than the more invasive surgical procedures. The manufacturing of prosthetic implants is dependent on the accuracy of digital data capturing techniques. Data capturing techniques such as computed tomography (CT) and magnetic resonance imaging (MRI) have the advantage of using digital scanned data that provides pre-operative insight into the pathogenesis of the body through the capturing of accurate medical data sets, which allows for further manipulation and the design of prosthetic implants (Petrovic et al. 2012). Various software programs are used in the process to manipulate the scanned imaging data sets to produce three-dimensional (3D) geometries that can be used in additive manufacturing (AM) to produce custom-made soft tissue prosthetic implants (Saour et al. 2008).

1.2 Aim and objectives

The main aim of this study was to design three-dimensional digital geometries of soft tissues for two Poland's syndrome patients that can be used for the production of soft tissue implants in the manufacturing process. A female and a male Poland's syndrome patient were included as two case studies; Case Study 1 (female patient) and Case Study 2 (male patient).

To achieve this aim the following objectives were devised:

- To obtain two-dimensional (2D) medical imaging scanned data sets of anonymous female and male Poland's syndrome patients;
- To translate and generate 3D digital geometry data of soft tissue from the 2D medical imaging scanned data sets of the two Poland's syndrome patients using a specialised processing and editing software program;
- To design different representative 3D digital geometries of soft tissue for each of the two Poland's syndrome patients using two different approaches in two different software programs;

- To briefly compare the 3D digital geometries of soft tissue produced using the two different approaches in the two software programs.

1.3 Limitations and delimitations

This study forms part of a larger study in which soft tissue geometries are designed for various parts of the body for different patients with soft tissue deformities, including Poland's syndrome. This study was thus limited to the design of 3D digital geometries of soft tissue for two Poland's syndrome patients. The software programs were specifically selected, because of their availability in the University where this study was registered.

1.4 Value of study

In this study various approaches to the design of 3D digital geometries of soft tissue were applied using more than one software program. This allowed the designer to refine the design process for the production of 3D soft tissue geometries for Poland's syndrome patients. These refined geometries will facilitate the manufacturing process of custom-made implants for Poland's syndrome patients. Furthermore, from the authors' best knowledge the application of the software program Freeform® Modeling™ was used for the first time to design 3D digital geometries of soft tissue for Poland's syndrome patients.

1.5 Layout of dissertation

This dissertation has been arranged into six chapters:

Chapter 1: This chapter introduces the field of study, highlights the problems and provides the aim and objectives.

Chapter 2: This chapter reviews previous literature on Poland's syndrome; CT and MRI technologies for capturing of digital data; 3D computer-aided design (CAD)

technologies and their application in digital geometry design; and AM for the manufacturing process of prosthetic implants.

Chapter 3: This chapter describes the two Poland's syndrome patients participating in this study. The research methodology followed to achieve the respective objectives is described in detail.

Chapter 4: This chapter describes the results of the female Poland's syndrome patient (Case Study 1) and presents an attempt to compare the different methods employed in this study.

Chapter 5: This chapter describes the results of the male Poland's syndrome patient (Case Study 2) and presents an attempt to compare the different methods employed in this study.

Chapter 6: In this concluding chapter the key findings from this study are discussed. The different techniques and case studies are also compared in an attempt to ascertain which of the design routes are the most applicable to these types of case studies.

Appendixes

Appendix 1: Deviation analysis reports of female Poland's syndrome patient.

A: Deviation analysis report for Magics, *Technique A*.

B: Deviation analysis report for Magics, *Technique B*.

C: Deviation analysis report for Freeform® Modeling™, *Technique A*.

D: Deviation analysis report for Freeform® Modeling™, *Technique B*.

Appendix 2: Deviation analysis reports of male Poland's syndrome patient.

A: Deviation analysis report for Magics, *Technique A*.

B: Deviation analysis report for Magics, *Technique B*.

C: Deviation analysis report for Freeform® Modeling™, *Technique A*.

D: Deviation analysis report for Freeform® Modeling™, *Technique B*.

Appendixes containing an extraction of the total *Geomagic Control Report* generated with Geomagic® Control™. The extractions consist of three pages of the approximate 40 pages of each deviation analysis report for the female and male Poland's syndrome patients.

Chapter 2:
Review of the Literature

2.1 Introduction to Poland's syndrome

Poland's syndrome is a medical condition comprising of congenital abnormalities of the thoracic area with soft tissue and skeletal deformities of the chest wall (Fokin et al. 2009; Costa et al. 2010a). Poland's syndrome was first described by Sir Alfred Poland in 1841 (Poland 1841). While, as an apprentice at Guy's Hospital in London, Alfred Poland dissected a deceased convict, 27-year-old George Elt, and identified the absence of the sternocostal part of the pectoralis major muscle, the absence of pectoralis minor and serratus anterior muscles (Poland 1841; Fox & Seyfer 2012). Based on his findings he reported on the abnormality in the anatomy of the convict in Guy's Hospital Reports under the title 'Deficiency of the Pectoral Muscles'. This original description was for the mildest form of Poland's syndrome (Majdak-Paredes et al. 2015). However, there were earlier reports by Lallemand (1826) and Froriep (1839) on a medical condition similar to that of Poland's syndrome. In these cases, only the chest wall deficiency with the absence of the pectoralis muscles were described (Fokin & Robicsek 2002; Moir & Johnson 2008; Fox & Seyfer 2012). Poland also identified the association of the abnormality, brachysyndactyly, with the common characteristics of Poland's syndrome (Poland 1841). This syndrome was first referred to as Poland's syndactyly named by Dr Patrick Clarkson in 1962 when he described similar cases to Poland's discovery, more than a century earlier. In a publication in 1967, 'Un cas de syndrome de Poland', by Dr Baudinne and colleagues the condition received the name known today as Poland's syndrome (Fokin & Robicsek 2002; Fox & Seyfer 2012). A clear historical timeline has been published by Ram and Chung (2009).

Poland's syndrome is rare (Akal & Kara 2002). It is difficult to estimate the incidence of Poland's syndrome. Currently, the estimates range from 1 in 7,000 to 1 in 100,000 births with more males

being affected, with a ratio of 3:1 (Kamburoğlu et al. 2011; Chen et al. 2012; Caouette-Laberge & Borsuk 2013; Chowdhury et al. 2015; Majdak-Paredes et al. 2015). Presently, approximately 400 cases of Poland's syndrome have been reported worldwide (Lantzsch et al. 2013; Majdak-Paredes et al. 2015). In 75% of the cases, the deformity is located in the right hemi-thorax (Goyal et al. 2014; Chowdhury et al. 2015).

The cause of Poland's syndrome remains controversial and relatively unknown (Hamburg et al. 2002; Li et al. 2011; Lantzsch et al. 2013). Most reports support the hypothesis that the syndrome is caused by the interruption of the embryonic blood supply from the ipsilateral subclavian arteries around the sixth week of foetal development (Chen et al. 2012; Caouette-Laberge & Borsuk 2013). Alternative theories, however, suggest that Poland's syndrome can commence with injury or developmental failure of the embryonic mesodermal plate, which gives rise to the pectoralis muscle, during the third and fourth weeks of gestation (Fokin & Robicsek 2002; Mathes et al. 2005).

The deformities of Poland's syndrome may include the unilateral absence of a number of anatomical structures of the chest wall. Anatomical structures often found to be absent in Poland's syndrome include the pectoralis major muscle, pectoralis minor muscle, the breast and/or nipple as well as hypoplasia or aplasia of the sternocostal head of the pectoralis major. The pectoralis muscles, the major and minor pectoralis muscles, form the main muscular thoracic wall and originate from the clavicle, the sternum and the seven upper costal cartilages (Stylianos et al. 2012). A total absence or hypoplasia of these muscles may lead to deformities of the chest wall. The syndrome can also affect other muscles, which include the absence of the anterior serratus magnus, the anterior abdominal oblique, the posterior latissimus dorsi, and the deltoid muscle. The syndrome also includes partial agenesis of ribs two, three and four or three, four and five, and various abnormalities of the chest wall. Various literatures have stated that the absence of the sternocostal head of the pectoralis major muscle is a common characteristic shared by all patients with Poland's syndrome (Mathes et al. 2005; Moir & Johnson 2008; Kamburoğlu et al. 2011; Dayal et al. 2014). Unilateral brachysyndactyly

of the fingers is also a clinical presentation associated with Poland's syndrome (Al-Qattan 2001). The collection of deformities differs from person to person, although the inclusion of all the deformities in one individual is rare (Pereira et al. 2008; Urschel 2009). Although Poland's syndrome is regarded as a syndrome presenting unilateral chest deformities, sporadic cases of additional bilateral deformities have been reported (Yiyit et al. 2015). Yiyit et al. (2014a) reported problems with the positions of the shoulders and limited abduction of both upper extremities in eight Poland's syndrome patients.

The deformities of Poland's syndrome are difficult to hide, because it leads to thoracic asymmetry. This syndrome is associated with significant psychological trauma and often social withdrawal (Costa et al. 2010a; Çelik et al. 2011). In most cases, the abnormalities in the thoracic region do not affect movement and the loss of function, or cause significant muscle weakness or serious health problems (Avci et al. 2003; Urschel 2009; Stylianos et al. 2012). Individuals affected by Poland's syndrome seek surgical correction for cosmetic purposes to improve their aesthetic appearance (Mathes et al. 2005; Pereira et al. 2008; Yadav et al. 2014). Although the syndrome is more predominantly found in males, reconstructive assistance is more often pursued by females because of the concern about their appearance (Ortiz 2014). Female patients with Poland's syndrome often present with deformities that are different when compared to the deformities presented in male patients. Together with the underlying muscle deformities, a female Poland's syndrome patient present with asymmetrical breasts, hypomastia, and a smaller nipple-areola complex on the affected side (Hodgkinson 2009; Goyal et al. 2014).

Poland's syndrome has been associated with a variety of syndromes and diseases. It has been associated with the syndromes such as Möbius and Klippel-Feil (Moir & Johnson 2008; Ahmad et al. 2012; Kelly & Shamberger 2012; Yiyit et al. 2014b). Möbius syndrome is characterised by facial paralysis and ocular abduction (Shamberger 1996; Gupta et al. 2003; Ahmad et al. 2012; Sharma et al. 2013). The abnormal, congenital fusion of two or more spinal bones (cervical vertebrae) is considered to be Klippel-Feil syndrome (Mirhosseini et al. 2013; Kerai et al. 2014). In 2011 a case

was reported where Poland's syndrome was associated with scapular winging in an 18-year-old youth, which caused much discomfort and pain (Uludag et al. 2011). A rare combination of Poland's syndrome with pulmonary hypertension and dextrocardia has also been reported (Raval et al. 2013). In 2006, an association of Poland's syndrome with a bleeding disorder was reported on for the first time by Legbo (2006). It is also known to be associated with some malignant diseases, such as breast invasive ductal carcinoma (Fukushima et al. 1999; Okamoto et al. 2002; Ji et al. 2008; Curcio et al. 2009; Zhang et al. 2011) and neurofibroma (Chen et al. 2012).

2.2 Classification of the different forms of Poland's syndrome

In patients presenting with Poland's syndrome the most important purpose of reconstruction is to improve chest wall and soft tissue deformities in an attempt to achieve thorax symmetry and thereby improving the overall aesthetic appearance (Moir & Johnson 2008). The severity of the chest wall and soft tissue deformities, gender and age determine the appropriate surgical approach (Foucras et al. 2003; Mathes et al. 2005; Pinsolle et al. 2008; Fokin et al. 2009; Lieber et al. 2012; Zhu et al. 2012). Therefore, classification systems for Poland's syndrome have been devised.

The clinical forms of Poland's syndrome are rather varied, thus Foucras, Grolleau-Raoux and Chavoin (2003) devised a classification system for the syndrome. In this classification system three grades were proposed based on the severity of the chest wall and soft tissue deformities. Grade I is referred to as 'mild' with minor deformities; Grade II, which refers to the classic Poland's syndrome is 'moderate', and Grade III presents the 'severe' form of the syndrome (Figure 2.1).

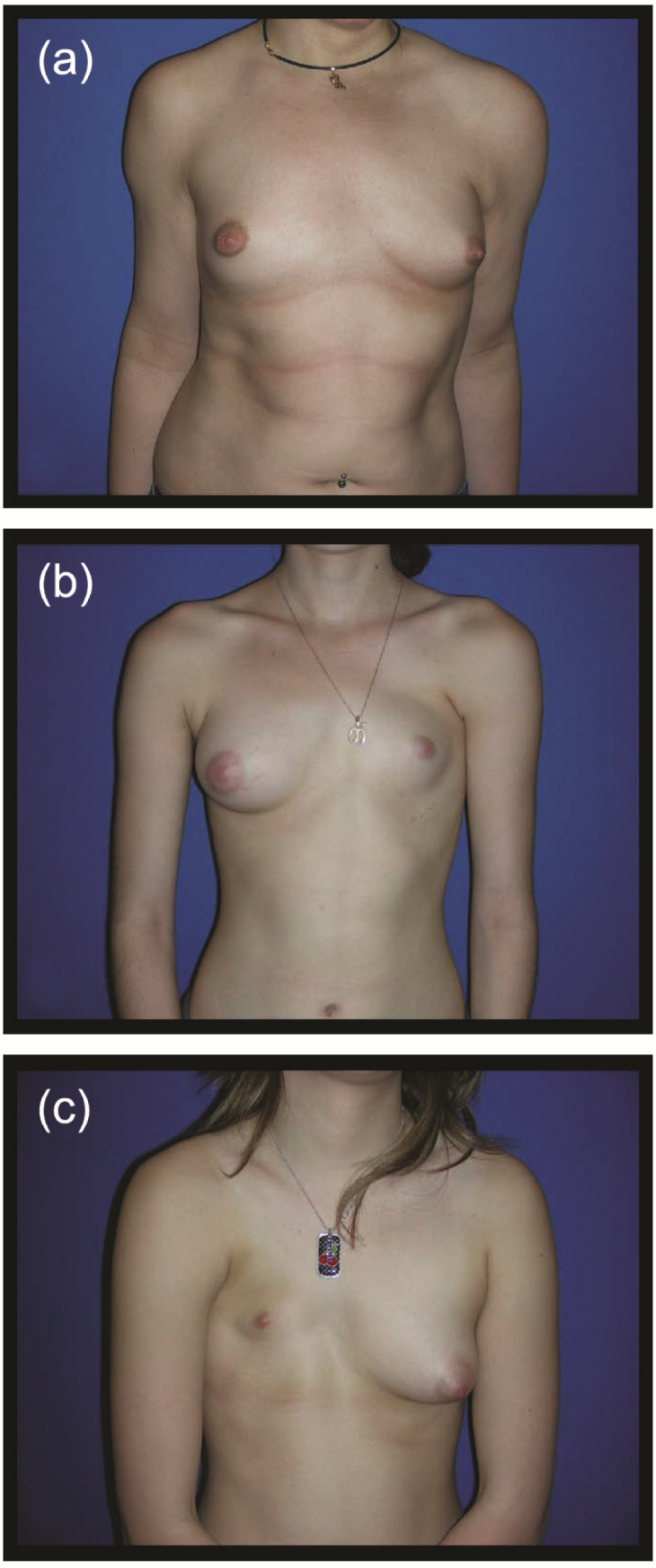

Figure 2.1 **Grades of Poland's syndrome.** (a) Grade I (mild), (b) Grade II (moderate), and (c) Grade III (severe) (Taken from Baratte et al. 2011).

The three grades of Poland's syndrome were defined by Foucras et al. (2003) as follows:

Grade I: Minor defect with muscle hypoplasia of the pectoralis major, and among women moderate hypoplasia of the breast. This phenomenon demonstrates a discreet asymmetry of the thorax in men and asymmetry of the breasts in women.

Grade II: Moderate deformity with major aplasia of the pectoralis major; significant breast asymmetry in women; and moderate costal deformity is possible. This phenomenon presents as an asymmetrical chest.

Grade III: Severe malformation with breast aplasia and complete muscle aplasia; associated major thoracic deformity with rib aplasia and sternal deformity. This phenomenon presents as severe asymmetry of the thorax.

A review of 20 cases of patients diagnosed with Poland's syndrome (12 males and eight females) was conducted in order to define a classification system of the hand deformities associated with the syndrome by Al-Qattan (2001). The hand deformities were divided into seven types according to the severity of the deformity. Type 1 was classified as normal hands; Type 2 presents with a form fruste (one hand is smaller than the contralateral hand and the arm of the affected side is also shorter); and Type 3 presents hand deformities with the classic anomaly of brachysyndactyly. Type 3A referred to as mild to moderate hypoplasia, while Type 3B denotes severe hypoplasia. Type 4 refers to hand anomalies with aplasia of one or more functional rays of the hand. Type 4A refers to radial club hand with floating or absent thumb; Type 4B refers to hand anomaly with adactyly of the index; Type 4C refers to adactyly of the index and long fingers; Type 4D refers to a cleft hand; and Type 4E refers to adactyly of the ulnar rays. Type 5 represents the anomaly where all the digits are functionless or absent. Type 6 represents the transverse deficiency that may be just distal to the wrist, while leaving rudimentary metacarpals, or proximal to the wrist. Type 7 represents the rarest and most severe

hand anomaly in Poland's syndrome (phocomelia-like deficiency). Figure 2.2 shows some of the hand deformities displayed by Poland's syndrome patients.

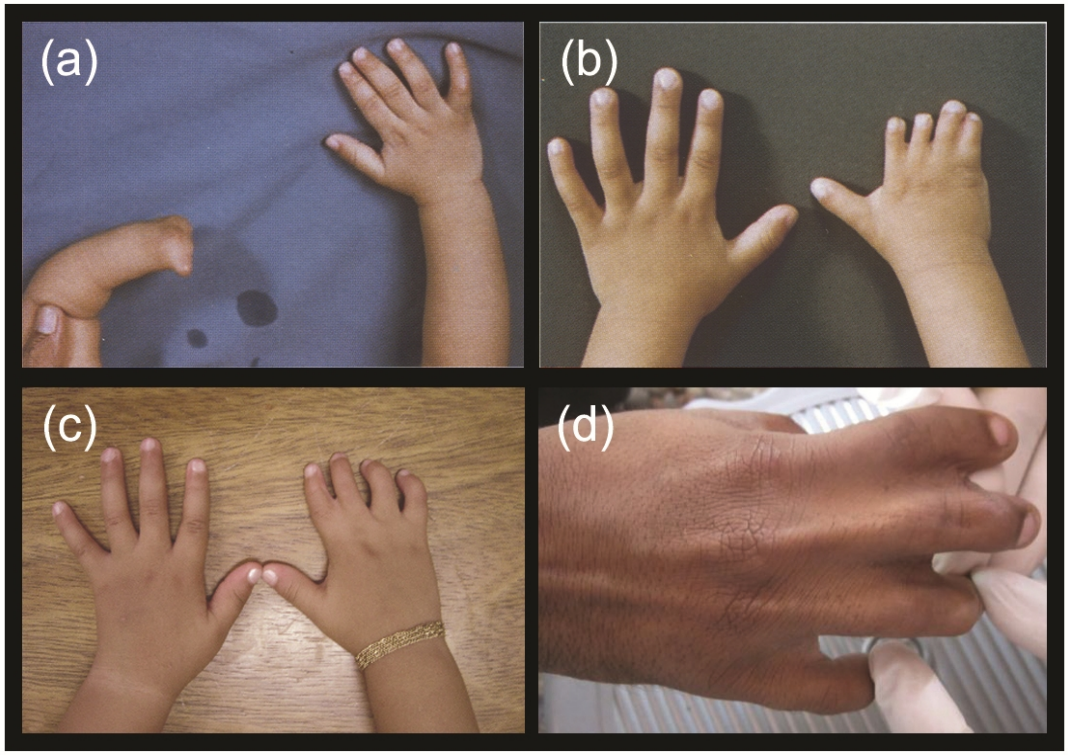

Figure 2.2 **Hand deformities in Poland's syndrome.** (a) Type 5 anomaly: functionless digits (Taken from Al-Qattan 2001), (b) Type 3B anomaly: Brachysyndactyly and severe hypoplasia of the hand (Taken from Al-Qattan 2001), (c) Brachysyndactyly of the 2nd and 3rd fingers digits (Taken from Da Silva Freitas et al. 2009), and (d) Syndactyly of 2nd and 3rd finger of right hand (Taken from Sharma et al. 2013).

With the development of sophisticated computer scanning technologies, Stylianos et al. (2012) developed an alternative classification system using a clinical and radiological approach. This approach consisted of scanning 10 patients using a computed tomography (CT) imaging scanner. The Poland's syndrome deformities were classified into four categories: First degree (hypoplasia of the pectoralis muscles); Second degree (absence of the sternocostal head of the major pectoralis muscle); Third degree (total absence of the major or both pectoralis muscles, including minor pectoralis); and Fourth degree (hypoplasia or absence of the pectoralis muscles combined with skeletal anomalies of the thoracic bones, including sternum and/or rib cage).

2.3 Medical reconstruction in Poland's syndrome

2.3.1 Introduction

Many different techniques have been used to correct Poland's syndrome chest wall and soft tissue deformities. Surgical reconstruction of the chest wall has included structural skeletal procedures and soft tissue procedures. Some of these procedures are more invasive than others and include a variety of single-stage and multi-stage interventions, such as the use of bone grafts, musculocutaneous flaps, omentum flaps, lipomodelling, and custom-made prosthetic implants (Urschel 2009; Majdak-Paredes et al. 2015). In the past, the reconstruction of the deformities of a Poland's syndrome patient involved invasive surgical procedures. However, in recent times the more minimal invasive types of reconstruction with less morbidity have gained popularity (Góes 2010).

2.3.2 Invasive surgical reconstruction techniques

There are a variety of different surgical approaches applied in the treatment of Poland's syndrome. Surgical reconstructive interventions may be indicated for the following reasons (Fokin & Robicsek 2002; Kanani et al. 2015): (1) Unilateral depression of the chest wall and the possibility of its progression; (2) Lack of adequate protection of the heart and lung; (3) Paradoxical movement of the chest wall; (4) Hypoplasia or aplasia of the female breast; and (5) Cosmetic defect due to lack of the pectoralis major muscle and axillary fold in male patients. The choice of a particular surgical approach is dependent on the patient's presentation of the severity of the syndrome (Moir & Johnson 2008; Fijałkowska & Antoszewski 2011). The patient's age and gender also play a role in the approach to surgical correction (Sood & Ahuja 2010). Surgical reconstruction of Poland's syndrome cannot be undertaken before 17 to 19 years of age, when the development of the body is complete (Costa et al. 2010b; Fijałkowska & Antoszewski 2011). The degree of difficulty of the surgical procedure depends on the type of chest deformity of a patient (Fijałkowska & Antoszewski 2011).

Poland's syndrome is a complex developmental deformity involving several tissues and requires access to a wide spectrum of reconstructive techniques to accomplish acceptable aesthetic results (Majdak-Paredes et al. 2015). In the past, surgical treatment of Poland's syndrome was undertaken by thoracic surgeons who reconstructed the chest wall and included breast augmentation. In contrast, when plastic surgeons became involved, the breast may have been reconstructed without chest wall reconstruction (Urschel 2009). However, neither of these two approaches was entirely satisfactory. Thus, single-stage reconstruction implicating the chest wall stabilisation and breast augmentation was recognised as the obvious next step in the development of suitable surgical approaches (Urschel 2009).

Currently the most widely used approach to surgical reconstruction is a method that was proposed by Ravitch (Fokin & Robicsek 2002; Urschel 2009). The classic Ravitch technique, first described by Ravitch and Handelsman in 1952, uses an autologous rib graft to achieve a more stabilised skeletal reconstruction together with a woven Dacron to replace the absent fascia providing a base for soft tissue repair (Fokin & Robicsek 2002; Urschel 2009). This classic technique is successful in achieving optimal results in a stable chest wall reconstruction, but is accompanied with disadvantages. These disadvantages include extensive and complex surgical procedures, extended painful recovery, scarring and infections (Blanco et al. 2011). The Ravitch technique has since been refined by using custom-made soft tissue implants supported by the harvesting of myocutaneous flaps (Moir & Johnson 2008). Single-stage reconstruction of the chest wall combined with simultaneous augmentation mammoplasty and transfer of an island pedicle myocutaneous flap of latissimus dorsi muscle are major improvements over previous multiple-stage procedures that provide less satisfactory cosmetic results in management of patients with Poland's syndrome (Urschel 2009). In a 15-year-old boy with Poland's syndrome a modified version of the Ravitch technique was used whereby the latissimus dorsi muscle was transferred to repair the chest wall deformity of the boy (Dingeldein et al. 2009).

Although the Ravitch technique does not address the aesthetic aspects of the Poland's syndrome deformity, it does lay the foundation for possible further aesthetic improvements (Urschel 2009). Currently, various reconstruction procedures are used to improve the aesthetic condition of Poland's syndrome patients. One of the best reconstructive alternatives to the Ravitch technique used today entails endoscopic harvesting and transpositioning of musculocutaneous flaps for soft tissue correction. This procedure includes the use of the latissimus dorsi myocutaneous flap, or the upper gluteal or transverse rectus abdominis muscle combined with the use of silicone implants. However, it is accompanied with side effects of additional scarring and deformity in the patient and carries the risk of the body rejecting the harvested soft tissue flaps (Zhu et al. 2012).

An alternative and less invasive procedure to the Ravitch technique is the Nuss technique (Swergold et al. 2013). This technique was developed by Dr Donald Nuss, a paediatric surgeon at Children's Hospital of The King's Daughters in Norfolk, Virginia. This technique uses a bar which is placed in front of the sternum and fixed to the ribs in a compressing position (Nuss & Kelly 2010; Poullis 2010). Advantages of the Nuss technique includes shorter operative times, less blood loss, stability of the chest wall, chest wall elasticity and small surgical incisions. The cosmetic results of the Nuss technique and its less invasive nature make it preferable to the Ravitch repair technique (Nuss & Kelly 2009; Swergold et al. 2013). The disadvantages associated with the Nuss technique include considerable pain requiring extensive pain management, lengthy hospitalisation, and lengthy recovery period. The Nuss technique is further known for an increased recurrence bar migration, hemothorax, and pneumothorax. In incidences of Poland's syndrome with rib sternal aberration, a modification of the Nuss technique has been applied (Nishibayashi et al. 2013; Koizumi et al. 2014). In the modified Nuss technique, an introducer is inserted under the ribs and in the subcutaneous layer in a 'sewing' fashion, followed by the insertion of a bar previously moulded to conform to the desired chest wall shape (Nishibayashi et al. 2013). This bar can be inserted above the sternum, decreasing the risk of puncturing vital organs.

Figure 2.3 shows examples of the Poland's syndrome reconstructive outcomes.

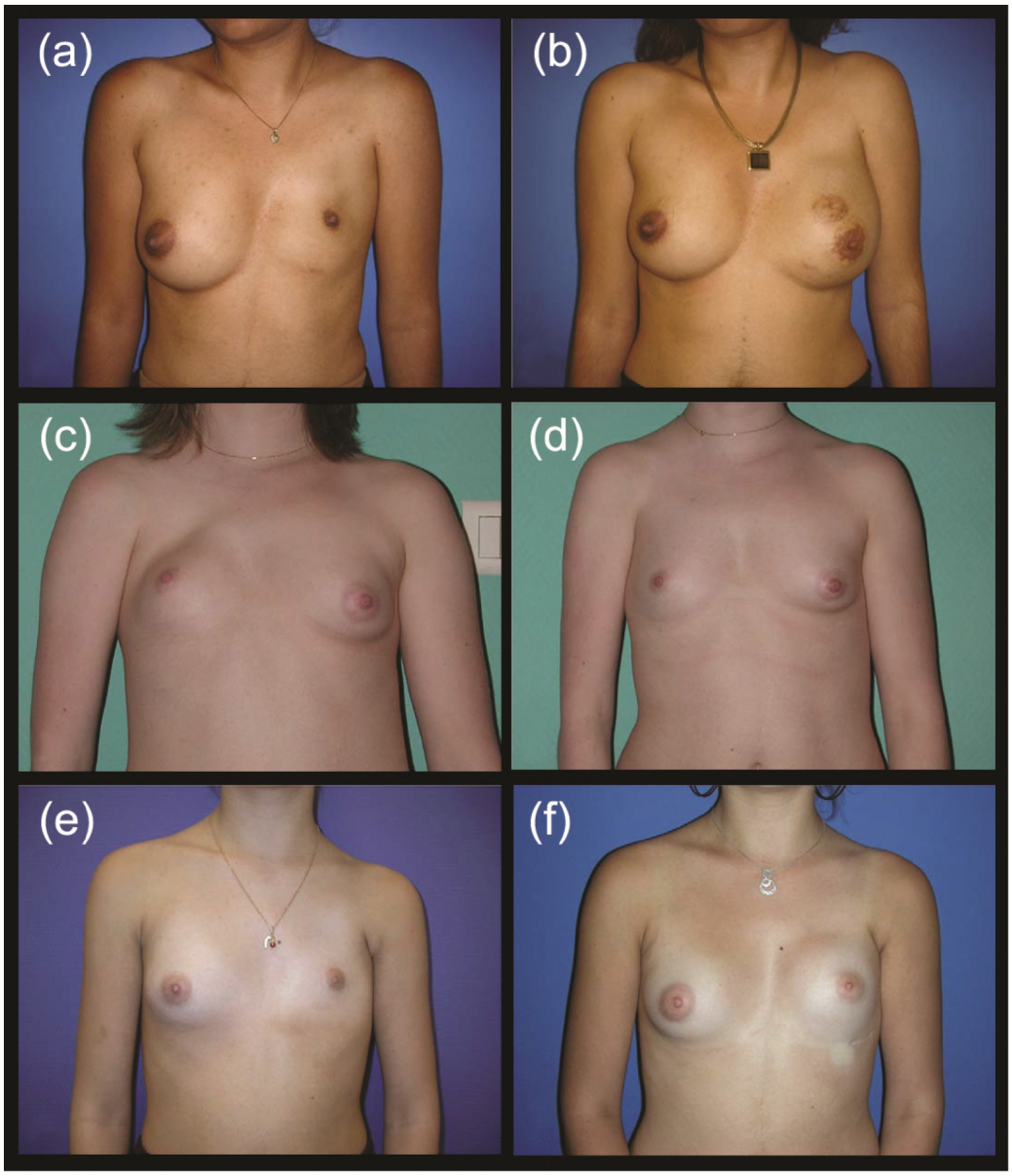

Figure 2.3 **Poland's syndrome reconstructive surgical outcomes.** (a) Poland's syndrome patient before reconstruction, (b) Patient showing a good result after insertion of latissimus dorsi and prosthesis on the left side, (c) Poland's syndrome patient before reconstruction, (d) Patient showing a good result after latissimus dorsi insertion and lipofilling on right side right, (e) Poland's syndrome patient before reconstruction, and (f) Patient showing an average result after insertion of prosthetic implant without latissimus dorsi insertion on the left side (Taken from Baratte et al. 2011).

2.3.3 Minimal invasive surgical reconstruction techniques

A variety of new minimal invasive surgical approaches to Poland's syndrome reconstruction have been developed. These include the insertion of a prosthetic implant, transfer of an omentum flap and lipomodelling. The insertion of silicone prostheses, for example, has evolved to become a successful alternative for the reconstruction of chest wall deformities, which is less complicated than the invasive types of surgical reconstruction (Saour et al. 2008). The aesthetic outcome using prosthetic implants is largely dependent on the design and production of the custom-made prosthesis, and how it is inserted into the chest wall of the Poland's syndrome patient (Saour et al. 2008). The implants are most commonly inserted from under the breast so that the scar is hidden by the infra-mammary fold, thereby achieving an acceptable aesthetic outcome. Implants, should however, only be considered from the age of 18 years and over (Mathes et al. 2005; Fijałkowska & Antoszewski 2011). A custom-made implant for females and males has aesthetical advantages because the outcome of the inserted implant may improve the contour deformity of the patient. Because of the safety of this technique, the overall satisfaction of patients and lack of significant complications make this procedure an attractive alternative to other reconstructive techniques (Mathes et al. 2005; Pereira et al. 2008; Fijałkowska & Antoszewski 2011). However, because an implant is a non-functional entity it cannot contribute to movement (Mathes et al. 2005).

Omentum flap transfer procedures have in recent times been used extensively in Poland's syndrome reconstructions. This procedure involves harvesting the omentum flap laparoscopically (Costa et al. 2010b; Góes 2010; Costa & Blotta 2012). The advantage of using the omentum flap is its malleable properties, which allows it to adapt easily to irregular surfaces and its reliable vascular pedicle (Costa & Blotta 2012). Costa et al. (2010b) performed laparoscopic omentum flap procedures on 13 Poland's syndrome patients. The outcomes of these procedures resulted in noteworthy improvements of the deformities caused by the syndrome. However, the final outcome is difficult to predict because of the flap's spontaneous growth characteristic (Costa et al. 2010a; Costa et al.

2010b). The application of laparoscopic harvesting of the omentum flap should be considered, because it is an excellent reconstructive option that offers superior aesthetic results in Poland's syndrome cases (Costa et al. 2010b; Romanini et al. 2013).

Lipomodelling, which involves the injection of autologous fat cells, is a more recent treatment of Poland's syndrome and is considered to be a feasible and safe technique (Sinna et al. 2010). In most patients, lipomodelling is combined with a latissimus dorsi flap reconstruction, although lipomodelling alone may be considered in some cases. One man and seven women were injected successfully with autologous fat cells after latissimus dorsi flap reconstruction. In one incidence fat necrosis occurred which was rectified with surgical drainage (Pinsolle et al. 2008). In a severe case of Poland's syndrome, several treatments of lipomodelling were performed after a latissimus dorsi flap reconstruction and resulted in successful remodelling of the body contours (Delay et al. 2010). The drawbacks of this technique are resorption of the transferred fat, repeated fat harvesting and requirement of several sessions of fat injections (Delay et al. 2010; Yang & Lee 2011). It has been found that lipomodelling is better identified using ultrasound (Costantini et al. 2013). In Turkey, lipomodelling was sufficient to correct the deformity in some patients; while tissue expansion together with fat grafting was performed on other patients. Finally, for these patients, silicone prostheses were used to replace the tissue expanders (Yesilada et al. 2013). In 2015, lipomodelling using fat transferred from the contralateral breast was performed on a 47-year-old male patient with Poland's syndrome for the first time (King et al. 2015). Although lipomodelling produces good results, most Poland's syndrome patients are physically thin with insufficient fat tissue thickness, often making this procedure unsuitable (Yang & Lee 2011; Romanini et al. 2013).

2.4 Implants for Poland's syndrome patients

In reconstructive surgery, implant structures are developed and fabricated to play very specific roles. For Poland's syndrome patients, implants are used mainly to improve body contours and aesthetic appearance. Self-esteem and social participation are also improved through such interventions

(Hönig 1999; Pereira et al. 2008). Prosthetic implant design is patient specific, mainly because patients' deformities are rarely the same. Achieving symmetry in patients with Poland's syndrome remains a significant challenge (Fijałkowska & Antoszewski 2011). In females with Poland's syndrome, an important consideration is the creation of a breast on the affected side that matches the contour of the healthy side, thereby producing a symmetrical result (Tvrdek et al. 2001).

The production of prosthetic implant structures has been accomplished using many different techniques. The conventional carving techniques for fabricating wax models are difficult and time-consuming, and cause discomfort to patients (Feng et al. 2010). Also, these techniques require that the patient is present for an extended period (Liacouras et al. 2011). These conventional techniques include several complex steps and rely on the exceptional artistic ability of the designer and the skills of the clinician (Feng et al. 2010; Karatas et al. 2011). Conventional prosthetic implant production consists of the following developmental steps (Liacouras et al. 2011): firstly, the creation of a duplication of the affected area by taking an impression of the area; secondly, the building of a clay or wax model of the anatomical structure(s) for which a prosthesis will be constructed; thirdly, the production of a 3-piece mould of the clay or wax model; and finally, the fabrication of the prosthesis in the desired material. In the case of an external prosthesis, the human likeness is hand painted onto the prosthesis, such as for a facial prosthesis.

The newer materials that are available for the production of prosthetic implants offer greater flexibility for the manufacturing of a custom-made implant specifically designed for a patient's unique anatomy (Mathes et al. 2005). The application of imaging technologies, computer-aided design (CAD) and computer-aided manufacturing (CAM) in this field has opened up a new approach to the fabrication of prostheses (Bai et al. 2014). Additive manufacturing (AM), although been available on the market for many years, is also a powerful tool for value-added design in medical device manufacturing (Petrovic et al. 2012).

Many authors consider implants as a method of choice in the treatment of patients with Poland's syndrome (Fokin & Robicsek 2002). Textured, rectangular-shaped silicone implants were inserted into eight male Poland's syndrome patients in Brazil (Pereira et al. 2008). Implant displacement occurred in only one patient which needed a second operation. In a clinical study of 18 Poland's syndrome patients individualised procedures were performed (Da Silva Freitas et al. 2007). In five female patients the latissimus dorsi flap transfer was combined with silicone gel implants.

2.5 Medical modelling

2.5.1 Introduction

Medical modelling is the term that describes the production of highly accurate physical models of the anatomy directly from 3D medical image data using computer controlled manufacturing machines commonly referred to as rapid prototyping (RP) (Bibb & Winder 2010). Medical models are routinely used for diagnosis, communication and pre-surgical planning (Salmi et al. 2012). However, medical models form today an integral part of the design and manufacture of medical implants and prostheses (Bibb & Winder 2010). In implant and prosthesis production, medical modelling involves the acquisition of 3D image data of the human anatomy and then the processing of these data to isolate the tissues or organs of interest, after which a medical model is produced. Such a medical model is then used to facilitate the manufacturing of an implant or prosthesis. Today, most of the manufacturing of implants and prostheses involve AM technologies.

2.5.2 Scanned image data

When a medical model is required, a 3D scan of the anatomy of interest is captured in three-dimensional format. The most commonly used medical imaging technologies employed for the capturing of 3D scanned data include computed tomography (CT), magnetic resonance imaging (MRI) and Ultrasound (Bibb & Winder 2010). These 3D scanned images are then imported into

specialist imaging editing and processing software to produce medical digital models which are used for 3D AM technologies.

In recent times medical imaging has shown rapid growth and is used extensively in modern medicine (Yen et al. 2014). The choice of imaging technology depends largely on the type of anatomical structures required for medical modelling and implant production. CT and MR imaging provide the most complete diagnostic information for medical modelling (Moir & Johnson 2008). CT is usually the modality of choice for the correction of chest wall deformities such as Poland's syndrome and provides in depth information which demonstrates the extent of the muscle abnormalities for planning any reconstructive surgery (Tagarakis et al. 2011; Uludag et al. 2011; Yadav et al. 2014).

Several Poland's syndrome reconstructions have been performed using CT scanned images (Sameuls et al. 1995; Moir & Johnson 2008; Colombani 2009; Uludag et al. 2011; Zhu et al. 2012; Dolas et al. 2014). CT works by focusing x-rays through the body and by detecting the signal on the opposite side of the body. Because CT uses ionising radiation in the form of x-rays, it is regarded as being a non-invasive modality (Bibb 2006). Scans are obtained in a series of slices, which may then be reconstructed to produce a 3D image. Each slice differentiates between the different anatomical structures by displaying them as pixel images in shades of grey. To maximise the data acquired, this distance should be minimised. Slice thickness maybe varied, but may be as thin as 0.5 mm. However, with modern scanners the radiation dose does increase with thinner slices, so a balance between the increased dose, the required detail and safety must be reached (Eggbeer 2008; Bibb & Winder 2010). A scan distance of 2 mm may be adequate for larger structures such as the long bones or pelvis (Bibb 2006). Figure 2.4 shows a CT scan of Poland's syndrome deformities.

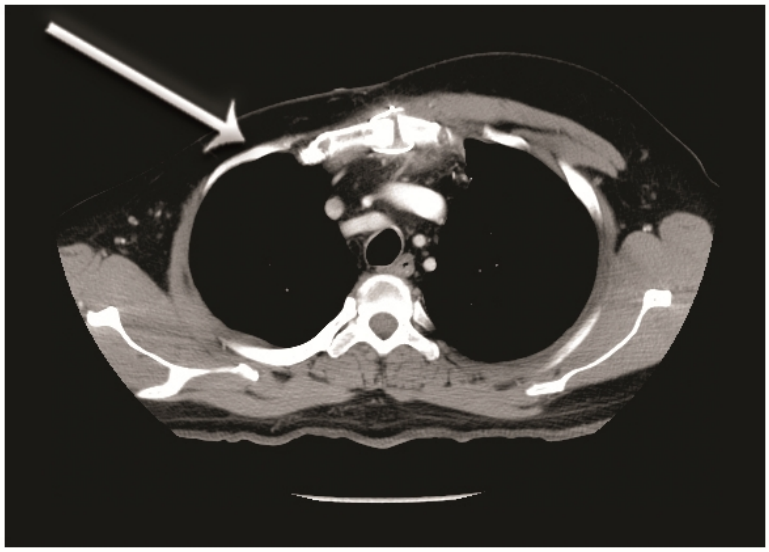

Figure 2.4 **CT scan of Poland's syndrome deformities.** The arrow shows the area where the pectoralis muscle is absent (http://radiopaedia.org/articles/poland-syndrome).

Modern computer technology enables 3D reconstruction of CT images in Digital Imaging and Communications in Medicine (DICOM) format, which are viewed as 2D images (Hatamleh & Watson 2011). When acquiring a CT medical image, it should be free from image artefacts with high resolution and high contrast between the anatomy of interest and the adjacent tissues (Bibb & Winder 2010). CT scans produce continuous 3D axial images of the area of interest which are perpendicular to the long axis of the body. These series of axial images must begin and end on either side of the anatomical structures of interest and also include anatomical structures above and below. The allowances to be included are dependent on the region that is being scanned (Bibb & Winder 2010). Digital models produced by CT scans are of high accuracy, detailed and reproducible, allowing for better visualisation of the region of interest in 3D orientation. These results are better when compared to conventional casts produced by conventional impression techniques (Hatamleh & Watson 2011).

MR imaging is similar to CT imaging and is also used to produce 3D representations in a pixel-based slice system. MRI exploits the situation that all atoms have a magnetic field that can be altered by

radio waves (Bibb 2006). MRI works by aligning atoms in the body using magnetic fields to temporarily disrupt the atom alignment and timing how long it takes the atoms to return to their aligned state (Eggbeer 2008; Moslehifard 2011). Because the human body comprises mostly of water, MRI scanning targets hydrogen nuclei present in water molecules. Thus, areas in the body with high water content will show up as lighter shades of grey, while those areas with less water will show up in darker shades of grey. For example, air shows up as black, while areas with high concentrations of fat will show up as white (Bibb 2006). Thus, MRI is an excellent modality for scanning soft tissue anatomy. Depending on what the region of interest is, the scan settings may be altered to highlight different tissue types more clearly.

A major advantage of CT imaging over MRI is its ability to rapidly produce images of multiple organs and of large portions of the body (Fletcher et al. 2013; Harih & Čretnik 2013). However, MRI has better soft tissue contrast than CT imaging, providing clearer high resolution images (Harih & Čretnik 2013; Pereira et al. 2014). A major concern with the increased use of CT imaging is the high exposure to ionizing radiation (Harih & Čretnik 2013; Chae et al. 2014). In 2010, a more than 20-fold increase in the use CT imaging was recorded in the USA since 1980, which resulted in approximately a 600% increase of ionizing radiation exposure per capita from 1980 to 2006 (Fletcher et al. 2013). The advantage of MR imaging over CT imaging is its lack of ionizing radiation, however, the lengthy acquisition times is a distinct disadvantage, causing much discomfort for many patients (Eggbeer 2008; Monsour & Dudhia 2008; Moslehifard 2011).

2.5.3 Processing of scanned imaging data for medical model production

For the production of a medical model, the scanned image data in DICOM format must be produced according to a specific scan protocol to obtain the data which is compatible with imaging software (Moslehifard 2011). Known imaging processing software packages for example, Mimics® (Materialise® N.V, Technologielaan 15, 3001 Leuven, Belgium), BioBuild™ (Anatomics® Pty. Ltd.

Suite 1, 23 – 27 Wellington Street, St Kilda, VIC, 3182, Australia) and 3D Doctor® (Able Software Corp®, 5 Appletree Lane, Lexington, MA 02420, USA), are used to convert slice image data of 2D slices into 3D computer models for analysis. For Poland's syndrome reconstruction, Mimics® is regularly used to process the scanned images by reformatting the scanned images into stereolithography (STL) format. An STL format of the data can then be transferred to personal computers for further processing. Such an STL file can thus be used directly by 3D printing technologies, or can be further manipulated to produce a medical model using CAD software before printing. A good quality medical model should be fit for purpose and should include the region of interest. Such a model should also be free from any artefacts and movement that could influence the accuracy of the resultant medical model (Bibb & Winder 2010).

The Mimics® software program was developed for working with STL files and files for 3D printing (Cronskär et al. 2012). Mimics® allows a user to import scanned images of a patient and to create 3D models that can be used to plan surgery or for medical implant production using 3D printing (Rahmati et al. 2012). The stack of scanned images that is imported into Mimics® usually consists of images in the XY plane (axial images). The program then calculates and creates images in the XZ (coronal) and YZ (sagittal) directions, which enables a more comprehensive 3D sense of the 2D data (Materialise® 2015). The conversion of the anatomical data from 2D images to 3D models entails a process called segmentation. During segmentation the region of interest is isolated in the scanned sliced image data. The simplest process to segment an anatomical region is through thresholding levels (Harih & Čretnik 2013). For the generation of meaningful information from images, it is important to isolate the region of interest accurately when using segmentation. This information is then used to generate a 3D model (Materialise® 2015).

An STL file is a simple mesh file format that describes objects as a series of triangular facets that form its surface in binary or text (ASCII) format (Bibb 2006). Large flat areas require fewer facets than curved surfaces. STL file format was originally developed by 3D Systems® (333 Three D

Systems, Circle Rock Hill, SC 29730, USA) to provide a transfer data format from CAD systems to stereolithography technology, but it has subsequently been adopted as the standard in the 3D printing industry (Wang et al. 2010). An STL file lists a description of each of the triangular facets, which make up the surface of a 3D model. The simplicity of applying triangular facets makes mathematical operations such as scaling, rotation, translation, calculation of surface area and volume straightforward. The format also allows the angle of facets to be identified, which is necessary for stereolithography (Materialise® 2015).

2.5.4 Design of a medical model

Design is a very complex task even for an experienced designer. In Poland's syndrome reconstruction, medical implants are custom-made parts making the design phase even more complex and challenging (Harih & Čretnik 2013). The designer has to consider the product-human-interaction and develop a medical model with high rate of efficiency and comfort (Hogberg et al. cited in Harih & Čretnik 2013). The prospective medical design determines the difficulty of the task and the constraints (Harih & Čretnik 2013). The traditional methods of design do not incorporate enough data of a patient to design a custom-made product, thus to overcome these limitations there has been an increased use of interdisciplinary medical imaging using 3D CAD software (Harih & Čretnik 2013). The introduction of the 3D CAD design option is one of the greatest advances in the manufacturing of medical devices (Bertol et al. 2009). As is the case with many new technologies, CAD software products were initially rather expensive and thus not accessible widely. However, in recent times the cost has reduced substantially making CAD software more accessible to smaller organisations or individuals (Eggbeer 2008).

The current literature in the field of medical modelling shows the development and extensive use of 3D CAD modelling for human anatomical structures (Dange et al. 2014). The introduction of CAD software brought about more accurate design products that could be visualised before the

manufacturing process. The process is further enhanced by its high level of repeatability, which has improved manufacturing accuracy (Eggbeer 2008).

A CAD process is based upon defining geometries and relationships between geometries. These geometries are defined by using, for example, simple 2D geometrical entities such as lengths, angles and curves. Typically, 2D geometrical entities are used to describe 3D entities such as surfaces and enclosed volumes (Eggbeer 2008). The major advantages of 3D CAD techniques include (Karatas et al. 2011): (1) elimination of impression taking because of the application of medical imaging technologies; (2) possibility to obtain a more realistic medical implant model; and (3) the ability to digitally store the information of a medical model. The only disadvantages of this method are its requirement of expensive computer software and a skilled operator.

Recent developments that have been incorporated into medical modelling design include the translation of real-world tools to their virtual reality equivalents. Among these virtual tools, the haptic interface is at the cutting edge of technology (Mazzoli et al. 2009). SensAble Technologies produced software, namely, Freeform® Modeling™ that is capable of defining and manipulating more anatomical forms than conventional CAD programs are able to manage. This software program was later purchased by 3D Systems® (333 Three D Systems, Circle Rock Hill, SC 29730, USA) and is currently marketed under the name of Geomagic® Freeform®. The program also includes the Geomagic® Touch™ haptic device previously revered to as the PHANTOM® Omni™ that allows users to touch and manipulate 3D virtual forms (Figure 2.5). The word 'haptic' originates from the Greek phrase haptesthai which means 'I touch' (Mazzoli et al. 2009). This haptic device provides precision positioning input and high fidelity force-feedback output. Thus, when using haptic modelling a designer is able shape models as if in the 'real' world. When the designer moves the cursor onto an object as seen on the monitor, the haptic feedback device gives the designer the 'feel' of an actual object which is achieved via an electromechanical system attached to the stylus arm of the haptic device (Evans et al. 2005; Van der Poorten et al. 2012). In essence the stylus arm translates

hand movement to the virtual environment. The model being worked on by the designer is referred to as 'clay' by the Freeform® Modeling™ software program and can be regarded as a virtual interpretation of a wax model produced through conventional carving techniques (Eggbeer 2008). Freeform® Modeling™ also provides a range of tools which a designer can use to model and manipulate the 'clay'.

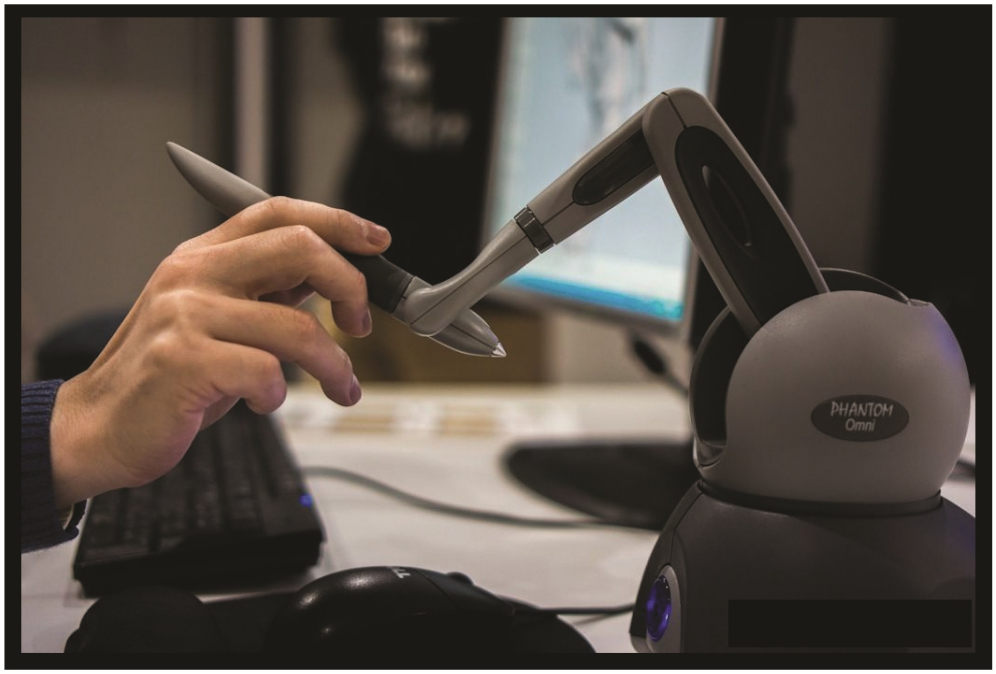

Figure 2.5 PHANTOM® Omni™ haptic device. (Taken from heartleaves.blog.techweb.com).

2.6 Medical implant manufacturing

During the last half of the previous century, major developments brought about important changes in engineering technologies. One of these developments refers to the design and manufacturing of industrial models. The introduction of CAD together with CAM revolutionised the design concept of industrial models (Bertol et al. 2009). Through the application of new rapid prototyping technologies, it has become possible to build real prototypes from a CAD created model. The processes whereby models are built in series of layers directly from computer CAD data are generally referred to as RP technologies (Bibb 2006; De Beer et al. 2009). Towards the late 1980s, RP technologies were

combined with medical imaging technologies to obtain solid medical models, which transformed surgical procedures (Tukuru et al. 2008; Bertol et al. 2009). These manufacturing technologies were later used to design custom-made implants and prostheses prior to surgical procedures (Bibb 2006; Viegas et al. 2010). RP technologies dominated the AM industry for many years; however, the AM industry has been transformed significantly from these early days (Scott et al. 2012).

AM was originally developed for the manufacturing industry to design components for numerous products by converting 3D CAD physical models using solid freeform fabrication (Kim et al. 2008; Bibb et al. 2011). There is a variety of terms used in the freeform fabrication sector, often introducing confusion. Freeform fabrication is regarded as a collection of technologies also known as rapid prototyping, rapid manufacturing and solid freeform fabrication, and more broadly viewed as a subset of additive manufacturing (Bourell et al. 2009). Synonyms for AM are additive fabrication, additive processes, additive techniques, additive layer manufacturing, layer manufacturing and freeform fabrication (ASTM International 2012). AM is an innovative technology that has evolved within the design and manufacturing industries. AM involves taking CAD virtual designs and transforming them into thin, virtual, horizontal, cross-sections, which are then placed into a physical space, one after the other; until the model is complete (Tukuru et al. 2008). Products and services using AM totalled almost $1.2 billion worldwide in 2008 (Bourell et al. 2009). AM is a process of joining materials to make objects from 3D CAD data, usually layer upon layer, as opposed to subtractive manufacturing methodologies (Bibb et al. 2011; Scott et al. 2012).

The most important advantages of AM are (Petrovic et al. 2012): (1) Reduced production time for custom-made products; (2) Flexible design and construction of a custom-made product; (3) Savings of production materials; (4) No tools, moulds or punches are required; (5) Production of parts with almost no residual porosity; and (6) Fabrication of free-form enclosed structures. AM has been extensively used in three key industries (Campbell et al. 2012). In the automotive industry, AM is used to develop new products rapidly, saving significantly on the overall vehicle development costs.

Aerospace industries apply AM for the manufacture of highly complex and high performance products. In the medical industry AM is used because of the ease in which 3D medical imaging data can converted into custom-made medical devices.

In medical modelling, six AM technologies are used to produce anatomic models (Tukuru et al. 2008; Karatas et al. 2011). These include: (1) Stereolithography, which is a photopolymerisation process used to produce parts from photopolymer materials in a liquid state using one or more lasers to selectively cure the predetermined thickness and harden the material into shape layer-by-layer (ASTM International 2012); (2) Laminated Object Manufacturing, which is a process whereby 3D models are created by laminating adhesive coated sheets of paper in which the adhesive is heat-activated by a focused laser beam (Karatas et al. 2011); (3) Selective Laser Sintering, which uses a powder bed fusion process to produce objects from powder materials; while using one or more lasers to selectively fuse or melt particles on the surface, layer-by-layer in an enclosed chamber (ASTM International 2012); (4) Solid Ground Curing, which is similar to stereolithography in that both use ultraviolet light to selectively harden photosensitive polymers (Tukuru et al. 2008); (5) 3D Printing, which selectively deposits binding material through a print head to fuse a thin layer of metallic or ceramic powder onto a previously fused layer which is then fired in a furnace for sinterizing (Karatas et al. 2011); and (6) Fused Deposition Modelling, which is an extrusion process used to make thermoplastic parts through heated extrusion and deposition of materials layer-by-layer (ASTM International 2012).

In prototype production of medical models, a variety of factors affect the quality of a prototype. The four major factors that influence the precision of a final prototype in medical modelling include: (1) Patient preparation; (2) CT scanning; (3) Image manipulation; and (4) Prototyping technology (Anchieta et al. 2011). The process of designing a medical model for the manufacturing of a custom-made implant is summarised in Figure 2.6.

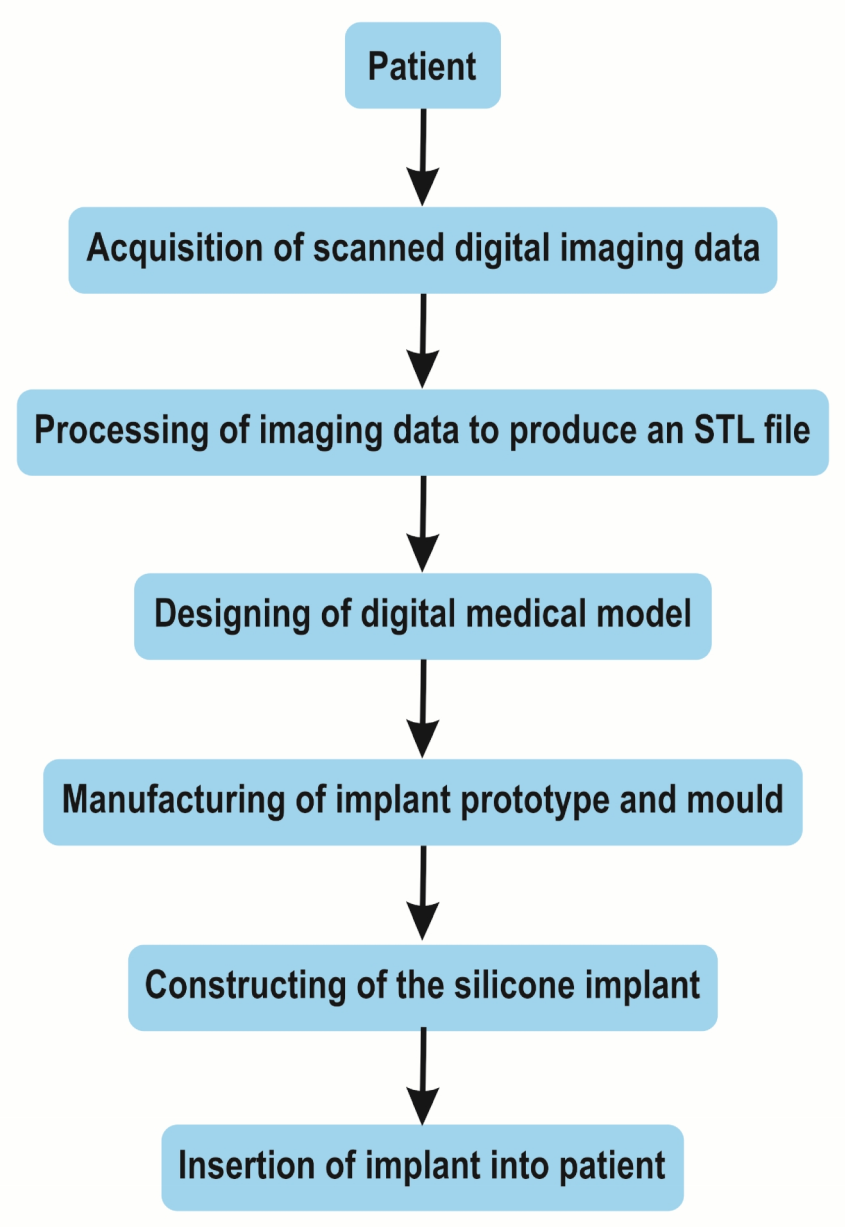

Figure 2.6 **Summary of the process to design and manufacture and insert a custom-made implant.**

Chapter 3:
Materials and Methods

3.1 Introduction

The nature of this study follows an interdisciplinary approach to the design of custom-made 3D digital geometries for soft tissue implants for Poland's syndrome patients. This multifaceted research project integrates information and data from the medical, engineering and design fields of study to develop an intervention. This intervention research project comprises of a process whereby 3D digital geometry designs are systematically developed for the manufacturing process of soft tissue implants. The process model of intervention research comprises of six steps (De Vos et al. 2011):

- Step 1: Problem analysis and project planning
- Step 2: Information gathering and synthesis
- Step 3: Design
- Step 4: Early development
- Step 5: Advanced development
- Step 6: Pilot testing and dissemination

The first two steps, as well as the last step are not addressed in this master's research project. Steps 1 and 2 involve the diagnosis and evaluation of patients with Poland's syndrome. Specifically, in Step 1, medical practitioners participating in the intervention research analyses and describe the disabilities and deformities of Poland's syndrome patients. Thereafter, in Step 2, scanned digital imaging data sets of the soft tissue deformities are captured for each patient. Steps 3 to 5 embraces the design process in which the scanned digital imaging data sets from Step 2 are processed,

manipulated and 3D digital geometries designed. In Step 6, the most suitable 3D digital geometry design is tested and used to manufacture soft tissue implants, which will finally be surgically inserted into the patients.

This research project, covering Steps 3 to 5 of the total intervention research model, used a mixed method research approach. The scanned digital imaging data sets of the Poland's syndrome patients were processed using mostly qualitative methods, while the assessment component was largely quantitative in nature (Figure 3.1).

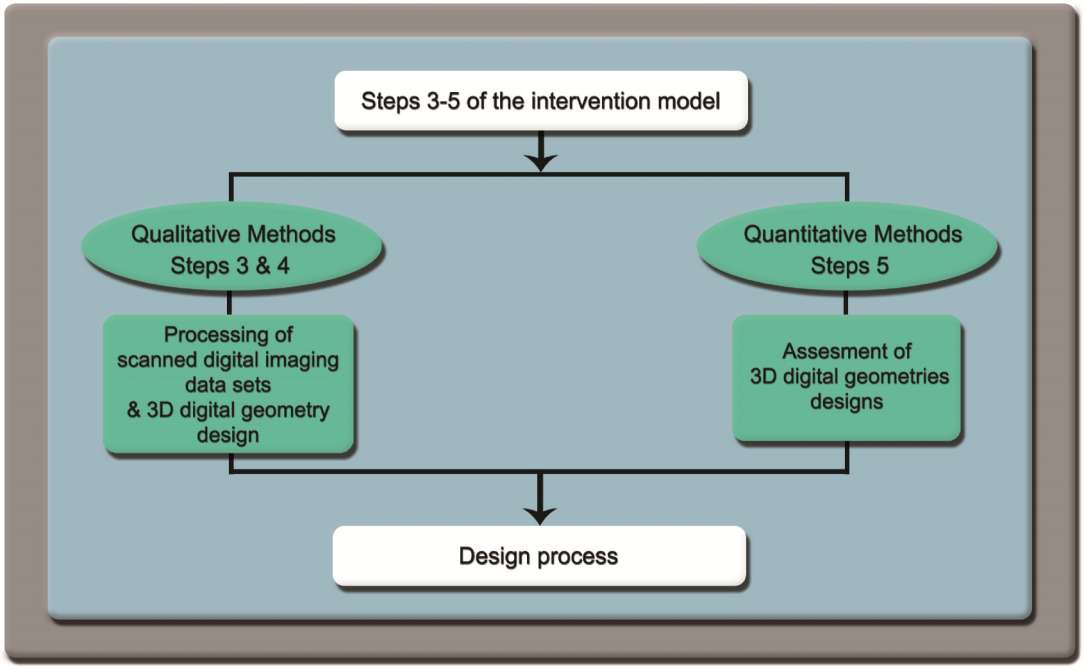

Figure 3.1 Research methods used in this study.

3.2 Study Design

This study formed part of a larger study in which soft tissue geometries were designed for various parts of the body for different patients with soft tissue deformities, including Poland's syndrome (Truscott et al. 2012). The anonymous scanned digital imaging data sets were supplied for this study by the project leader of the main project, Professor M. Truscott from the Faculty of Engineering and Information Technology at the Central University of Technology, Free State, Bloemfontein. These

anonymous scanned digital imaging data sets were captured by a Siemens Sensation Model 16 computed tomography (CT) image scanner at a hospital in Pretoria.

This study comprised of two case studies which included a female and a male patient, each presenting with Poland's syndrome soft tissue deformities. The digital data sets of these patients were processed following four phases (Figure 3.2). Phase 1 involved the acquisition of CT digital data sets; while in the second phase the digital data sets were processed and edited to isolate the regions of interest using the software program Mimics® (Materialise® N.V, Technologielaan 15, 3001 Leuven, Belgium). In Phase 3, the digital data sets of the isolated regions of interest were manipulated and 3D digital geometries of soft tissue implants designed using two different software programs, namely, Magics (Materialise® N.V, Technologielaan 15, 3001 Leuven, Belgium) and Freeform® Modeling™ (333 Three D Systems, Circle Rock Hill, SC 29730, USA). Although, an in depth assessment of the performance of Magics and Freeform® Modeling™ is beyond the scope of this study; an attempt was however made to compare the outputs of these programs in Phase 4.

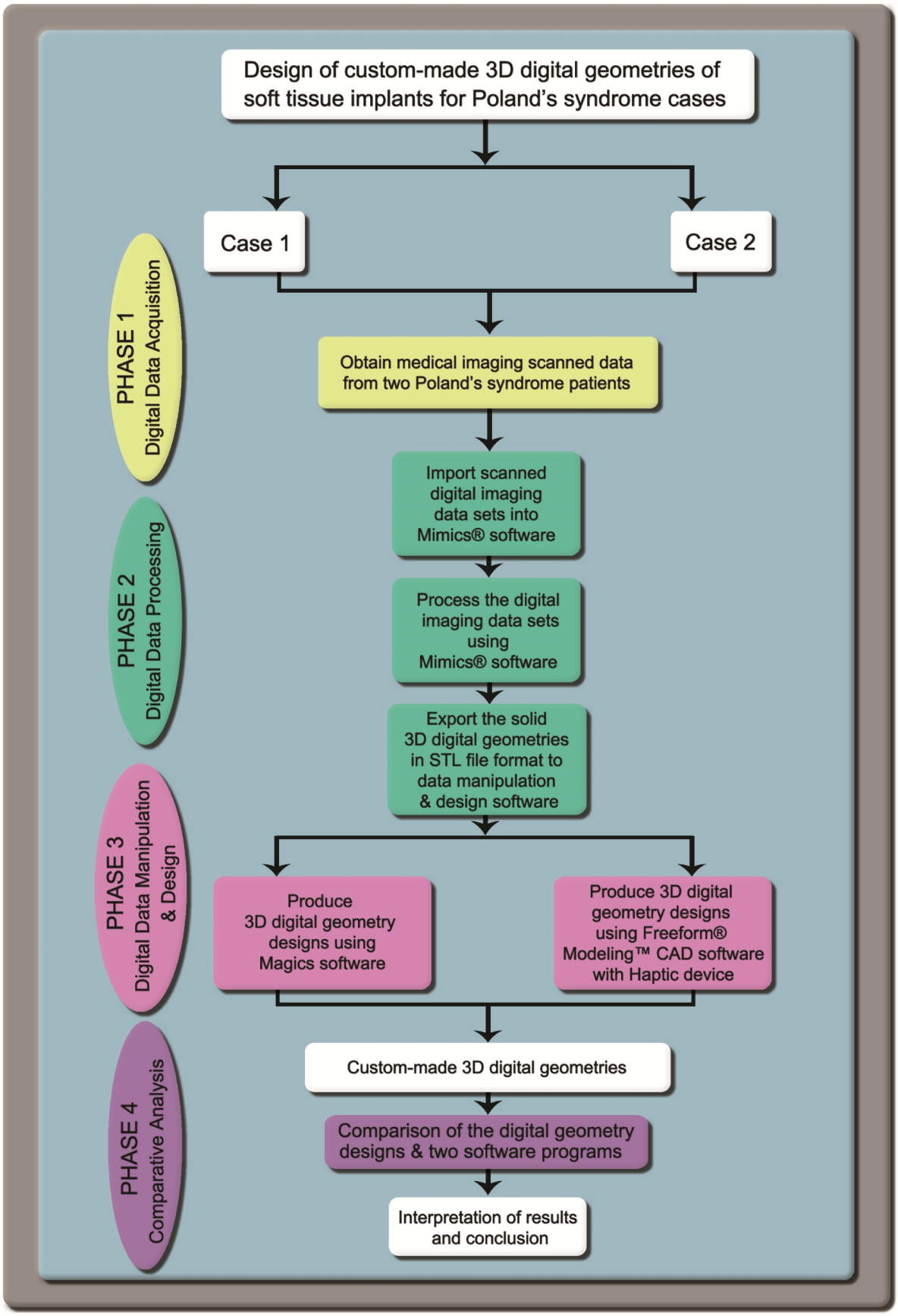

Figure 3.2 **Flow diagram depicting the four phases of the research project.**

3.3 Materials: Patient details

A female and a male patient were selected for this study, because females and males generally present with different deformities of the thorax area and therefore requires different approaches to soft tissue reconstruction. These patients presented with some form of upper extremity deficiency together with the absence of chest wall muscles confined to one side of the body. The details of the presentation of Poland's syndrome in the two patients are summarised in Table 3.1.

Table 3.1 Details of the two patients with Poland's syndrome used in this study.

Poland's syndrome descriptor	Case Study 1	Case Study 2
Gender	Female	Male
Age	16 years	17 years
Affected side of body	Right	Right
Soft tissue deformity	Pectoralis major muscle	Pectoralis major and minor muscle

3.3.1 Software

Materialise® in Belgium developed a software program which enables the processing and editing of medical images obtained from a medical image scanner. The program *Materialise's Interactive Medical Image Control System*, namely Mimics® Version 17 of 2014, allows the user to import scanned digital imaging data sets from a CT image scanner into the correct format suitable for processing of the digital data. The two software programs used to design and manipulate data generated in Mimics® were the STL editor Magics, and the computer-aided design (CAD) software program Freeform® Modeling™. Magics was selected because it was originally exclusively used for the development of medical geometries for soft tissue implants at the institute where this study was conducted (Truscott et al. 2012). However, at the inception of this project, the software program

Freeform® Modeling™ was purchased for design purposes of all types of models, including medical models. Limited understand of the functionality of Freeform® Modeling™ existed in the department at that time, thus it was decided that both these software programs should be implemented in this study. The development information of the two design software programs is presented in Table 3.2.

Table 3.2 Development information of Magics and Freeform® Modeling™ software programs.

Software program properties	Magics	Freeform® Modeling™
Version	17	12
Developer	Materialise®	3D Systems®
Year	2013	2012
Head office	Belgium	USA
Program characteristics	STL digital editor & build preparations	3D digital CAD modelling and virtual sculpting

3.4 Methods of Phase 1: Digital data acquisition

The digital data acquisition phase comprised of Steps 1 and 2 of the intervention research model. Scanned digital imaging data sets are successive 2D images (sequence of slices) that collectively form a 3D image. The scanned digital imaging data sets of the two Poland's syndrome patients were captured in a Digital Imaging and Communications in Medicine file format (DICOM file format). These scanned digital imaging data sets of the two patients were defined by different parameter dimensions (Table 3.3). For the female Poland's syndrome patient, the CT scanned slice thickness and slice increment were of equal size, thus the CT scanned slices did not overlap. In contrast, the slice increment of the male Poland's syndrome patient was smaller than the slice thickness, thus producing overlapping CT scanned slices.

Table 3.3 Parameters of the scanned digital imaging data sets of the two patients with Poland's syndrome used in this study.

CT parameters	Female	Male
Number of CT scanned slices	152	533
Slice thickness (mm)	2	1
Slice increment (mm)	2	0.7
Pixel size (mm)	0.883	0.779
Resolution (pixels)	512 × 512	512 × 512

3.5 Methods of Phase 2: Digital data processing

Digital data processing involves the isolation of anatomical digital data of anatomical structures, including skin, soft tissue, bone and organs, using the *Segmentation Functions* of Mimics®. In this study the anatomical structures that were isolated for each Poland's syndrome patient were the whole thorax and the pectoralis muscle. These anatomical structures are regarded as the regions of interest (ROIs). The *Segmentation Functions* allows for the removal of all unwanted anatomical digital data from the ROIs.

The digital data processing phase comprises of three major components. The first component involves the importing of the DICOM files of the scanned digital imaging data sets into Mimics®, while in the second component the processing of the DICOM files involves the isolation of the digital data of the ROIs, from which *solid 3D digital geometries* (*solid 3D-DGs*) are produced. The third component comprises of the conversion of the *solid 3D-DGs* into STL file format suitable for the digital data manipulation and design phase (Phase 3). Thus, using Mimics®, *solid 3D-DG* models of the isolated whole thorax and pectoralis muscle of the two Poland's syndrome patients were generated.

3.5.1 Component 1: Digital data importing

The DICOM files of the scanned digital imaging data sets of the two Poland's syndrome patients were imported into the Mimics® *Work Area*. Thereafter, the DICOM files were compressed using the CT algorithm. The compressed DICOM files were then displayed in three views in the Mimics® *Work Area*, namely, the XZ-view or Front-view (coronal cross-sectional images) was displayed in the top left window, the XY-view or Top-view (axial cross-sectional images) was displayed in top right window, while the YZ-view or Side-view (sagittal cross-sectional images) was displayed in the bottom left window of the *Work Area* (Figure 3.3). These images were displayed in grey scale values representing the density values of different anatomical structures. The lowest density tissues were presented in black, while the tissues with the highest density, for example bone, were presented in white. These density values of the images were depicted as pixels.

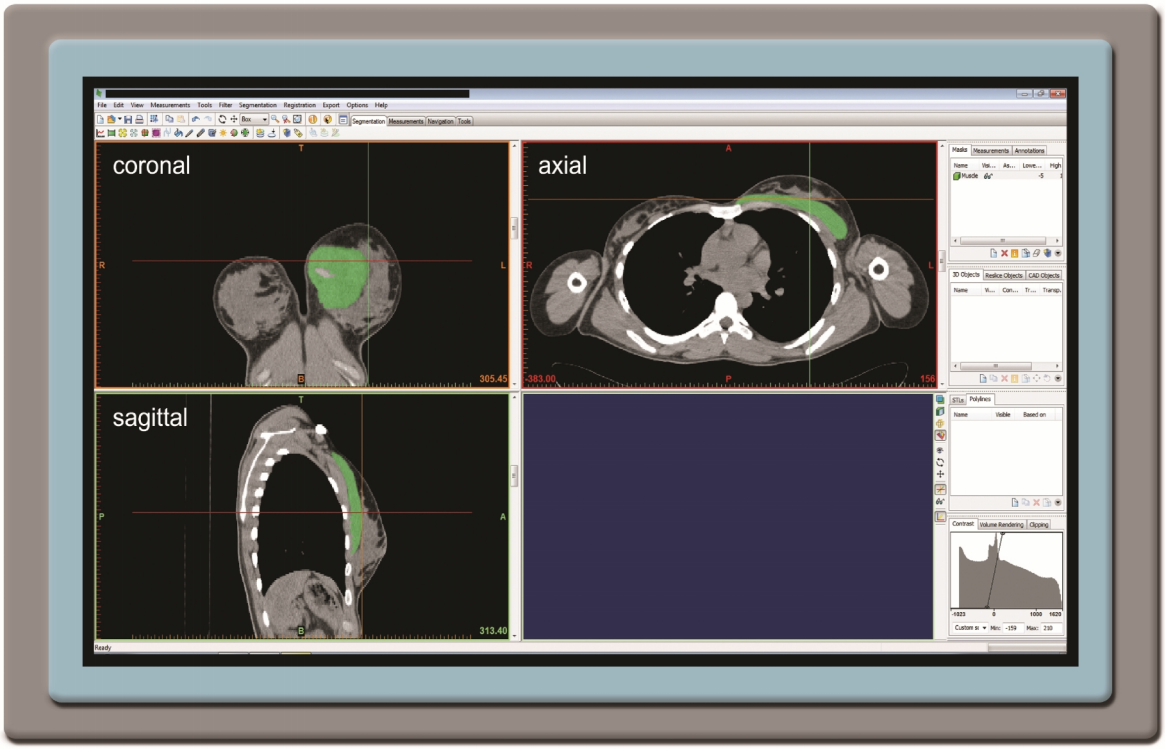

Figure 3.3 Mimics® *Work Area*.

It is essential to ensure that when importing DICOM files, the images in the *Work Area* are in the appropriate window orientations. For example, the left-right positioning and top-bottom positioning of the coronal cross-sectional images may be in the wrong orientation and must thus be switched to the correct orientation using the switching handles (Figure 3.4).

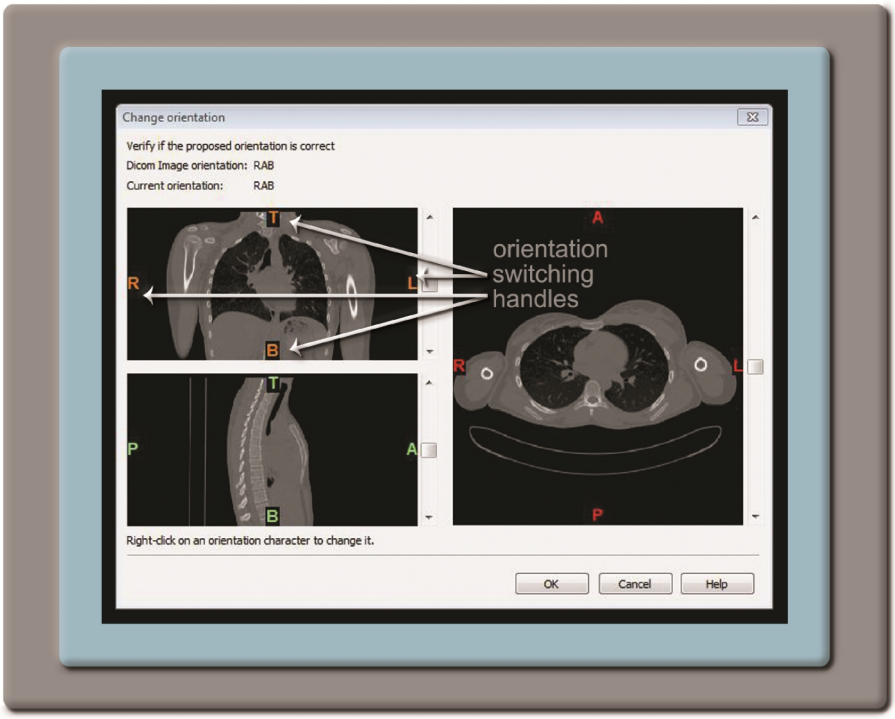

Figure 3.4 Mimics® orientation switching handles.

3.5.2 Component 2: Digital data processing

To enable the user to isolate the ROIs from the digital data in the DICOM files, *Segmentation Masks* are used to highlight these regions. *Segmentation Masks* are created using different functions of Mimics®. These functions include *Thresholding* and *Region Growing*, which also involves the editing and refining of the masks (*Mask Editing*) to ultimately calculate and produce the 3D soft tissue geometries (*Calculate 3D*). These *Segmentation Masks* each have fixed colour codes assigned to them. Several different *Segmentation Masks* can be defined in one project and named accordingly, for example, a muscle mask, bone mask, skin mask and organ mask.

Thresholding is used to exclude all anatomical structures beyond the boundaries of the ROIs. This process thus leaves, for the thorax, a selection which included the thorax anatomical structures, bones, organs and soft tissues, and also the pectoralis muscle. However, the isolation of the pectoralis muscle included only the soft tissue muscle volume. *Thresholding* can be achieved in two different ways, namely through the use of the *Thresholding Profile Line* and through the use of the *Thresholding toolbar*. When applying the *Thresholding Profile Line* method, a profile line is drawn to cross over the ROI and into surrounding regions to display how grey values change along the line. In this study the *Thresholding toolbar* was used because of its ease of use and because it allows the user to make manual adjustments when creating the *Segmentation Masks*.

Thresholding was achieved in the following manner:

The *Thresholding tool* was selected to activate the *Thresholding toolbar*, which contains different pre-defined ranges of threshold values for the entire imported scanned digital imaging data set. Figure 3.5 shows a pre-defined range of CT soft tissue threshold values ranging from -700 to 225 (indicated in green). These pre-defined threshold values can now be manually changed to include the soft tissue anatomy volume so that it includes all the soft tissue ROI by moving the sliders. This *Thresholding* process selects pixels on all the 2D slices within the threshold value range to construct a mask (indicated in green) of all the soft tissue within the given segmentation.

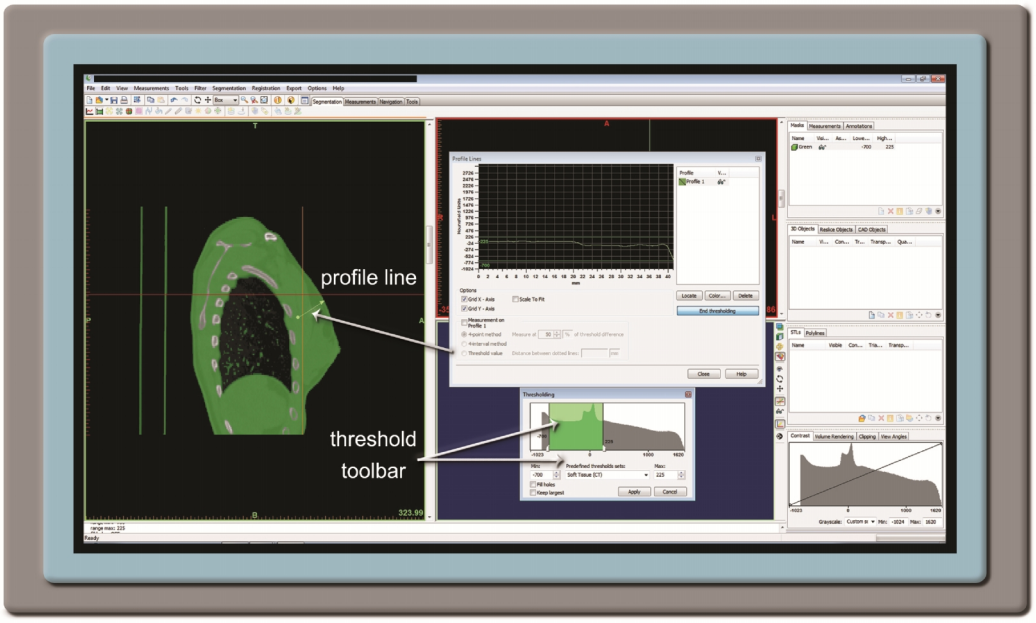

Figure 3.5 **Dialog boxes indicating the *Thresholding toolbar* and *Thresholding Profile Line*.**

The *Segmentation Masks* produced by *Thresholding* contains, besides the ROIs, digital data of superfluous tissue. These ROIs must now be isolated from this segmentation mask using the *Region Growing tool.* The *Region Growing tool* thus allows the user to split a *Segmentation Mask* into different 3D anatomical structures (sub-masks of the *Segmentation Mask).* During the splitting of a *Segmentation Mask*, some anatomical structures are easily separated from adjacent anatomical parts because of explicit boundaries between them, such as solid bone structures from soft tissue anatomical structures. On the other hand, the separation of the different soft tissues in close proximity to one another is a difficult task to achieve, because of the similarity of the grey values. In this study, for the pectoralis muscle isolation, the task of separating the ROI from the superfluous soft tissue muscle volume was time consuming and was achieved by manually removing floating pixels around the boundaries (*Mask Editing*). Once a sub-mask has been accurately edited, a *solid 3D-DG* model can be generated for exportation as an STL file.

Region Growing and *Mask Editing* were achieved in the following manner:

The *Region Growing toolbar* was activated by selecting the *Region Growing tool* to split the *Segmentation Mask* formed while performing the *Thresholding* action. After splitting the *Segmentation Mask* (identified in the source space of the *Region Growing toolbar*), sub-masks were formed of the ROI. A sub-mask is created as a *New Target Mask* by editing the original *Segmentation Mask* to contain only the ROI as defined by the *New Target Mask*. Figure 3.6 shows the *Region Growing toolbar* which was used to split the *Segmentation Mask* into sub-masks.

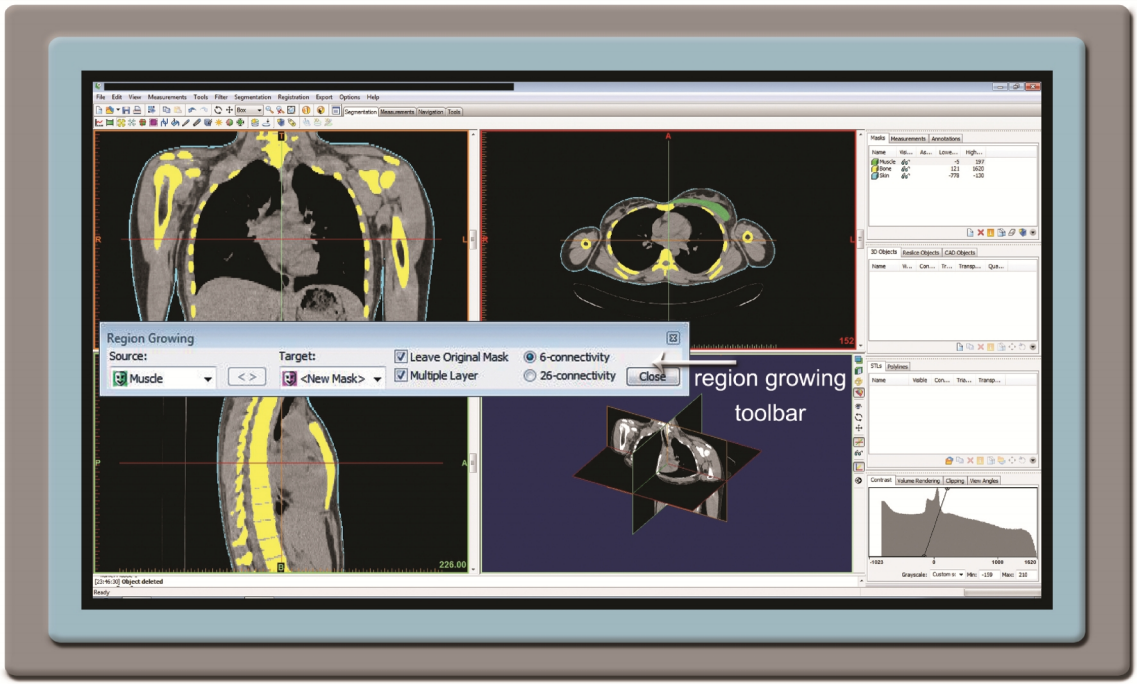

Figure 3.6 ***Region Growing toolbar*** **used to split a** ***Segmentation Mask*** **into sub-masks.**

To remove the floating pixels from the ROI, editing functions were performed manually on the active sub-mask. These editing functions were performed using the *Edit Mask tool* and the *Multiple Slice Edit tool* allowing the user to add or subtract from 2D slice(s) or to restore when needed. The *Edit Mask tool* was used to edit a single 2D slice, while the *Multiple Slice Edit tool* was used to edit a few 2D sequential slices simultaneously (Figure 3.7).

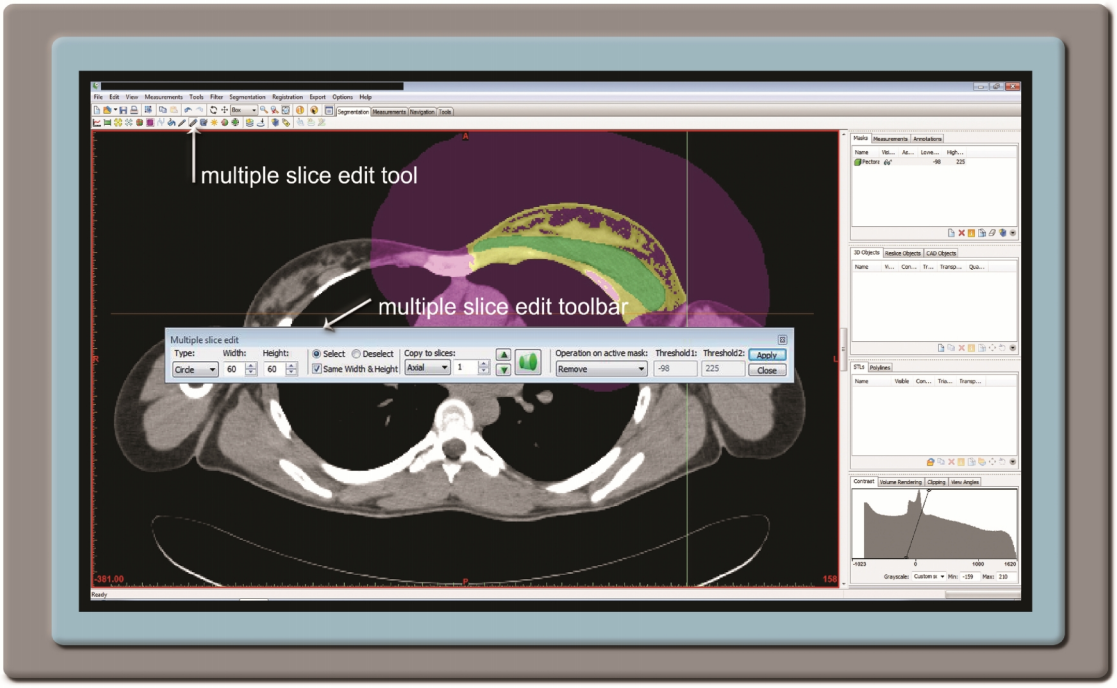

Figure 3.7 ***Multiple Slice Edit tool*** **used to edit 2D slices.**

In the final step of digital data processing component, the edited sub-mask containing only the digital data of the ROI must be transformed into a *solid 3D-DG.*

Generation of a solid 3D-DG model was achieved in the following manner:

> *Solid 3D-DG* models were generated by transforming the edited *Segmentation Masks* using the *Calculate 3D tool*. A mask of the desired ROI, for example the pectoralis muscle, was selected and then a *solid 3D-DG* model was generated. Once the *solid 3D-DG* model had been generated, it could be visualised using the fast and advanced 3D rendering and shaping algorithms of Mimics® (Figure 3.8).

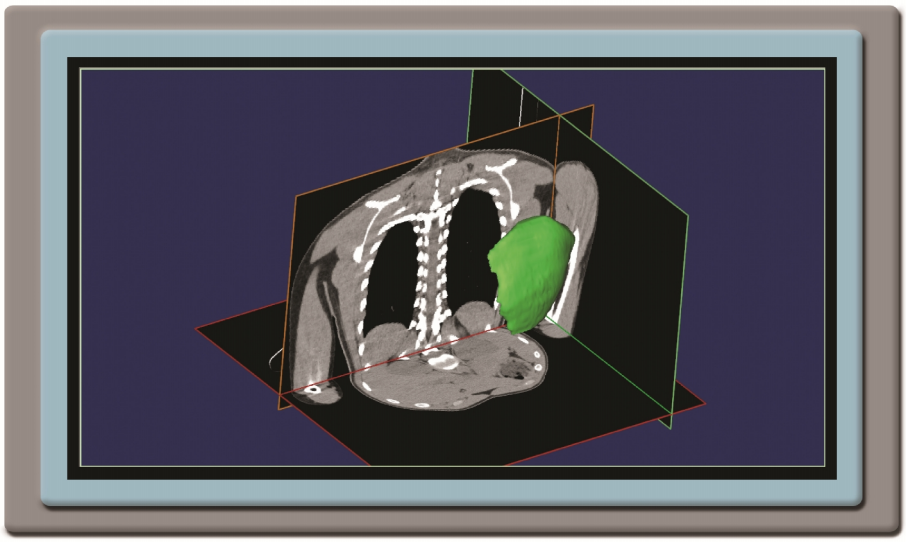

Figure 3.8 Visualisation of the pectoralis muscle prior to exportation (green).

3.5.3 Component 3: Exporting of STL file

In the final stage of digital data processing, the edited sub-mask containing only the digital data of the ROI must be exported and then imported into the two software programs, Magics and Freeform® Modeling™, used for the digital data manipulation and design phase. Both these programs require that the digital data are in STL format (Shimamura et al. 2012). STL is an abbreviation that was derived from the term stereolithography, which is a standard interface for additive manufacturing technologies. The STL format, in binary and ASCII, uses triangular facets to approximate the shape of an object (ASTM International 2012). The higher the number of triangular facets, the greater the quality of the reconstructed 3D digital geometry model will be. For many anatomical structures a large number of triangles are required to render a smooth surface because of curvature.

Exporting of an STL file was achieved in the following manner:

The *solid 3D-DG* models were exported in STL file format by selecting the STL+ option. The STL+ dialog box was activated allowing the user to select one or more options; namely, Mask, 3D, CAD objects or Finite Element Analysis (FEA) meshes. For this study the 3D option was selected, after which the *solid 3D-DG* models were exported as binary STL files (Figure 3.9).

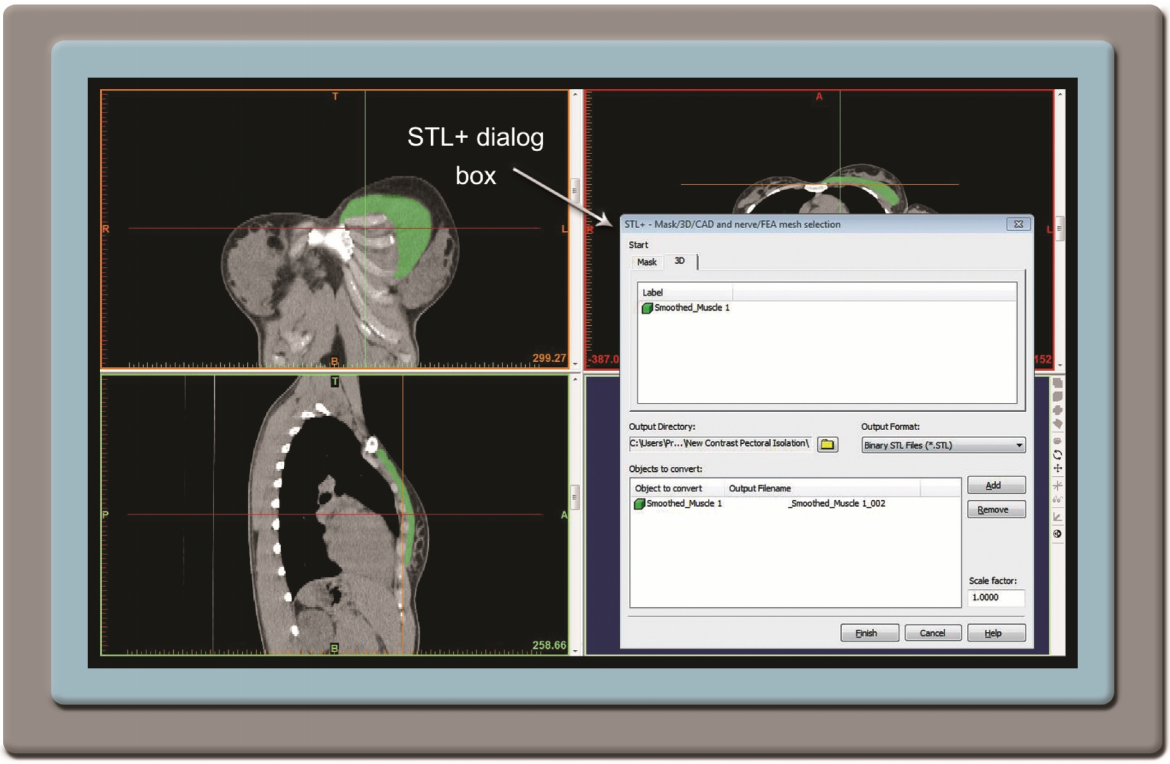

Figure 3.9 STL+ dialog box used to export a *solid 3D digital geometry* model.

3.6 Methods of Phase 3: Digital data manipulation and design

For this study the two software programs, Magics and Freeform® Modeling™, were used to manipulate the digital data of *solid 3D-DG* models exported from Mimics® in STL format. Magics software has two main characteristics; firstly it is used for STL editing and secondly it is used to prepare 3D digital geometry models for the AM process. The software offers a variety of powerful 3D tools suitable for STL manipulation and the production of high quality prototypes. Furthermore, Magics allows 3D models to be sliced into thin layers suitable for 3D printing. On the other hand, the Freeform® Modeling™ program allows for 3D digital manipulation and design in a digital 3D virtual space with sculpting capabilities, as well as advanced features of 3D CAD modelling. Freeform® Modeling™ is combined with a haptic device's integrated sense of touch and is able to handle voxels, polygons, subdivisions and non-uniform rational basis splines, which allows the user to undertake sculpting and modelling in virtual space.

For the digital data manipulation and design phase, two different design routes were applied to achieve a reconstruction of Poland's syndrome deformities. The one design route involved using a mirror image of the whole thorax, referred to as *Technique A*, while the other design route involved the use of a mirror image of the isolated pectoralis muscle from the healthy side of the thorax; referred to as *Technique B*. These design routes were followed in both software programs, Magics and Freeform® Modeling™. This resulted in producing four different *final 3D digital geometries* (*final 3D-DGs*) of the pectoralis muscle for each of the two patients. Although *Technique A* uses the whole thorax and *Technique B* uses the isolated pectoralis muscle, both procedures resulted in a *final 3D-DGs* model of the pectoralis muscle (Figure 3.10).

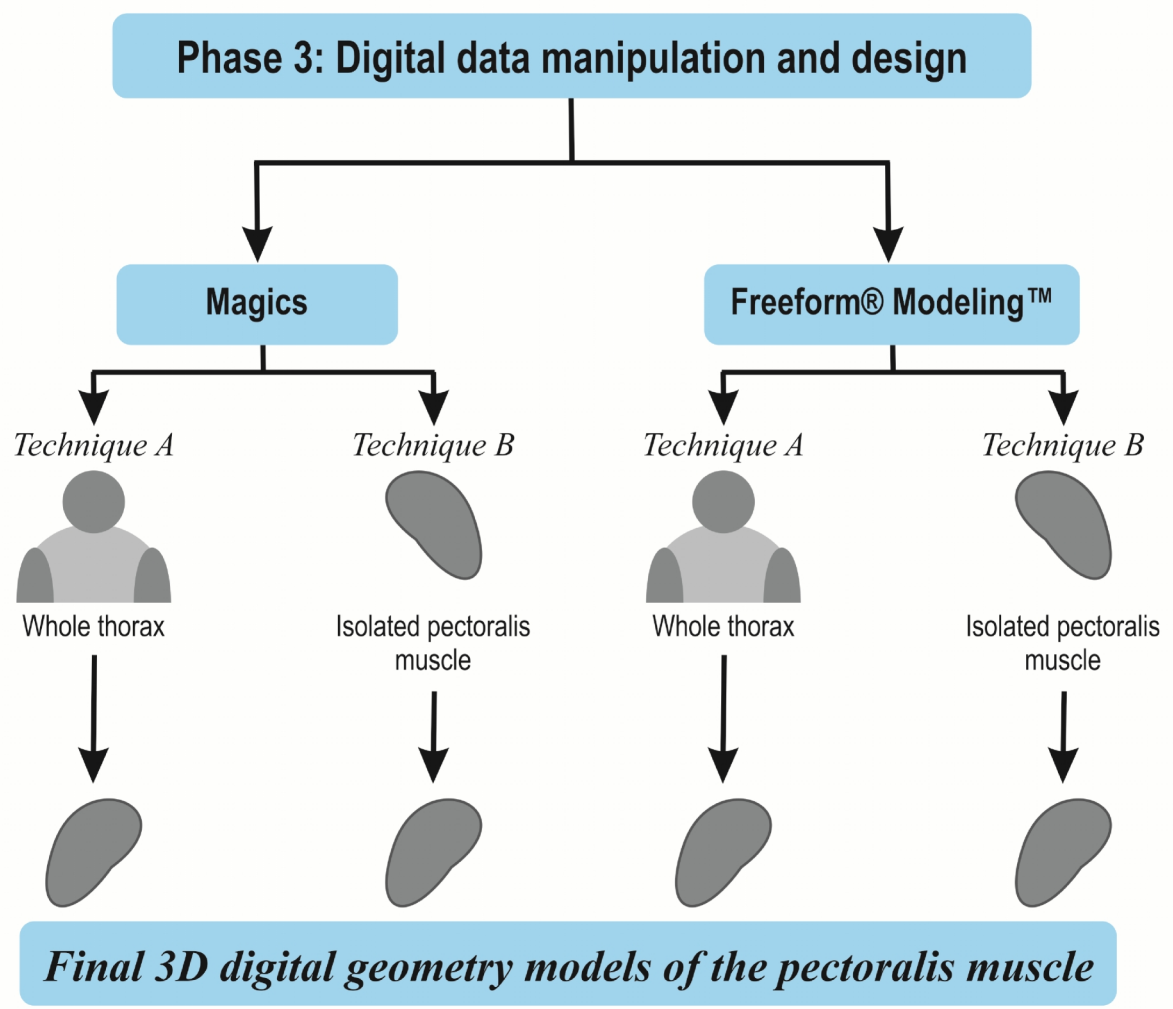

Figure 3.10 **Flow diagram demonstrating the application of *Technique A* and *B* in Magics and Freeform® Modeling™ which results in four *final 3D digital geometry* models of the pectoralis muscle.**

3.6.1 *Technique A* using Magics

In Magics, *Technique A* entailed many operational steps to manipulate the STL file. These steps included the *activation of the coordinate planes*, the *bisection of the whole thorax*, followed by the *mirroring of the healthy half onto the affected half*, after which a number of *Boolean operations* are performed to produce a *final 3D-DG* model of the pectoralis muscle (Figure 3.11).

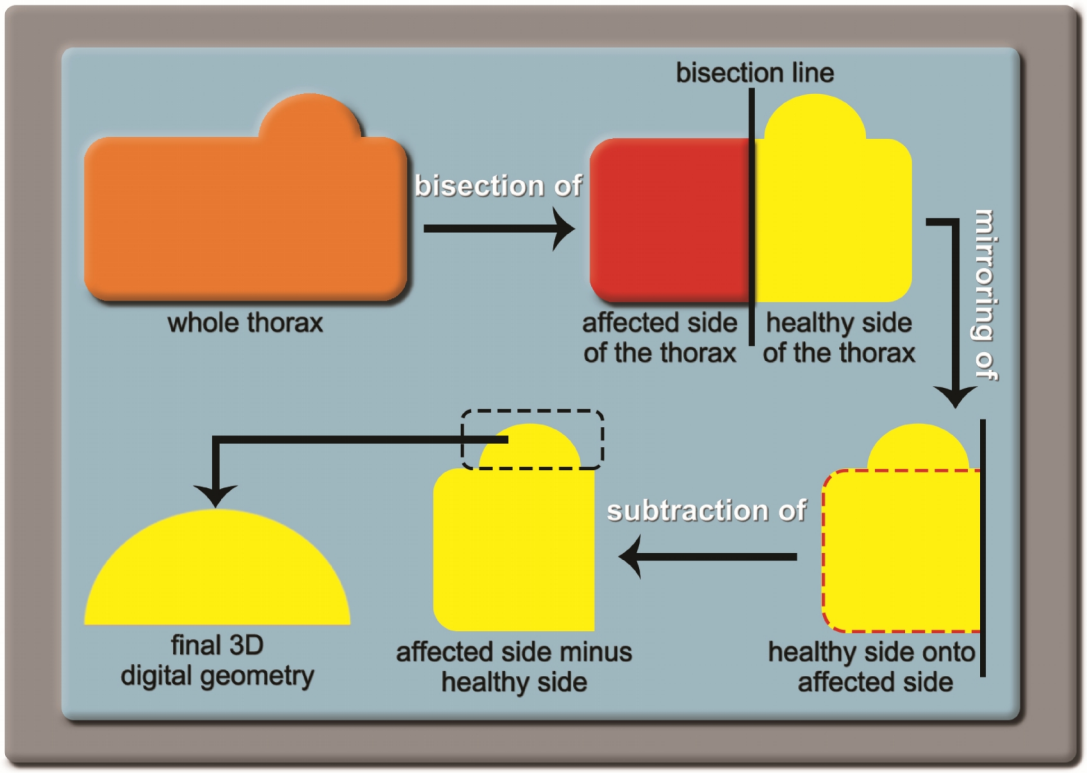

Figure 3.11 **Work flow using Magics *Technique A* to design a *final 3D digital geometry* model of the pectoralis muscle using the whole thorax.**

Digital data manipulation and design phase using Technique A was performed in the following manner:

Activation of the coordinate planes

1. The *solid 3D-DG* model of the whole thorax that was exported from Mimics® in STL file format was imported into the work area of Magics using the *Import Part function*.

2. In the *View Menu* of Magics a number of toolbars are available. When these toolbars are activated different function tabs are displayed; namely, *Tools* tab, *Fixing* tab, *View* tab, *Marking* tab, *Scenes* tab, *Slicing* tab, *Support Generation* tab, and *Tooling* tab, as well as the *Main toolbar* (Figure 3.12).

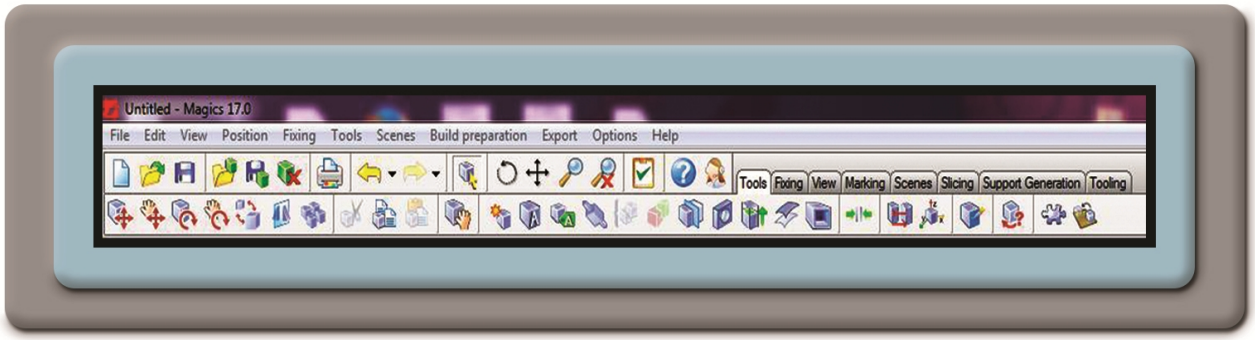

Figure 3.12 Magics toolbars displaying the different function tabs.

3. In the *Tools* tab the *Pick & Place Parts function* was selected to activate the bounding box around the 3D digital geometry model (referred to as part in the program). This allows the user to move and rotate the part in the work area.

4. The *View* tab was then opened in which the *Coordinate System function* and/or an *Orientation Indicator function* could be selected to activate the display of the *XYZ* coordinates (Cartesian coordinate system) in the work area.

5. The *X plane* (central plane or mirror plane) and *Y plane* listed in the *Multi-Section* tab was then activated by ticking the appropriate boxes (Figure 3.13).

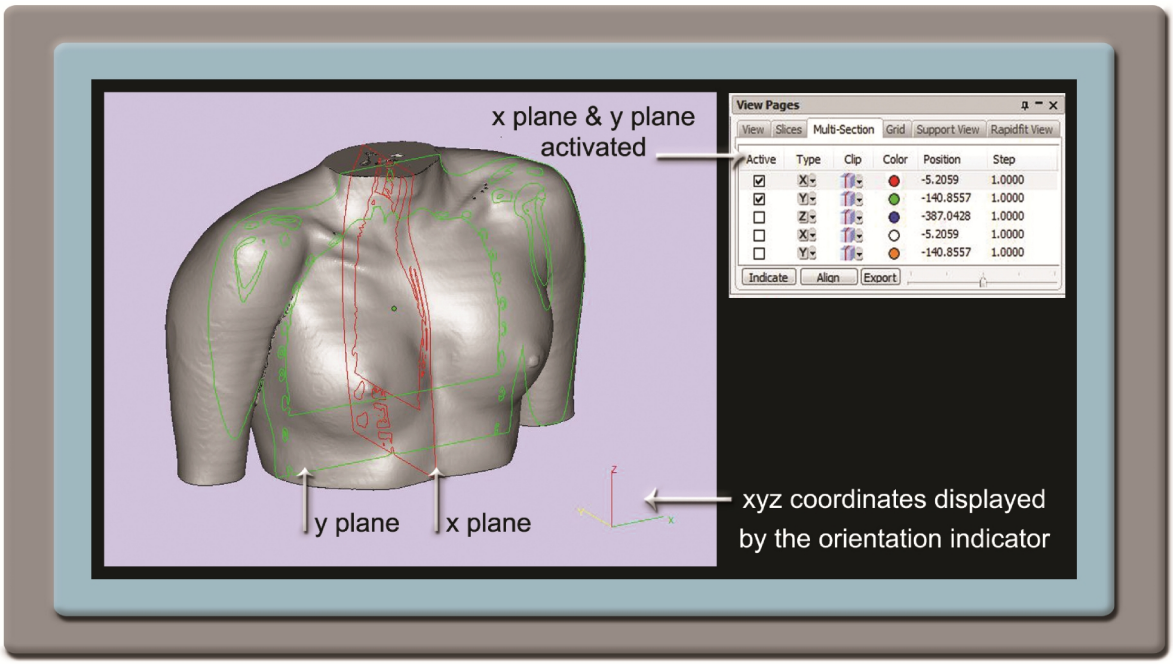

Figure 3.13 Activated *X plane* (displayed in red) and *Y plane* (displayed in green).

Bisection and mirroring of the healthy half onto the affected half

The term symmetry refers to a body that can be divided along a central plane into two identical halves, referred to as bilateral symmetry (Tomkinson & Olds 2000; The American Heritage® Dictionary of the English Language 2011; Ursyn 2015). The bisection of a body part using a CAD program requires the accurate placement of a central plane (mirror plane) of the coordinate system to achieve as close as possible complete symmetry (Truscott et al. 2012). Although a variety of studies exist on how to determine and calculate facial symmetry (Benz et al. 2002; Meyer-Marcotty et al. 2010; Meyer-Marcotty et al. 2011; Wu et al. 2011; Mcavinchey et al. 2014), none could be found on methods to achieve body symmetry, particularly of the thorax. However, if such methodology does exist, it would be impractical to apply it in this study, because of the extreme asymmetrical thoracic deformities demonstrated by the two participating Poland's syndrome patients. Therefore, in this study the best-fit central plane (mirror plane) position was found through an iterative process of trial and error.

Bisection and mirroring of the healthy half of the thorax (part) onto the affected half of the thorax was achieved in the following manner:

6. After the *X* and *Y planes* were selected, the part was brought into alignment with the planes before any mirroring and Boolean operations could be performed. These alignment adjustments were achieved by manually rotating the part until an acceptable alignment was achieved as shown by the red arrows indicating the rotation deviation in Figures 3.14a and b.

7. Thereafter, the *X plane* (central plane) was adjusted in the *Front View* for further cutting and mirroring purposes.

8. The *Cut\Punch tool* was selected to cut the 3D digital geometry model of the whole thorax into two halves along the *X plane*. The *Cut\Punch* dialog box was activated which provided a list of different cutting option tabs, namely, *Polyline*, *Circle Cut*, *Teeth Cut*, and *Section Cut*. For this study the *Section Cut* tab was selected to bisect the thorax.

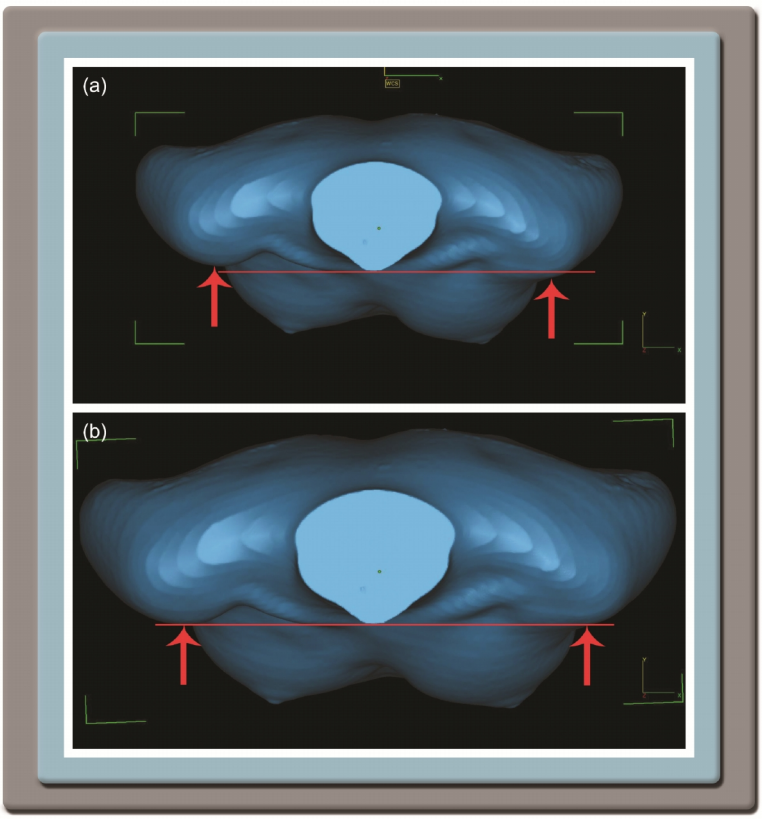

Figure 3.14 **Alignment of the thorax using rotation.** (a) Arrows indicate places of poor alignment at the shoulders of the thorax in *Top view*, and (b) Arrows indicate

places of acceptable alignment at the shoulders of the thorax after rotation in *Top view*.

9. After the 3D digital geometry model of the whole thorax model was cut into two separate halves, the healthy and the affected halves of the thorax were each assigned different colours (Figure 3.15).

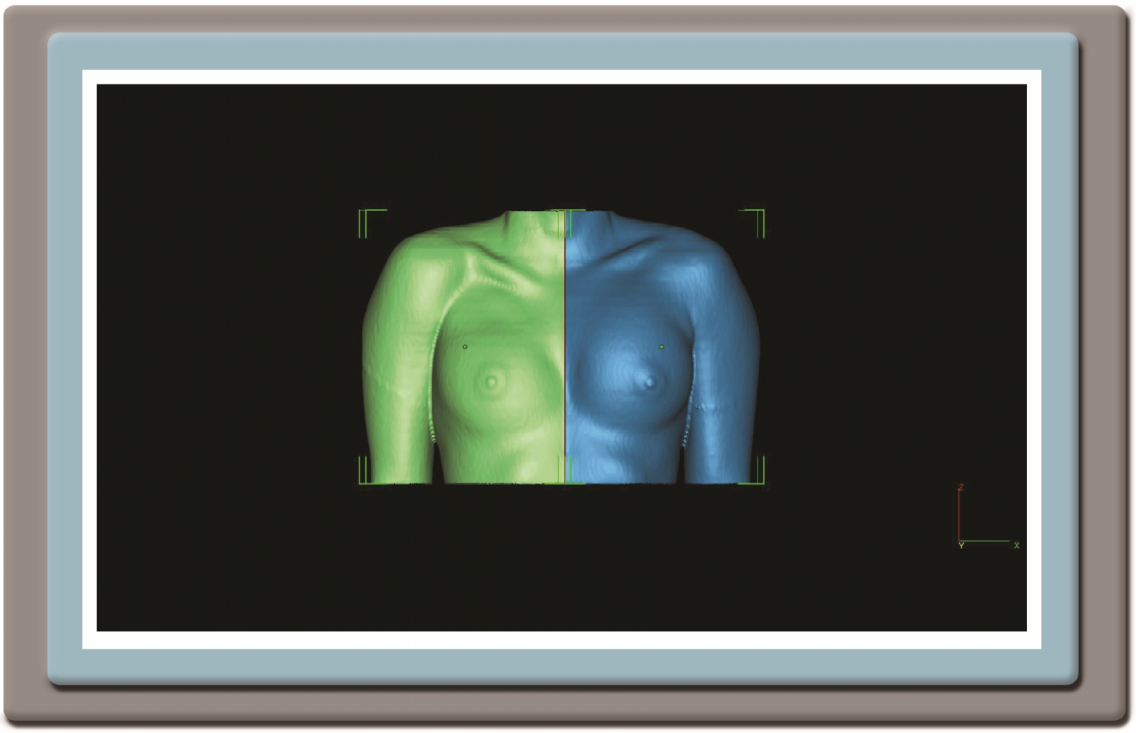

Figure 3.15 Model of the bisected thorax showing the healthy half (blue) and the affected half (green) in different colours.

10. The healthy half of the bisected thorax was then mirrored along the *YZ planes* onto the affected half using the *Mirror tool*.

11. After the healthy half of the thorax was mirrored onto the affected half, the 3D digital geometry model was viewed from all angles to ascertain how well the halves were aligned with one another. The alignment was inspected visually to determine at which places the alignment was acceptable and at which places the aligned was poor (Figure 3.16). Steps 7 to 11 were repeated until an acceptable mirror was produced with as few as possible places that were poorly aligned.

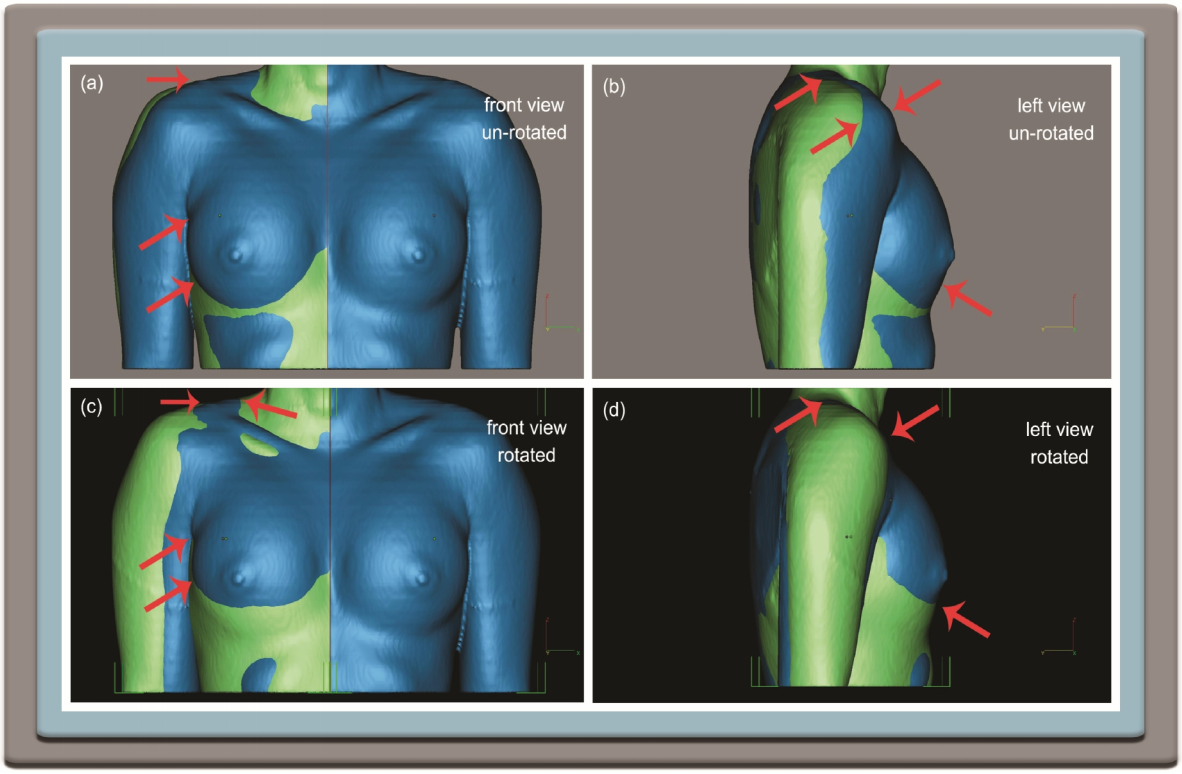

Figure 3.16 **Examples of alignment after mirroring the healthy half of the thorax onto the affected half of the thorax.** (a) Arrows indicate places of poor alignment of an un-rotated thorax in a *Front view*, (b) Arrows indicate places of poor alignment of an un-rotated thorax in a *Left side view*, (c) Arrows indicate places of acceptable alignment of a rotated thorax in a *Front view*, and (d) Arrows indicate places of acceptable alignment of a rotated thorax in a *Left side view*.

Boolean operations

Boolean operations were first introduced by George Boole in 1847 in his book, *The Mathematical Analysis of Logic* (Bornet 2013; Gopinath et al. 2015). Boolean operations are used in geometric modelling for the purpose of creating new geometries from solid objects by manipulating a solid object using one of four possible tools (Feito et al. 2013; Mei & Tipper 2013; Douze et al. 2015). These tools are (Mei 2014; Jirásek et al. 2015): *union* which unites two or more objects resulting in a single object; *intersect* which intersects two or more objects resulting in an overlapping object outcome; *difference* which subtracts one object from another; and *symmetric difference* which unifies two or more objects that result in an object outcome which excludes the overlapping intersecting

parts (Figure 3.17). In this study the *difference* Boolean operation was used to subtract the affected half from the healthy half of the thorax of the two Poland's syndrome patients. This resulted in 3D digital geometry models of soft tissue, which were then cut to produce the *final 3D-DG* models.

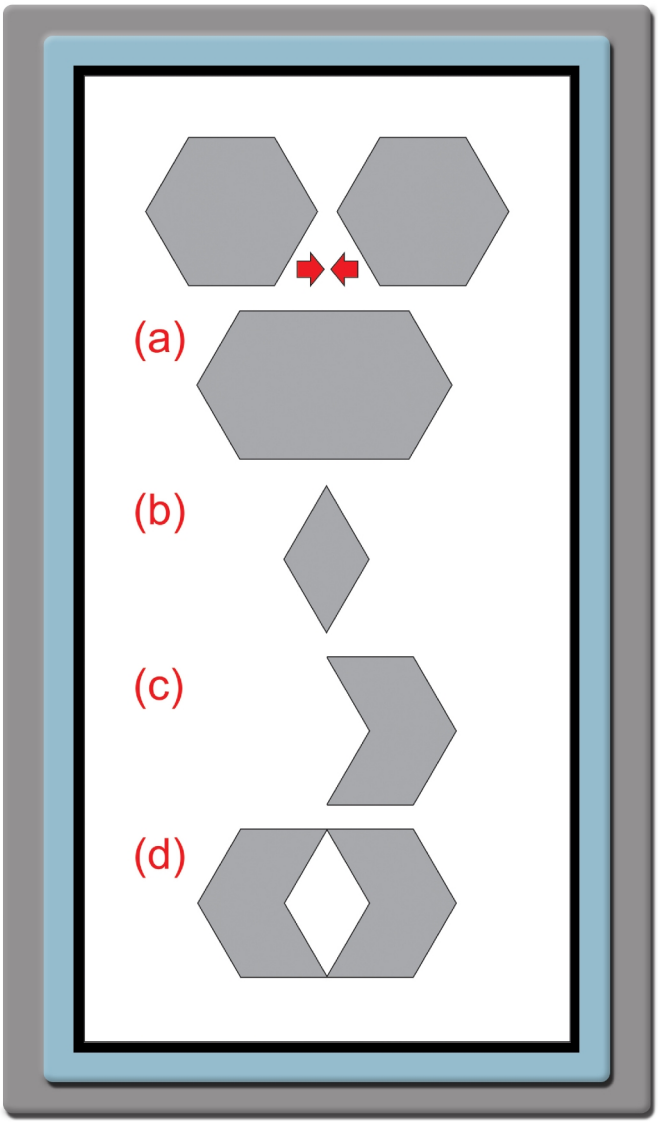

Figure 3.17 **Boolean tool operations.** (a) union, (b) intersect, (c) difference, and (d) symmetric difference.

Boolean operations were performed in the following manner:

12. The *difference* Boolean operation, referred to as *Subtract* in Magics, was used to subtract the affected half of the thorax from the healthy half of the thorax. After subtraction this *difference* part was named (Figure 3.18).

13. Before this *difference* part could be processed further, all excess parts were deleted using the *Cut\Punch tool*, which removes the larger excess parts. Thereafter, the small excess parts, still attached to the part of interest, were removed with the *Mark Surface tool*.

14. Finally, the *difference* part was inspected to detect the presence of holes, which were then filled by either using *Automatic Hole Filling* or *Manual Hole Filling*. This shaped and filled part was now referred to as the *final 3D-DG* model in Magics, *Technique A*.

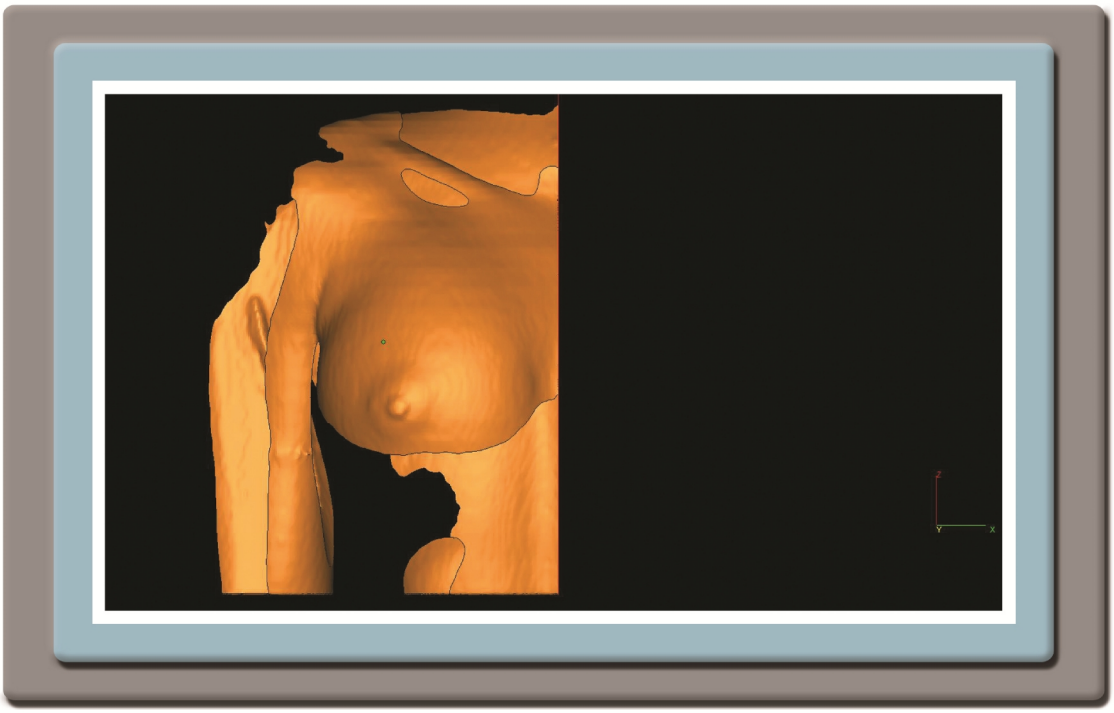

Figure 3.18 Result after the affected half of the thorax was subtracted from the healthy half.

3.6.2 *Technique B* using Magics

In *Technique B*, the *solid 3D-DG* model in STL file format of the isolated pectoralis muscle was manipulated to create a *final 3D-DG* model that can be used for the manufacturing process. In contrast to *Technique A*, this manipulation involved creating a mirror image of the isolated healthy pectoralis muscle.

Digital data manipulation and design phase using Technique B was performed in the following manner:

1. Activation of the coordinate planes was achieved in a similar manner to that of *Technique A*, except that only the *X plane* was activated.

2. A mirror image of the isolated healthy pectoralis muscle was created around the *X plane* in a similar manner as was accomplished in *Technique A* (Figure 3.19).

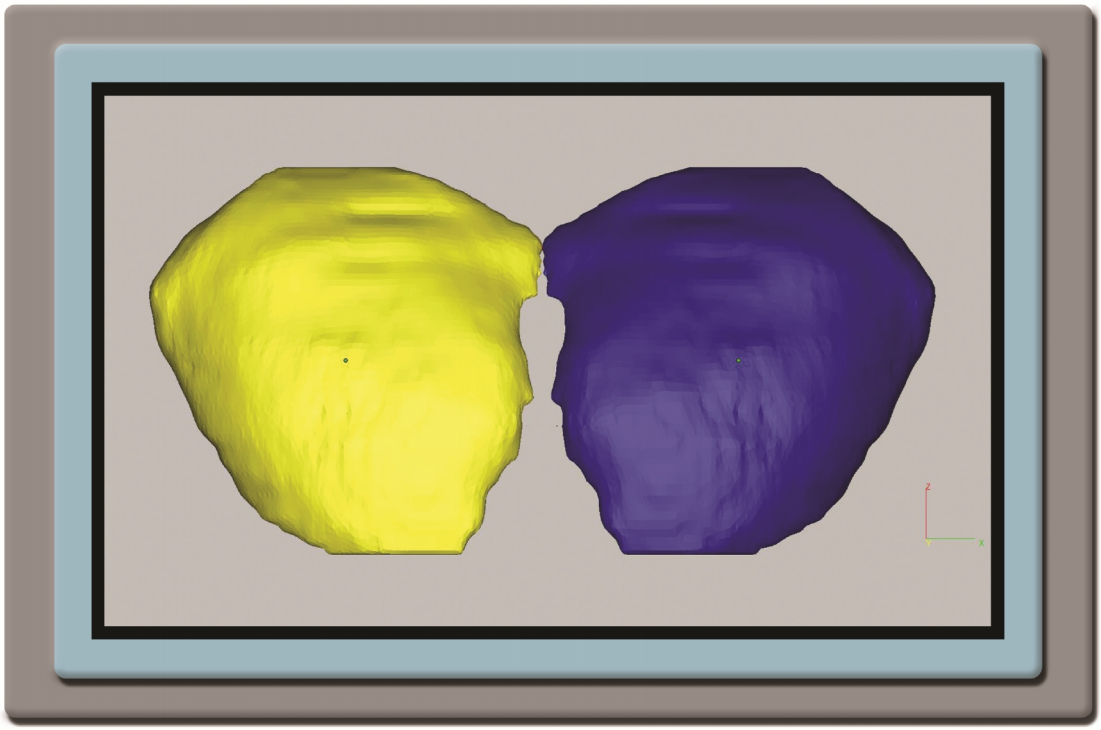

Figure 3.19 ***Technique B*** **showing the isolated healthy pectoralis muscle and its mirror image in yellow.**

3.6.3 *Technique A* using Freeform® Modeling™

Similar to the Magics, *Techniques A* and *B* were also applied in the digital data manipulation and design phase using the Freeform® Modeling™ CAD software program. However, the interface of Freeform® Modeling™ differs extensively from that of Magics bringing about completely different tools sets, particularly 3D CAD sculpting and modelling tools that are not available in Magics.

Technique A follows the same broad steps as were described for *Technique A* in Magics, namely the *activation of the coordinate planes*, *bisection and mirroring of the healthy half onto the affected half* of the thorax and *Boolean operations* (Figure 3.20).

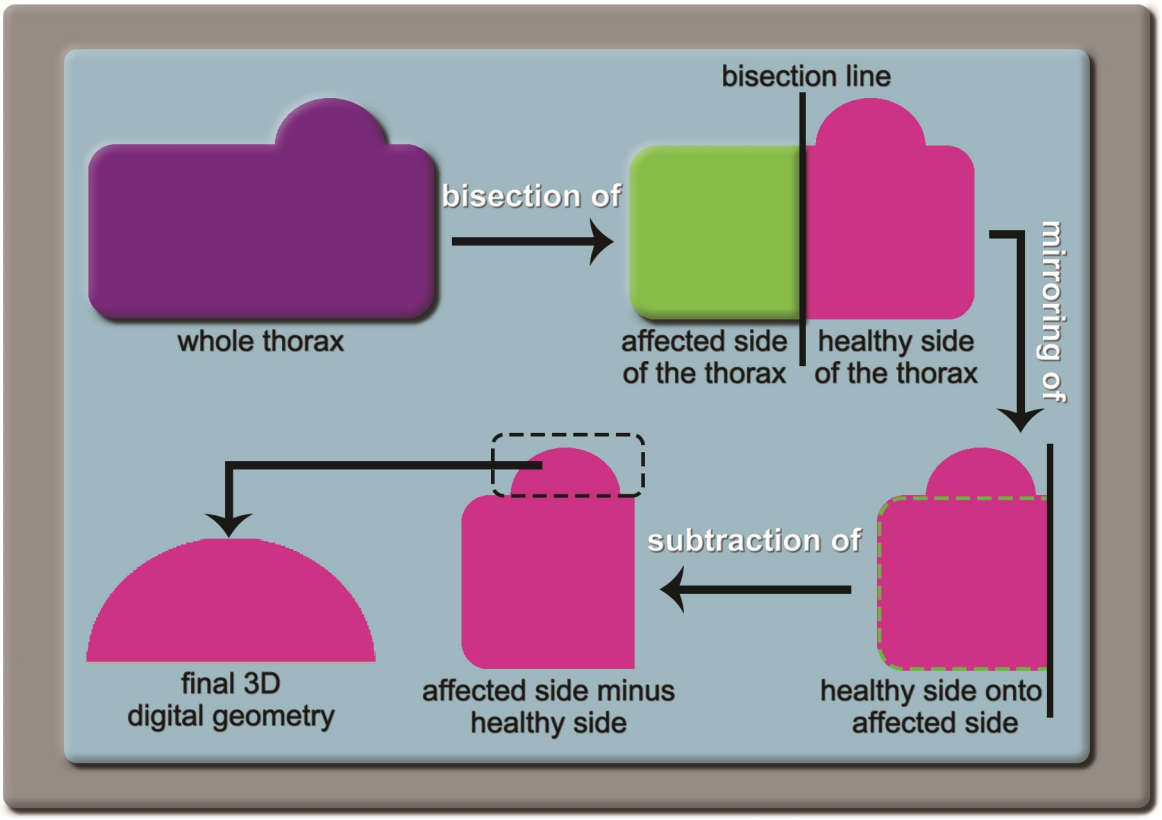

Figure 3.20 Workflow using Freeform® Modeling™ *Technique A* to design a *final 3D digital geometry* model using the whole thorax.

Digital data manipulation and design phase using Technique A was performed in the following manner:

Activation of the coordinate planes

1. Before any data manipulation could be implemented, the *solid 3D-DG* model in STL file format of the whole thorax was imported into Freeform® Modeling™ using the *Import Model function*. The *Buck setting* of this function was specifically selected to protect the data against inadvertent carving; therefore *Import As* was set to *Buck*.

2. After importing the *solid 3D-DG* model, a number of functions were activated prior to activation of the coordinate planes:

    a) The *Object List* dialog box was activated, which allows the user to access the different layers and different planes.

    b) An additional view window was then selected from the *Side Views* list found in the *View Menu* in order to view the placement of the *stylus arm* of the haptic device in the 3D virtual space.

    c) In the *Object List* dialog box the *buck model* was duplicated with the *Duplicate function* to create a new *clay model* (equivalent to the 'part' mentioned in Magics), which allows the user to work on an active *clay model*.

3. The *Coordinate System* used in this project was then set to the *World* coordinate system.

4. Thereafter, a number of working planes were activated one-by-one via the *Create Plane tool* found in the *Planes Palette toolbox*.

5. Each plane was then individually orientated and positioned in relationship with the *clay model*. The *Edit Plane Dynabar toolbar* was thus activated and the angle of each plane adjusted, by selecting the *Switch Orientation* option.

6. Finally, the *clay model* was rotated in the *Top view* and brought into alignment with the *Y plane* so that both shoulders were aligned with the plane (Figure 3.21). This was achieved by activating the *Reposition Piece tool* found in the *Select/Move Clay Palette toolbox*.

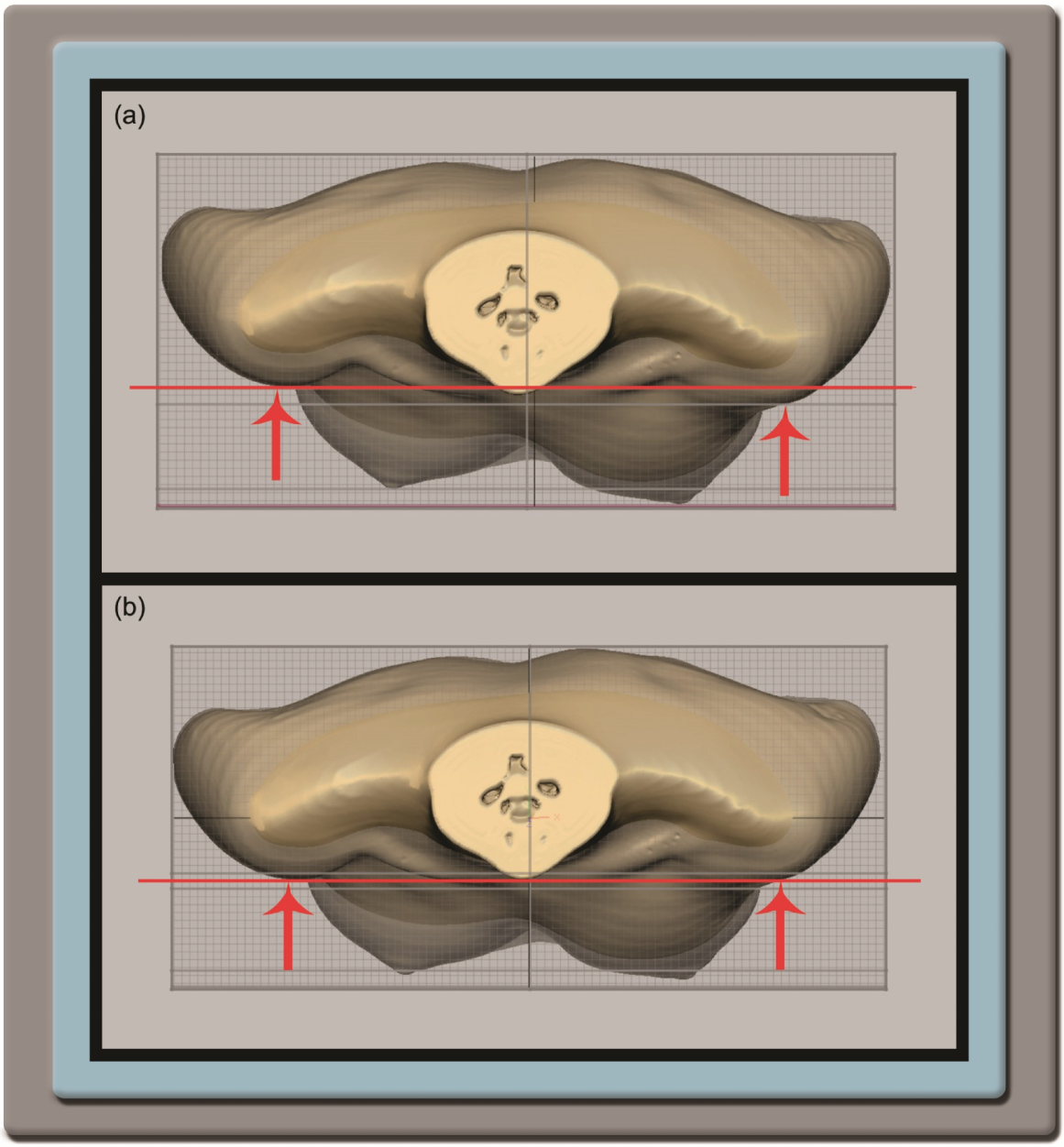

Figure 3.21 **Alignment of the thorax using rotation.** (a) Arrows indicate places of poor alignment at the shoulders of the thorax in *Top view*, and (b) Arrows indicate places of acceptable alignment at the shoulders of the thorax after rotation in *Top view*.

Bisection and mirroring of the healthy half of the thorax onto the affected half

7. After the rotation of the thorax was completed, a number of slicing actions were applied to the thorax to achieve a 3D digital geometry model that can be subjected to Boolean operations. The first slicing action involved the slicing of the thorax along the *Y plane* to separate the frontal section (which

includes the pectoralis muscle) of the thorax from the back section. This slicing action was applied to reduce the data volume. This was achieved by selecting the *Separate tool*. Thereafter, the *stylus arm* of the haptic device was used to separate the frontal section from the rest of the whole thorax using the *Select Separate Piece function* using the *Y plane* (Figure 3.22).

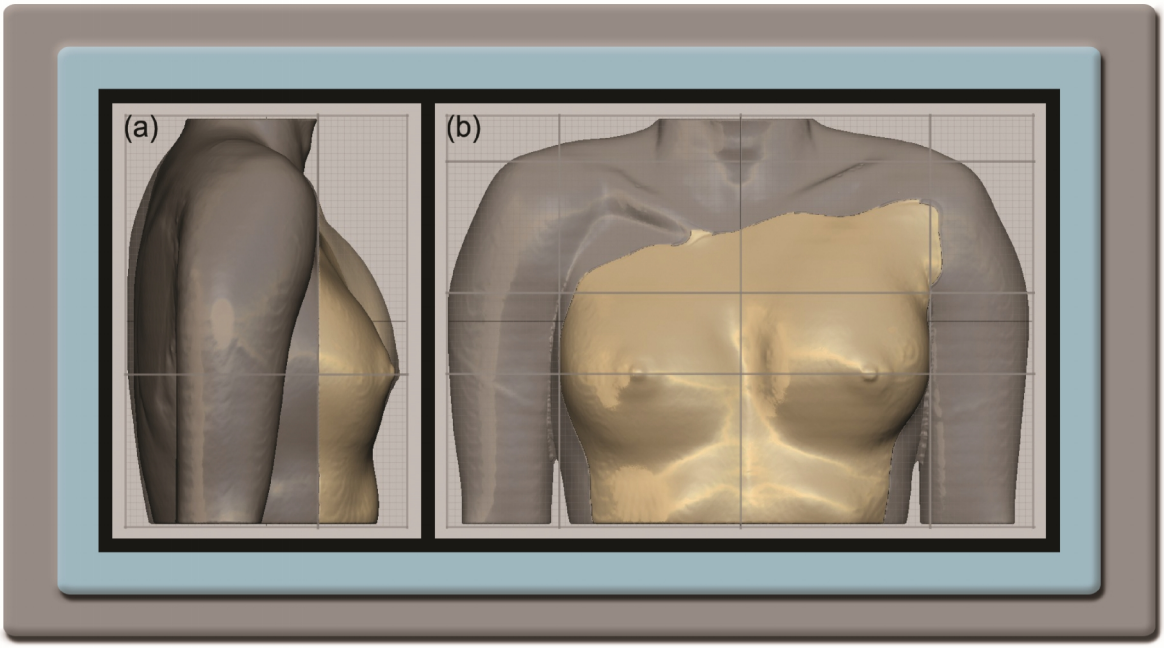

Figure 3.22 **Separated frontal section from the back section of the thorax.** (a) *Left side view* showing the frontal section in yellow (clay colour) and back section in grey, and (b) *Front view* showing the showing the frontal section in yellow (clay colour) and back section in grey.

8. Before the next slicing action could be applied, the *X plane* was inspected and if it was out of alignment it was moved to the central position in the *Front View*. The next slicing action was then applied using the *X plane* to separate the healthy half of the frontal section of the thorax from the affected half of the frontal section. The *Separate tool* and the *Select Separate Piece function* were used to achieve this slicing action.

9. The healthy half of the frontal section of the thorax was then mirrored onto the affected half of the frontal section of the thorax. Mirroring was performed by selecting the *Mirror Clay tool* and mirroring along the *X plane* that was used for the slicing action in step 8.

10. The alignment of the two halves was then visually inspected by viewing the 3D digital geometry model from all angles. This inspection was performed to ascertain if an acceptable mirror alignment of the healthy half of the frontal section onto the affected half was achieved (Figure 3.23). Steps 8 and 9 were repeated until an acceptable alignment was achieved.

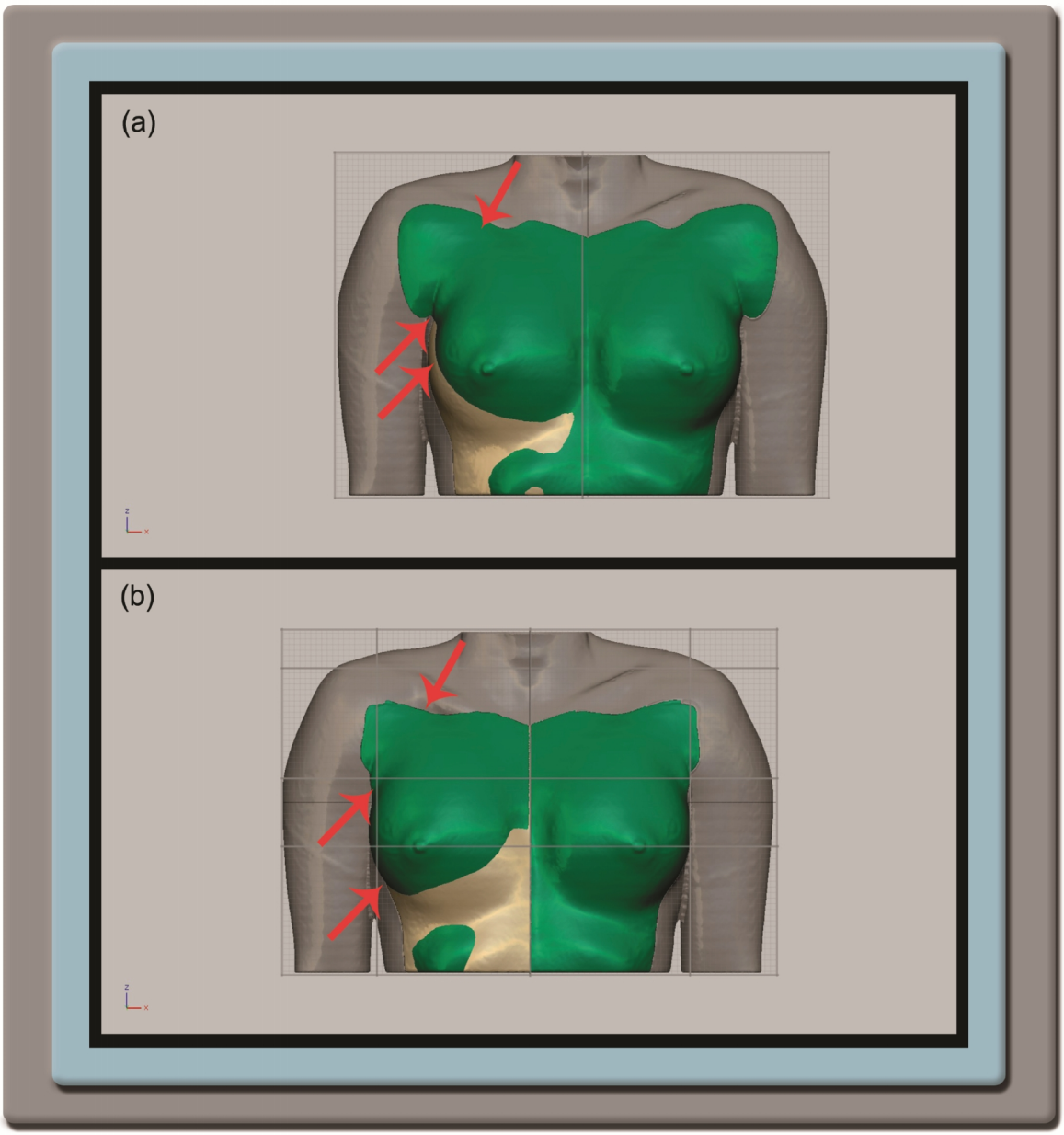

Figure 3.23 **Alignment of the mirrored half of the frontal section onto the affected half.** (a) Arrows indicate places of poor alignment of an un-rotated thorax in a *Front view*, and (b) Arrows indicate places of acceptable alignment of a rotated thorax in a *Front view*.

11. Finally, the mirrored half of the frontal section was separated from the healthy half of the frontal section by repeating the process followed in step 7. For this separation the same *X plane* that was used in step 7 was used for the separation of the two halves.

Boolean Operations

12. In Freeform® Modeling™ the *difference* Boolean operation is referred to as *Remove Pieces*. This operation was applied to the affected side of the frontal section of the thorax, because the mirrored healthy half lies on top of the affected section of the thorax (Figure 3.23b), which has to be removed. To achieve the removal, the *Remove Pieces* option was used to subtract the affected side of the frontal section from the mirrored healthy side (Figure 3.24). This results in producing a 3D digital geometry containing the anatomical section that was originally absent from the deformed side of the thorax in the correct mirrored orientation.

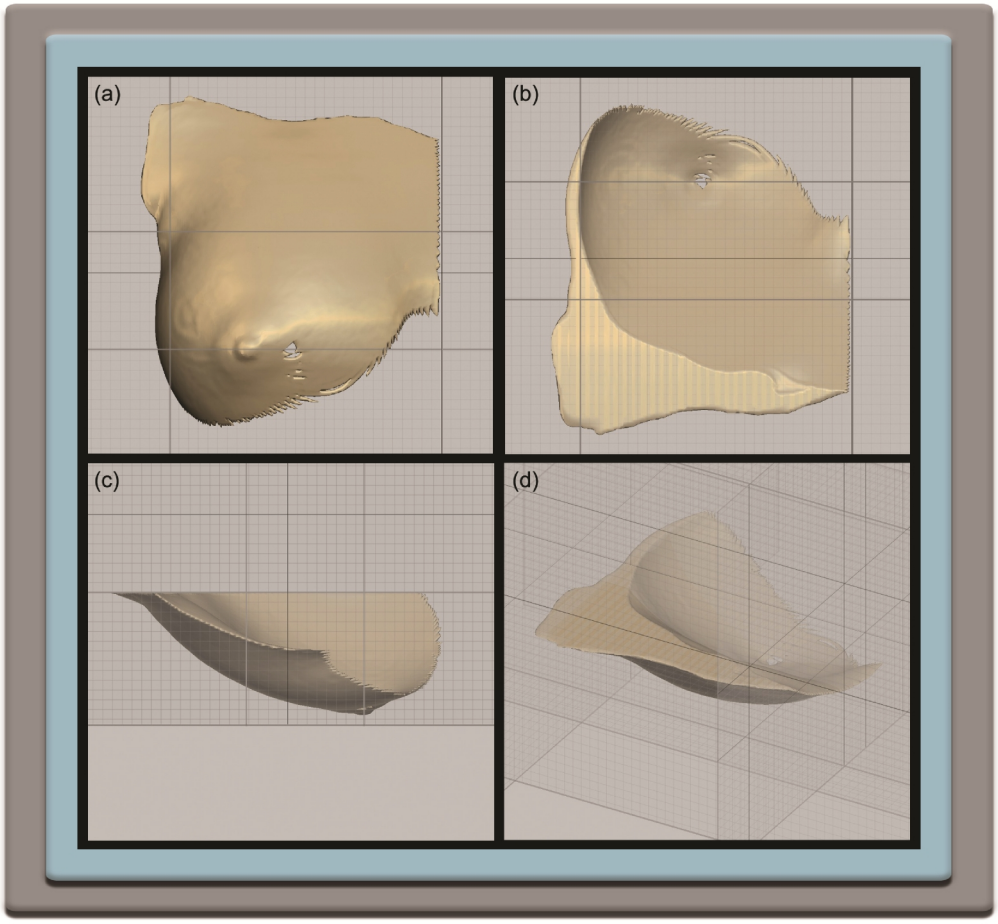

Figure 3.24 ***Difference* piece of the Boolean subtraction operation.** (a) *Front view*, (b) *Bottom view*, (c) *Right side view*, and (d) *Bottom angle view*.

13. Digital data manipulation and design involved the sculpting of the *difference* Boolean piece for the development of a *final 3D-DG* model. This was achieved using the *Smooth tool* and the *Tug tool* until the final *clay model* was blended into the available space in the affected half (Figure 3.25).

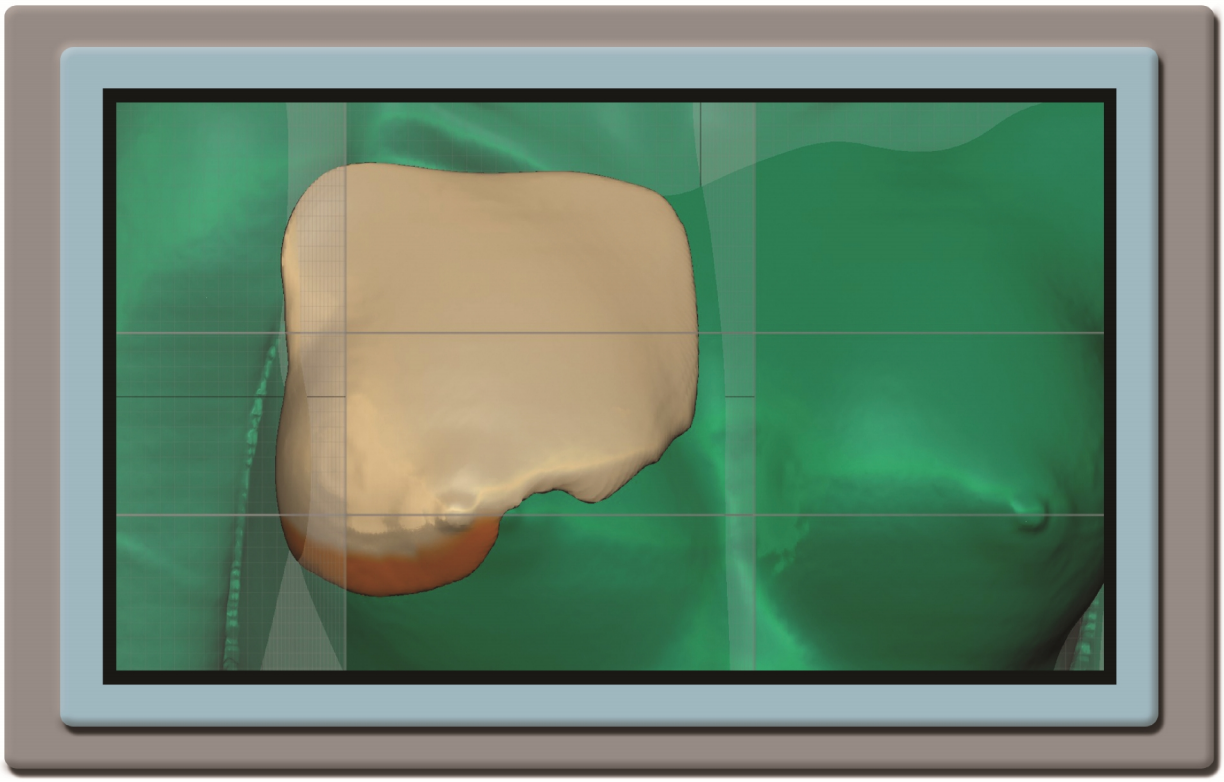

Figure 3.25 ***Smooth tool*** **used to smooth the Boolean piece in the area indicated in orange.**

3.6.4 *Technique B* using Freeform® Modeling™

Similarly to *Technique B* using Magics, the isolated pectoralis muscle in STL file format was manipulated to create a *final 3D-DG* model. However, for Freeform® Modeling™ *Technique B*, the whole thorax was also imported to act as a reference piece. The whole thorax provided a background matrix displaying the affected region into which the pectoralis muscle would be projected and fitted.

Digital data manipulation and design phase using Technique B was performed in the following manner:

1. After importing the whole thorax and pectoralis muscle in STL file format, steps 1 - 5 of *Technique A* were repeated to activate the coordinate planes.

2. Thereafter, a number of curves were drawn on the healthy half of the thorax using *Boundary Curves* by selecting the *Draw Curve tool* (Figure 3.26).

3. The *Fit Curve tool* was then selected to move the curve points of each curve so that the curve snapped back to the surface of the active *clay model* of the whole thorax.

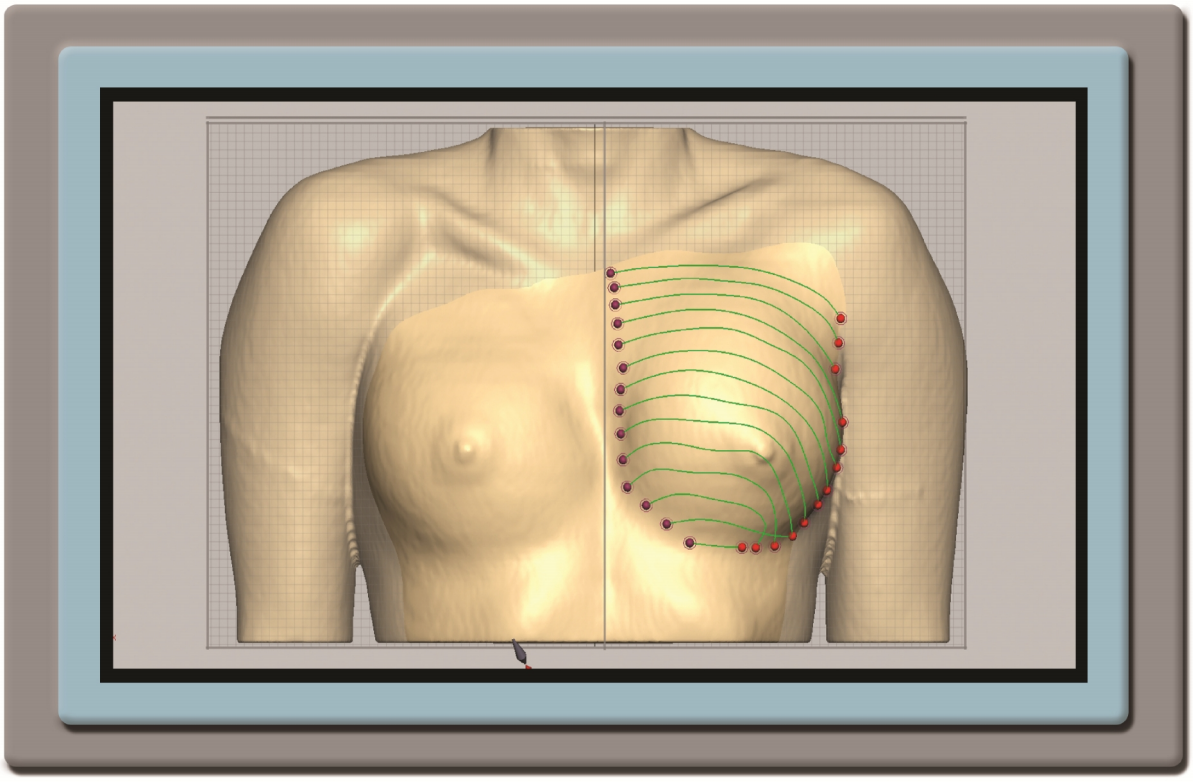

Figure 3.26 *Boundary Curves* on the healthy side of the thorax.

4. The *Boundary Curves* on the healthy half of the thorax were then mirrored onto affected half using the *X plane* prior to the importing of the pectoralis muscle (Figure 3.27). Each curve was mirrored individually by selecting the *Mirror Curve tool*.

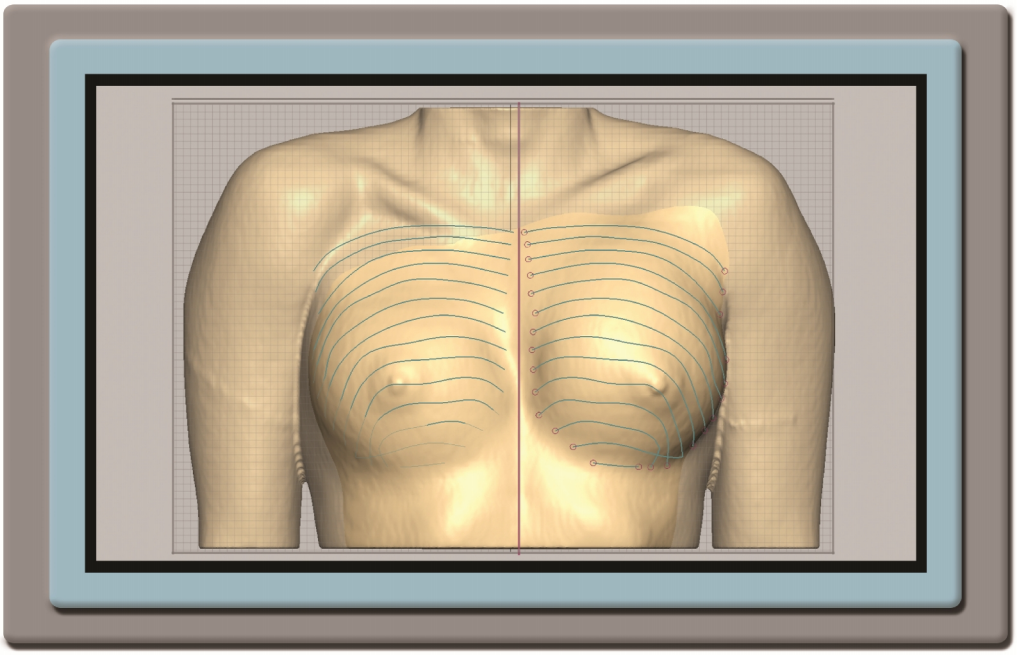

Figure 3.27 Mirrored *Boundary Curves* on the affected side of the thorax.

5. The pectoralis muscle in STL format was then imported using the activated functions described in step 1 (Figure 3.28). Thereafter, the pectoralis muscle was rotated on the *Z plane* to match the rotation position of the whole thorax.

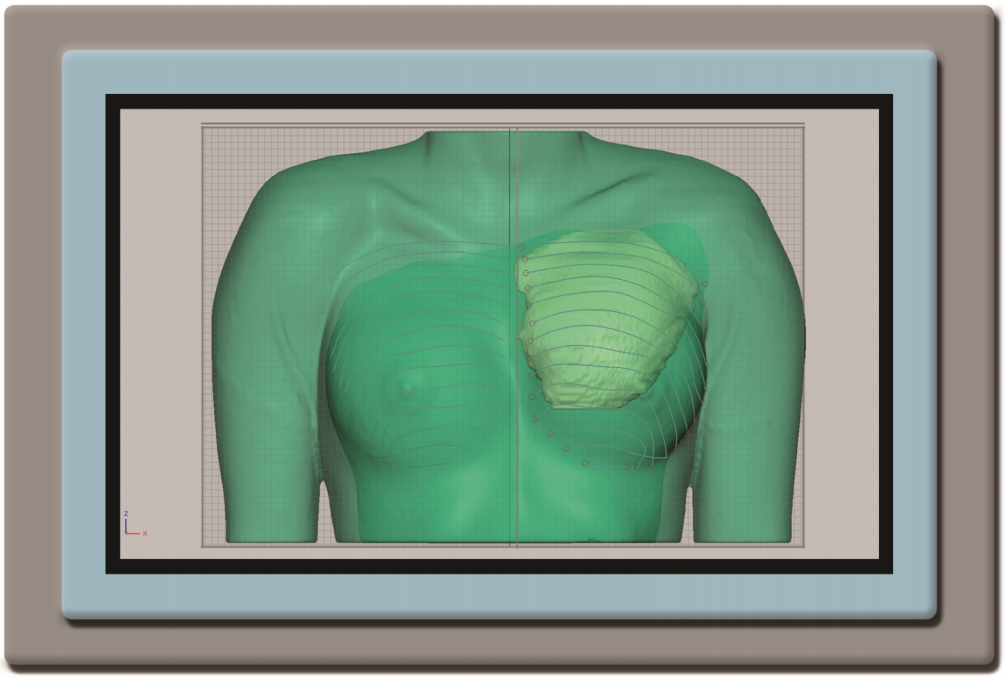

Figure 3.28 Imported and rotated pectoralis muscle.

6. The pectoralis muscle was then mirrored onto the affected half using the activated *X plane* (Figure 3.29).

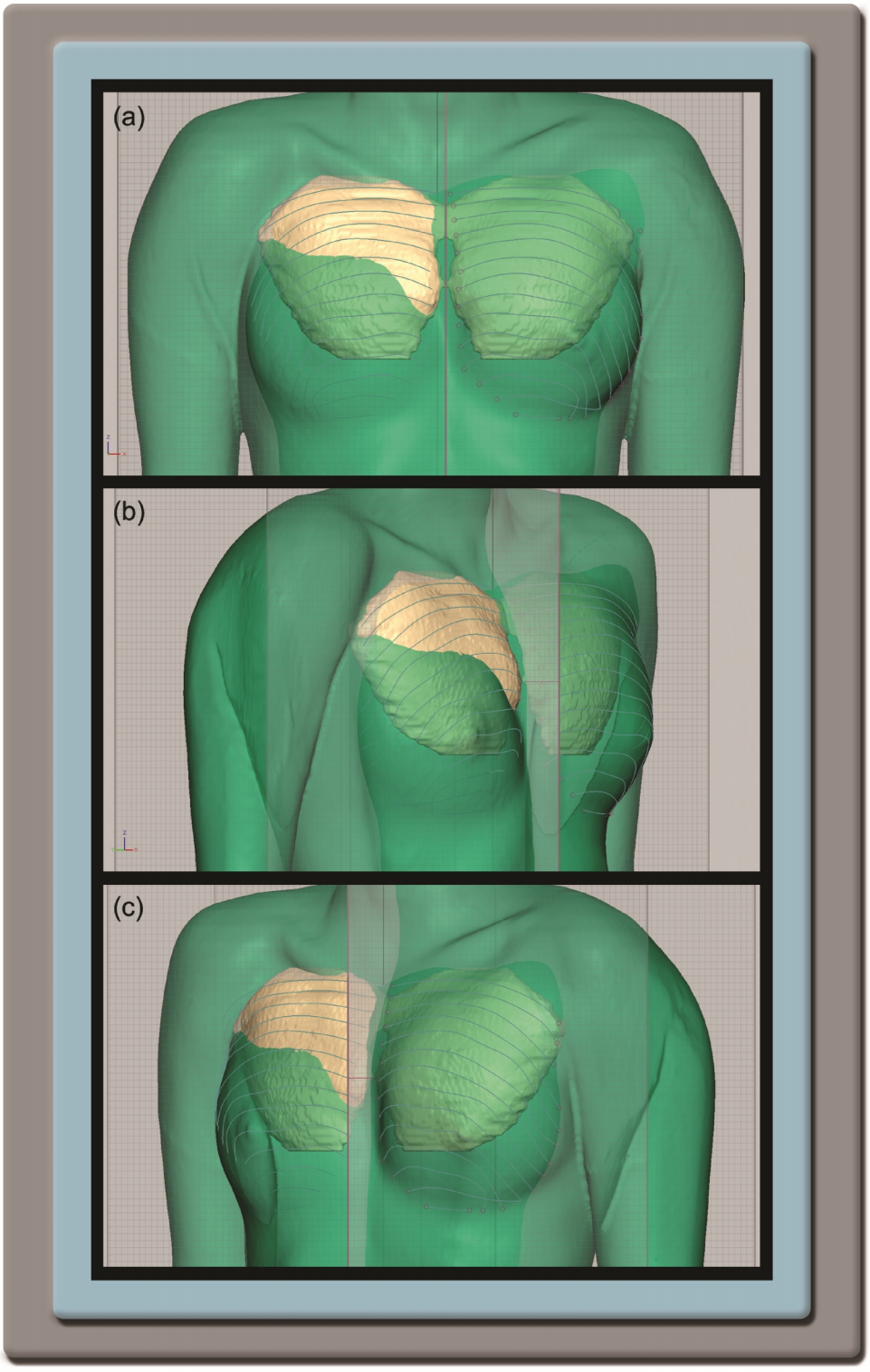

Figure 3.29 Model of the pectoralis muscle mirror indicated in yellow. (a) *Front view*, (b) *Left angle view*, and (c) *Right angle view*.

7. Finally, the 3D digital geometry model of the pectoralis muscle was manipulated using the *Tug tool* to fill the space underneath the boundary curves in the affected half (Figure 3.30).

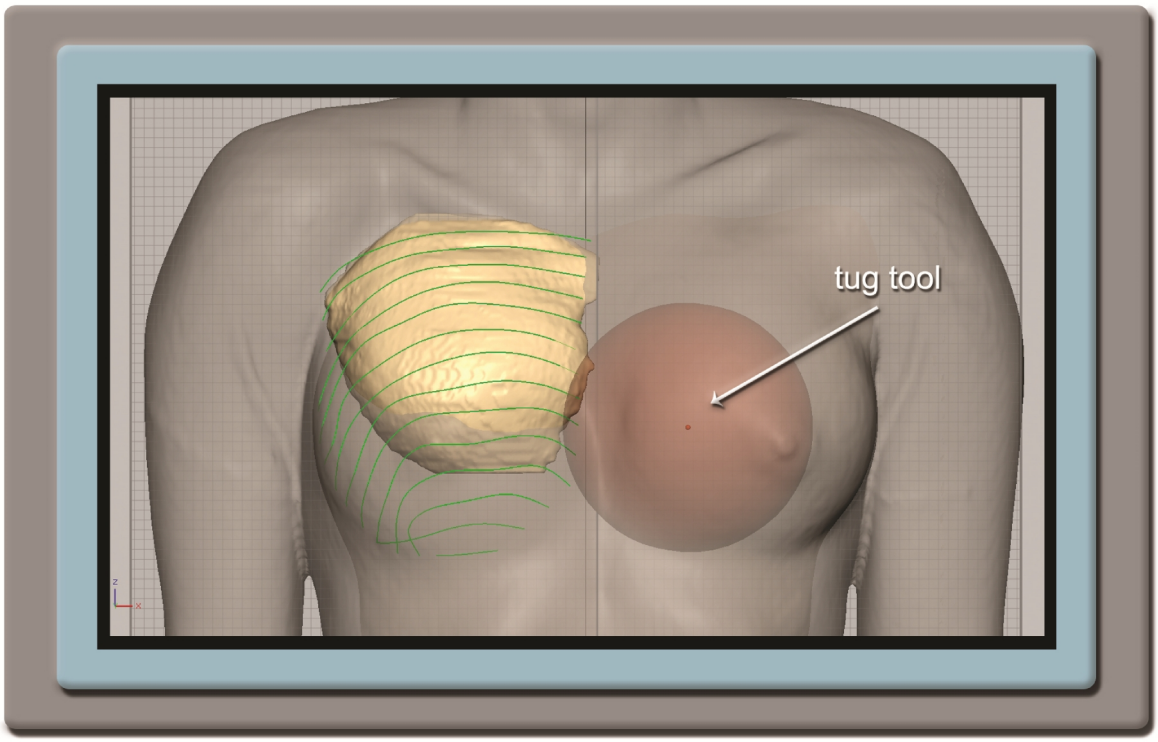

Figure 3.30 ***Tug tool*** **used to manipulate the pectoralis muscle into place underneath the boundary curves shown in red.**

3.7 Methods of Phase 4: Comparative analysis of the different techniques

Although Phases 1 to 3 were the main focus of this study, it was deemed appropriate to compare the different techniques used to produce the *final 3D-DG* models, so as to obtain some understanding of how these digital models compared with a test model of the original data. Three different comparisons were undertaken. These comprised of a deviation analysis using the software program Geomagic® Control™, an implant mass property analysis using Freeform® Modeling™, and a body conformation analysis also using Freeform® Modeling™. Prior to the various comparative analyses,

digital test models had to be produced using Freeform® Modeling™ against which the *final 3D-DG* models could be compared to.

3.7.1 Production of a digital test model

Digital test models were produced in the following manner (Figure 3.31):

1. Firstly, the original STL file of the thorax of each patient, prior to manipulation in Phase 3, was unified separately, with the four *final 3D-DG* models of the pectoralis muscles in the program in which they were designed. These unified digital products were referred to as *assembled models* resulting in four temporary models for each patient; two originating from Magics (*Techniques A* and *B*) and two from Freeform® Modeling™ (*Techniques A* and *B*). These *assembled models* were then used to produce the *digital test models* in Magics.

2. Before the *digital test models* could be produced, unwanted internal structures (noise) had to be removed from the *assembled models*.

3. The *digital test models* were finally produced by mirroring the *assembled models*, after noise removal, to produce a mirror image of the healthy side in the same orientation as the affected side. These *digital test models* were used in the various comparative analyses.

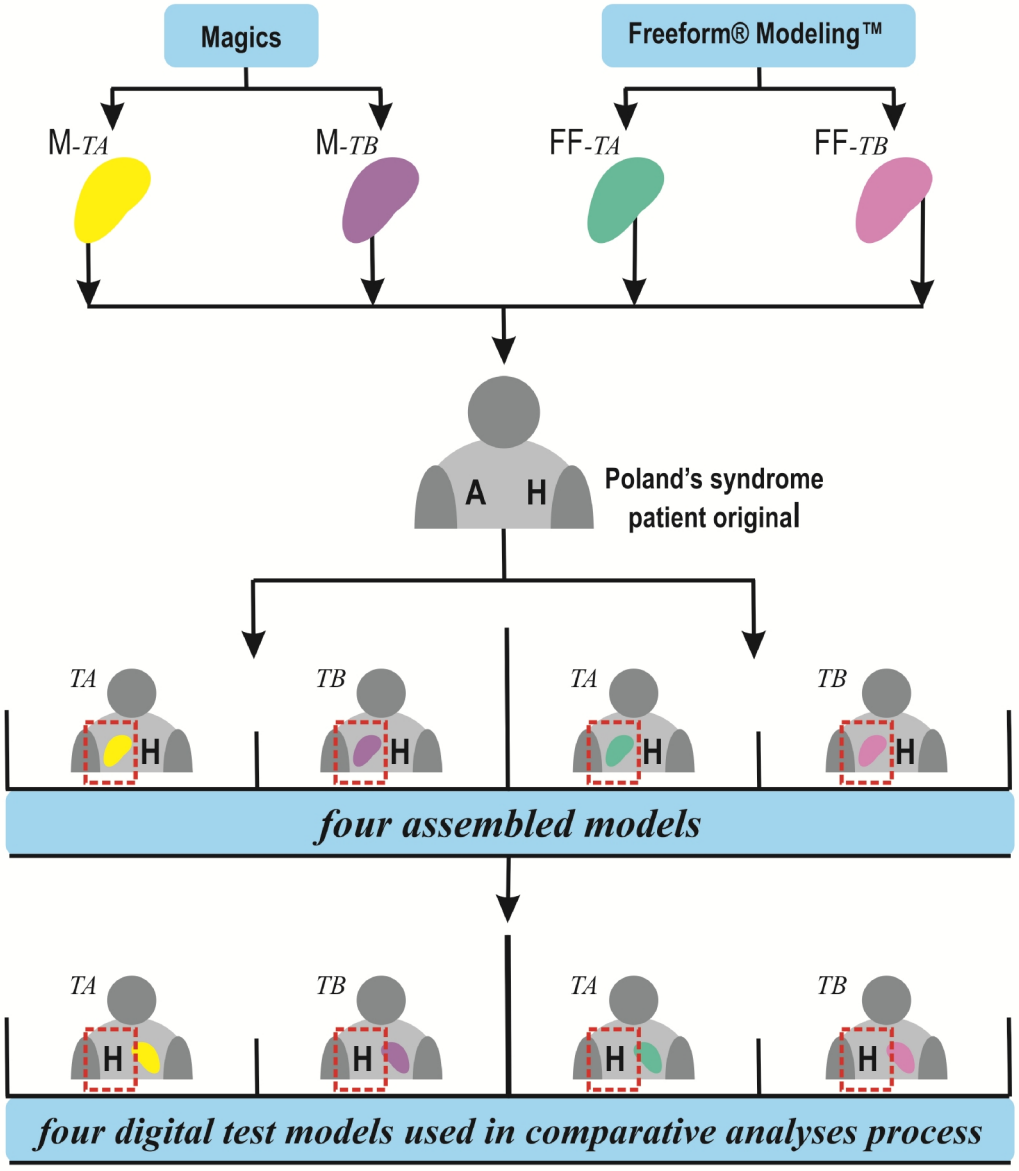

* M = Magics; FF = Freeform® Modeling™; *TA* = *Technique A*; *TB* = *Technique B*; A = Affected half; H = Healthy half.

Figure 3.31 Flow diagram depicting the production of *digital test models.*

3.7.2 Noise removal from the assembled models

The *final 3D-DG* models produced in Phase 3 using Magics and Freeform® Modeling™ contain data of other internal organs besides the regions of interest. These internal organs are for example, lung, bone, rib cage and heart. They were also transferred to the *assembled models* produced in Magics and Freeform® Modeling™ during the production of the *digital test models*. Because these anatomical structures did not influence the design of the *final 3D-DG* models, they were not removed

during Phases 2 and 3. These anatomical structures (also referred to as noise), do however, have an influence on the comparative analyses and therefore required removal.

There are two possibilities to remove noise. Firstly, noise may be removed from the original scanned digital imaging data sets of the successive 2D images used in Phase 2, following a lengthy and laborious pixel-by-pixel removal through Mimics®. Secondly, noise may be removed directly from the *assembled models* using Magics. This removal process is much less time consuming and less laborious than the process employing Mimics®, because it does not require pixel-by-pixel removal, but rather the removal of internal organs as a whole. Therefore, in this study, Magics was used to remove the noise from all the *assembled models* prior to mirroring.

Noise was removed from the assembled models in the following manner:

1. The *Import Part function* was used to import the different *assembled models* individually into the work area of Magics.

2. The *Z plane* was then activated in the *Multi-Section* tab and the *Clip function* selected to view an *assembled model* in slices from top to bottom. This indicated that internal organs were still present and therefore needed to be removed (Figures 3.32a, b).

3. For the successful removal of noise from an *assembled model*, the top and bottom edge of the thorax must be opened so that the internal organs can be seen. To attain the opening of the edges, the *assembled model* was sliced to remove a few millimetres off the top and bottom edges of the model to create raw cutting edges. This was achieved by moving the activated *Z plane* close to top and bottom edges of the *assembled model* using the slider found in the *Multi-Section* tab. Thereafter, the *Cut\Punch tool* was used to slice off a few millimetres from the top and bottom edges of the *assembled model*.

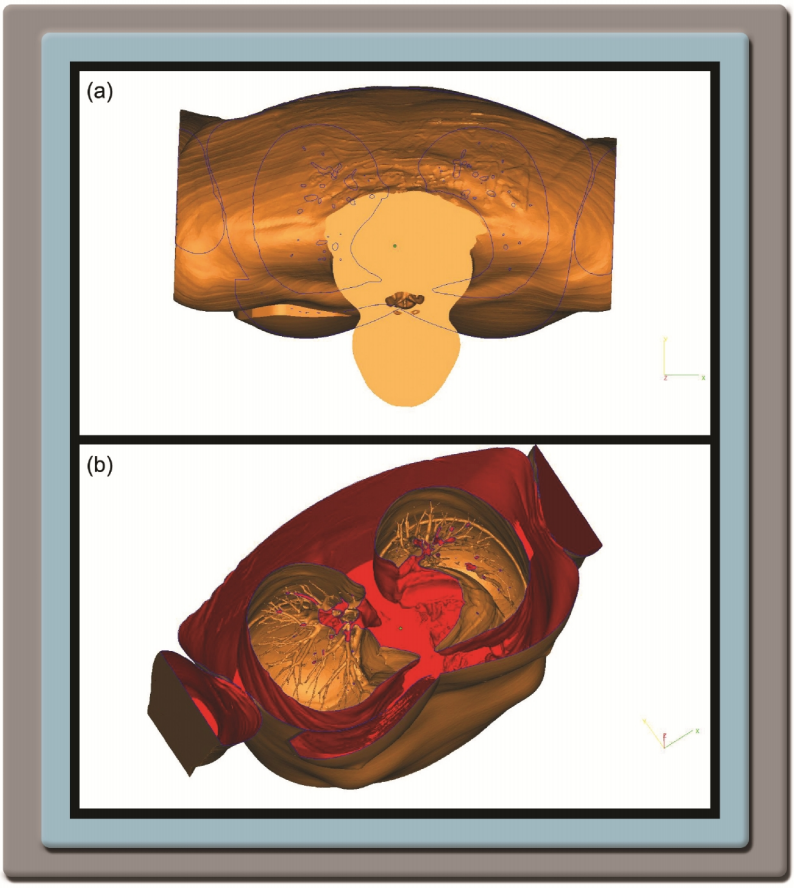

Figure 3.32 **Internal organs of the *assembled model*.** (a) *Top view* showing the internal organs outlined in blue, and (b) *Angled top view* showing the internal organs.

4. After applying the *Cut\Punch tool*, the *assembled model* was opened by activating the *Mark Plane tool* and deleting the raw cutting edges at the top and bottom of the model (Figure 3.33).

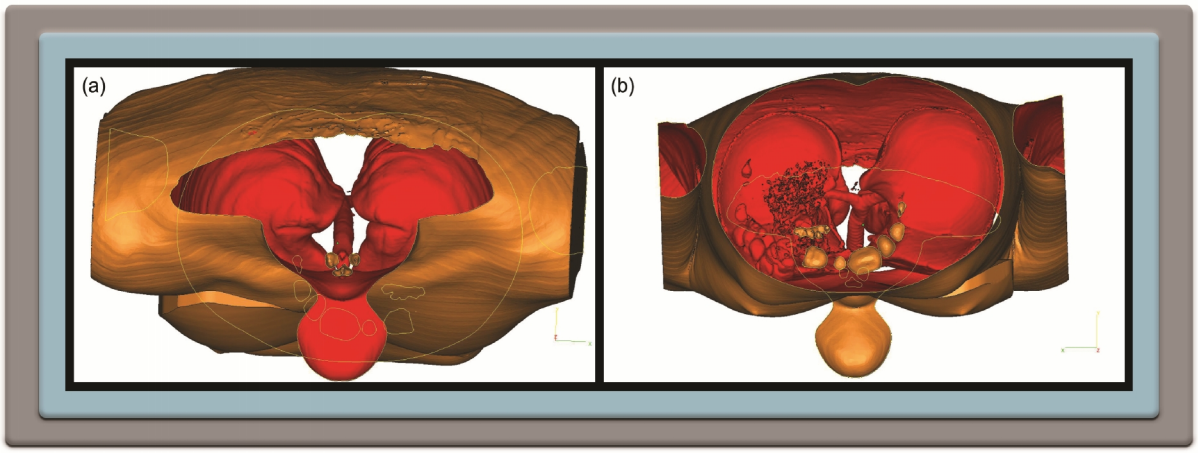

Figure 3.33 **Open *assembled model*.** (a) *Top view* showing the open edge at the top of the thorax, and (b) *Bottom view* showing the open bottom edge of the thorax.

5. After the outer structures of the *assembled model* was selected with the *Mark Shell tool* as shown in green in Figure 3.34a, the inverse of the *assembled model* showing the internal organs was activated by selecting the *Toggle Marked tool*. This inverse of the model was then deleted so that the empty outer structures of the *assembled model* remained (Figures 3.34b, c).

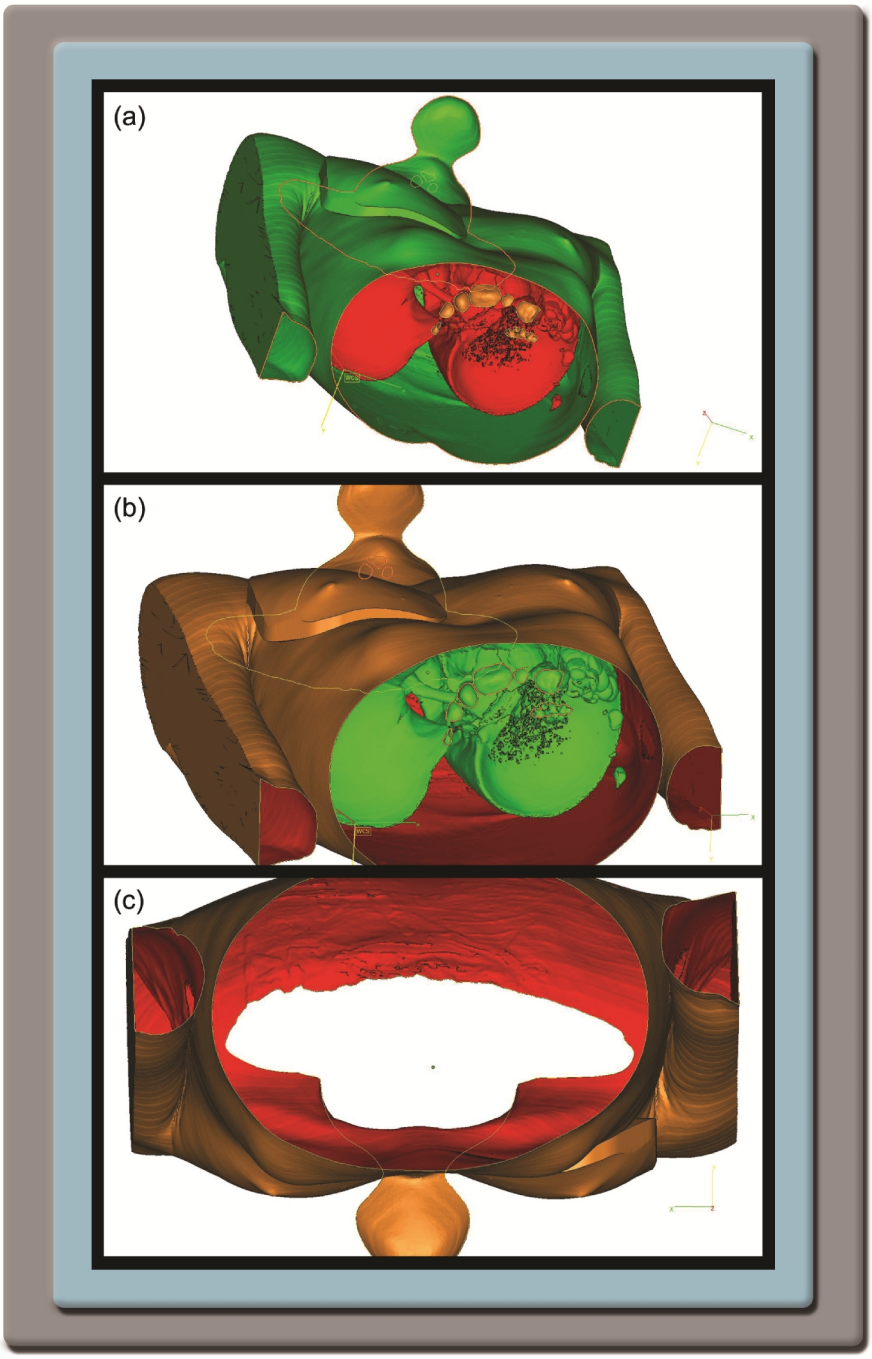

Figure 3.34 **Steps followed to remove noise from the *assembled model*.** (a) Selected outer structures of the *assembled model* indicated in green, (b) Selected internal organs (noise) indicated in green, and (c) Remaining empty outer structures of the *assembled model*.

6. After the removal of the internal organs, the *assembled model* had to be closed to produce a closed model. Firstly, the contour edges of the openings at the top and bottom of the *assembled model* had to be activated using the *Mark Edge tool*. Secondly, the *Fill Marked Contours function* was selected to close the openings at the top and bottom of the *assembled model*.

7. Finally, the *assembled model* was checked for residual noise, holes, bad edges, overlapping triangles and intersecting triangles. This was achieved by ticking all the boxes found in the *Part Fixing Info* tab and running a scan (Figure 3.35).

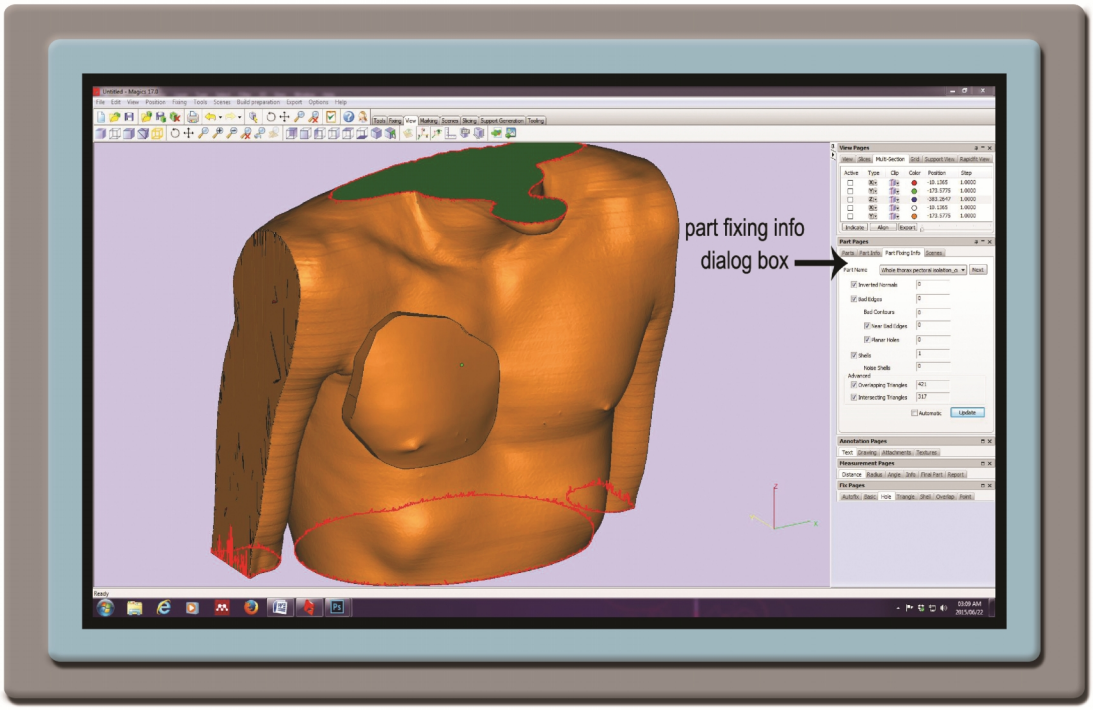

Figure 3.35 *Part Fixing Info* tab used to check for residual noise.

8. After updating the scan, the resulting fault report was then inspected and the irregularities corrected. This was achieved by selecting the *Fix Wizard tool* which allowed the user to check different fields/profiles for irregularities, for example, *Normals*, *Stitching*, *Noise Shells*, *Holes*, *Triangles*, *Overlaps*, and *Shells*. Thereafter, for each profile a *Diagnostics* report was generated indicating the faults in the *assembled model* and provided two options for fixing; the *Automatic Fixing function* and the *Manual function* (Figure 3.36).

9. Finally, the *assembled model,* from which the noise had been removed, was rechecked following step 7 and then exported as an *assembled model* in STL file format for the production of the separate *digital test models* used in the three comparative analyses.

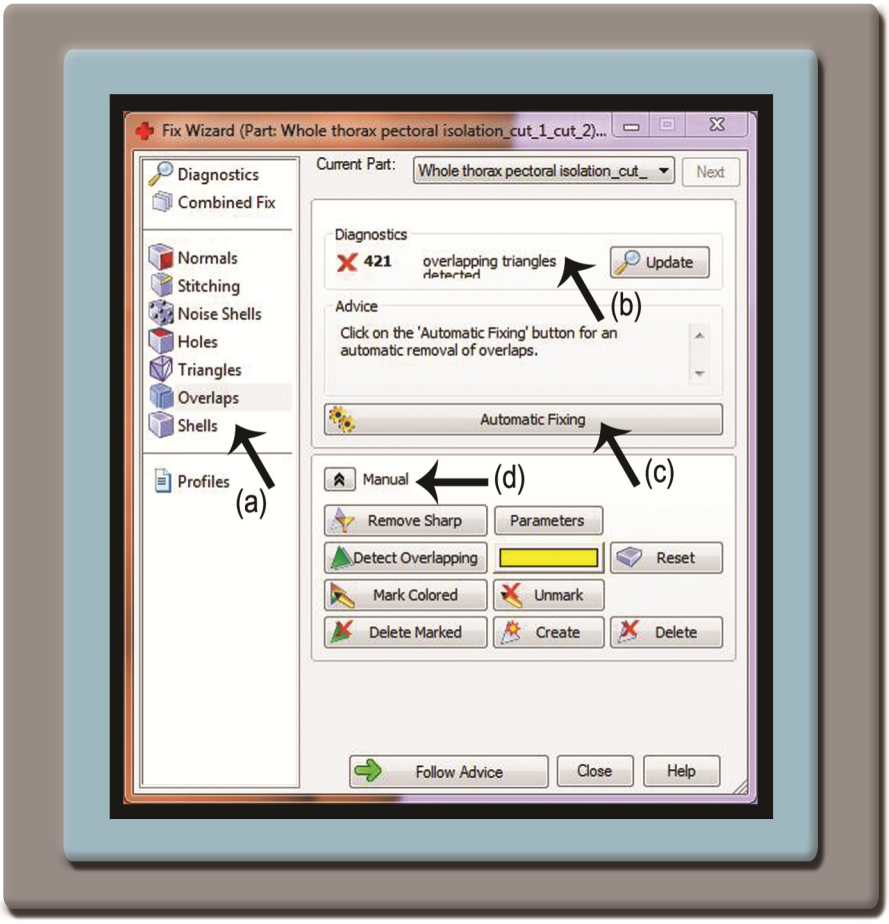

Figure 3.36 ***Fix Wizard*** **dialog box.** (a) Different profiles of the *assembled model* checked for irregularities, (b) Profile *Diagnostics* report, (c) *Automatic Fixing function*, and (d) *Manual function*.

3.7.3 Deviation analysis

A deviation analysis was performed between each of the four *final 3D-DG* models produced using the four techniques; *Techniques A* and *B* with Magics and *Techniques A* and *B* with Freeform® Modeling™; with their corresponding constructed *digital test models*. This was achieved with the 3D CAD inspection software program Geomagic® Control™. Geomagic® Control™ is a program which is

used for the systematic inspection of digital models created in various software programs. This application can manage many different types of entities ranging from scanned data to CAD data. It offers options to analyse deviations, as well as geometric dimensioning and tolerance using a variety of functions.

The deviation analysis involved comparing each of the *final 3D-DG* models against its corresponding *digital test model* to obtain data points that fell within a defined nominated tolerance interval, as well as data points that fell beyond this interval. For this study, the nominated tolerance interval was set at ≥-5 mm and ≤+5 mm. Two regions beyond the nominated interval were also defined. The critical plus interval showed data points where the *final 3D-DG* models were larger than the *digital test model*, while the critical minus interval showed data points where the *final 3D-DG* models were smaller than the *digital test models*. The critical plus interval was defined as the interval from >5 mm to ≤50 mm, while critical minus interval was defined as the interval from ≥-50 mm to <-5 mm. Figure 3.37 demonstrates the different tolerance intervals used for the deviation analyses.

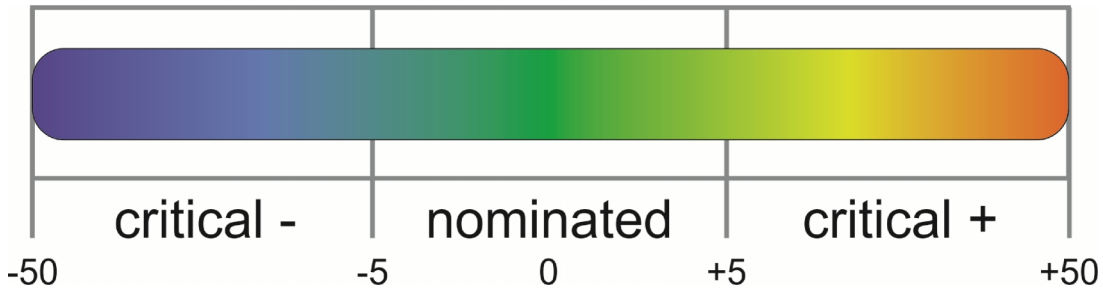

Figure 3.37 Tolerance interval scale.

Deviation analysis was performed in the following manner:

After importing the *final 3D-DG* models and *digital test models* into Geomagic® Control™ the corresponding models were aligned. Thereafter, the function *Deviation 3D compare* was selected to generate 3D colour-codes map showing the differences between the selected models. The colour map was then adjusted to reflect the different tolerance intervals. Finally, a *Geomagic Control Report*

was generated showing the number of data points in each of the tolerance intervals. The deviation analysis data of the two patients have been taken up in appendixes 1 and 2.

3.7.4 Implant mass properties analysis

Implant mass properties (surface and volume) were determined for the *final 3D-DG* models of the pectoralis muscles of the two Poland's syndrome patients created using the four methods; *Techniques A* and *B* with Magics and *Techniques A* and *B* with Freeform® Modeling™. For this comparative analysis of the implant mass properties, the model representing the original healthy pectoralis muscle was represented by the *final 3D-DG* model produced using Magics *Techniques B*, because it was produced directly from the scanned digital imaging data set of the successive 2D images.

3.7.5 Body conformation analysis

Body conformation analysis was undertaken by determining the mass properties of the different models of the two Poland's syndrome patients using Freeform® Modeling™. These properties were generated in the same manner as the implant mass properties. For this analysis the surface areas and volumes were determined for the four *assembled models*, the *original body conformation model* (original scanned digital imaging data set) and an *ideal body conformation model*.

Body conformation properties were determined in the following manner:

The different models were imported into by Freeform® Modeling™ using the custom import settings. Because this program operates with clay models, the clay coarseness was set to 0.10000 for all the models during importation. To determine the surface areas and volumes the *Mass Properties* option in the *Tools Menu* was selected to generate a report using the density set to 0.1000 g/mm^3. Although the report also provided the weight of a model, this property was excluded from the analysis because the weight was calculated as a solid clay entity in g/mm^3, which produced values that were identical to volume values.

Ideal body conformation model was produced for each patient in the following manner:

The *original body conformation model* (original scanned digital imaging data set) was bisected by separating the healthy half of the thorax from the affected half as described in *Technique A* using Freeform® Modeling™. Thereafter, the affected half of the thorax was deleted and the healthy half mirrored into the space vacated by the affected half of the thorax. This resulted in an *ideal body conformation model* containing two healthy halves of the thorax.

3.8 Conclusion

In order to comprehend all the facets of this investigation, the major steps and models used are presented as a summary flow diagram in Figure 3.38.

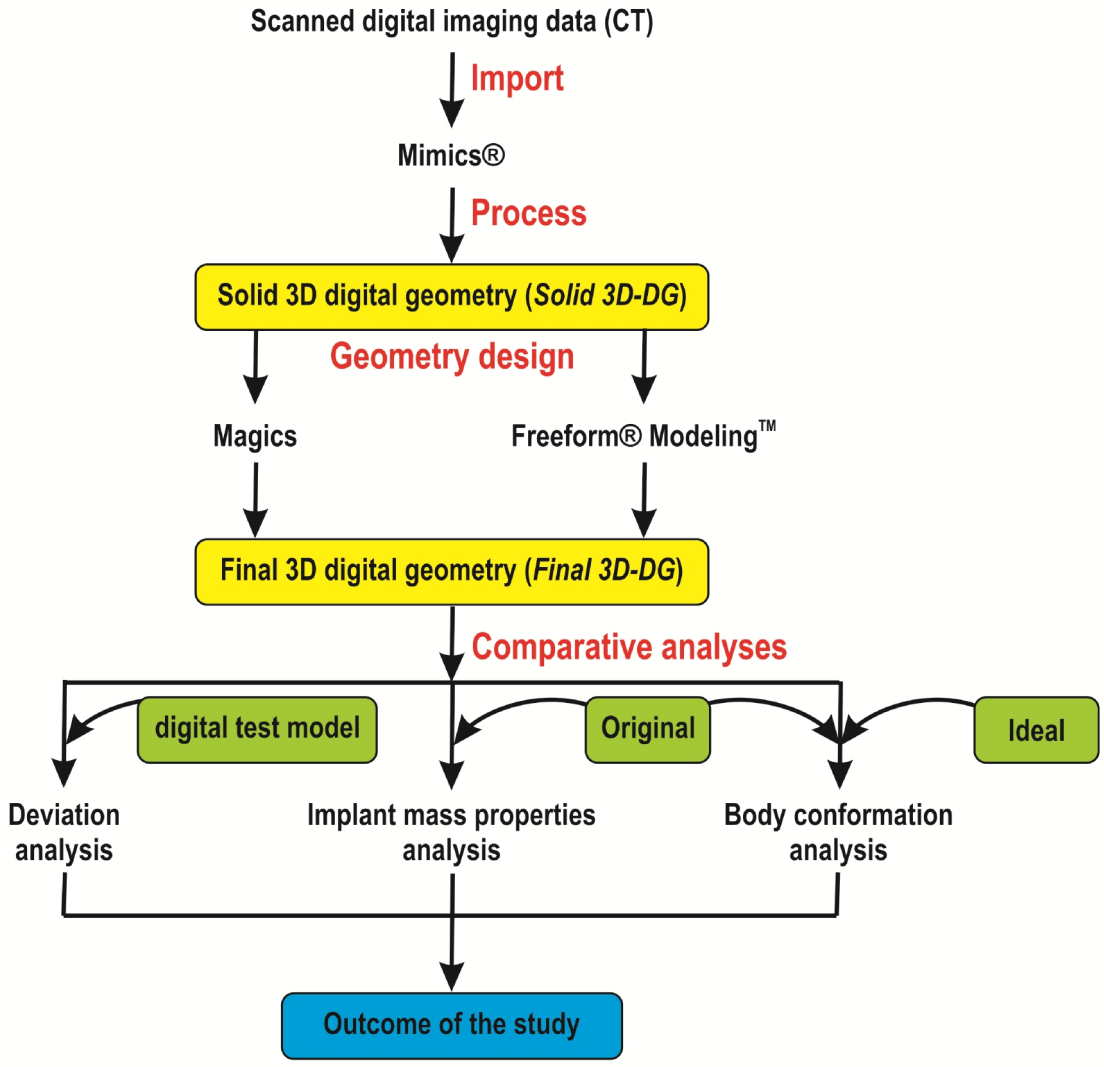

Figure 3.38 Summary of the development and assessment of 3D digital geometry models.

Chapter 4:

Case Study 1: Design of 3D Digital Geometries of Soft Tissue Models for a Female Poland's Syndrome Patient

4.1 Introduction

3D digital geometries for soft tissue prosthetic implants were designed for a 16-year-old Poland's syndrome female patient presenting with pectoralis major muscle deformities. These 3D soft tissue digital geometries were designed following three procedural phases, namely, digital data acquisition, digital data processing and digital data manipulation and design. The Mimics® software program was used for digital data processing, while the two software programs, Magics and Freeform® Modeling™, were used for the digital data manipulation and design of *final 3D digital geometries* (*final 3D-DGs*). In both Magics and Freeform® Modeling™, two design routes were followed using different source digital data to produce these *final 3D-DG* models. In *Technique A* the whole thorax was used, while in *Technique B* the pectoralis muscle was used. The models designed through these design routes were then assessed using the software programs Geomagic® Control™ and Freeform® Modeling™.

To demonstrate to what extent the Poland's syndrome female patient's deformities had resulted in an asymmetrical body type of the thorax, the Freeform® Modeling™ software was used to indicate the difference between the healthy and affected sides of the thorax. A vertical plane touching the shoulder was inserted together with an oblique plane stretching from the shoulder to the upper contour of a breast. The angle between vertical plane and the oblique plane was determined for each half of the thorax. Figure 4.1 shows the angle between the vertical planes and the oblique planes of the healthy and affected sides of the thorax. The difference between the two angles was 6.5º.

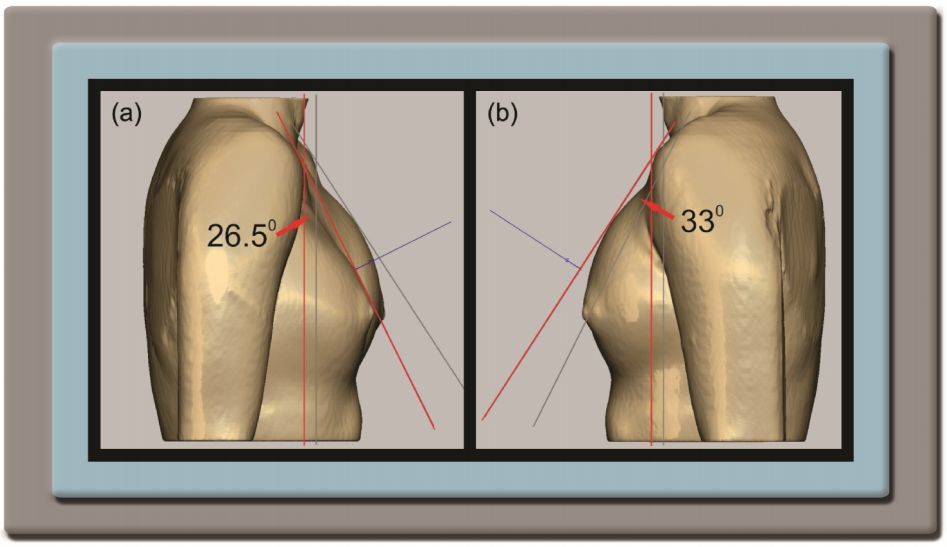

Figure 4.1 **Angles between vertical and oblique planes of the healthy and affected sides of the thorax.** (a) *Left view* depicting the angle of the affected side of the thorax, and (b) *Right view* depicting the angle of the healthy side of the thorax.

4.2 Results of Phase 1: Digital data acquisition

A scanned digital imaging data set of the female Poland's syndrome patient was obtained from a hospital in Pretoria. This data set comprised of 152 2D sequential scanned images in DICOM file format. Figure 4.2 provides an example of a number of the 2D sequential scanned images of this patient.

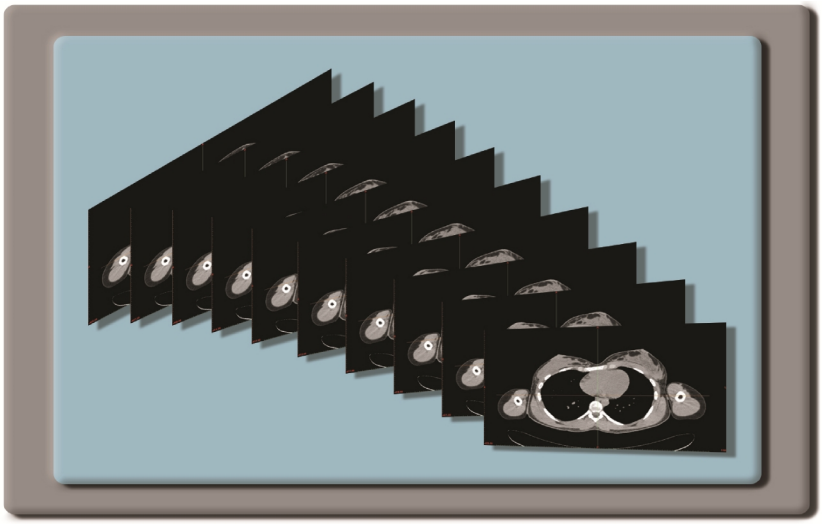

Figure 4.2 **2D sequential scanned images of the female Poland's syndrome patient in a DICOM file format.**

4.3 Results of Phase 2: Digital data processing

After the acquisition of the scanned digital imaging data set of the female Poland's syndrome patient, it was imported into Mimics®. In Mimics®, these data were processed to create models, referred to as *solid 3D digital geometries* (*solid 3D-DGs*), in STL file format; one of the whole thorax and one of the pectoralis muscle.

The processing of the scanned digital images involved a number of manipulations through the application of *Segmentation masks*, which resulted in the isolation of the two regions of interest (ROIs); the whole thorax and the pectoralis muscle. The application of *Segmentation masks* involved a number of steps, namely, *Thresholding*, *Region Growing*, *Mask Editing* and, finally, the generation of two *solid 3D-DGs* in STL format. *Thresholding* involved the exclusion of all anatomical structures beyond the boundaries of the ROI. For the whole thorax isolation, this included bone, organs and soft tissues (Figure 4.3a). For the pectoralis muscle isolation this included the entire soft tissue muscle volume (Figure 4.3b). In the case of the pectoralis muscle, *Region Growing* was then used to isolate all soft tissues beyond the boundaries of the pectoralis muscle (Figure 4.3c). The isolated pectoralis muscle was then inspected and further edited manually (pixel-by-pixel) to remove all floating pixels around the boundaries, thereby producing a *solid 3D-DG* of a model of the pectoralis muscle with refined boundaries in STL format (Figure 4.3d). The STL models of the whole thorax and the pectoralis muscle were then exported to Magics and Freeform® Modeling™ for further manipulation to design *final 3D-DGs* (Figures 4.3e and f).

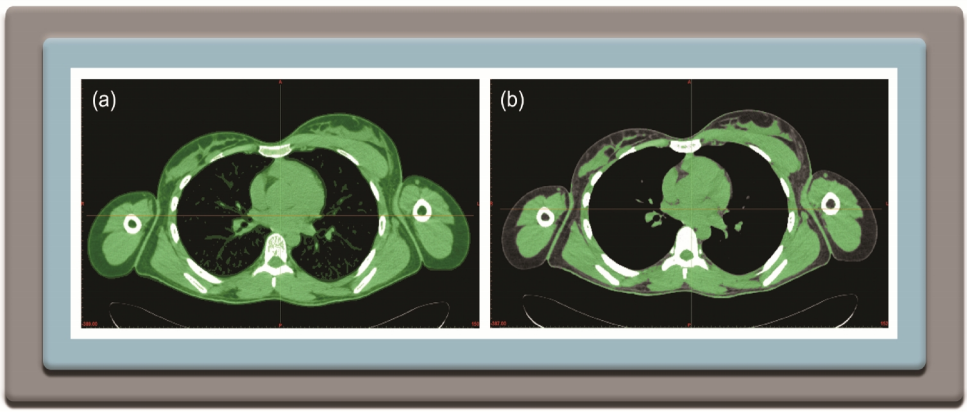

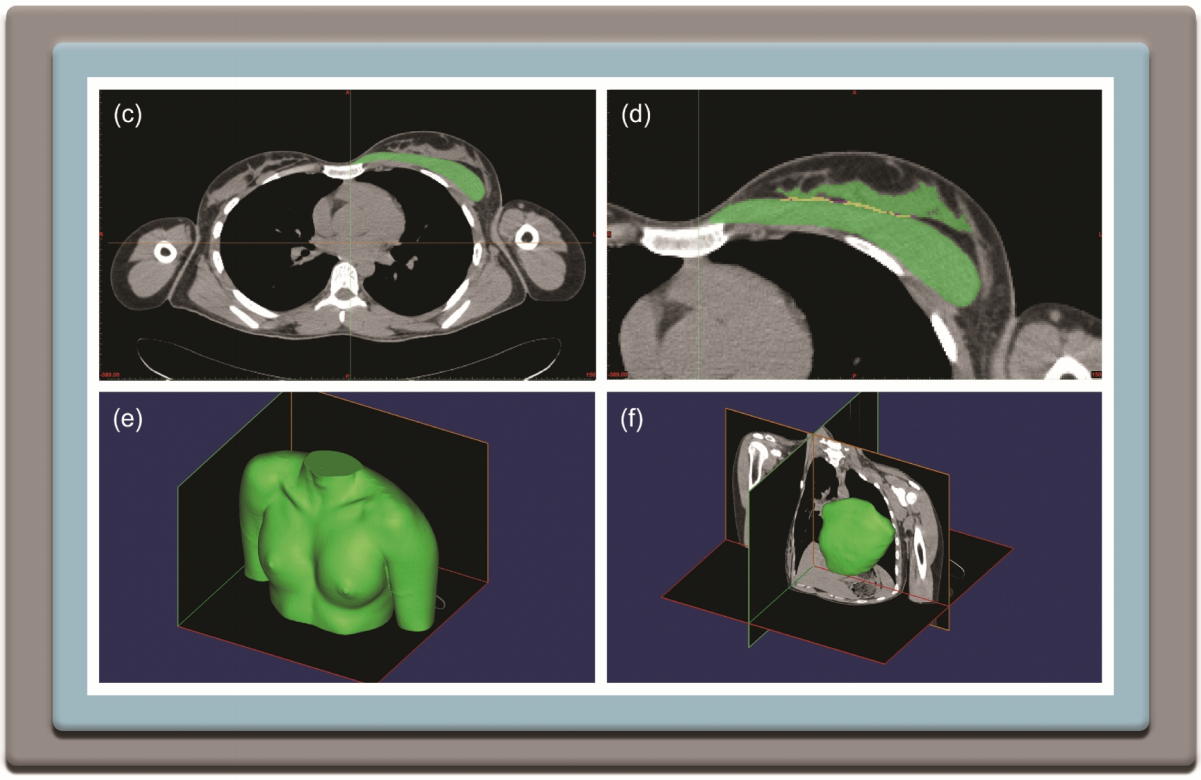

Figure 4.3 **Segmentation process.** (a) Anatomical structures after *Thresholding* of the whole thorax (indicated green), (b) Muscle soft tissue volume after *Thresholding* for the pectoralis muscle (indicated green), (c) *Region Growing* of the pectoralis muscle isolation (indicated green), (d) Editing of the boundaries of the pectoralis muscle (indicated in yellow and purple), (e) Isolated thorax as a *solid 3D digital geometry* STL model, and (f) Isolated pectoralis muscle as a *solid 3D digital geometry* STL model.

4.4 Results of Phase 3: Digital data manipulation and design

After the importing of the *solid 3D-DG* soft tissue STL models into Magics and Freeform® Modeling™, they were manipulated to design digital geometries of soft tissue implants for the female Poland's syndrome patient. In *Technique A,* the whole thorax was used to design a 3D digital geometry model; one in Magics and one in Freeform® Modeling™. Similarly, in *Technique B,* two 3D digital geometry models were designed in these software programs using the pectoralis muscle. This process thus resulted in the design of four *final 3D-DG* models, which could be used in the manufacturing process of prosthetic implants.

4.4.1 Digital data manipulation and design using Magics

In *Technique A*, the manipulation of the whole thorax was subjected to a number of steps, namely, the *activation of the coordinate planes*, *bisection of the thorax*, and the *mirroring of the healthy half of the thorax onto the affected half*; after which a number of *Boolean operations* were performed to produce a model as a *final 3D-DG*. Figure 4.4 demonstrates the *final 3D-DG* designed from the whole thorax in four different views using Magics. The geometry margin thicknesses (implant edges) of the isolated *final 3D-DG* model have been indicated in mm.

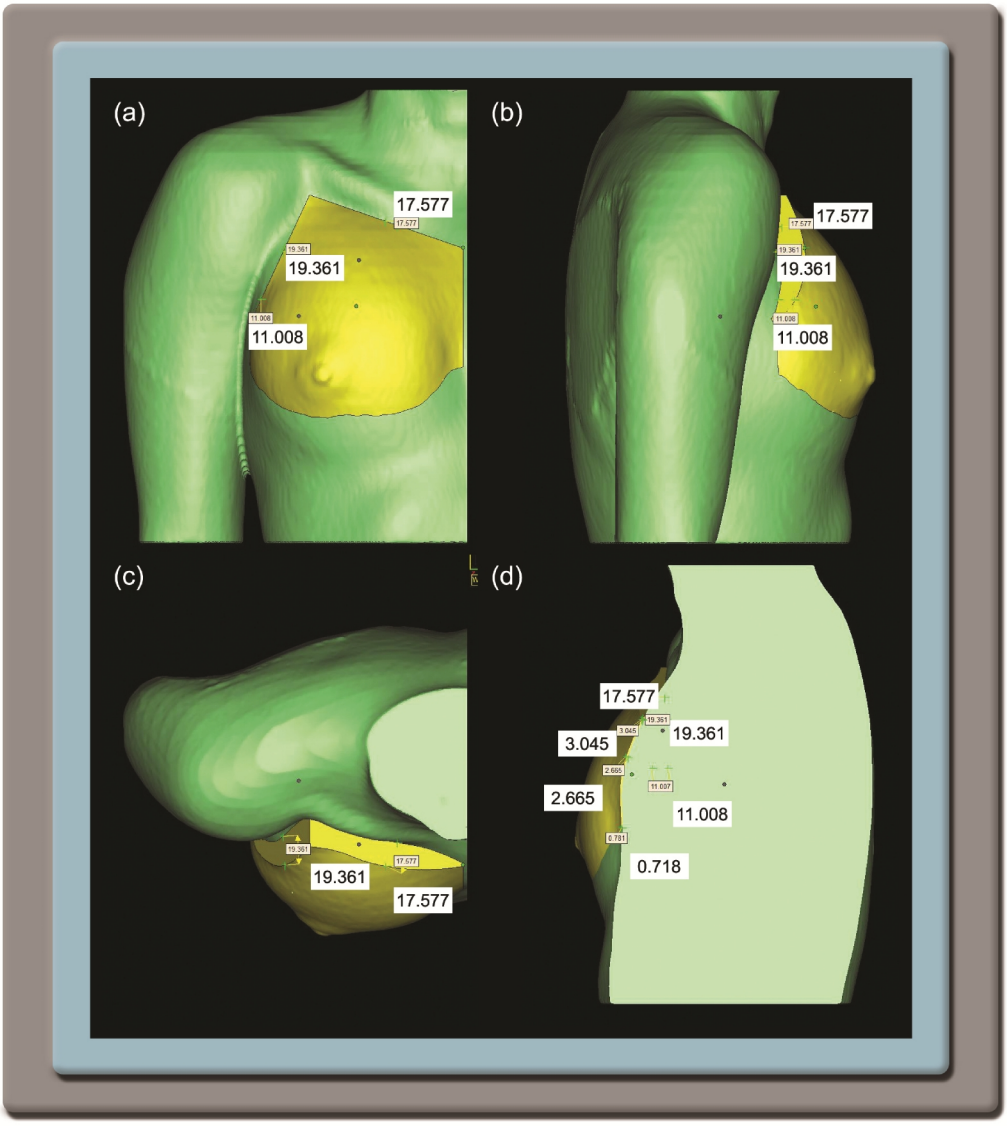

Figure 4.4 **Model of *final 3D digital geometry* designed from the whole thorax in four different views using Magics.** (a) *Front view*, (b) *Left side view*, (c) *Top view*, and (d) *Right side view*.

In *Technique B*, the pectoralis muscle was manipulated to design a *final 3D-DG* model by mirroring the isolated healthy pectoralis muscle onto the affected half. Figure 4.5 demonstrates the *final 3D-DG* model designed from the pectoralis muscle in six different views using Magics. Similarly to *Technique A,* the geometry margin thicknesses (implant edges) of the isolated *final 3D-DG* model have been indicated in mm.

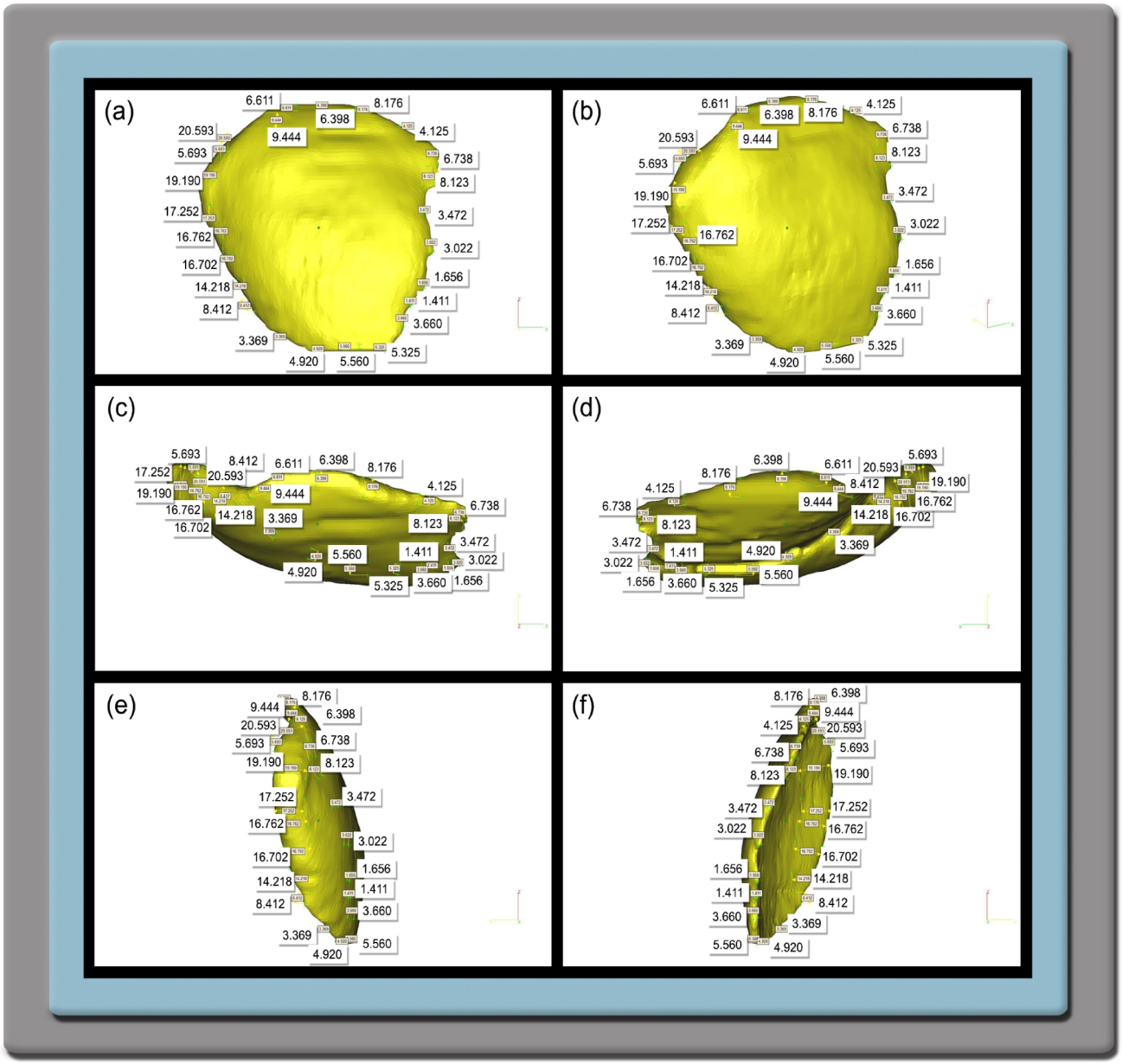

Figure 4.5 **Model of *final 3D digital geometry* designed from the pectoralis muscle in six different views using Magics.** (a) *Front view*, (b) *Angle view*, (c) *Top view*, (d) *Bottom view*, (e) *Left side view*, and (f) *Right side view*.

4.4.2 Digital data manipulation and design using Freeform® Modeling™

In *Technique A*, using Freeform® Modeling™, the whole thorax was subjected to similar steps as was used in *Technique A* with Magics. These steps included the *activation of the coordinate planes*, *bisection of the thorax*, and the *mirroring of the healthy half of the thorax onto the affected half*, as well as the application of *Boolean operations*. Figure 4.6 demonstrates the *final 3D-DG* designed from the whole thorax in ten different views using Freeform® Modeling™.

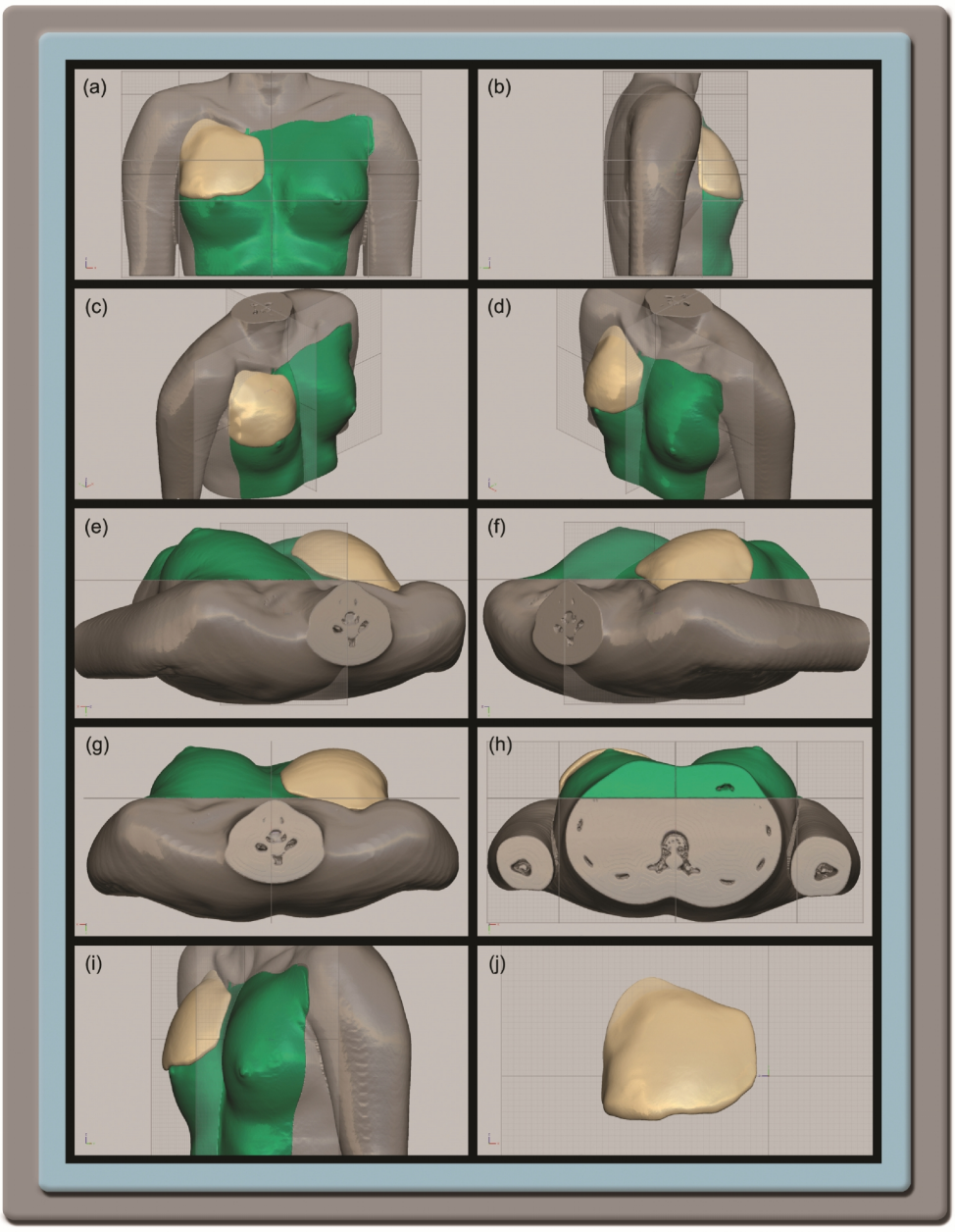

Figure 4.6 **Model of *final 3D digital geometry* designed from the whole thorax in ten different views using Freeform® Modeling™.** (a) *Front view*, (b) *Left side view*,

(c) *Angle view* from the top-left side, (d) *Angle view* from the top-right side, (e) *Angle view* from the top, (f) *Angle top view*, (g) *Top view*, (h) *Bottom view*, (i) *Right side view*, and (j) The *final 3D digital geometry* model of the pectoralis muscle.

In *Technique B*, the pectoralis muscle was manipulated to design a model as a *final 3D-DG* by mirroring the isolated healthy pectoralis muscle onto the affected half. In contrast with *Technique B* of Magics, the 3D digital geometry model was further manipulated by tugging and pulling to fill the space in the affected half which produced the newly designed *final 3D-DG*. Figure 4.7 demonstrates the model of the *final 3D-DG* designed from the pectoralis muscle in six different views using Freeform® Modeling™.

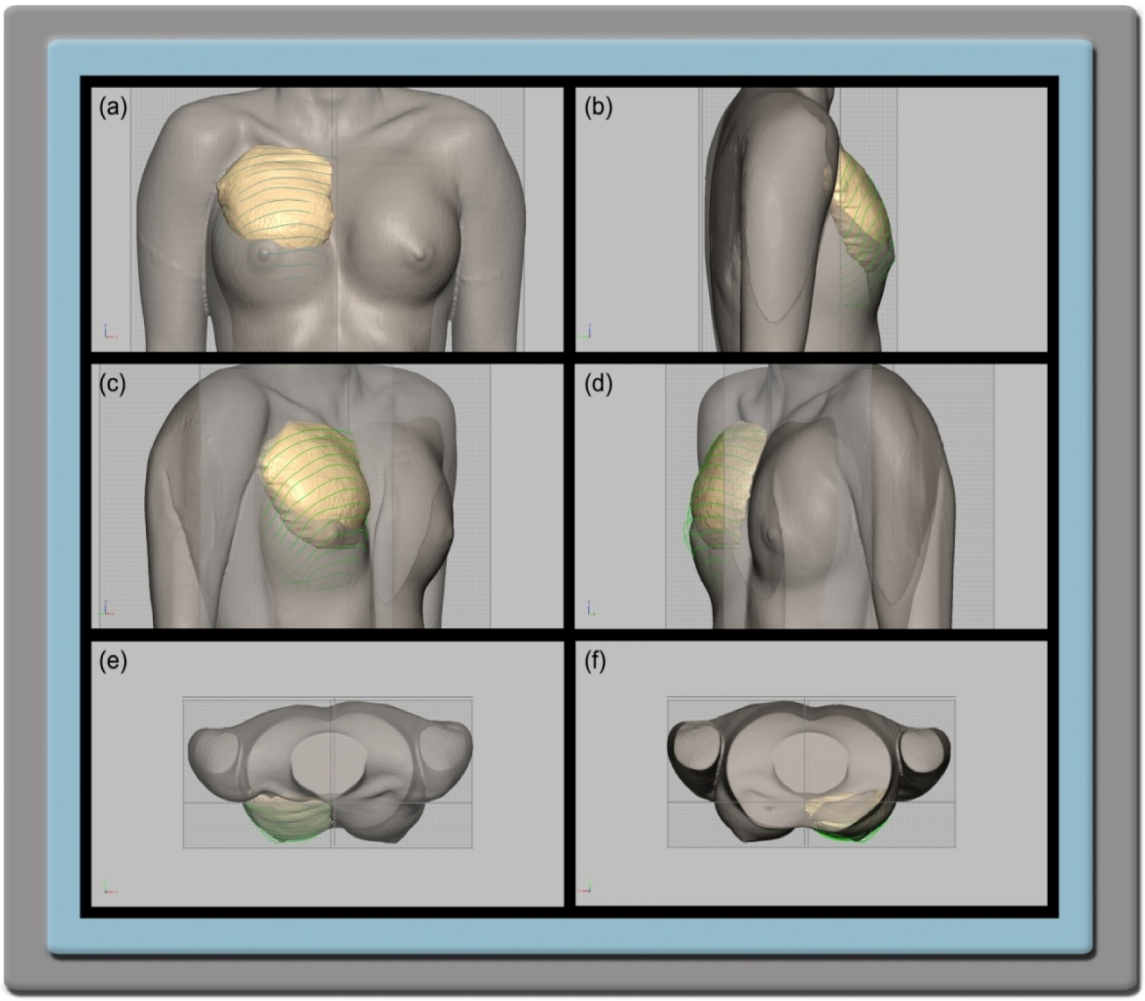

Figure 4.7 **Model of *final 3D digital geometry* designed from the pectoralis muscle in six different views using Freeform® Modeling™.** (a) *Front view*, (b) *Left side view*, (c) *Left angle view*, (d) *Right angle view*, (e) *Top view*, and (f) *Bottom view*.

4.5 Comparative analysis of the different models of the *final 3D digital geometries*

Comparative analyses were conducted to obtain some understanding of how the different techniques performed relative to a *digital test model.* Therefore, the four *final 3D-DG* models produced using the four techniques; *Technique A* and *B* with Magics and *Technique A* and *B* with Freeform® Modeling™; were compared to constructed *digital test models*. Three comparative analyses were undertaken in this study. They included a deviation analysis, an implant mass property analysis and a body conformation analysis.

4.5.1 Deviation analysis

In the deviation analysis of the different techniques, the software program Geomagic® Control™ allocated different numbers of deviation test points. For Magics *Technique A*, Geomagic® Control™ allocated approximately 50% less deviation test points than for Freeform® Modeling™ *Technique A*, while for Magics *Technique B*, the program allocated approximately 34% less deviation test points than for Freeform® Modeling™ *Technique B* (Table 4.1). Although the number of test points differed for the different techniques, the overall outcome of the comparison was similar for all four techniques, where most of the deviation test points (more than 70%) fell within the nominated tolerance region of $\geq$-5 and $\leq$+5 mm showing a high level of alignment between the models of the *final 3D-DGs* and the *digital test models.* For all the techniques the critical minus interval contained approximately 20% of the number of deviation test points showing that the models of the *final 3D-DGs* were smaller than the *digital test models* at these points. Very few of the deviation test points, less than 1%, of the *final 3D-DG* models were larger than the *digital test models* at these points.

Table 4.1 **Comparison between *digital test models* and *final 3D digital geometry* models designed for the female patient with Poland's syndrome.**

Deviation analysis criterion	Technique used to produce a *final 3D digital geometry* model			
	Magics *Technique A*	Magics *Technique B*	Freeform® Modeling™ *Technique A*	Freeform® Modeling™ *Technique B*
Number of data points	91524	64729	178194	184957
% (number) data points in the nominated tolerance interval	78 (70968)	73 (47119)	82 (146224)	78 (144658)
% (number) data points in the critical minus tolerance interval	22 (20217)	27 (17568)	18 (31957)	21 (38866)
% (number) data points in the critical plus tolerance interval	0.400 (339)	0.070 (42)	0.007 (13)	0.800 (1433)
Standard deviation	4.78	5.32	3.78	7.22

The standard deviations revealed that both the Magics *Techniques A* and *B* produced *final 3D-DG* models with approximately 68% of the deviation test points falling within a narrow interval; -4.7 to +4.7 for Magics *Technique A* and -5.3 and +5.3 for Magics *Technique B* (Table 4.1). In contrast, approximately 68% of the deviation test points for Freeform® Modeling™ *Technique A* fell within a smaller interval when compared to the Magics intervals; -3.8 to +3.8. The interval for Freeform® Modeling™ *Technique B* was the largest of the four design routes; -7.2 to +7.2. This can probably be attributed to the particular designing technique used in this route. The 3D digital geometry model of the pectoralis muscle was manipulated using the *Tug tool* to fill the space underneath the boundary curves, thereby expanding the surface edge and volume of the *final 3D-DG* model.

To obtain a visual perspective of the deviations of the *final 3D-DG* models from the *digital test models*, histograms were constructed showing the percentage of deviation test points that fell within the set tolerance interval of ≥-5 and ≤+5 mm (nominated interval) and in the critical plus (>5 and ≤50 mm) and minus (≥-50 and <-5 mm) tolerance regions (Figure 4.8a-d). These histograms show that

the vast majority of deviation test points fell within the nominated tolerance interval, while most of the remainder of the deviation test points fell within the and critical minus region (≥-50 and <-5 mm).

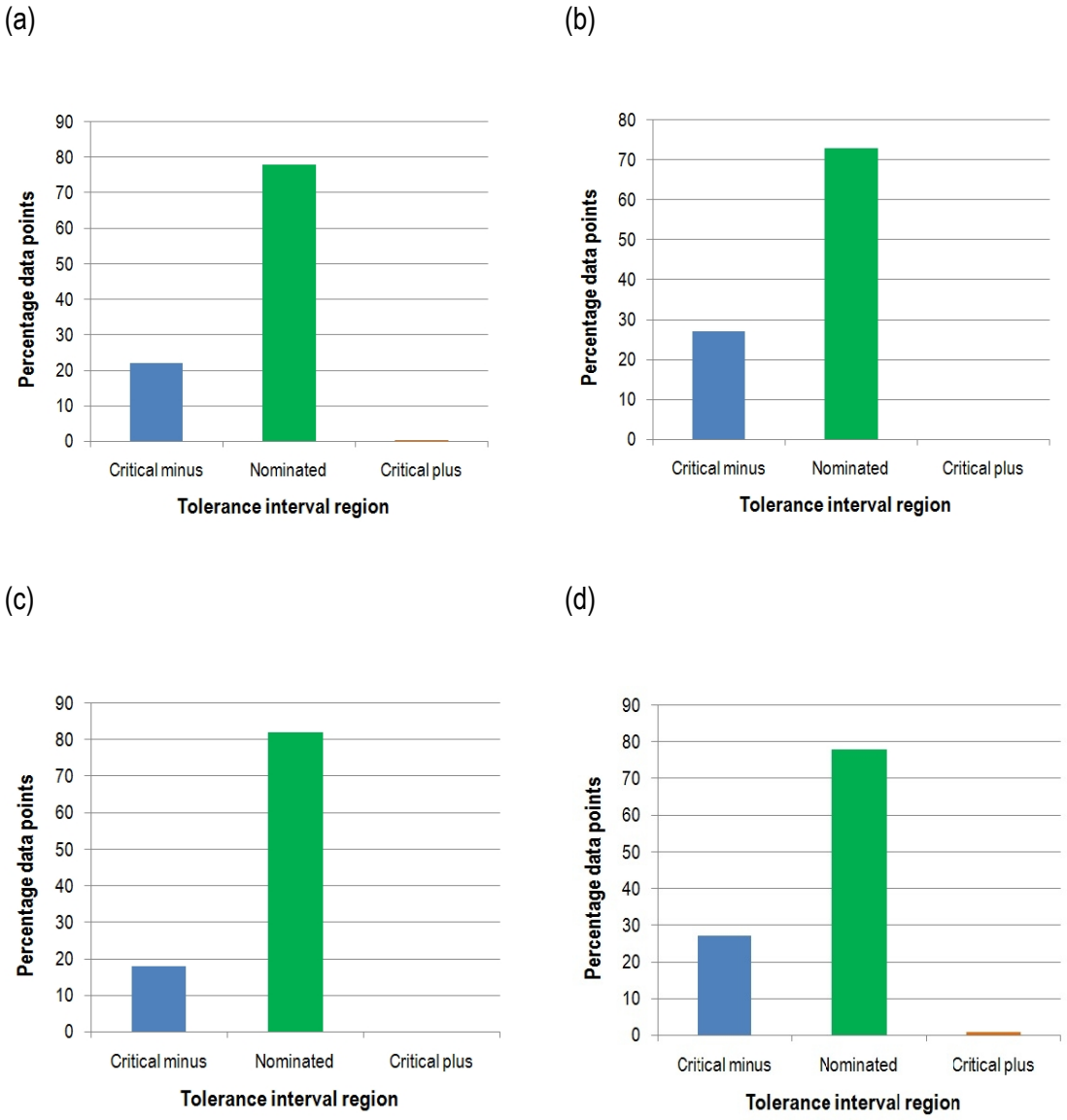

Figure 4.8 **Histograms showing percentage data points in different tolerance intervals using different techniques.** (a) Magics *Technique A*, (b) Magics *Technique B*, (c) Freeform® Modeling™ *Technique A*, and (d) Freeform® Modeling™ *Technique B*.

Colour deviation maps revealed that the different programs using the same technique produced similar deviation maps. *Technique A* of Magics and of Freeform® Modeling™ indicated similar aligned areas between the models of the *final 3D-DGs* and the *digital test models*, as well as the

areas of the *final 3D-DG* models that were smaller than the *digital test models*. Figures 4.9a and b indicates for *Technique A* the aligned areas in green and the areas that were smaller in blue. A similar outcome was found for *Technique B* of Magics and Freeform® Modeling™ (Figures 4.9c, d). Other views, including frontal views, of the deviation maps are presented in Figure 4.10, Plate 1 (Magics *Technique A*), Plate 2 (Magics *Technique B*), Plate 3 (Freeform® Modeling™ *Technique A*), and Plate 4 (Freeform® Modeling™ *Technique B*) at the end of this chapter.

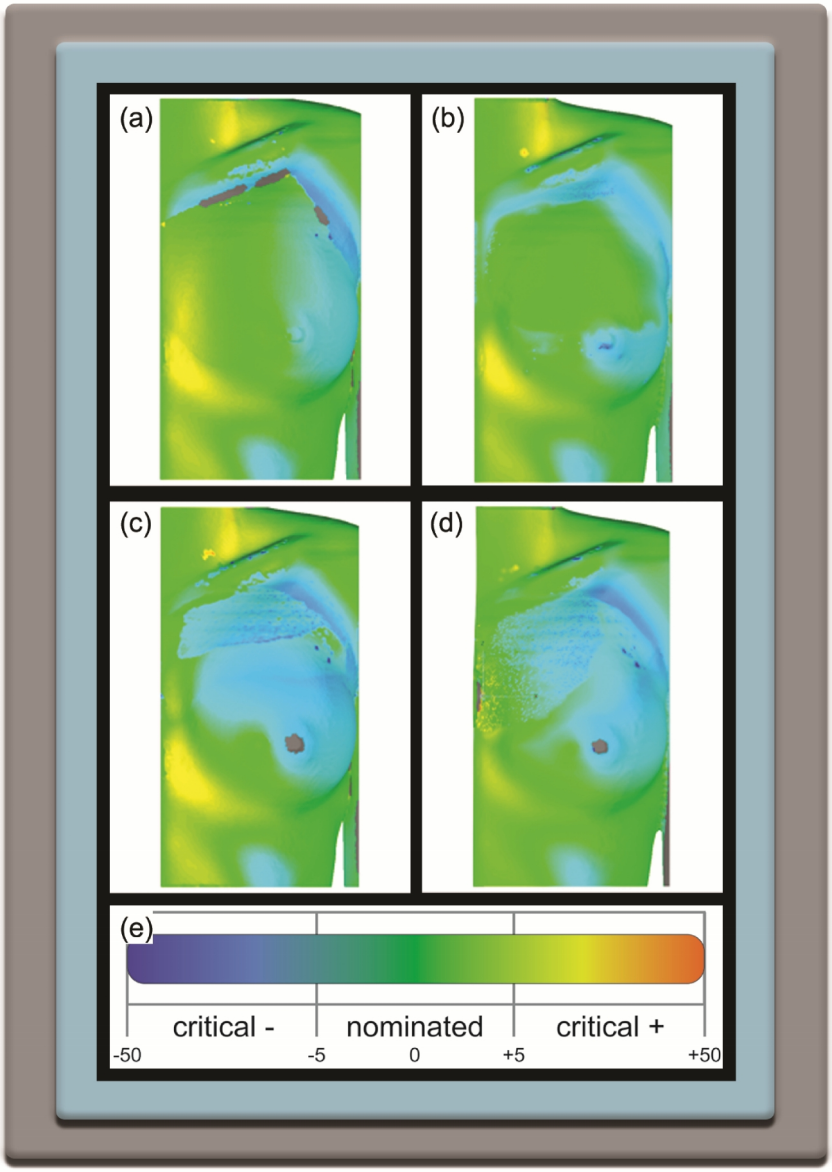

Figure 4.9 **Deviation colour maps showing the frontal views of the different techniques.** (a) Magics *Technique A*, (b) Freeform® Modeling™ *Technique A*, (c) Magics *Technique B*, (d) Freeform® Modeling™ *Technique B*, and (e) Tolerance intervals scale.

4.5.2 Implant mass property analysis

An implant mass property analysis was performed using Freeform® Modeling™ to compare the surface areas and volumes of the different *final 3D-DG* models of the pectoralis muscle. The *final 3D-DG* model that was produced directly from the scanned digital imaging data set using Magics *Techniques B* represented the original healthy pectoralis muscle. The surface areas of the four pectoralis muscles produced by the different techniques ranged from approximately 34,000 to 44,000 mm^2, while the volumes ranged from 160,000 to 210,000 mm^3 (Table 4.2). The *final 3D-DG* model of the pectoralis muscle produced using Freeform® Modeling™ *Technique A* was closest in dimensions to that of the *original model* (Magics *Technique B*).

Table 4.2 Implant mass properties of *the final 3D digital geometry* models.

Implant mass property	Techniques used to produce a *final 3D digital geometry* model			
	Magics *Technique A*	Magics *Technique B**	Freeform® Modeling™ *Technique A*	Freeform® Modeling™ *Technique B*
Surface area × 10^3 (mm^2)	44.010	34.515	34.135	42.113
Volume × 10^4 (mm^3)	21.375	16.839	21.368	19.512

* Represents the original healthy pectoralis muscle (original).

4.5.3 Body conformation analysis

A body conformation analysis was performed to ascertain to what extent the different techniques used to produce the *final 3D-DGs* had the potential to reconstruct the soft tissue deformities of the female Poland's syndrome patient. Four *assembled models* were compared to the *original body conformation* (original scanned digital imaging data set) of the female patient and an *ideal body conformation* produced using Freeform® Modeling™. The four *assembled models* comprised of a

unified *original body conformation* with each of the *final 3D-DG* models (pectoralis muscle) of each technique. An *ideal body conformation* comprised of two healthy sides of the thorax.

The body conformation properties of the *original body conformation* was, as expected, slightly less than that of the *ideal body conformation*, because the *ideal body conformation* consists of a thorax with two healthy pectoralis muscles (Table 4.3). All four techniques produced dimensions relatively close to the *ideal body conformation* dimensions.

Table 4.3 Body conformation mass properties of the *assembled models*, *original* and *ideal body conformation models*.

Body conformation mass property	**Original**	**Ideal**	**Technique used to produce a *final 3D digital geometry* model**			
			Magics *Technique A*	Magics *Technique B*	Freeform® Modeling™ *Technique A*	Freeform® Modeling™ *Technique B*
Surface area $\times 10^3$ (mm^2)	389.550	396.264	390.383	396.957	393.098	405.474
Volume $\times 10^4$ (mm^3)	1522.826	1586.796	1505.659	1498.183	1515.938	1507.945

4.6 Conclusion

Four different *final 3D-DGs* models of pectoralis muscles were produced for the female Poland's syndrome patient using a scanned digital imaging data set. These models were designed following four techniques using two different software programs. A comparison of these pectoralis muscle implant geometries revealed that the four design techniques applied delivered results with relatively small variation. It was thus not possible to select a preferred design route in this case study.

Figure 4.10 **Deviation colour maps of the four techniques.**

Plate 1. Magics *Technique A*. (a) *Isometric view*, (b) *Frontal view*, (c) *Left side view*, (d) *Right side view*, (e) *Top view*, and (f) *Bottom view*.

Plate 2. Magics *Technique B*. (a) *Isometric view*, (b) *Frontal view*, (c) *Left side view*, (d) *Right side view*, (e) *Top view*, and (f) *Bottom view*.

Plate 3. Freeform® Modeling™ *Technique A*. (a) *Isometric view*, (b) *Frontal view*, (c) *Left side view*, (d) *Right side view*, (e) *Top view*, and (f) *Bottom view*.

Plate 4. Freeform® Modeling™ *Technique B*. (a) *Isometric view*, (b) *Frontal view*, (c) *Left side view*, (d) *Right side view*, (e) *Top view*, and (f) *Bottom view*.

Plate 1

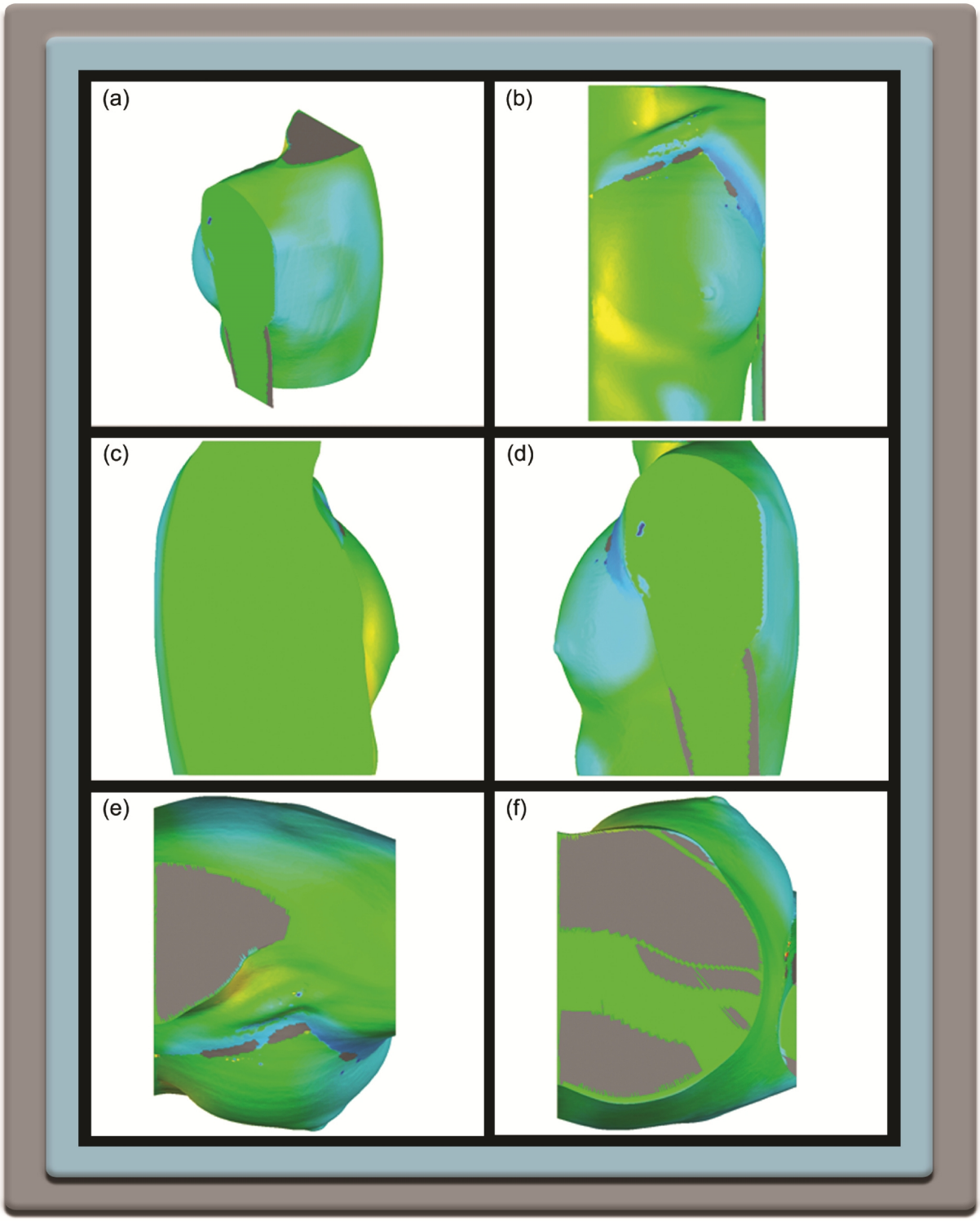

Plate 2

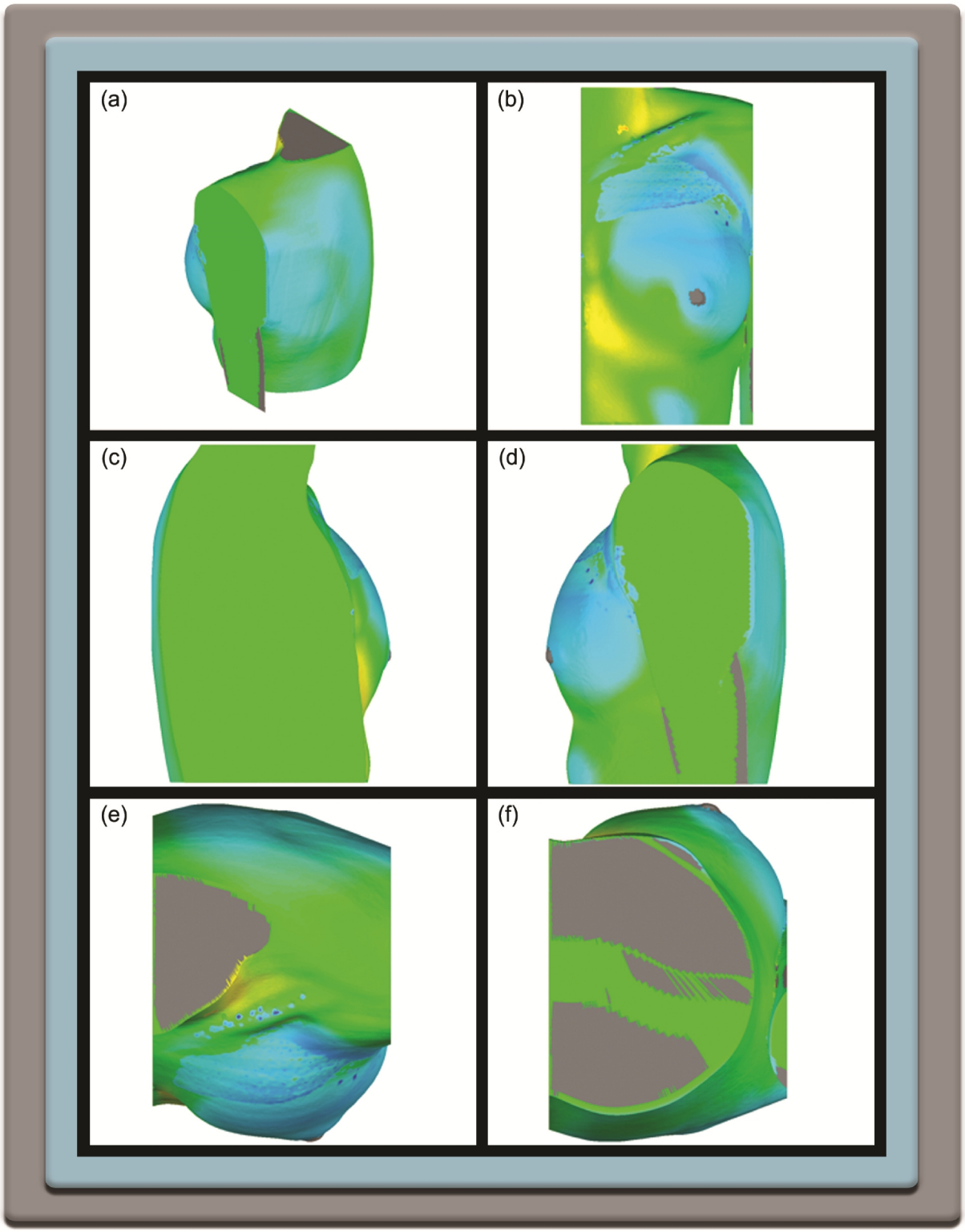

Plate 3

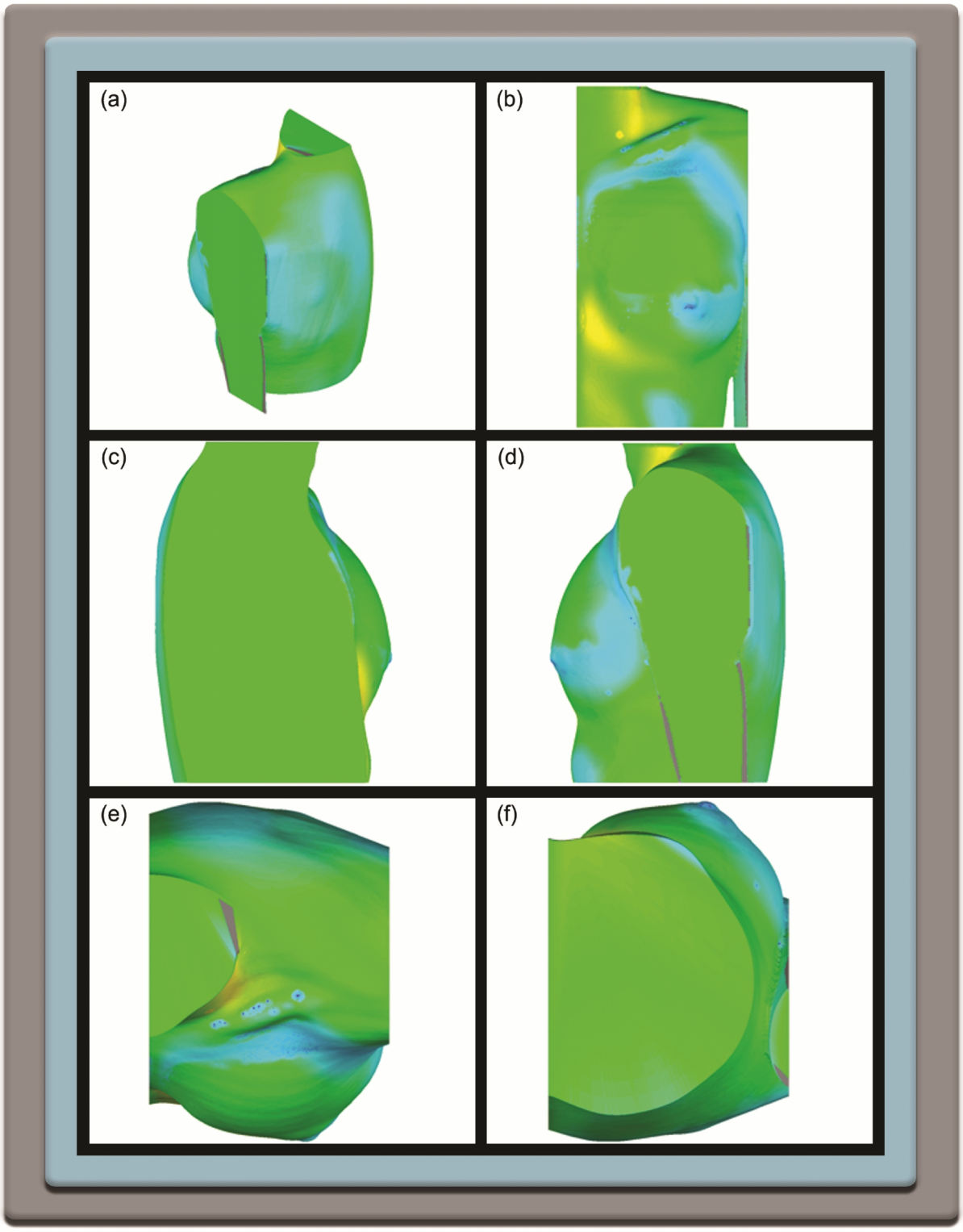

Plate 4

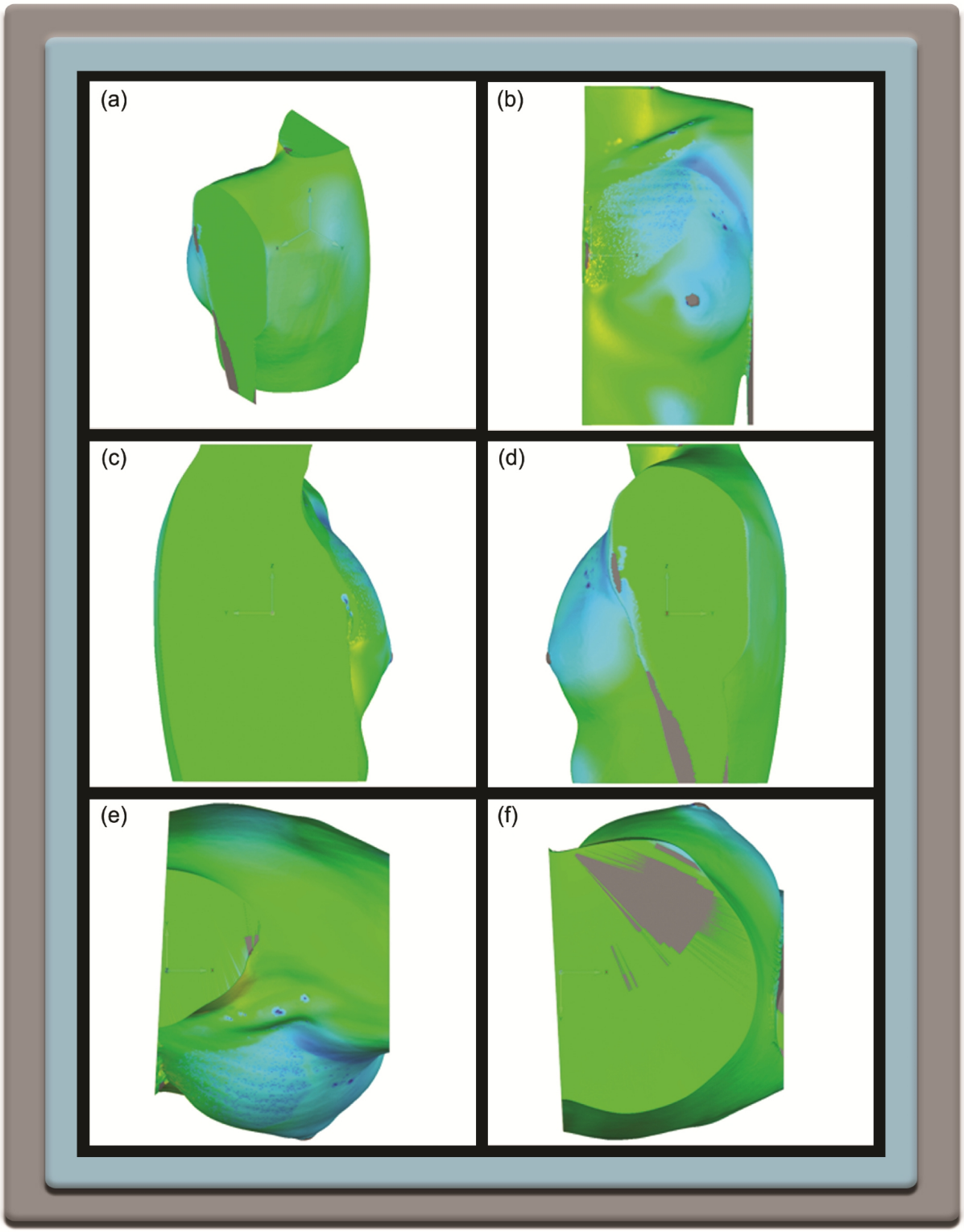

Chapter 5:

Case Study 2: Design of 3D Digital Geometries of Soft Tissue Models for a Male Poland's Syndrome Patient

5.1 Introduction

3D digital geometries for soft tissue prosthetic implants were designed for a 17-year-old Poland's syndrome male patient presenting with pectoralis major and pectoralis minor muscle deformities. These 3D digital geometries were designed following the same three procedural phases as for Case Study 1, namely, digital data acquisition, digital data processing and digital data manipulation and design.

Similarly to Case Study 1, the extent of the asymmetrical conformation body type of the thorax was also demonstrated. This was achieved by determining the difference between the angles formed by a vertical plane touching the shoulder and an oblique plane stretching from the shoulder to the upper contour of the breast on each side of the thorax. Figures 5.1a and b show that the difference between the two sides of the thorax was 14º. This difference was substantially greater than that of the female patient which was 6.5º.

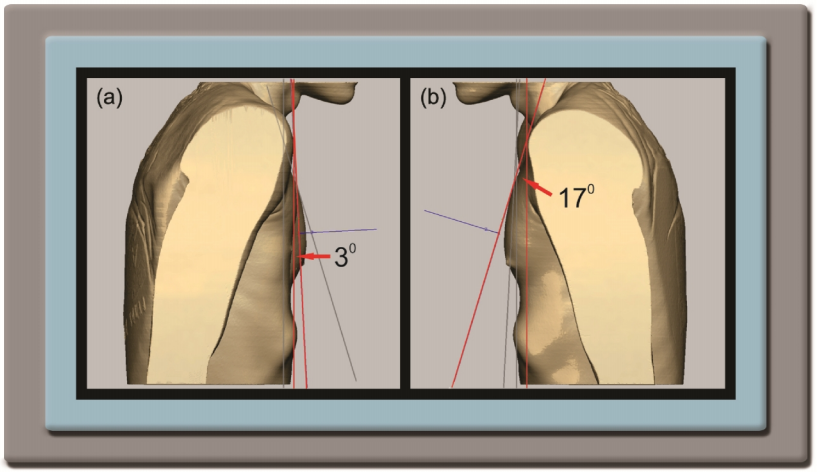

Figure 5.1 Angles between vertical and oblique planes of the healthy and affected sides

of the thorax. (a) *Left view* depicting the angle of the affected side of the thorax, and (b) *Right view* depicting the angle of the healthy side of the thorax.

5.2 Results of Phase 1: Digital data acquisition

The scanned digital imaging data set of the male Poland's syndrome patient was also obtained from a hospital in Pretoria. This data set was substantially larger than the data set used in Case Study 1 (152 images) and comprised of 533 2D sequential scanned images in a DICOM file format. In contrast to Case Study 1, the scanning slice thickness was thinner, 1 mm as compared to Case Study 1 that was 2 mm. Figure 5.2 provides an example of a number of the 2D sequential scanned images of this patient.

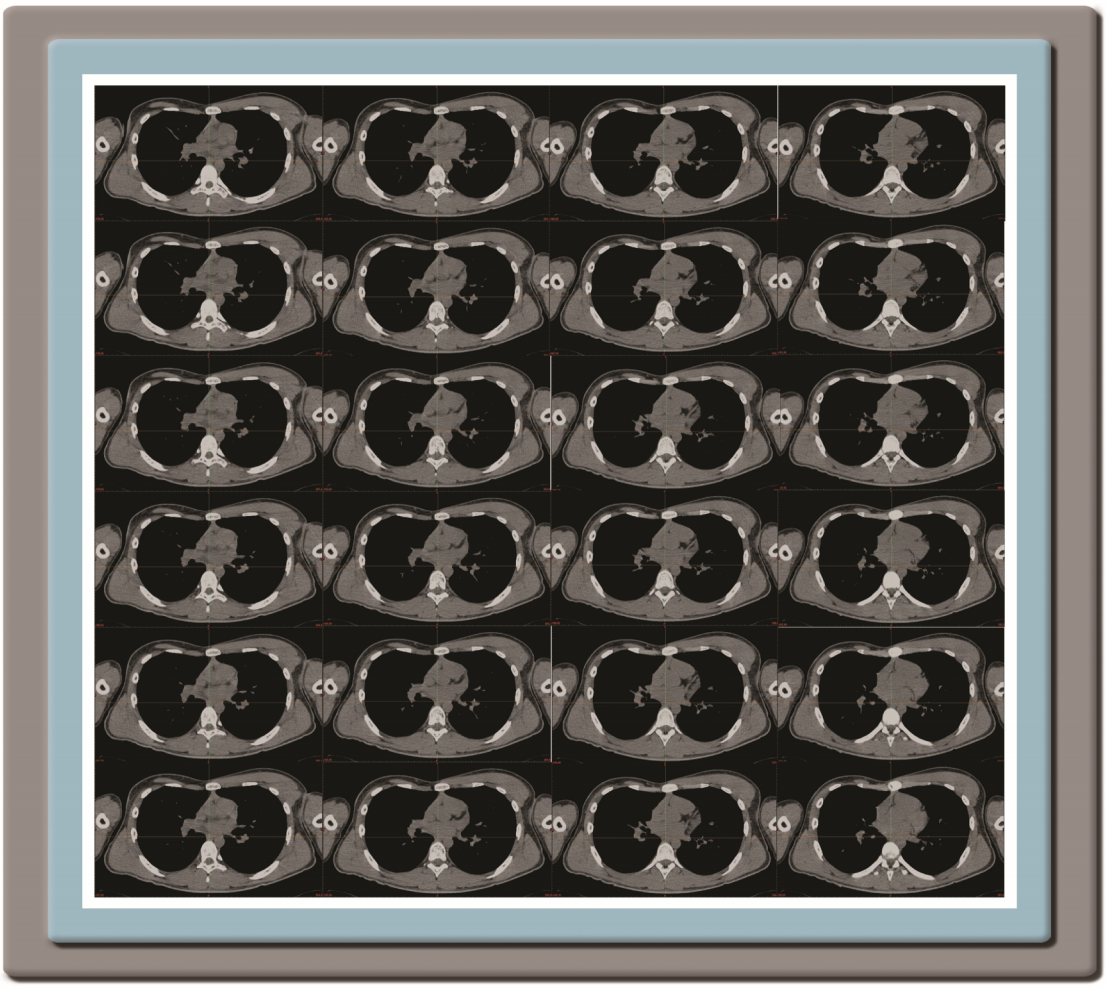

Figure 5.2 2D sequential scanned images of the male Poland's syndrome patient in a DICOM file format.

5.3 Results of Phase 2: Digital data processing

After the acquisition of the scanned digital imaging data set of the male Poland's syndrome patient, it was imported into Mimics®. Similarly to Case Study 1, the digital imaging data were then processed to create two *solid 3D digital geometries* (*solid 3D-DGs*) in STL file format; one for the whole thorax and one of the pectoralis muscle. Both these STL models were finally exported to Magics and Freeform® Modeling™ for further manipulation to design *final 3D digital geometries* (*final 3D-DGs*). Figure 5.3 demonstrates the procedural steps to create *Segmentation masks* in Mimics® for the manipulation of the digital data to create the two *solid 3D-DGs* models in STL file format.

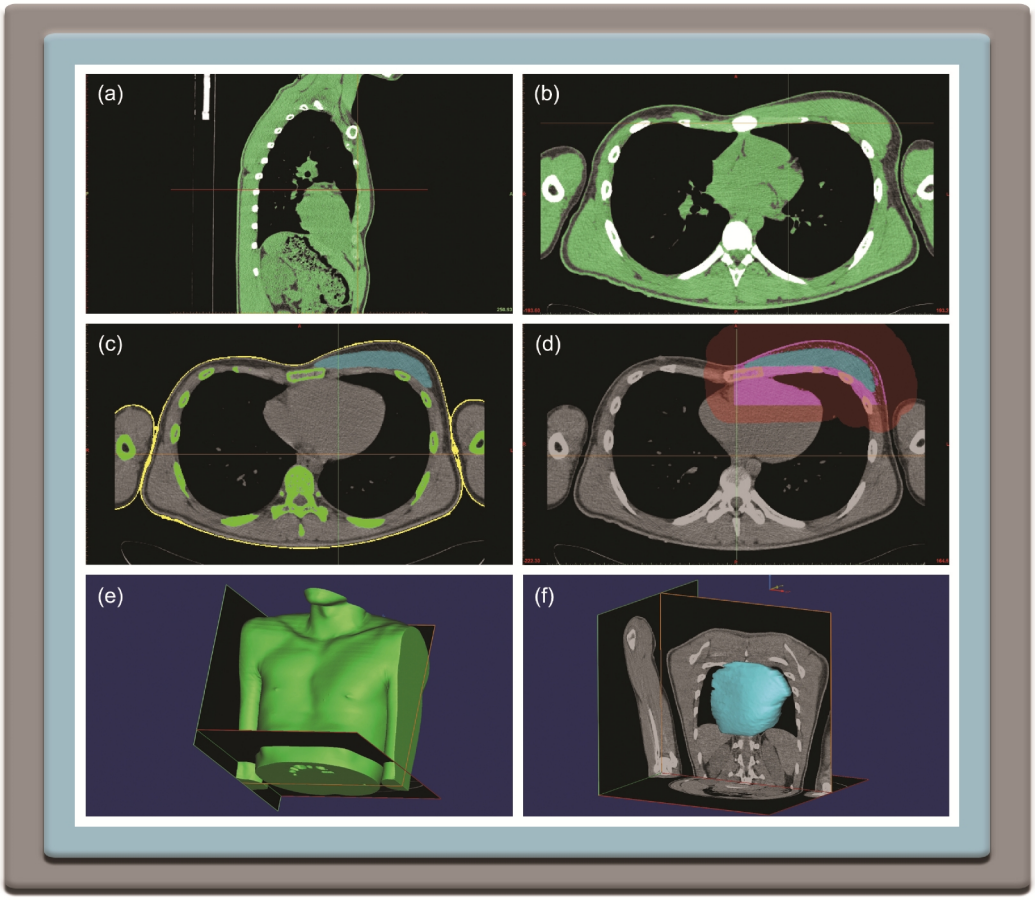

Figure 5.3 **Segmentation process.** (a) Anatomical structures after *Thresholding* of the whole thorax (indicated green), (b) Muscle soft tissue volume after *Thresholding* for the pectoralis muscle (indicated green), (c) *Region Growing* of the pectoralis muscle isolation (indicated blue), (d) Editing of the boundaries of the pectoralis muscle (indicated in purple), (e) Isolated thorax as a *solid 3D digital geometry* STL model, and (f) Isolated pectoralis muscle as a *solid 3D digital geometry* STL model.

5.4 Results of Phase 3: Digital data manipulation and design

After importing the *solid 3D-DGs* STL models into the software programs Magics and Freeform® Modeling™, they were manipulated to design *final 3D-DGs* of soft tissue prosthetic implants for the male Poland's syndrome patient. Similarly to Case Study 1, four *final 3D-DGs* were designed, which could be used for the manufacturing process of prosthetic implants.

5.4.1 Digital data manipulation and design using Magics

Technique A was used to manipulate the whole thorax in a similar manner as in Case Study 1. By applying the steps of *activating the coordinate planes*, the *bisection of the thorax*, the *mirroring of the healthy half of the thorax onto the affected half*; and the application of *Boolean operations*, *a final 3D-DG* was designed. Figure 5.4 demonstrates the *final 3D-DG* model of the pectoralis muscle designed from the whole thorax in an *Angled view*. The geometry margin thicknesses (implant edges) have been indicated in mm.

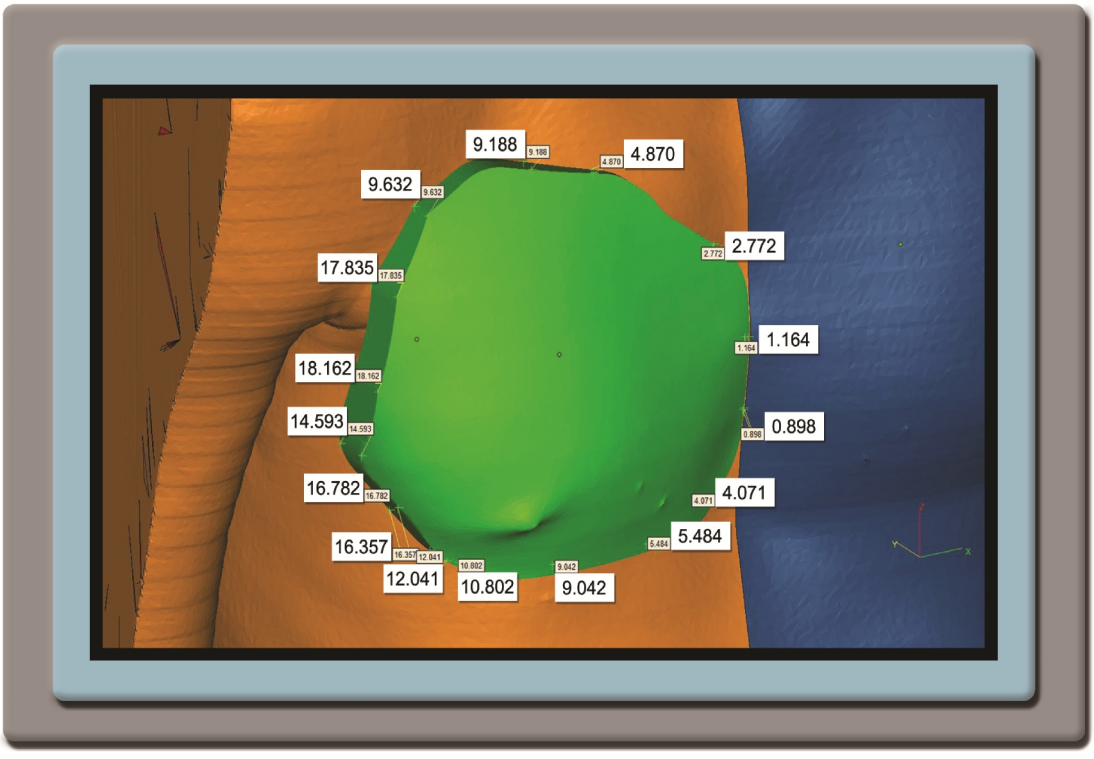

Figure 5.4 Model of *final 3D digital geometry* designed from the whole thorax in an *Angled view* using Magics.

Different views of the *final 3D-DG* model designed from the whole thorax provide a perspective of the model. Figures 5.5a-f demonstrates the *final 3D-DG* model of the pectoralis muscle in ten views using Magics, while Figures 5.5g-j depicts the geometry margin thicknesses of the model in mm.

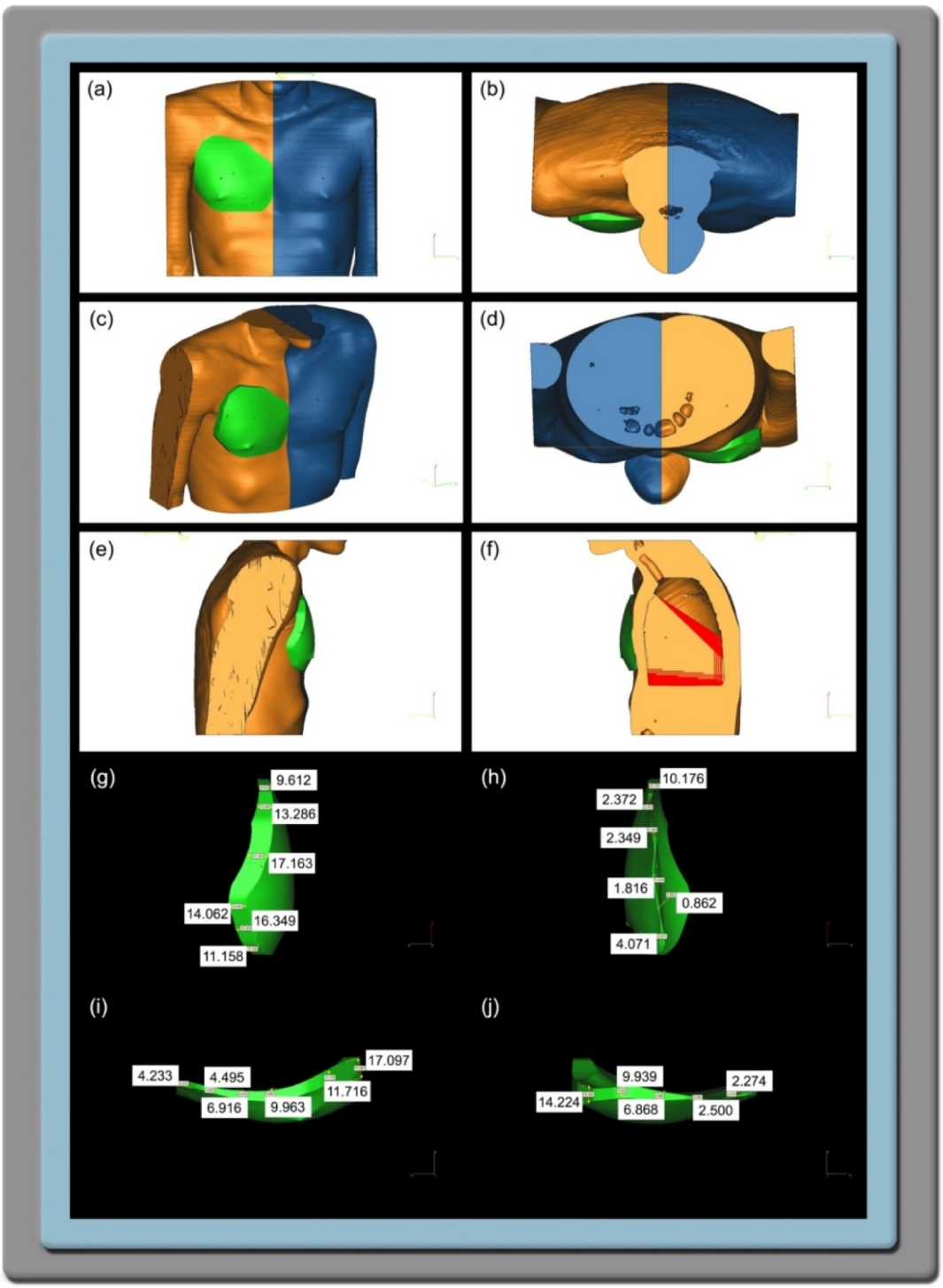

Figure 5.5 **Model of *final 3D digital geometry* designed from the whole thorax in ten different views using Magics.** (a) Thorax *Front view*, (b) Thorax *Top view*, (c) Thorax *Angle view*, (d) Thorax *Bottom view*, (e) Thorax *Left side view*, (f) Thorax

Right side view, (g) Margin thicknesses in *Left side view* in mm, (h) Margin thicknesses in *Right side view* in mm, (i) Margin thicknesses in *Bottom view* in mm, and (j) Margin thicknesses in *Top view* in mm.

In *Technique B* the pectoralis muscle was manipulated to design a *final 3D-DG* model by mirroring the isolated healthy pectoralis muscle onto the affected half of the thorax. Figure 5.6 demonstrates the *final 3D-DG* model designed from the pectoralis muscle in six views using Magics. Similarly to *Technique A,* the geometry margin thicknesses of the final isolated soft tissue model have been indicated in mm.

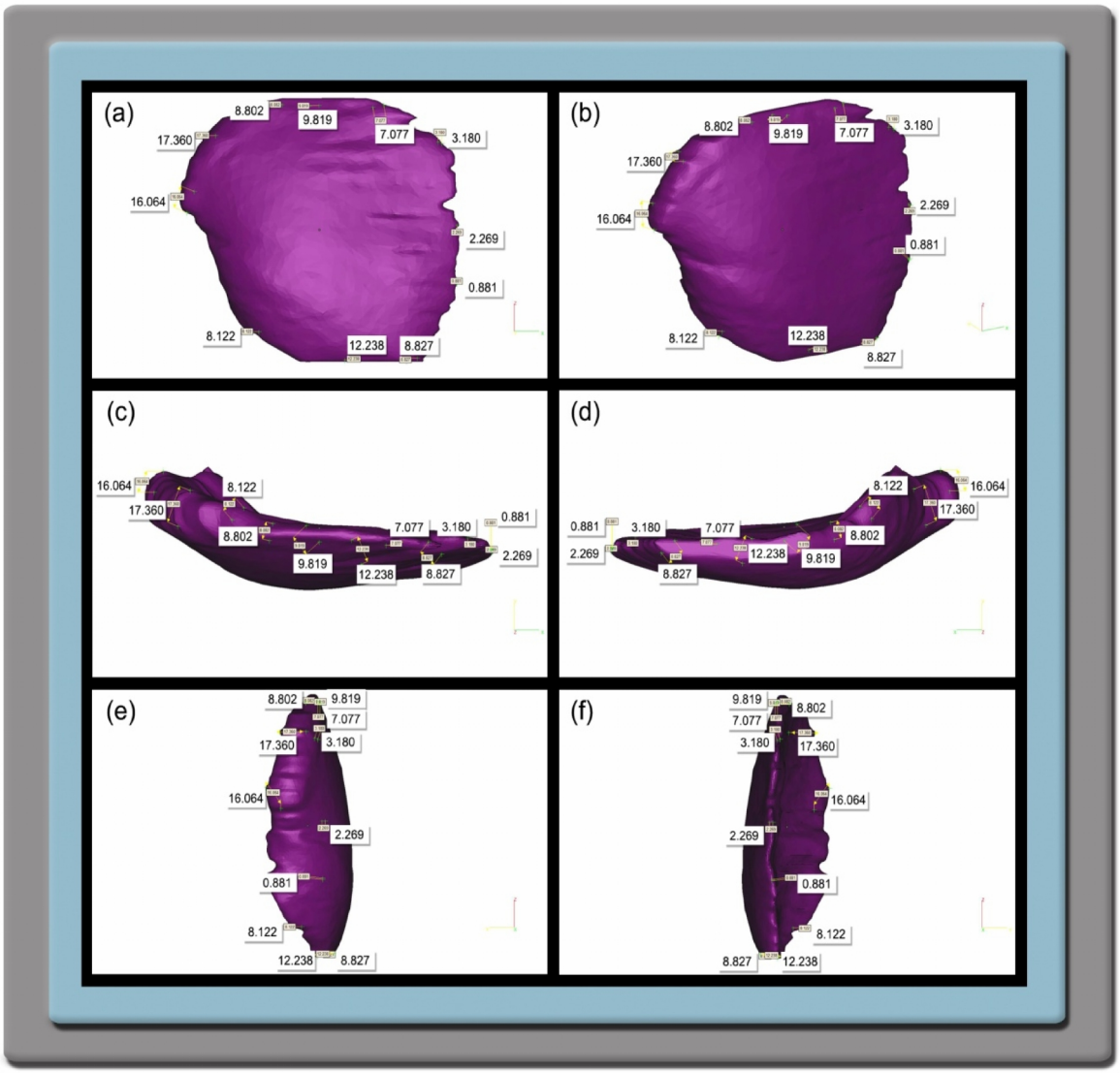

Figure 5.6 Model of *final 3D digital geometry* designed from the pectoralis muscle in six different views using Magics. (a) *Front view*, (b) *Angle view*, (c) *Top view*, (d) *Bottom view*, (e) *Left side view*, and (f) *Right side view*.

5.4.2 Digital data manipulation and design using Freeform® Modeling™

In *Technique A*, using Freeform® Modeling™, the whole thorax was subjected to similar steps as was used in *Technique A* with Magics. Figure 5.7 demonstrates the *final 3D-DG* model designed from the whole thorax in ten different views using Freeform® Modeling™.

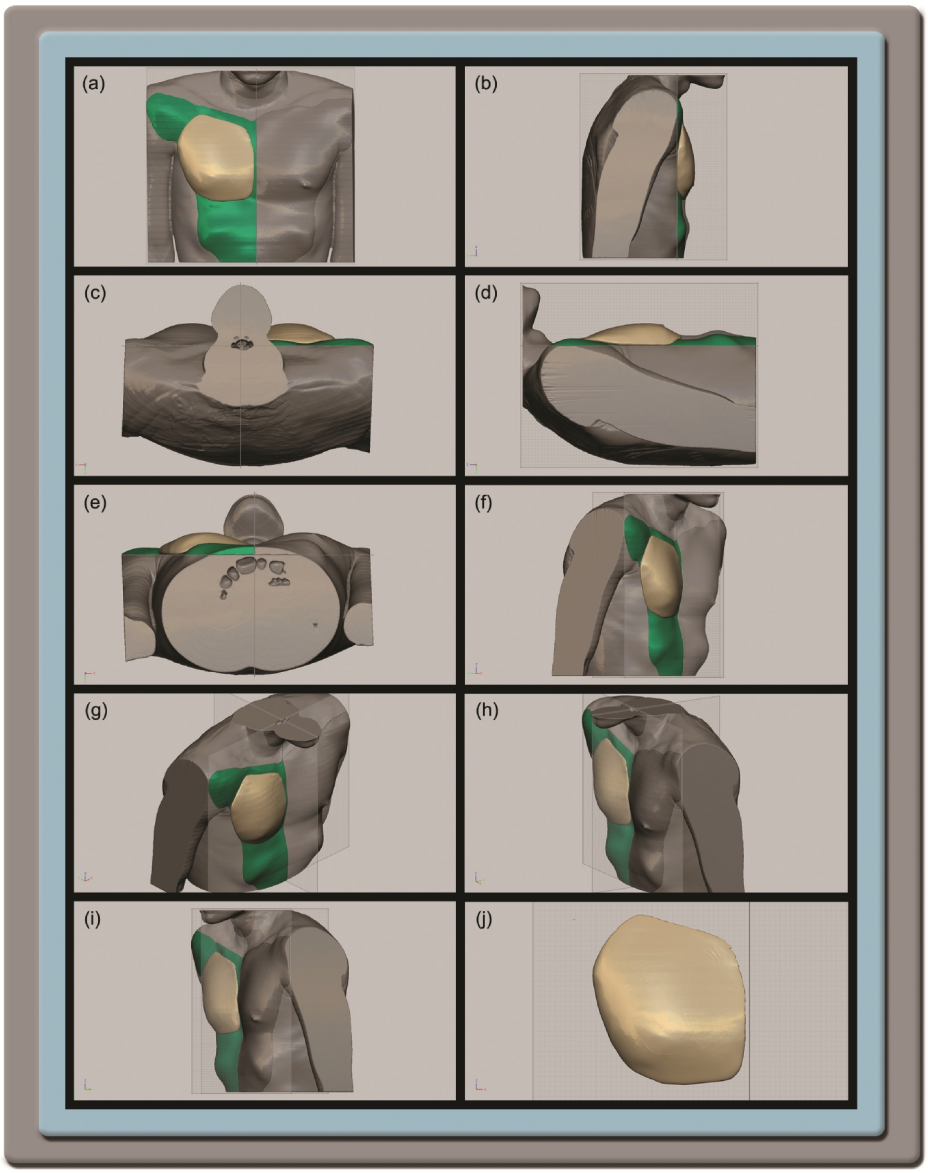

Figure 5.7 **Model of *final 3D digital geometry* designed from the whole thorax in ten different views using Freeform® Modeling™.** (a) *Front view*, (b) *Left side view*, (c) *Top view*, (d) *Right side view*, (e) *Bottom view*, (f) *Angle view* from the left side, (g) *Angle view* from the top-left side, (h) *Angle view* from the top-right side, (i) *Angle view* from the right side, and (j) The *final 3D digital model* of the pectoralis muscle.

In *Technique B*, the pectoralis muscle was manipulated to design a *final 3D-DG* model by mirroring the isolated healthy pectoralis muscle onto the affected half of the thorax and then further manipulating the geometry by means of tugging the muscle so that the space was filled by the newly designed *final 3D-DG* model. Figure 5.8 demonstrates the *final 3D-DG* model that was designed from the pectoralis muscle in six different views using Freeform® Modeling™.

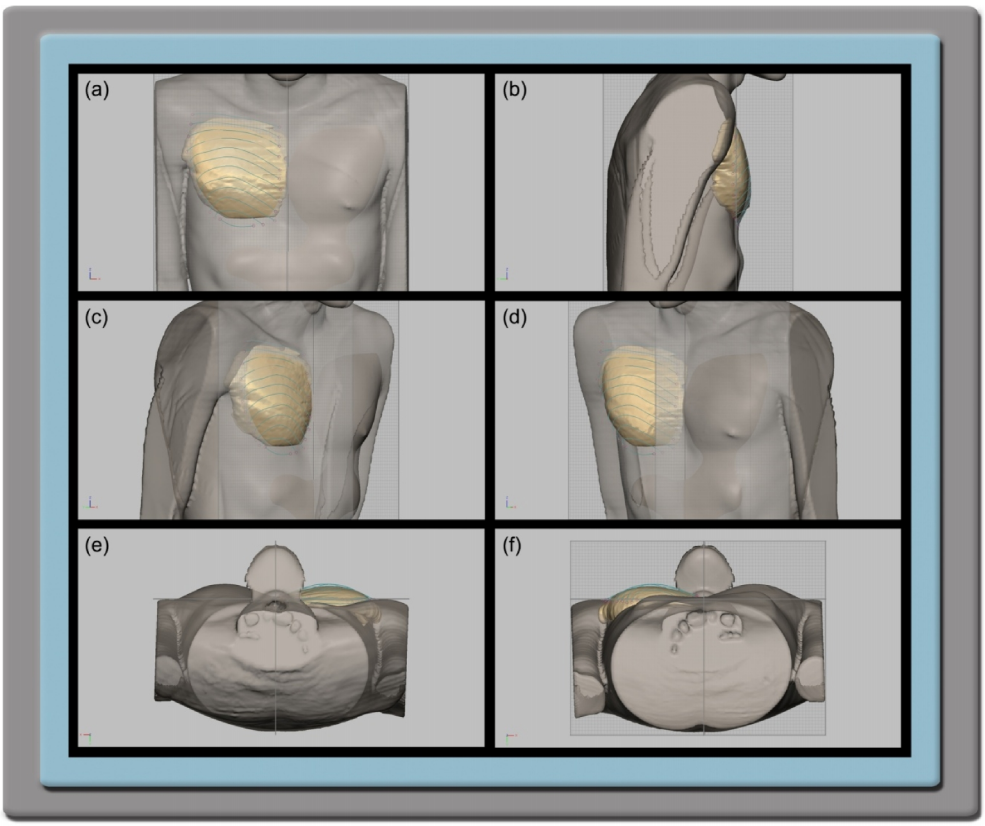

Figure 5.8 **Model of *final 3D digital geometry* designed from the pectoralis muscle in six different views using Freeform® Modeling™.** (a) *Front view*, (b) *Left side view*, (c) *Left angle view*, (d) *Right angle view*, (e) *Top view*, and (f) *Bottom view*.

5.5 Comparative analysis of the different models of the *final 3D digital geometries*

To obtain some understanding of how the different techniques performed, different comparative analyses were conducted, namely, a deviation analysis, an implant mass property analysis and a body conformation analysis. The four *final 3D-DG* models produced using the four techniques;

Technique A and *B* with Magics and *Technique A* and *B* with Freeform® Modeling™; were compared to constructed *digital test models*.

5.5.1 Deviation analysis

Similarly to Case Study 1, the software program Geomagic® Control™ allocated different numbers of deviation test points. The number of test points allocated to the models produced with Freeform® Modeling™ was approximately 10× more than those allocated for the Magics models. As was the case with Case Study 1, the overall outcome of the comparison was similar for all four techniques, where most of the deviation test points (more than 80%) fell within the nominated tolerance region of ≥-5 and ≤+5 mm showing a high level of alignment between the *final 3D-DG* models and the *digital test models.* The critical minus interval (≥-50 mm to <-5 mm) contained the next most number of deviation test points; ranging from 10% to 15%, while the critical plus interval (>5 mm to ≤50 mm) contained less than 2% of the deviation test points (Table 5.1).

Table 5.1 Comparison between *digital test models* and *final 3D digital geometry* models designed for the male patient with Poland's syndrome.

Deviation analysis criterion	Technique used to produce a *final 3D digital geometry* model			
	Magics *Technique A*	Magics *Technique B*	Freeform® Modeling™ *Technique A*	Freeform® Modeling™ *Technique B*
Number of data points	45582	47804	396627	525131
% (number) data points in the nominated tolerance interval	86 (38971)	83 (39861)	89 (351071)	88 (463566)
% (number) data points in the critical minus tolerance interval	13 (6055)	15 (7094)	11 (42142)	10 (54835)
% (number) data points in the critical plus tolerance interval	1.2 (556)	1.8 (849)	0.9 (3414)	1.3 (6730)
Standard deviation (mm)	5.12	5.28	4.26	3.75

The standard deviations revealed that both the Magics *Techniques A* and *B* produced *final 3D-DG* models with approximately 68% of the deviation test points falling within narrow intervals, similar to those of Case Study 1; -5.1 to +5.1 for Magics *Technique A* and -5.3 and +5.3 for Magics *Technique B* (Table 5.1). In contrast to Case Study 1, both the 68% intervals of Freeform® Modeling™ *Technique A* and *Technique B* were narrower than those of the Magics; -4.3 to +4.3 for Freeform® Modeling™ *Technique A* and -3.8 to +3.8 for Freeform® Modeling™ *Technique B*. Although the *Tug tool* was used to manipulate the 3D digital geometry model of the pectoralis muscle of the male patient in Freeform® Modeling™ *Technique B,* very little manipulation was employed because the male's deformed thoracic cavity was less extreme than that of the female Poland's syndrome patient.

Histograms were constructed to provide a visual perspective of the deviations of the *final 3D-DG* models from the *digital test models*. These histograms indicate that the vast majority of the deviation test points fell within the nominated tolerance interval of ≥-5 and ≤+5 mm (Figure 5.9).

(a)

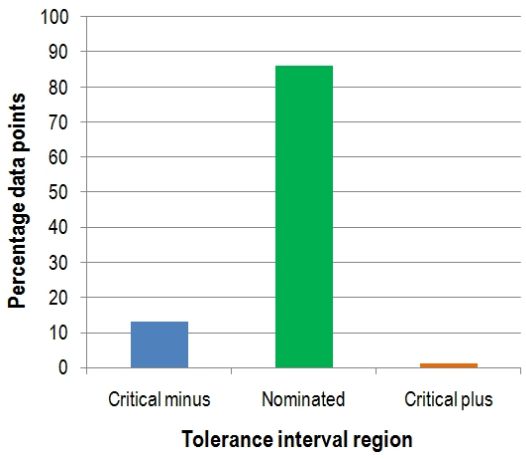

(b)

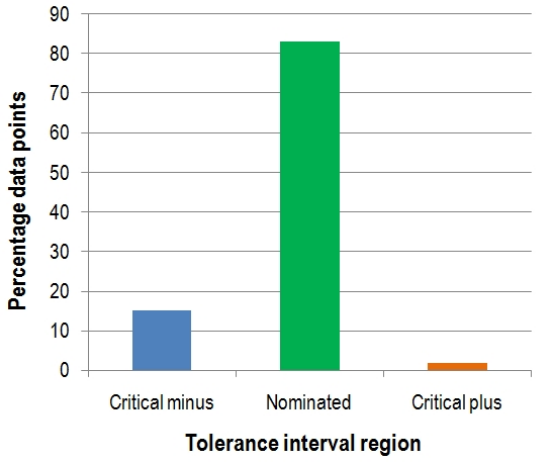

(c) (d)

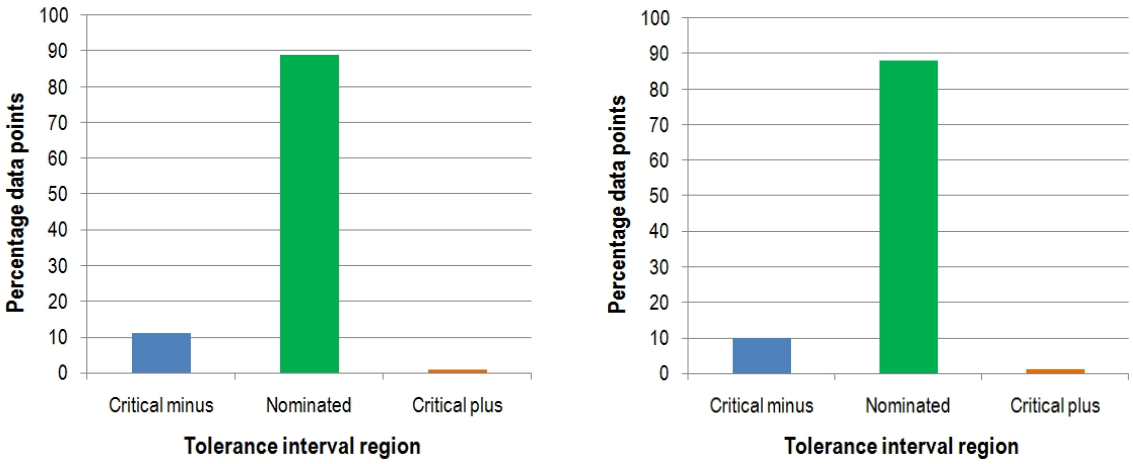

Figure 5.9 **Histograms showing percentage data points in different tolerance intervals using different techniques.** (a) Magics *Technique A*, (b) Magics *Technique B*, (c) Freeform® Modeling™ *Technique A*, and (d) Freeform® Modeling™ *Technique B*.

In contrast with Case Study 1, the colour deviation maps revealed that the different programs produced similar deviation maps. *Techniques A* and *B* of Magics and *Techniques A* and *B* of Freeform® Modeling™ showed similar aligned areas (green) between the produced *final 3D-DG* models and the *digital test models*, while the blue areas indicated were the produced *final 3D-DG* models were smaller than the *digital test model*s. Figure 5.10 shows frontal views of the deviation maps for all four techniques. Other views, including the frontal views, of the deviation maps are presented in Figure 5.11, Plate 1 (Magics *Technique A*), Plate 2 (Magics *Technique B*), Plate 3 (Freeform® Modeling™ *Technique A*), and Plate 4 (Freeform® Modeling™ *Technique B*) at the end of this chapter.

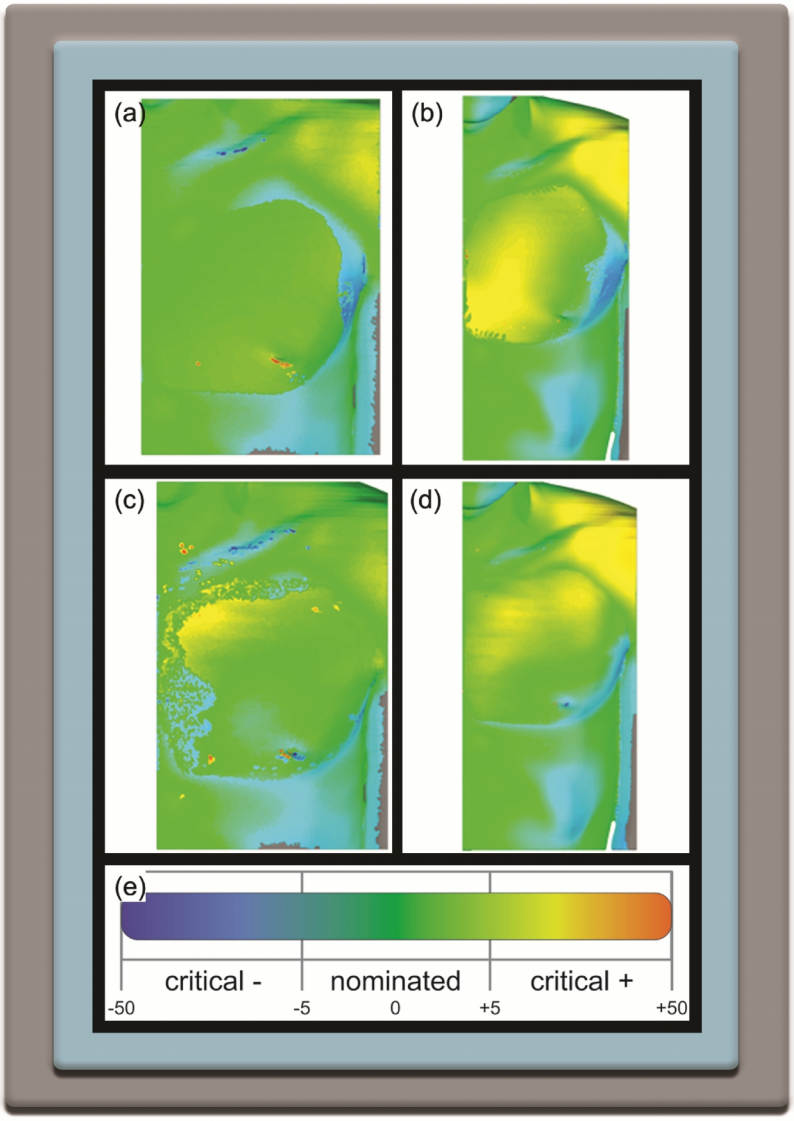

Figure 5.10 **Deviation colour maps showing the frontal views of the different techniques.** (a) Magics *Technique A*, (b) Freeform® Modeling™ *Technique A*, (c) Magics *Technique B*, (d) Freeform® Modeling™ *Technique B*, and (e) Tolerance intervals scale.

5.5.2 Implant mass property analysis

For the comparative analysis of the implant mass properties, the surface areas and volumes of the different *final 3D-DG* models of the pectoralis muscle were compared using Freeform® Modeling™. The model representing the original healthy pectoralis muscle was represented by the *final 3D-DG*

model produced using Magics *Techniques B,* because it was produced directly from the scanned digital imaging data set of the successive 2D images.

Similarly to Case Study 1, the results of the implant mass property analysis of the four *final 3D-DG* models of the pectoralis muscle were comparable. The surface areas of the four pectoralis muscles ranged from 43,000 to 54,000 mm^2, while the volumes ranged from 260,000 to 370,000 mm^3 (Table 5.2). The *final 3D-DG* model of the pectoralis muscle produced using Freeform® Modeling™ *Technique B* was closest in dimensions to that of the *original model* (Magics *Technique B*).

Table 5.2 Implant mass properties of the *final 3D digital geometry* models.

Implant mass property	Technique used to produce a *final 3D digital geometry* model			
	Magics *Technique A*	Magics *Technique B**	Freeform® Modeling™ *Technique A*	Freeform® Modeling™ *Technique B*
Surface area × 10^3 (mm^2)	43.125	50.276	44.928	53.625
Volume × 10^4 (mm^3)	28.082	34.850	26.345	36.222

* Represents the original healthy pectoralis muscle (original).

5.5.3 Body conformation analysis

A body conformation analysis was performed to ascertain to what extent the different techniques used to produce the *final 3D-DGs* had the potential to reconstruct the soft tissue deformities of the male Poland's syndrome patient. All four techniques produced dimensions relatively close to the *original body conformation* (Table 5.3). The body conformation properties of the *original body conformation* was, as expected, less than that of the *ideal body conformation*, because the *ideal body conformation* consists of a thorax with two healthy pectoralis muscles.

Table 5.3 **Body conformation mass properties of the *assembled models*, *original* and *ideal body conformation models*.**

Body conformation mass property	Original	Ideal	Technique used to produce a *final 3D digital* model			
			Magics *Technique A*	Magics *Technique B*	Freeform® Modeling™ *Technique A*	Freeform® Modeling™ *Technique B*
Surface area $\times 10^3$ (mm^2)	551.348	658.764	553.893	513.908	536.322	533.875
Volume $\times 10^4$ (mm^3)	2219.156	2131.744	2228.836	2237.628	2274.913	2272.853

5.6 Conclusion

Four different *final 3D-DGs* models of pectoralis muscles were produced for the male Poland's syndrome patient using a scanned digital imaging data set. These models were designed following four techniques using two different software programs. A comparison of these pectoralis muscle implant geometries revealed that the four design routes applied delivered similar results as for Case Study 1, with relatively small variation. It was thus not possible to select a preferred design route.

Figure 5.11 **Deviation colour maps of the four techniques.**

Plate 1. Magics *Technique A*. (a) *Isometric view*, (b) *Frontal view*, (c) *Left side view*, (d) *Right side view*, (e) *Top view*, and (f) *Bottom view*.

Plate 2. Magics *Technique B*. (a) *Isometric view*, (b) *Frontal view*, (c) *Left side view*, (d) *Right side view*, (e) *Top view*, and (f) *Bottom view*.

Plate 3. Freeform® Modeling™ *Technique A*. (a) *Isometric view*, (b) *Frontal view*, (c) *Left side view*, (d) *Right side view*, (e) *Top view*, and (f) *Bottom view*.

Plate 4. Freeform® Modeling™ *Technique B*. (a) *Isometric view*, (b) *Frontal view*, (c) *Left side view*, (d) *Right side view*, (e) *Top view*, and (f) *Bottom view*.

Plate 1

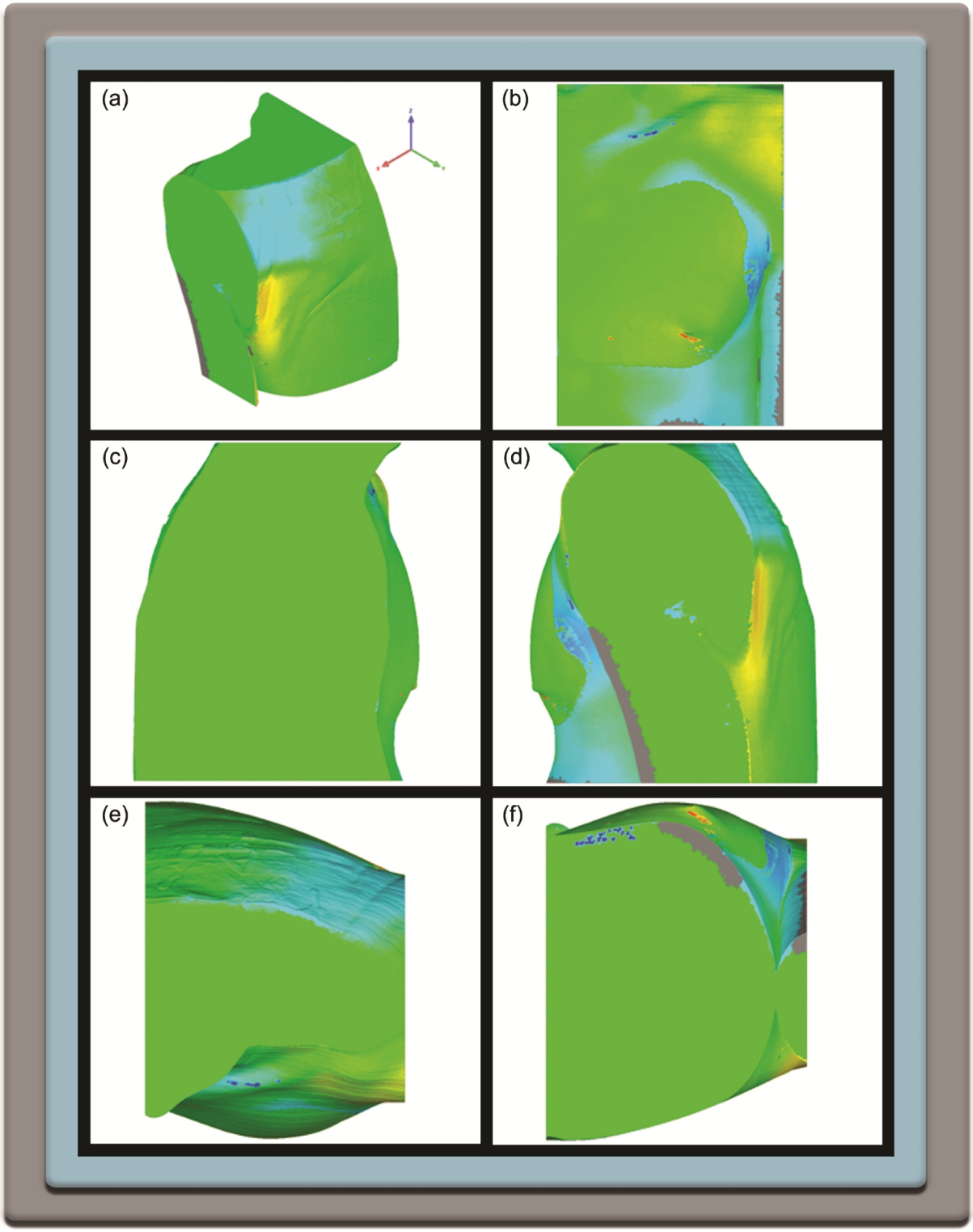

Plate 2

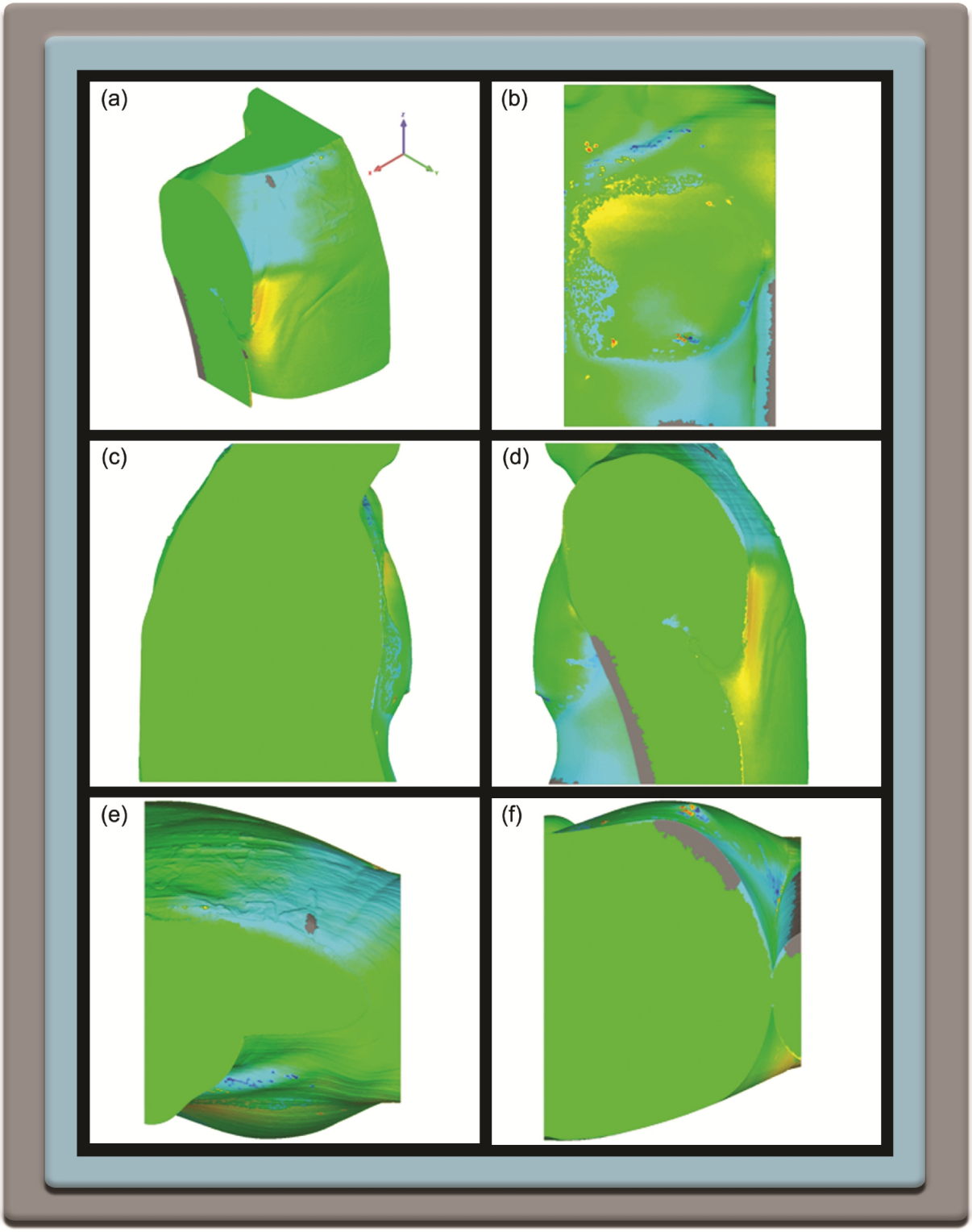

Plate 3

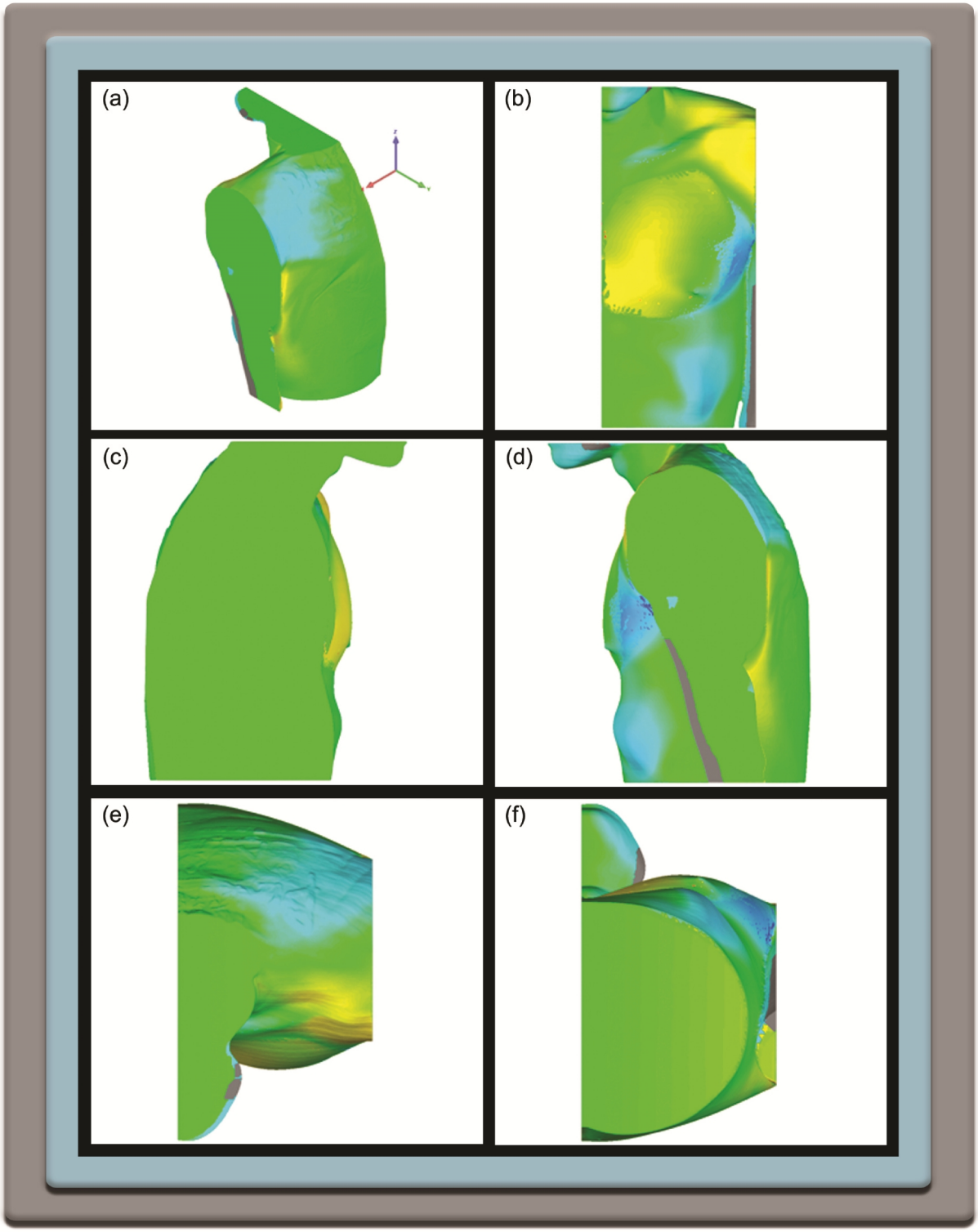

Plate 4

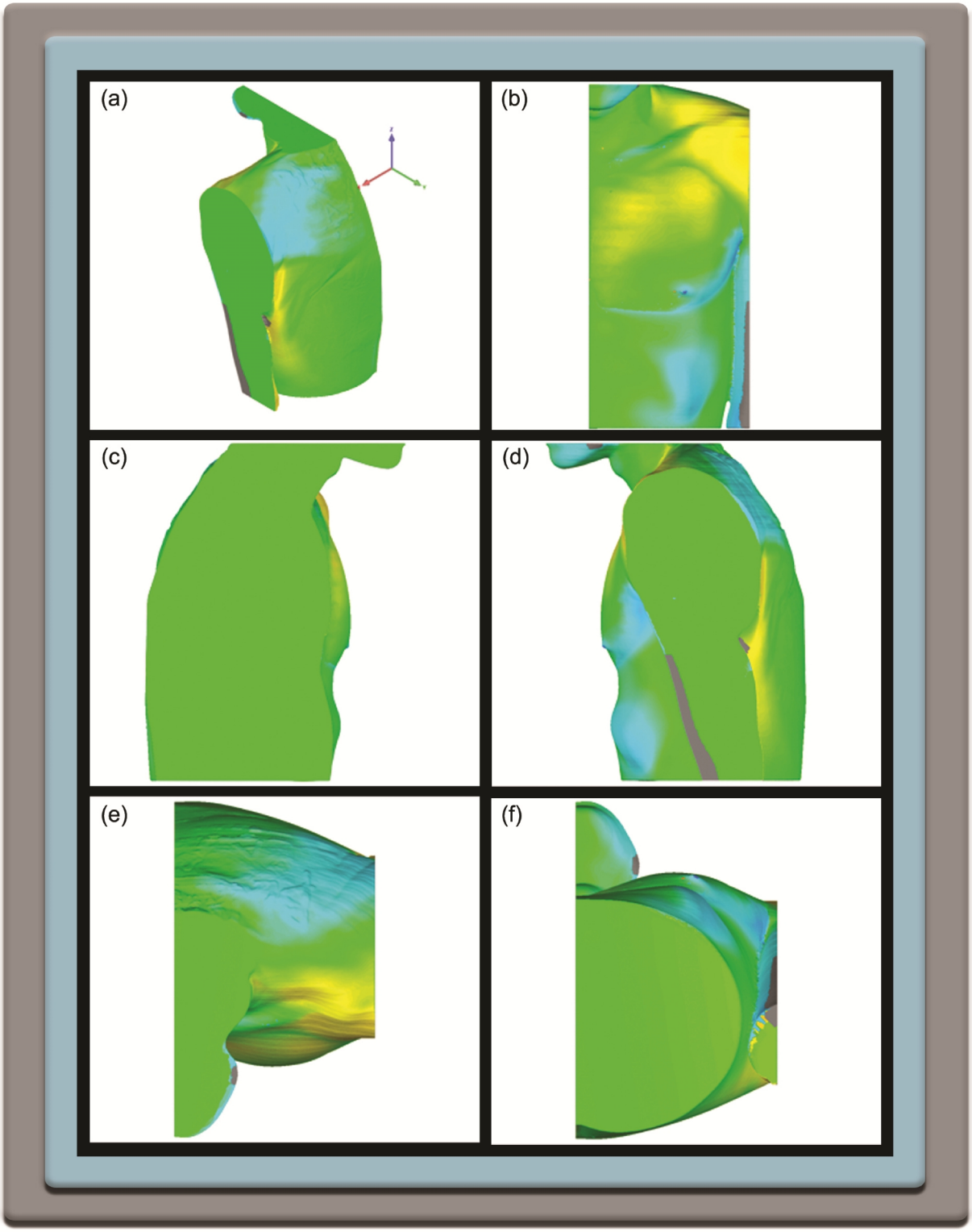

Chapter 6:
Discussion and Conclusions

6.1 Introduction

Poland's syndrome is a unilateral congenital defect displaying a wide variety of deformities mostly of soft tissues and the skeleton (Dustagheer et al. 2009; Gashegu et al. 2009; Baltayiannis et al. 2011; Majdak-Paredes et al. 2015). The severity of the deformities in Poland's syndrome patients vary from person to person, however, all the manifestations of the syndrome are rarely simultaneously present in one individual (Pereira et al. 2008; Urschel 2009; Lee et al. 2012; Al Faleh et al. 2014). The syndrome commonly affects the right side of the thorax and is more often found in males (Urschel 2009; Stylianos et al. 2012). Many Poland's syndrome patients display the absence of the pectoralis major muscle, although other muscles such as the pectoralis minor may also be affected (Lacorte et al. 2010). Poland's syndrome is also often associated with hand deformities of varying severities (Mentzel et al. 2002; Ersen et al. 2015).

Individuals affected by Poland's syndrome usually seek some or other medical intervention to improve their aesthetic appearance (Mathes et al. 2005; Pereira et al. 2008; Yadav et al. 2014), although full correction of the asymmetry is unattainable due to the complexity of the syndrome (Majdak-Paredes et al. 2015). Most of the interventions involve some or other surgical reconstruction, which is often invasive in nature requiring extended recovery times and may be rather traumatic for the patient (Urschel 2009). There is a constant search for less invasive and less traumatic approaches to the reconstruction of Poland's syndrome deformities.

In recent times it has been recognised that implants that are inserted surgically have the potential to improve the aesthetic contours and appearance of a Poland's syndrome patient. With the advances in medical modelling and the accompanying development of medical imaging technologies, design

technologies and manufacturing technologies it has become possible to produce custom-made prosthetic implants for more complex medical conditions.

This study was undertaken to design 3D digital geometries of soft tissue implants of pectoralis muscles for two Poland's syndrome patients. A female (Case Study 1) and a male (Case Study 2) patient were selected for this study, because females and males generally present with different manifestations of the deformities of the thoracic area (Chang & Kahn 2012).

The intention was that the geometries designed in this study could be used for the manufacturing of prototypes for implant production, although this step is beyond the scope of this study. Because of the novel nature of this study, the two software programs Magics and Freeform® Modeling™ were used to design soft tissue digital geometries for the two patients.

6.2 Comparison of Case Study 1 and Case Study 2

In this study, CT scanned digital imaging data sets were acquired for each of the two Poland's syndrome patients. These data sets were processed to create 3D digital geometries in STL file format using Mimics® software. The processing of these data sets involved a number of manipulations and pixel-by-pixel editing steps to isolate the regions of interest. The execution of these steps was time consuming in both instances, thereby contributing to a relatively lengthy development time of the 3D digital geometries.

In the design phase, two design routes were followed to design soft tissue digital geometries of the pectoralis muscle for each of the two patients. The one design route involved using a mirror image of the whole thorax (*Technique A*), while the other design route involved firstly the isolation of the pectoralis muscle from the healthy side of the thorax and thereafter producing a mirror image thereof (*Technique B*). These design routes were followed using both software programs Magics and

Freeform® Modeling™. This resulted in producing four different soft tissue digital geometries of the pectoralis muscle for each of the two patients.

Three different analyses were performed in an attempt to compare the outcomes of the different design routes and software programs. At close scrutiny, the deviation analysis, implant mass properties analysis and the body conformation analysis could not clearly differentiate between the different design routes or software programs with a reasonable margin. It was thus not possible to select definitively a preferred design route or software program. However, an attempt was made to select a design route and program based upon the analyses performed. The outcomes of the different performance criteria used in the deviation analysis of the two case studies were compared with one another. The criteria of the implant mass properties and a body conformation analyses were excluded from this comparison, because of a limited understanding of their true contribution to discriminate between the different performance outcomes. Table 6.1 provides the percentages of data points that occurred in the tolerance intervals found in the outcomes of the deviation analyses performed with the data of the two Poland's syndrome patients to facilitate the comparison of the performances of the two design software programs.

Table 6.1 Percentage data points in the tolerance intervals of the two Poland's syndrome patients.

Case Study	Tolerance interval (% data points)	Technique used to produce a *final 3D digital geometry* model			
		Magics *Technique A*	Magics *Technique B*	Freeform® Modeling™ *Technique A*	Freeform® Modeling™ *Technique B*
1	Nominated	78	73	82	78
	Critical minus	22	27	18	21
	Critical plus	0.400	0.070	0.007	0.800
	Standard deviation	4.78	5.32	3.78	7.22
2	Nominated	86	83	89	88
	Critical minus	13	15	11	10
	Critical plus	1.200	1.800	0.900	1.300
	Standard deviation	5.12	5.28	4.26	3.75

Four criteria of the deviation analysis were used to compare the performance outcomes of the design routes and software programs of the two case studies. The best performing design route and program were listed and compared (Table 6.2). For both case studies, the software program Freeform® Modeling™ produced the best results for all criteria. In Case Study 1, the technique involving the mirroring of the whole thorax (*Technique A*) emerged, overall, as the best technique to use to produce soft tissue digital geometries of the pectoralis muscle for the female patient. In contrast, Case Study 2 revealed a more ambiguous outcome. For the nominated tolerance interval the performance outcome was similar to that of Case Study 1. However, for the two critical tolerance intervals the outcomes were different. *Technique A* proved to produce a better outcome for the critical plus interval, while the isolation and mirroring of the pectoralis muscle, *Techniques B,* produced the better outcome for the critical minus interval. Although Freeform® Modeling™ displayed the lowest standard deviations; the variation in the size of the values was small. The range of the standard deviation for the female was 3.44 mm and for the male 1.53 mm, which is an

acceptable deviation for the medical practitioners (personal communication with a medical practitioner).

Table 6.2 Performance of the design software programs for Case Study 1 and Case Study 2.

Criterion	Case Study 1	Case Study 2
% (number) data points in the nominated tolerance interval	Freeform® Modeling™ *Technique A*	Freeform® Modeling™ *Technique A*
% (number) data points in the critical minus tolerance interval	Freeform® Modeling™ *Technique A*	Freeform® Modeling™ *Technique B*
% (number) data points in the critical plus tolerance interval	Freeform® Modeling™ *Technique A*	Freeform® Modeling™ *Technique A*
Standard deviation	Freeform® Modeling™ *Technique A*	Freeform® Modeling™ *Technique B*

6.3 Comparison of design software

In the past, the program Magics was exclusively used at the institute where this study was conducted for the development of medical geometries for soft tissue implants (Truscott et al. 2012). With the inception of this project, the software program Freeform® Modeling™ was purchased for design purposes of all types of models, including medical models. Because of a limited understanding of the versatility and ease-of-use of the program Freeform® Modeling™ at that time, it was used together with Magics in this project. It was thus deemed appropriate to ascertain how Magics and Freeform® Modeling™ performed in the design of digital geometries of pectoralis muscles for the Poland's syndrome patients. To this end a list of criteria were composed to compare different attributes of the two programs (Table 6.3). These criteria included software functionality, hardware possibilities, and geometry development time and software/hardware costs. It could be concluded that, in this study, Freeform® Modeling™ appeared to be the better suited software program for the designing of 3D digital geometries of soft tissue implants.

Table 6.3 Comparison of the design software programs.

Criterion	Description	3D modelling software	
		Magics	Freeform® Modeling™
Ease of user software interaction	The program is relatively easy to learn and to apply the diverse range of design tools effectively by an experienced software user.	Yes	Yes (some elements pose some difficulty)
Scope of design tools and tool options	The program allows the user to select from a variety of tools with a relatively large range of options.	Few	Many
Availability of multiple display views	The program can display a model from multiple angles simultaneously.	No	Yes
Versatility of order of workflow	The program allows the user to change and select the order of the workflow.	No	Yes
Possibility of fine refinement of a geometry	The program allows the user to refine geometries with design and sculpting tools.	Minimal	Yes
Availability of a high level sculpting device (haptic device)	The program allows for the attachment of a haptic device which creates a virtual environment of 'touching' virtual objects with which the user can interact with.	No	Yes
Length of geometry development time	The time that the user takes to design a 3D digital geometry for export for manufacturing purposes.	Relatively fast	Relatively slower because of more design steps
Availability of a help function that connects the user with developers	There are software specialists available to provide software assistance through a direct help link provided in the software.	Minimal	Yes
Cost of software	Cost to purchase the software.	Cheaper than Freeform® Modeling™ (22% cheaper)	Expensive (in the order of R150 000 with the PHANTOM® Omni™ haptic device)

Although Freeform® Modeling™ outperformed Magics in all the software functionality criteria, it should be recognised that the soft tissue geometries developed in this study using Freeform® Modeling™ were only marginally superior when compared to the soft tissue geometries developed using Magics. When attempting to estimate development times of the soft tissue geometry designs using the respective software programs, it was difficult because of the lengthy software learning component of the study. Limited knowledge in the use of particularly Freeform® Modeling™ existed in the department where this study took place at its commencement. This required an extensive manual-driven self-teaching process of Freeform® Modeling™ and to a lesser extent of Magics. Besides these limitations, it was possible to conclude that the design process using Freeform® Modeling™ was at least five times longer than the time spent using Magics. Furthermore, when considering the cost and shorter development time when using Magics, it may be an attractive option for individual users or in instances where design geometries are required for implants with relatively smooth and less intricate contours.

A major advantage of Freeform® Modeling™ is the possibility of using a haptic device. The device allows the user to move a hand-held stylus arm of the haptic device similarly to a pen or sculpting tool (Bibb 2006). The stylus arm can be used to manipulate solid, complex, shapes and forms in a 3D virtual space. A solid model in the virtual space can be ground away, stretched, pushed or added in a manner comparable to sculpting with clay (Eggbeer 2008). In Freeform® Modeling™, the haptic device and the range of tools provide for a versatile design environment, which allows a designer many design options (Petrovic et al. 2012). Other advantages include the wide range of viewing angles, the possibility to protect a model from inadvertent carving using a protective ‘mask’ or ‘buck’ setting, and a variety of virtual sculpting and modelling tools (Bibb et al. 2010).

6.4 Concluding remarks

This first attempt to produce 3D digital geometries of soft tissue implants for Poland's syndrome patients using, in particular, the software program Freeform® Modeling™, has proven to be successful. However, the final realisation of this research can only be appreciated once implants have been manufactured and tested in the real world. This will provide an understanding of how well these implants fit in patients and how easily the implants can be modified for a better fit.

This project has highlighted potential studies that can be conducted in the future. Particularly, studies to refine scanning parameters will facilitate the design process and could contribute to the shortening of development times. Also, the use of scanned images produced with magnetic resonance imaging technology in the design process needs consideration as it is known that these images differentiate soft tissue better than those of CT scans (Harih & Čretnik 2013; Pereira et al. 2014). Furthermore, in the evaluations of the observed data deviations, more studies are needed to determine to what extent the user and the software capabilities contribute to the deviations.

Evolving technologies in the fields of design, medicine and engineering, permits for interdisciplinary studies to be conducted and to create more accurate and more detailed project outcomes. The use of free-form computer-aided design programs together with advanced design skills have the potential to reduce the design and fabrication times of implants to hours or even minutes in the future. The integration of technologies such as computer-aided design, medical imaging, computer-aided manufacturing and computer-aided engineering in the field of medical modelling together with prospects of new developments could lead to significant improvements in treatment times, effectiveness and cost in the future.

References

Ahmad, M., Redondo, C.S. & Rodríguez, M.H., 2012. Moebius-Poland syndrome: A case report Síndrome Moebius-Poland: Reporte de un caso. *Salud Uninorte. Barranquilla*, 28(1), pp.171–177.

Akal, M. & Kara, M., 2002. The use of a homologous preserved costal cartilage in an infant with Poland's syndrome. *European Journal of Cardio-thoracic Surgery*, 21(1), pp.146–148.

Al Faleh, K., Al Saadi, M. & Khalid-Bantuas, S., 2014. Poland's Syndrome with Absent Limb Anomalies. *Journal of Clinical Neonatology*, 3(1), pp.44–46.

Al-Qattan, M.M., 2001. Classification of hand anomalies in Poland's syndrome. *British Journal of Plastic Surgery*, 54(2), pp.132–136.

Anchieta, M.V.M., Quaresma, M.M. & De Salles, F.A., 2011. Rapid Prototyping Applied to Maxillofacial Surgery. In M. E. Hoque, ed. *Advanced Applications of Rapid Prototyping Technology In Modern Engineering*. Brasilia: InTech, pp. 153–172.

ASTM International, 2012. Standard Terminology for Additive Manufacturing Technologies. *Edition F292-12a*.

Avci, G., Misirlioğlu, A., Eker, G. & Aköz, T., 2003. Mild Degree of Poland's Syndrome Reconstruction with Customized Silicone Prosthesis. *Aesthetic Plastic Surgery*, 27(2), pp.112–115.

Bai, S.-Z., Feng, Z.-H., Gao, R., Dong, Y., Bi, Y.-P., Wu, G.-F. & Chen, X., 2014. Development and application of a rapid rehabilitation system for reconstruction of maxillofacial soft-tissue defects related to war and traumatic injuries. *Military Medical Research*, 1(1), p.11.

Baltayiannis, N., Ifantidis, F., Gavressea, T., Papatheodorou, H., Kayianni, E. & Rizos, S., 2011. A very unusual case of poland syndrome with amastia-athelia and dextrocardia. *Hellenic Journal of Surgery*, 83(1), pp.33–38.

Baratte, A., Bodin, F., Del Pin, D., Wilk, A. & Bruant, C., 2011. Syndrome de Poland chez la femme: indications thérapeutiques en fonction du stade. À propos de 11 cas et revue de la littérature. *Annales de Chirurgie Plastique Esthétique*, 56(1), pp.33–42.

Benz, M., Laboureux, X., Maier, T., Nkenke, E., Seeger, S. & Neukam, F.W., 2002. The Symmetry of Faces Introduction 2 Computation of the Symmetry Plane. *Faces*.

Bertol, L.S., Da Silva, F.P. & Kindlein Junior, W., 2009. Design and health care: a study of virtual design and direct metal laser sintering of titanium alloy for the production of customized facial implants. *Australasian Medical Journal*, 1(11), pp.136–141.

Bibb, R., 2006. *Medical modelling: The application of advanced design and development techniques in medicine*, Cambridge England: Woodhead Publishing Limited.

Bibb, R., Eggbeer, D. & Evans, P., 2010. Rapid prototyping technologies in soft tissue facial prosthetics: current state of the art. *Rapid Prototyping Journal*, 16(2), pp.130–137.

Bibb, R., Thompson, D. & Winder, J., 2011. Computed tomography characterisation of additive manufacturing materials. *Medical Engineering & Physics*, 33(5), pp.590–596.

Bibb, R. & Winder, J., 2010. A review of the issues surrounding three-dimensional computed tomography for medical modelling using rapid prototyping techniques. *Radiography*, 16(1), pp.78–83.

Blanco, F.C., Elliott, S.T. & Sandler, A.D., 2011. Management of Congenital Chest Wall Deformities. *Seminars in Plastic Surgery*, 25(1), pp.107–116.

Bornet, G., 2013. *A Boole Anthology: Recent and Classical Studies in the Logic of George Boole* Volume 291. J. Gasser, ed., Springer Science & Business Media, 2013.

Bourell, D.L., Beaman, J.J., Leu, M.C. & Rosen, D.W., 2009. A Brief History of Additive Manufacturing and the 2009 Roadmap for Additive Manufacturing: Looking Back and Looking Ahead. *US-Turkey Workshop on Rapid Technologies*.

Campbell, I., Bourell, D. & Gibson, I., 2012. Additive manufacturing: rapid prototyping comes of age. *Rapid Prototyping Journal*, 18(4), pp.255–258.

Caouette-Laberge, L. & Borsuk, D., 2013. Congenital Anomalies of the Breast. *Seminars in Plastic Surgery*, 27(1), pp.36–41.

Çelik, A., Tülüce, K., Sayan, M. & Kurul, Í.C., 2011. A Rare Chest Wall Deformity; Poland Syndrome: Case Report. *Gazi Medical Journal*, 22(2), pp.49–51.

Chae, I.H., Kim, Y., Lee, S.W., Park, J.E., Shim, S.S. & Lee, J.H., 2014. Standard chest CT using combined automated tube potential selection and iterative reconstruction: image quality and radiation dose reduction. *Clinical Imaging*, 38(5), pp.641–647.

Chang, E. & Kahn, D.M., 2012. Congenital disorders of the breast. In Z. P. Seth Thaller, ed. *Aesthetic and Reconstructive Breast Surgery: Solving Complications and Avoiding Unfavorable Results*. CRC Press, p. 206.

Chen, C., Lu, J., Lu, X., Wu, W. & Han, W., 2012. Neurofibroma and Pectoralis Muscle Hypoplasia: A Mild Degree of Poland's Syndrome. *Breast Care*, 7(6), pp.490–492.

Chowdhury, M.K.S., Chakrabortty, R. & Gope, S., 2015. Poland 's syndrome : a case report and review of literature. *Journal of Pakistan Medical Association*, 65(1), pp.87–89.

Colombani, P.M., 2009. Preoperative Assessment of Chest Wall Deformities. *Seminars in Thoracic and Cardiovascular Surgery*, 21(1), pp.58–63.

Costa, S.D.S. & Blotta, R.M., 2012. The Omentum Flap. In M. Salgarello, ed. *Breast Reconstruction - Current Techniques*. p. 276.

Costa, S.D.S., Blotta, R.M., Mariano, M.B., Meurer, L. & Edelweiss, M.I.A., 2010a. Aesthetic Improvements in Poland's Syndrome Treatment with Omentum Flap. *Aesthetic Plastic Surgery*, 34(5), pp.634–639.

Costa, S.D.S., Blotta, R.M., Mariano, M.B., Meurer, L. & Edelweiss, M.I.A., 2010b. Laparoscopic treatment of Poland's syndrome using the omentum flap technique. *Clinics*, 65(4), pp.401–406.

Costantini, M., Cipriani, A., Belli, P., Bufi, E., Fubelli, R., Visconti, G., Salgarello, M. & Bonomo, L., 2013. Radiological findings in mammary autologous fat injections: A multi-technique evaluation. *Clinical Radiology*, 68(1), pp.27–33.

Cronskär, M., Rännar, L.-E. & Bäckström, M., 2012. Implementation of Digital Design and Solid Free-Form Fabrication for Customization of Implants in Trauma Orthopaedics. *Journal of Medical and Biological Engineering*, 32(2), pp.91–96.

Curcio, A., Giuricin, M., Lelli, D., Falcini, F., Nava, M.B. & Folli, S., 2009. Poland's syndrome and thoracic duct anomaly. *European Journal of Plastic Surgery*, 32(3), pp.155–156.

Dange, J.J., Mantha, S.S. & Deshmukh, S.P., 2014. Investigation and Estimation of Geometric Differences between the Left and Right distal Femur via 3D solid models Developed from CT Scans Using CAD tools. *International Journal of Mechanical Engineering and Computer Applications*, 2(1), pp.6 – 10.

Da Silva Freitas, R., Tolazzi, A.R.D., Martins, V.D.M., Knop, B.A., Graf, R.M. & De Oliveira e Cruz, G.A., 2007. Poland's Syndrome: Different Clinical Presentations and Surgical Reconstructions in 18 Cases. *Aesthetic Plastic Surgery*, 31(2), pp.140–146.

Da Silva Freitas, R., Tolazzi, A.R.D., Dos Santos, A.R., Graf, R.M. & De Oliveira e Cruz, G.A., 2009. Poland 's Syndrome. In M. A. Shiffman, ed. *Breast Augmentation*. Springer Berlin Heidelberg, pp. 345–358.

Dayal, S., Bhat, R. & Shankar, N., 2014. Complete unilateral right-sided absence of the pectoralis major and serratus anterior muscles in an adult male cadaver of South Indian origin. *Anatomical Science International*, 89(1), pp.53–56.

De Beer, D.J., Campbell, R.I., Truscott, M., Barnard, L.J. & Booysen, G.J., 2009. Client-centred design evolution via functional prototyping. *International Journal of Product Development*, 8(1), p.22.

Delay, E., Sinna, R., Chekaroua, K., Delaporte, T., Garson, S. & Toussoun, G., 2010. Lipomodeling of Poland's Syndrome: A New Treatment of the Thoracic Deformity. *Aesthetic Plastic Surgery*, 34(2), pp.218–225.

De Vos, A.S., Delport, C.S.L., Fouché, C.B. & Strydom, H., 2011. *Research at grass roots - for the social sciences and human service professions 4/e* 4th editio. D. V. A. Strydom H., Delport C.S.L., ed., Van Schaik Publishers.

Dingeldein, M.W., Lu, C.J., Kim, A.W., Ostric, S., Liptay, M.J. & Holterman, M.J., 2009. Simultaneous costal cartilage-sparing modified Ravitch procedure and latissimus dorsi transfer for chest wall deformity repair in Poland's syndrome. *Journal of Pediatric Surgery*, 44(1), pp.e29–e32.

Dolas, S.C., Poovamma, C.U., Prema, M., Khandelwal, R., Pais, A.V. & Kaul, A., 2014. Poland's syndrome : A case report with review of literature regarding management. *Breast Disease*, 34(3), pp.121–125.

Douze, M., Franco, J.-S. & Raffin, B., 2015. QuickCSG : Arbitrary and Faster Boolean Combinations of N Solids. *Research Report: RR-8687, Inria - Research Centre Greno- ble*, p.36.

Dustagheer, S., Basheer, M.H., Collins, A. & Hill, C., 2009. Further support for the vascular aetiology of Poland syndrome - a case report. *Journal of Plastic, Reconstructive and Aesthetic Surgery*, 62(10), pp.e360–e361.

Eggbeer, D., 2008. *The Computer Aided Design and Fabrication of Facial Prostheses*. University of Wales Institute, Cardiff.

Ersen, B., Kahveci, R., can Saki, M., Sahin, A., Tunali, O. & Aksu, I., 2015. A variant of Poland's syndrome: axillary web containing rudimentary pectoralis major muscle. *European Journal of Plastic Surgery*, 38(2), pp.161–162.

Evans, M., Wallace, D., Cheshire, D. & Sener, B., 2005. An evaluation of haptic feedback modelling during industrial design practice. *Design Studies*, 26(5), pp.487–508.

Feito, F.R., Ogayar, C.J., Segura, R.J. & Rivero, M.L., 2013. Fast and accurate evaluation of regularized Boolean operations on triangulated solids. *Computer-Aided Design*, 45(3), pp.705–716.

Feng, Z., Dong, Y., Zhao, Y., Bai, S., Zhou, B., Bi, Y. & Wu, G., 2010. Computer-assisted technique for the design and manufacture of realistic facial prostheses. *British Journal of Oral and Maxillofacial Surgery*, 48(2), pp.105–109.

Fijałkowska, M. & Antoszewski, B., 2011. Surgical treatment of patients with Poland's syndrome--own experience. *Polski Przeglad Chirurgiczny*, 83(12), pp.662–667.

Fletcher, J.G., Kofler, J.M., Coburn, J.A., Bruining, D.H. & McCollough, C.H., 2013. Perspective on radiation risk in CT imaging. *Abdominal Imaging*, 38(1), pp.22–31.

Fokin, A.A. & Robicsek, F., 2002. Poland's syndrome revisited. *Annals of Thoracic Surgery*, 74(6), pp.2218–2225.

Fokin, A.A., Steuerwald, N.M., Ahrens, W.A. & Allen, K.E., 2009. Anatomical, Histologic, and Genetic Characteristics of Congenital Chest Wall Deformities. *Seminars in Thoracic and Cardiovascular Surgery*, 21(1), pp.44–57.

Foucras, L., Grolleau-Raoux, J.L. & Chavoin, J.P., 2003. Syndrome de Poland: Série clinique de reconstructions thoraco-mammaires. À propos de 27 patients opérés. *Annales de Chirurgie Plastique Esthétique*, 48(2), pp.54–66.

Fox, CPT Justin P. & Seyfer, A.E., 2012. Setting the record straight: The real history of Poland's syndrome. *Bulletin of the American College of Surgeons*, 97(3), pp.27–29.

Fukushima, T., Otake, T., Yashima, R., Nihei, M., Takeuchi, S., Kimijima, I. & Tsuchiya, A., 1999. Breast Cancer in Two Patients with Poland's Syndrome. *Breast Cancer*, 6(2), pp.127–130.

Gashegu, J., Byiringiro, J.C., Nyundo, M., Uwineza, A. & Mutesa, L., 2009. Poland 's Syndrome : A Case Report. *East and Central African Journal of Surgery*, 14(2), pp.112–114.

Góes, J.C.S., 2010. Aesthetic Improvements in Poland's Syndrome Treatment with Omentum Flap.

Aesthetic Plastic Surgery, 34(5), pp.640–641.

Gopinath, B., Sangeetha, N., Nancy, J.S. & Umarani, T., 2015. Design and Implementation of High Speed Carry Select Adder. *International Journal of Engineering Research & Technology*, 4(2), pp.419–422.

Goyal, H., Naaz, F. & Gulati, R.K., 2014. Poland Syndrome : A Case Report. *PARIPEX - Indian Journal of Research*, 3(3), pp.126–127.

Gupta, R.K., Gupta, C.R. & Singh, D., 2003. An Unusual Presentation of Poland's Syndrome. *JK Science: Journal of Medical Education & Research*, 5(I), pp.38–39.

Hamburg, S.M., Oldenbeuving, N.B., Nicolai, J.P.A., Bauland, C.G. & Spauwen, P.H.M., 2002. Poland's syndrome: A review of 23 cases. *European Journal of Plastic Surgery*, 25(1), pp.1–6.

Harih, G. & Čretnik, A., 2013. Interdisciplinary Approach to Tool-Handle Design Based on Medical Imaging. *BioMed Research International*, 2013, p.8.

Hatamleh, M.M. & Watson, J., 2011. 3D Innovations of Cranioplasty Plate Construction: A Case Report. *Smile Dental Journal*, 6(2), pp.22–24.

Hodgkinson, D.J., 2009. Management of Anterior Chest Wall Deformity in Breast Augmentation. In M. A. Shiffman, ed. *Breast Augmentation*. Springer Berlin Heidelberg, pp. 333–343.

Hönig, J.F., 1999. Correction of Poland's syndrome in a male with solid chest wall implants. *European Journal of Plastic Surgery*, 22(2), pp.128–131.

Ji, J., Zhang, S., Shao, C., Xu, M., Chen, S., Lu, C., Wang, Z., Zhao, Z., Fan, X. & Tu, J., 2008. Poland's Syndrome Complicated with Breast Cancer: Mammographic, Ultrasonographic, and Computed Tomographic Findings. *Acta Radiologica*, 49(4), pp.387–390.

Jirásek, J.Š., Jirásková, G. & Szabari, A., 2015. Operations on Self-Verifying Finite Automata. In Lev D. Beklemishev & D. V. Musatov, eds. *Computer Science -Theory and Applications*. Listvyanka, Russia: Springer International Publishing, pp. 231–261.

Kamburoğlu, H.O., Sönmez, E., Aksu, A.E., Evrenos, M.K., Şafak, T. & Keçik, A., 2011. A Rare Poland Syndrome Deformity: Humero-Pectoral Band. *Journal of Hand and Microsurgery*, 3(1), pp.28–30.

Kanani, M., Elliott, M.J., Withey, S. & Pearl, R., 2015. Chest Wall Reconstruction. In S. C. Ross Farhadieh, Neil Bulstrode, ed. *Plastic and Reconstructive Surgery: Approaches and Techniques*. John Wiley & Sons, p. 1208.

Karatas, M.O., Cifter, E.D., Ozenen, D.O., Balik, A. & Tuncer, E.B., 2011. Manufacturing Implant Supported Auricular Prostheses by Rapid Prototyping Techniques. *European Journal of Dentistry*, 5(4), pp.472–477.

Kelly, R.E. & Shamberger, R.C., 2012. Congenital Chest Wall Deformities. In and R. S. Arnold G. Coran, Anthony Caldamone, N. Scott Adzick, Thomas M. Krummel, Jean-Martin Laberge, ed. *Pediatric Surgery, Volume 2*. Philadelphia: Elsevier Saunders, pp. 779–808.

Kerai, S., Saxena, K. & Taneja, B., 2014. Klippel–Feil syndrome and neuraxial anaesthesia. *Indian*

Journal of Anaesthesia, 58(3), pp.341–343.

Kim, M.S., Hansgen, A.R., Wink, O., Quaife, R.A. & Carroll, J.D., 2008. Rapid prototyping: A New Tool in Understanding and Treating Structural Heart Disease. *Circulation*, 117(18), pp.2388–2394.

King, I.C.C., Fung, V. & Dunkin, C.S.J., 2015. Concurrent Poland's syndrome and gynaecomastia: achieving the balance using lipomodelling. *European Journal of Plastic Surgery*, 38(3), pp.237–240.

Koizumi, T., Mitsukawa, N., Saiga, A. & Satoh, K., 2014. Clinical application of Nuss procedure for chest wall deformity in Poland syndrome. *Polish Journal of Cardio-Thoracic Surgery*, 11(4), pp.421–423.

Lacorte, D., Marsella, M. & Guerrini, P., 2010. A case of Poland Syndrome associated with dextroposition. *Italian Journal of Pediatrics*, 36(1), pp.21–23.

Lantzsch, T., Lampe, D. & Kantelhardt, E.J., 2013. Correction of Poland's Syndrome: Case Report and Review of the Current Literature. *Breast care (Basel, Switzerland)*, 8(2), pp.139–142.

Lee, S.H., Kim, J.B., Park, N.H., Keum, D.Y. & Kim, Y.H., 2012. Rare Combination of Dextrocardia with Right-Sided Poland Syndrome. *Annals of Thoracic Surgery*, 94(4), pp.e103–e104.

Legbo, J.N., 2006. Poland 's Syndrome : Report of a Variant. *Journal of the National Medical Association*, 98(1), pp.97–99.

Li, W., Zhang, L., Zhang, Q., Du, J., Zhang, S. & Liu, X., 2011. Poland Syndrome Associated with Ipsilateral Lipoma and Dextrocardia. *Annals of Thoracic Surgery*, 92(6), pp.2250–2252.

Liacouras, P., Garnes, J., Roman, N., Petrich, A. & Grant, G.T., 2011. Designing and manufacturing an auricular prosthesis using computed tomography, 3-dimensional photographic imaging, and additive manufacturing: A clinical report. *The Journal of Prosthetic Dentistry*, 105(2), pp.78–82.

Lieber, J., Kirschner, H.J. & Fuchs, J., 2012. Chest wall repair in Poland syndrome: complex single-stage surgery including Vertical Expandable Prosthetic Titanium Rib stabilization--a case report. *Journal of Pediatric Surgery*, 47(3), pp.e1–5.

Majdak-Paredes, E.J., Shafighi, M. & Fatah, F., 2015. Integrated algorithm for reconstruction of complex forms of Poland syndrome: 20-year outcomes. *Journal of Plastic, Reconstructive & Aesthetic Surgery*, 68(10), pp.1386–1394.

Materialise®, 2015. Mimics® Materialise®. *Mimics® Student Edition Course Book*, p.83. Available at: http://uc.materialise.com/mimics.

Mathes S.J.; Seyfer A.E. & Miranda E.P., 2005. Congenital Anomalies of the Chest Wall. In M. Stephen J. Mathes, MD and Vincent Rod Hentz, ed. *Plastic Surgery, Second Edition*. Philadelphia: Saunders, pp. 457–537.

Mazzoli, A., Germani, M. & Raffaeli, R., 2009. Direct fabrication through electron beam melting technology of custom cranial implants designed in a PHANToM-based haptic environment. *Materials & Design*, 30(8), pp.3186–3192.

Mcavinchey, G., Maxim, F., Nix, B., Djordjevic, J. & Linklater, R., 2014. The perception of facial asymmetry using 3-dimensional simulated images. , 84(6).

Mei, G., 2014. Summary on Several Key Techniques in 3D Geological Modeling. *The Scientific World Journal*, 2014, p.11.

Mei, G. & Tipper, J.C., 2013. Simple and Robust Boolean Operations for Triangulated Surfaces. *arXiv*, pp.1–18.

Mentzel, H.-J., Seidel, J., Sauner, D., Vogt, S., Fitzek, C., Zintl, F. & Kaiser, W.A., 2002. Radiological aspects of the Poland syndrome and implications for treatment: a case study and review. *European Journal of Pediatrics*, 161(8), pp.455–459.

Meyer-Marcotty, P., Alpers, G.W., Gerdes, A.B.M. & Stellzig-Eisenhauer, A., 2010. Impact of facial asymmetry in visual perception: A 3-dimensional data analysis. *American Journal of Orthodontics and Dentofacial Orthopedics*, 137(2), pp.168.e1–168.e8.

Meyer-Marcotty, P., Stellzig-Eisenhauer, A., Bareis, U., Hartmann, J. & Kochel, J., 2011. Three-dimensional perception of facial asymmetry. *European Journal of Orthodontics*, 33(6), pp.647–653.

Mirhosseini, S.A., Mirhosseini, S.M.M., Bidaki, R. & Boshrabadi, A.P., 2013. Sprengel deformity and Klippel-Feil syndrome leading to cervical myelopathy presentation in old age. *Journal of Research in Medical Sciences*, 18(6), pp.526–528.

Moir, C.R. & Johnson, C.H., 2008. Poland's syndrome. *Seminars in Pediatric Surgery*, 17(3), pp.161–166.

Monsour, P.A. & Dudhia, R., 2008. Implant radiography and radiology. *Australian Dental Journal*, 53(1), pp.S11–S25.

Moslehifard, E., 2011. Computer Aided Techniques Developed for Diagnosis and Treatment Planning in Implantology. In P. I. Turkyilmaz, ed. *Implant Dentistry – The Most Promising Discipline of Dentistry*. InTech, pp. 409 – 436.

Nishibayashi, A., Tomita, K., Yano, K. & Hosokawa, K., 2013. Correction of complex chest wall deformity in Poland's syndrome using a modified Nuss procedure. *Journal of Plastic, Reconstructive & Aesthetic Surgery*, 66(2), pp.e53–e55.

Nuss, D. & Kelly, R.E., 2009. Chest Wall Deformities. In P. Puri & M. Höllwarth, eds. *Pediatric Surgery: Diagnosis and Management*. Berlin: Springer Berlin Heidelberg, pp. 247–256.

Nuss, D. & Kelly, R.E., 2010. Congenital Chest Wall Deformities. In G. W. Holcomb, P. Murphy, & D. J. Ostlie, eds. *Ashcraft's Pediatric Surgery*. Philadelphia: Saunders Elsevier, pp. 249–265.

Okamoto, H., Miura, K., Yamane, T., Fujii, H. & Matsumoto, Y., 2002. Invasive Ductal Carcinoma of the Breast Associated with Poland's Syndrome: Report of a Case. *Surgery today*, 32(3), pp.257–260.

Ortiz, J.A., 2014. Poland's Breast Reconstruction With Decellularized Human Dermal Allograft. *Military Medicine*, 179(2), pp.e249–e252.

Pereira, G.C., Traughber, M. & Muzic, R.F., 2014. The Role of Imaging in Radiation Therapy Planning: Past, Present, and Future. *BioMed Research International*, 2014, p.9.

Pereira, L.H., Sabatovich, O., Santana, K.P., Picanço, R. & Sterodimas, A., 2008. Surgical correction of Poland's syndrome in males - a purposely designed implant. *Journal of Plastic, Reconstructive & Aesthetic Surgery : JPRAS*, 61(4), pp.393–399.

Petrovic, V., Haro, J.V., Blasco, J.R. & Portolés, L., 2012. Additive Manufacturing Solutions for Improved Medical Implants. In D. C. Lin, ed. *Biomedicine*. Spain: InTech, pp. 147–180.

Pinsolle, V., Chichery, A., Grolleau, J.-L. & Chavoin, J.P., 2008. Autologous fat injection in Poland's syndrome. *Journal of Plastic, Reconstructive and Aesthetic Surgery*, 61(7), pp.784–791.

Poland, A., 1841. Deficiency of the Pectoral Muscles. In George H. Barlow and James P. Babington, ed. *Guy's Hospital Reports*. London, pp. 191 – 193.

Poullis, M., 2010. Modified Nuss repair for pectus carinatum. *Interactive Cardiovascular and Thoracic Surgery*, 11(3), pp.221–222.

Rahmati, S., Abbaszadeh, F. & Farahmand, F., 2012. An improved methodology for design of custom-made hip prostheses to be fabricated using additive manufacturing technologies. *Rapid Prototyping Journal*, 18(5), pp.389 – 400.

Ram, A.N. & Chung, K.C., 2009. Poland's syndrome: Current Thoughts in the Setting of a Controversy. *Plastic and Reconstructive Surgery*, 123(3), pp.949–953.

Raval, J., Nagaraja, V., Burgess, D., Eshoo, S., Sadick, N. & Denniss, A.R., 2013. A Rare Association of Pulmonary Hypertension and Dextrocardia with Poland Syndrome. *Heart, Lung and Circulation*, 22(9), pp.778–780.

Romanini, M.V., Vidal, C., Godoy, J. & Morovic, C.G., 2013. Laparoscopically harvested omental flap for breast reconstruction in Poland syndrome. *Journal of Plastic, Reconstructive & Aesthetic Surgery*, 66(11), pp.e303–e309.

Salmi, M., Tuomi, J., Paloheimo, K.-S., Björkstrand, R., Paloheimo, M., Salo, J., Kontio, R., Mesimäki, K. & Mäkitie, A.A., 2012. Patient specific reconstruction with 3D modeling and DMLS additive manufacturing. *Rapid Prototyping Journal*, 18(3), pp.209–214.

Sameuls, T.H., Haider, M.A. & Peter, K., 1995. Poland's Syndrome: A Mammographic Presentation. *American Journal of Roentgenology*, 166(2), pp.347–348.

Saour, S., Shaaban, H., McPhail, J. & McArthur, P., 2008. Customised silicone prostheses for the reconstruction of chest wall defects: technique of manufacture and final outcome. *Journal of Plastic, Reconstructive & Aesthetic Surgery*, 61(10), pp.1205–1209.

Scott, J., Gupta, N., Weber, C., Newsome, S., Wohlers, T. & Caffrey, T., 2012. Additive manufacturing: Status and opportunities. *Science and Technology Policy Institute*, (March), pp.1–29.

Shamberger, R.C., 1996. Congenital chest wall deformities. *Current Problems in Surgery*, 33(6), pp.469–542.

Sharma, A., Singh, H.P. & Sharma, S., 2013. Case Report: An unusual case report showing overlapping Features of Poland and Moebius syndrome. *American Journal of Advances in Medical Science*, 1(1), pp.28–32.

Shimamura, J., Kubota, H., Endo, H., Tsuchiya, H., Kawashima, N. & Sudo, K., 2012. Three-Dimensional Replica of a Life-Sized Model of Aortic Arch Aneurysm for Preoperative Assessments. *Annals of Thoracic Surgery*, 93(5), pp.1699–1702.

Sinna, R., Delay, E., Garson, S., Delaporte, T. & Toussoun, G., 2010. Breast fat grafting (lipomodelling) after extended latissimus dorsi flap breast reconstruction: A preliminary report of 200 consecutive cases. *Journal of Plastic, Reconstructive and Aesthetic Surgery*, 63(11), pp.1769–1777.

Sood, A. & Ahuja, N., 2010. Interesting Case Series: Chest Wall Reconstruction in Male Poland Syndrome. *Eplasty*, 10.

Stylianos, K., Constantinos, P., Alexandros, T., Aliki, F., Nikolaos, A., Demetriou, M. & Petros, P., 2012. Muscle abnormalities of the chest in Poland's syndrome: variations and proposal for a classification. *Surgical and Radiologic Anatomy*, 34(1), pp.57–63.

Swergold, N., Sridharan, P., Loukas, M. & Chamberlain, R.S., 2013. Advances in the management of pectus deformities in children. *Open Journal of Pediatrics*, 3(3), pp.211–223.

Tagarakis, G.I., Karangelis, D., Tsantsaridou, A., Tsolaki, F., Daskalopoulos, M.E., Hevas, A., Kyriakaki, K., Stamoulis, K., Lampoura, S. & Tsilimingas, N.B., 2011. Poland's syndrome and recurrent pneumothorax: is there a connection? *Journal of Cardiothoracic Surgery*, 6(1), pp.32–33.

The American Heritage® Dictionary of the English Language, 2011. *The American Heritage® Dictionary of the English Language* 5th edition., Houghton Mifflin Harcourt.

Tomkinson, G.R. & Olds, T.S., 2000. Physiological Correlates of Bilateral Symmetry in Humans. *International Journal of Sports Medicine*, 21(8), pp.545–550.

Truscott, M., Booysen, G. & De Beer, D., 2012. Additive Manufacturing of Soft Tissue Geometries for Reconstruction Purposes. In T. M. D. F. Paulo Jorge Bártolo, Ana Cristina Soares de Lemos, Ana Patrícia Oliveira Tojeira, António Mário Henriques Pereira, Artur Jorge Mateus, Ausenda Luís Avelar Mendes, Cyril dos Santos, Dino Miguel Fernandes Freitas, Helena Maria Bártolo, Henrique de, ed. *Innovative Developments in Virtual and Physical Prototyping*. London: Taylor and Francis Group, pp. 139–144.

Tukuru, N., Gowda, S., Ahmed, S.M. & Badami, S., 2008. Rapid Prototype Technique in Medical Field. *Research Journal of Pharmacy and Technology*, 1(4), pp.341–344.

Tvrdek, M., Kletenský, J. & Svaboda, S., 2001. Aplasia of the breast--reconstruction using a free tram flap. *Acta Chirurgiae Plasticae*, 43(2), pp.39–41.

Uludag, M., Cece, H., Incebiyik, S., Demirkol, A., Karakas, E. & Akgun, K., 2011. Scapular winging in Poland syndrome. *Clinics (Sao Paulo, Brazil)*, 66(5), pp.929–930.

Urschel, H.C., 2009. Poland Syndrome. *Seminars in Thoracic and Cardiovascular Surgery*, 21(1), pp.89–94.

Ursyn, A., 2015. Handbook of Research on Maximizing Cognitive Learning through Knowledge. In A. Ursyn, ed. *Handbook of Research on Maximizing Cognitive Learning through Knowledge Visualization*. IGI Global, p. 600.

Van der Poorten, E.B., Demeester, E. & Lammertse, P., 2012. Haptic feedback for medical applications , a survey. *Actuator*, pp.1–6.

Viegas, V.N., Dutra, V., Pagnoncelli, R.M. & De Oliveira, M.G., 2010. Transference of virtual planning and planning over biomedical prototypes for dental implant placement using guided surgery. *Clinical Oral Implants Research*, 21(3), pp.290–295.

Wang, C.-S., Wang, W.-H.A. & Lin, M.-C., 2010. STL rapid prototyping bio-CAD model for CT medical image segmentation. *Computers in Industry*, 61(3), pp.187–197.

Wu, J., Tse, R., Heike, C.L., Shapiro, L.G. & Children, S., 2011. Learning to Compute the Plane of Symmetry for Human Faces Categories and Subject Descriptors.

Yadav, G.K., Lal, S., Dange, N., Marwah, K.G. & Singh, J.P., 2014. Poland 's Syndrome with Unusual Hand and Chest Anomalies: A Rare Case Report. *The Indian Journal of Chest Diseases & Allied Sciences*, 56(3), pp.191–194.

Yang, H. & Lee, H., 2011. Successful Use of Squeezed-Fat Grafts to Correct a Breast Affected by Poland Syndrome. *Aesthetic Plastic Surgery*, 35(3), pp.418–425.

Yen, T.-C., Visvikis, D., Pan, T. & Fang, Y.-H.D., 2014. Biomedical Imaging : Role and Opportunities of Medical Imaging in the "' Omics '" Era. *BioMed Research International*, 2014, pp.2–4.

Yesilada, A.K., Sevim, K.Z., Sirvan, S.S., Karsidag, S. & Tatlidede, H.S., 2013. Our Surgical Approach to Treatment of Congenital, Developmental, and Acquired Breast Asymmetries: A Review of 30 Cases. *Aesthetic Plastic Surgery*, 37(1), pp.77–87.

Yiyit, N., Işıtmangil, T. & Öksüz, S., 2015. Clinical analysis of 113 patients with Poland syndrome. *The Annals of Thoracic Surgery*, 99(3), pp.999–1004.

Yiyit, N., Işitmangil, T. & Saygin, H., 2014a. Eight Patients with Multiple Bilateral Thoracic Anomalies: A New Syndrome or Bilateral Poland's Syndrome? *Annals of Thoracic Surgery*, 97(5), pp.1758–1763.

Yiyit, N., Işıtmangil, T. & Öztürker, C., 2014b. The abnormalities of trapezius muscle might be a component of Poland's syndrome. *Medical Hypotheses*, 83(5), pp.533–536.

Zhang, F., Qi, X., Xu, Y., Zhou, Y., Zhang, Y., Fan, L., Zhong, L., Yang, X. & Jiang, J., 2011. Breast Cancer and Poland's Syndrome: A Case report and literature review. *The Breast journal*, 17(2), pp.196–200.

Zhu, L., Zeng, A., Wang, X., Liu, Z. & Zhang, H., 2012. Poland's syndrome in women: 24 cases study and literature review. *Chinese Medical Journal*, 125(18), pp.3283–3287.

Appendixes

Appendixes containing an extraction of the total *Geomagic Control Report* generated with Geomagic® Control™. The extractions consist of three pages of the approximate 40 pages of each deviation analysis report for the female and male Poland's syndrome patients.

Appendix 1: Deviation analysis reports of female Poland's syndrome patient.

A: Deviation analysis report for Magics, *Technique A*.

B: Deviation analysis report for Magics, *Technique B*.

C: Deviation analysis report for Freeform® Modeling™, *Technique A*.

D: Deviation analysis report for Freeform® Modeling™, *Technique B*.

Appendix 2: Deviation analysis reports of male Poland's syndrome patient.

A: Deviation analysis report for Magics, *Technique A*.

B: Deviation analysis report for Magics, *Technique B*.

C: Deviation analysis report for Freeform® Modeling™, *Technique A*.

D: Deviation analysis report for Freeform® Modeling™, *Technique B*.

Geomagic Control™

Appendix 1: A

Geomagic Control Report

Date Inspected: 7/7/2015

Date Generated: 7/7/2015, 1:48 pm

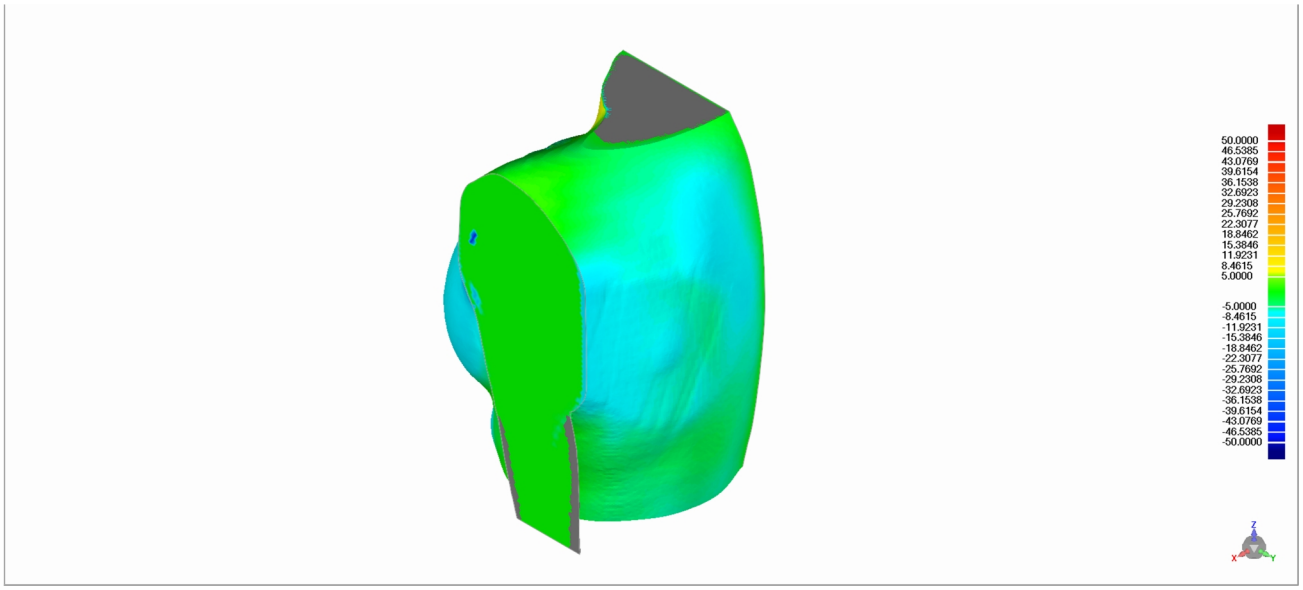

Author: cpotgiet:CPOTGIETPC2

Client Name: 3D Systems, Inc.

Reference Model: FWTPI

Test Model: FWTPI_Mirror

3D Comparison Results

Reference Model	FWTPI
Test Model	FWTPI_Mirror
No. of Data Points	91524
# Outliers	27

Tolerance Type	3D Deviation
Units	mm
Max. Critical	50.0000
Max. Nominal	5.0000
Min. Nominal	-5.0000
Min. Critical	-50.0000

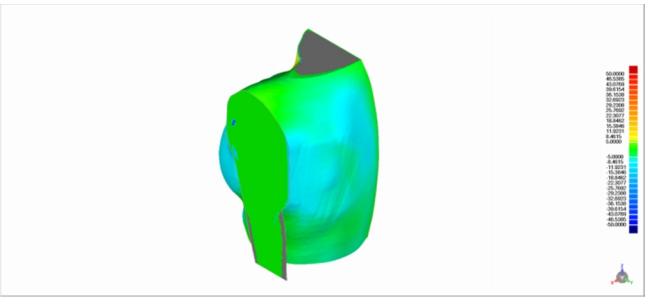

Deviation	
Max. Upper Deviation	49.2837
Max. Lower Deviation	-47.3255
Average Deviation	1.4389 / -4.7686
Standard Deviation	4.7800

Deviation Distribution

>=Min	<Max	# Points	%
-50 0000	-46 5385	6	0 0066
-46 5385	-43 0769	38	0 0415
-43 0769	-39 6154	37	0 0404
-39 6154	-36.1538	15	0 0164
-36.1538	-32 6923	41	0 0448
-32 6923	-29 2308	30	0 0328
-29 2308	-25.7692	17	0 0186
-25.7692	-22 3077	24	0 0262
-22 3077	-18 8462	305	0 3332
-18 8462	-15 3846	433	0.4731
-15 3846	-11 9231	740	0 8085
-11 9231	-8.4615	3370	3 6821
-8.4615	-5.0000	15161	16.5651
-5.0000	5.0000	68582	74.9334
5.0000	8.4615	2386	2 6070
8.4615	11 9231	18	0 0197
11 9231	15 3846	16	0 0175
15 3846	18 8462	13	0 0142
18 8462	22 3077	9	0 0098
22 3077	25.7692	15	0 0164
25.7692	29 2308	1	0 0011

Deviation Distribution

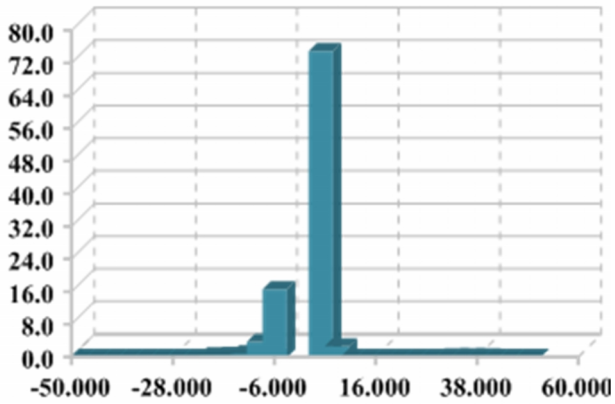

29 2308	32 6923	76	0 0830
32 6923	36.1538	83	0 0907
36.1538	39 6154	90	0 0983
39 6154	43 0769	4	0 0044
43 0769	46 5385	7	0 0076
46 5385	50 0000	7	0 0076

Out of Upper Critical	0	0 0000
Out of Lower Critical	0	0 0000

Standard Deviations

Distribution (+/-)	# Points	%
-6 * Std. Dev.	184	0.2010
-5 * Std. Dev.	99	0.1082
-4 * Std. Dev.	564	0.6162
-3 * Std. Dev.	946	1.0336
-2 * Std. Dev.	10232	11.1796
-1 * Std. Dev.	25712	28.0932
1 * Std. Dev.	46260	50.5441
2 * Std. Dev.	7120	7.7794
3 * Std. Dev.	88	0.0961
4 * Std. Dev.	19	0.0208
5 * Std. Dev.	16	0.0175
6 * Std. Dev.	284	0.3103

Standard Deviations

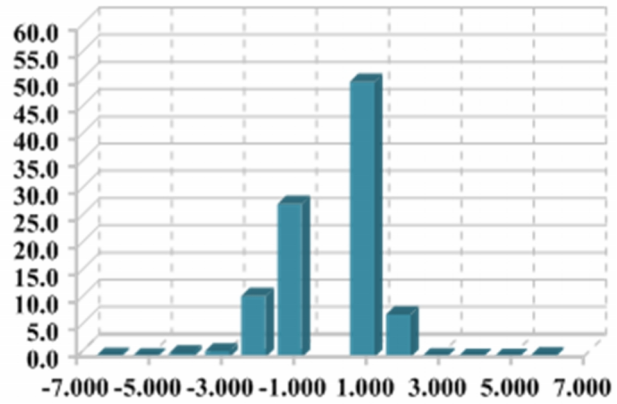

Geomagic Control™

Appendix 1: B

Geomagic Control Report

Date Inspected: 7/7/2015

Date Generated: 7/7/2015, 1:43 pm

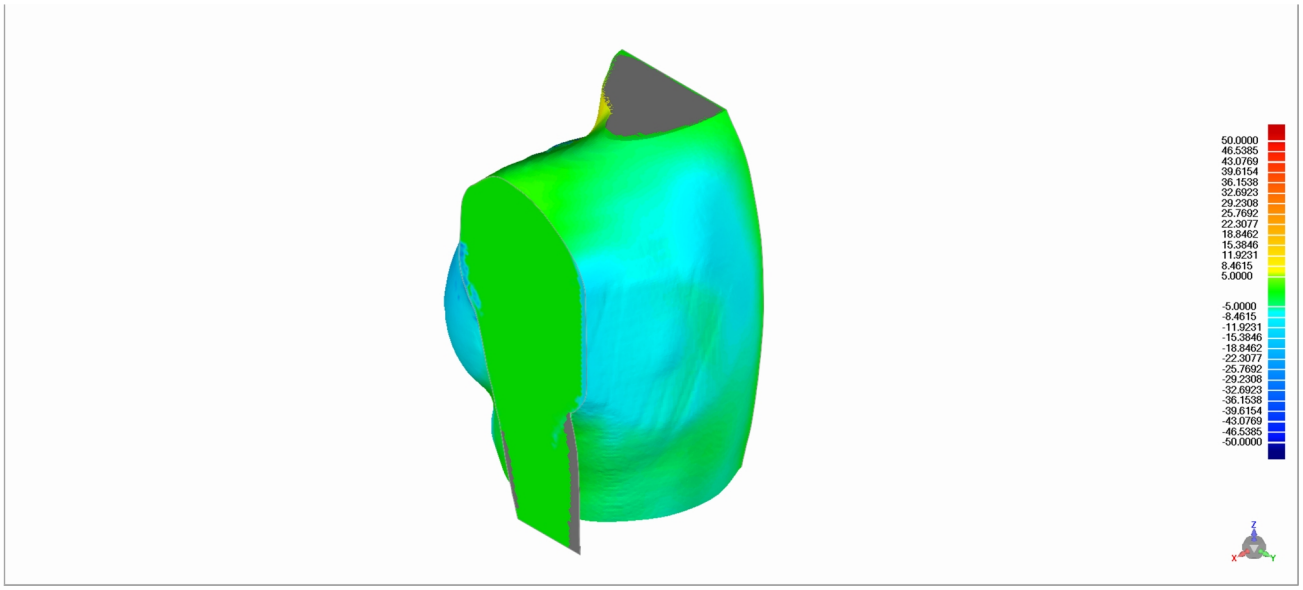

Author: cpotgiet:CPOTGIETPC2

Client Name: 3D Systems, Inc.

Reference Model: FPI

Test Model: FPI_Mirror

3D Comparison Results

Reference Model	FPI
Test Model	FPI_Mirror
No. of Data Points	64729
# Outliers	1646

Tolerance Type	3D Deviation
Units	mm
Max. Critical	50.0000
Max. Nominal	5.0000
Min. Nominal	-5.0000
Min. Critical	-50.0000

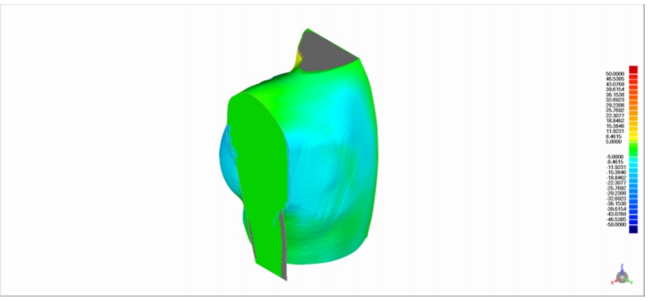

Deviation	
Max. Upper Deviation	33.4880
Max. Lower Deviation	-49.8563
Average Deviation	0.9819 / -5.5737
Standard Deviation	5.3224

Deviation Distribution

>=Min	<Max	# Points	%
-50 0000	-46 5385	14	0 0216
-46 5385	-43 0769	24	0 0371
-43 0769	-39 6154	12	0 0185
-39 6154	-36.1538	14	0 0216
-36.1538	-32 6923	8	0 0124
-32 6923	-29 2308	15	0 0232
-29 2308	-25.7692	16	0 0247
-25.7692	-22 3077	359	0 5546
-22 3077	-18 8462	740	1.1432
-18 8462	-15 3846	1219	1 8832
-15 3846	-11 9231	2393	3 6970
-11 9231	-8.4615	3100	4.7892
-8.4615	-5.0000	9654	14.9145
-5.0000	5.0000	45814	70.7782
5.0000	8.4615	1305	2 0161
8.4615	11 9231	32	0 0494
11 9231	15 3846	1	0 0015
15 3846	18 8462	0	0 0000
18 8462	22 3077	0	0 0000
22 3077	25.7692	8	0 0124
25.7692	29 2308	0	0 0000

Deviation Distribution

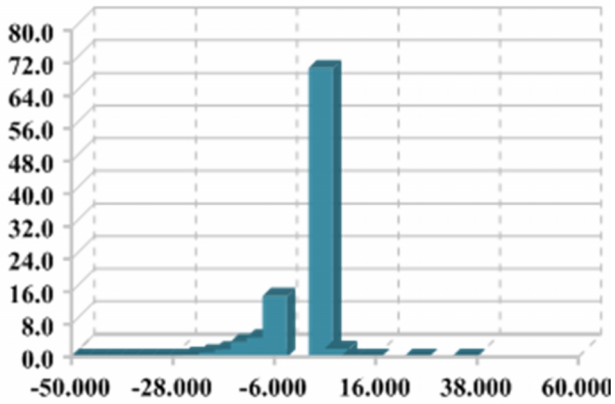

29 2308	32 6923	0	0 0000
32 6923	36.1538	1	0 0015
36.1538	39 6154	0	0 0000
39 6154	43 0769	0	0 0000
43 0769	46 5385	0	0 0000
46 5385	50 0000	0	0 0000

Out of Upper Critical	0	0 0000
Out of Lower Critical	0	0 0000

Standard Deviations

Distribution (+/-)	# Points	%
-6 * Std. Dev.	87	0.1344
-5 * Std. Dev.	21	0.0324
-4 * Std. Dev.	1053	1.6268
-3 * Std. Dev.	2366	3.6552
-2 * Std. Dev.	4450	6.8748
-1 * Std. Dev.	17506	27.0451
1 * Std. Dev.	35147	54.2987
2 * Std. Dev.	3950	6.1024
3 * Std. Dev.	139	0.2147
4 * Std. Dev.	1	0.0015
5 * Std. Dev.	2	0.0031
6 * Std. Dev.	7	0.0108

Standard Deviations

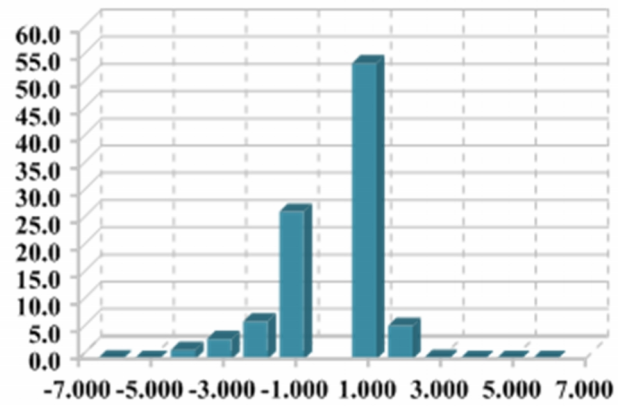

Appendix 1: C

Geomagic Control Report

Date Inspected: 7/7/2015

Date Generated: 7/7/2015, 1:36 pm

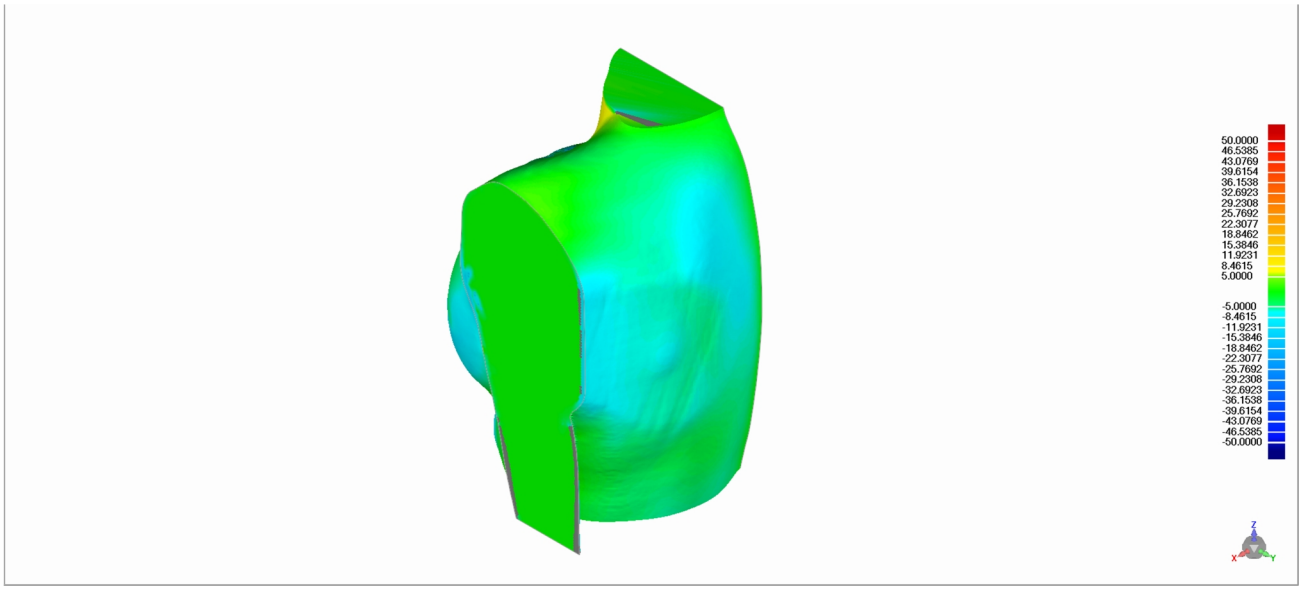

Author: cpotgiet:CPOTGIETPC2

Client Name: 3D Systems, Inc.

Reference Model: FWTPI 2

Test Model: FWTPI 2_Mirror

3D Comparison Results

Reference Model	FWTPI 2
Test Model	FWTPI 2_Mirror
No. of Data Points	178194
# Outliers	2738

Tolerance Type	3D Deviation
Units	mm
Max. Critical	50.0000
Max. Nominal	5.0000
Min. Nominal	-5.0000
Min. Critical	-50.0000

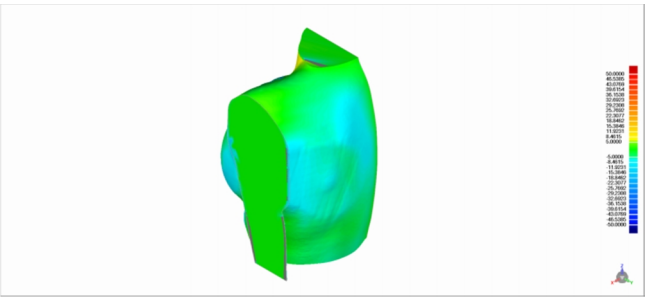

Deviation	
Max. Upper Deviation	43.9845
Max. Lower Deviation	-49.5605
Average Deviation	0.7999 / -4.1893
Standard Deviation	3.7821

Deviation Distribution

>=Min	<Max	# Points	%
-50 0000	-46 5385	16	0 0090
-46 5385	-43 0769	25	0 0140
-43 0769	-39 6154	28	0 0157
-39 6154	-36.1538	27	0 0152
-36.1538	-32 6923	18	0 0101
-32 6923	-29 2308	7	0 0039
-29 2308	-25.7692	14	0 0079
-25.7692	-22 3077	17	0 0095
-22 3077	-18 8462	367	0 2060
-18 8462	-15 3846	938	0 5264
-15 3846	-11 9231	2323	1 3036
-11 9231	-8.4615	4757	2 6696
-8.4615	-5.0000	23420	13.1430
-5.0000	5.0000	143590	80.5807
5.0000	8.4615	2634	1.4782
8.4615	11 9231	0	0 0000
11 9231	15 3846	0	0 0000
15 3846	18 8462	0	0 0000
18 8462	22 3077	5	0 0028
22 3077	25.7692	5	0 0028
25.7692	29 2308	0	0 0000

Deviation Distribution

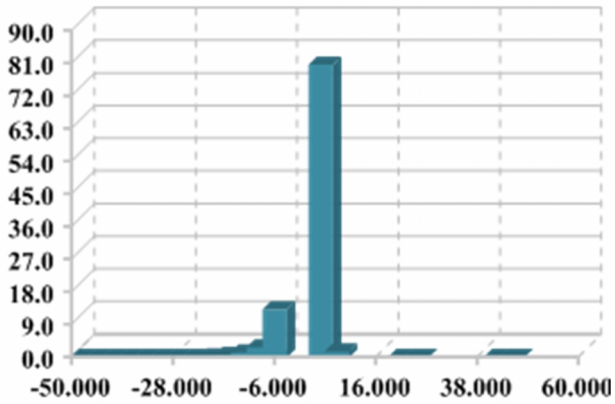

29 2308	32 6923	0	0 0000
32 6923	36.1538	0	0 0000
36.1538	39 6154	0	0 0000
39 6154	43 0769	1	0 0006
43 0769	46 5385	2	0 0011
46 5385	50 0000	0	0 0000

Out of Upper Critical	0	0 0000
Out of Lower Critical	0	0 0000

Standard Deviations

Distribution (+/-)	# Points	%
-6 * Std. Dev.	271	0.1521
-5 * Std. Dev.	575	0.3227
-4 * Std. Dev.	1919	1.0769
-3 * Std. Dev.	3536	1.9844
-2 * Std. Dev.	16824	9.4414
-1 * Std. Dev.	48957	27.4740
1 * Std. Dev.	93880	52.6842
2 * Std. Dev.	10207	5.7280
3 * Std. Dev.	2012	1.1291
4 * Std. Dev.	0	0.0000
5 * Std. Dev.	0	0.0000
6 * Std. Dev.	13	0.0073

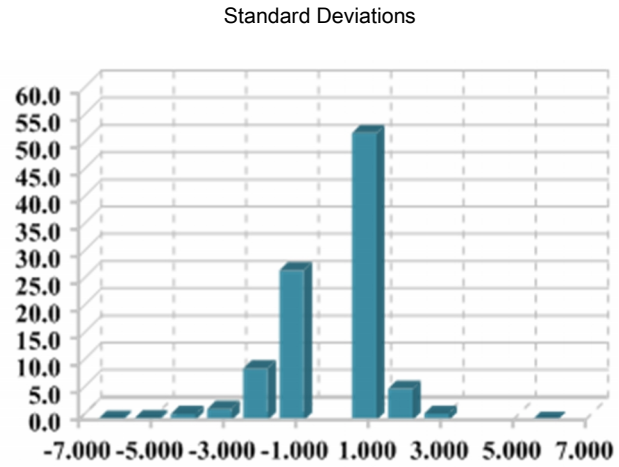

Appendix 1: D

Geomagic Control Report

Date Inspected: 7/7/2015

Date Generated: 7/7/2015, 12:25 pm

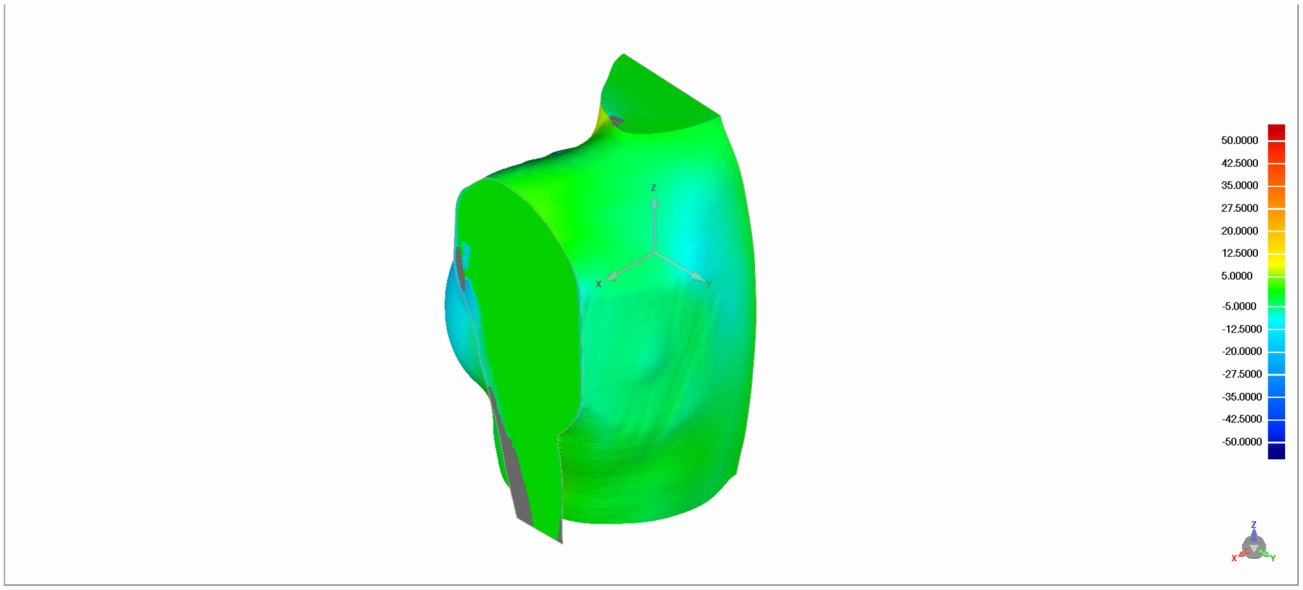

Author: cpotgiet:CPOTGIETPC2

Client Name: 3D Systems, Inc.

Reference Model: FPI 2

Test Model: FPI 2_Mirror

3D Comparison Results

Reference Model	FPI 2
Test Model	FPI 2_Mirror
No. of Data Points	184957
# Outliers	5891

Tolerance Type	3D Deviation
Units	mm
Max. Critical	50.0000
Max. Nominal	5.0000
Min. Nominal	-5.0000
Min. Critical	-50.0000

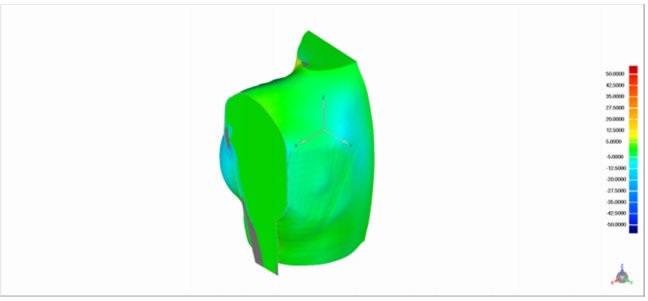

Deviation	
Max. Upper Deviation	49.9857
Max. Lower Deviation	-49.9915
Average Deviation	1.6643 / -6.0430
Standard Deviation	7.2189

Deviation Distribution

>=Min	<Max	# Points	%
-50 0000	-42 5000	663	0 3585
-42 5000	-35 0000	604	0 3266
-35 0000	-27 5000	551	0 2979
-27 5000	-20 0000	3460	1 8707
-20 0000	-12 5000	9884	5 3439
-12 5000	-5.0000	23704	12.8160
-5.0000	5.0000	139648	75.5030
5.0000	12 5000	5010	2.7087
12 5000	20 0000	298	0.1611
20 0000	27 5000	305	0.1649
27 5000	35 0000	302	0.1633
35 0000	42 5000	306	0.1654
42 5000	50 0000	222	0.1200

Deviation Distribution

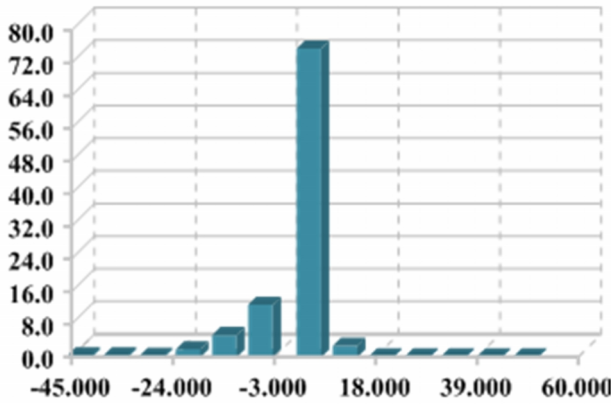

Out of Upper Critical	0	0 0000
Out of Lower Critical	0	0 0000

Standard Deviations

Distribution (+/-)	# Points	%
-6 * Std. Dev.	985	0.5326
-5 * Std. Dev.	489	0.2644
-4 * Std. Dev.	1222	0.6607
-3 * Std. Dev.	4654	2.5163
-2 * Std. Dev.	12272	6.6351
-1 * Std. Dev.	46334	25.0512
1 * Std. Dev.	111450	60.2572
2 * Std. Dev.	5946	3.2148
3 * Std. Dev.	420	0.2271
4 * Std. Dev.	296	0.1600
5 * Std. Dev.	283	0.1530
6 * Std. Dev.	606	0.3276

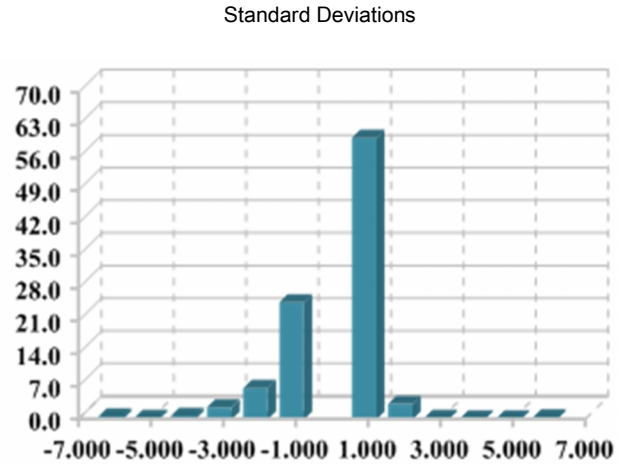

Appendix 2: A

Geomagic Control Report

Date Inspected: 7/7/2015

Date Generated: 7/7/2015, 12:12 pm

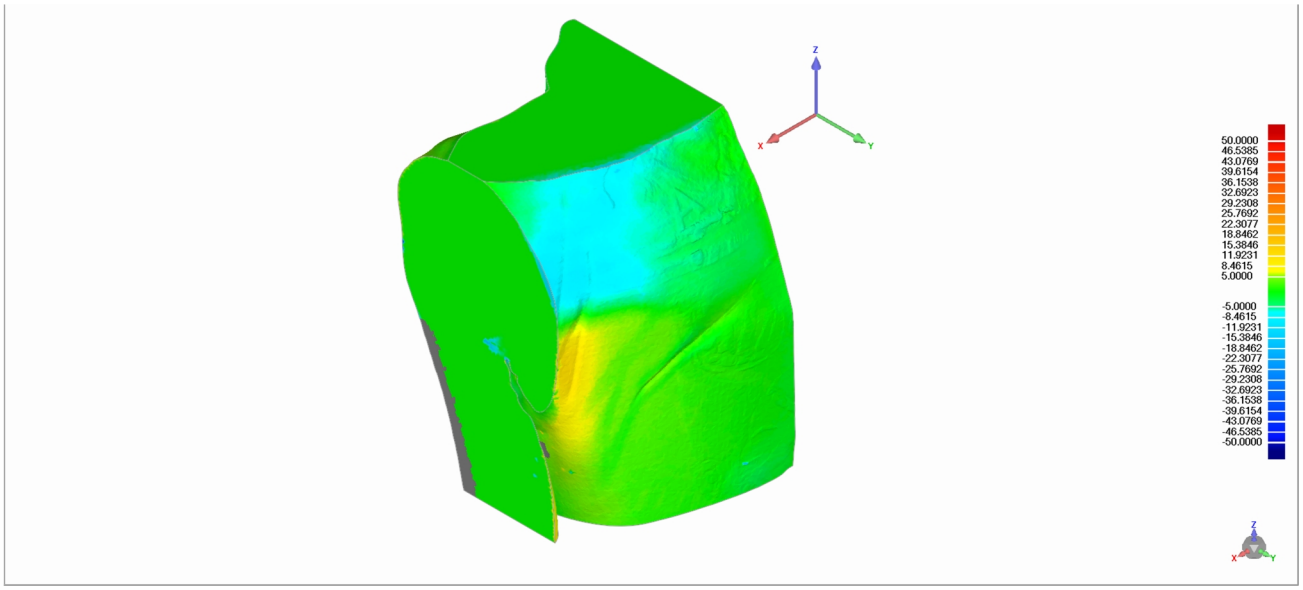

Author: cpotgiet:CPOTGIETPC2

Client Name: 3D Systems, Inc.

Reference Model: MWTPI - redo

Test Model: MWTPI - redo_Mirror

3D Comparison Results

Reference Model	MWTPI - redo
Test Model	MWTPI - redo_Mirror
No. of Data Points	45582
# Outliers	212

Tolerance Type	3D Deviation
Units	mm
Max. Critical	50.0000
Max. Nominal	5.0000
Min. Nominal	-5.0000
Min. Critical	-50.0000

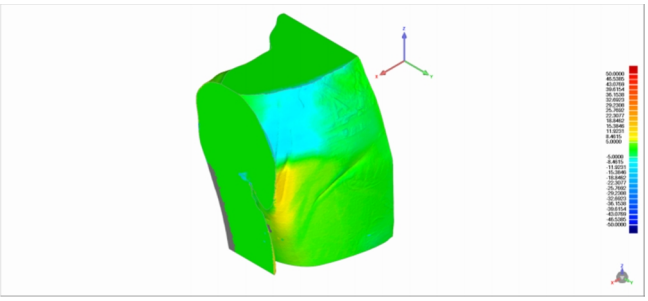

Deviation	
Max. Upper Deviation	45.9438
Max. Lower Deviation	-49.9737
Average Deviation	1.3928 / -4.9078
Standard Deviation	5.1270

Deviation Distribution

>=Min	<Max	# Points	%
-50 0000	-46 5385	56	0.1229
-46 5385	-43 0769	50	0.1097
-43 0769	-39 6154	36	0 0790
-39 6154	-36.1538	21	0 0461
-36.1538	-32 6923	10	0 0219
-32 6923	-29 2308	15	0 0329
-29 2308	-25.7692	10	0 0219
-25.7692	-22 3077	36	0 0790
-22 3077	-18 8462	120	0 2633
-18 8462	-15 3846	360	0.7898
-15 3846	-11 9231	544	1.1935
-11 9231	-8.4615	1090	2 3913
-8.4615	-5.0000	3707	8.1326
-5.0000	5.0000	37738	82.7915
5.0000	8.4615	1233	2.7050
8.4615	11 9231	341	0.7481
11 9231	15 3846	98	0 2150
15 3846	18 8462	13	0 0285
18 8462	22 3077	4	0 0088
22 3077	25.7692	14	0 0307
25.7692	29 2308	20	0 0439

Deviation Distribution

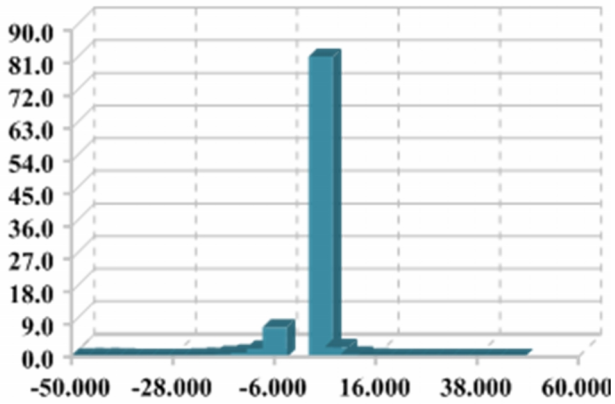

29 2308	32 6923	26	0 0570
32 6923	36.1538	19	0 0417
36.1538	39 6154	15	0 0329
39 6154	43 0769	4	0 0088
43 0769	46 5385	2	0 0044
46 5385	50 0000	0	0 0000

Out of Upper Critical	0	0 0000
Out of Lower Critical	0	0 0000

Standard Deviations

Distribution (+/-)	# Points	%
-6 * Std. Dev.	193	0.4234
-5 * Std. Dev.	70	0.1536
-4 * Std. Dev.	320	0.7020
-3 * Std. Dev.	821	1.8011
-2 * Std. Dev.	3546	7.7794
-1 * Std. Dev.	8431	18.4963
1 * Std. Dev.	29799	65.3745
2 * Std. Dev.	1956	4.2912
3 * Std. Dev.	323	0.7086
4 * Std. Dev.	21	0.0461
5 * Std. Dev.	12	0.0263
6 * Std. Dev.	90	0.1974

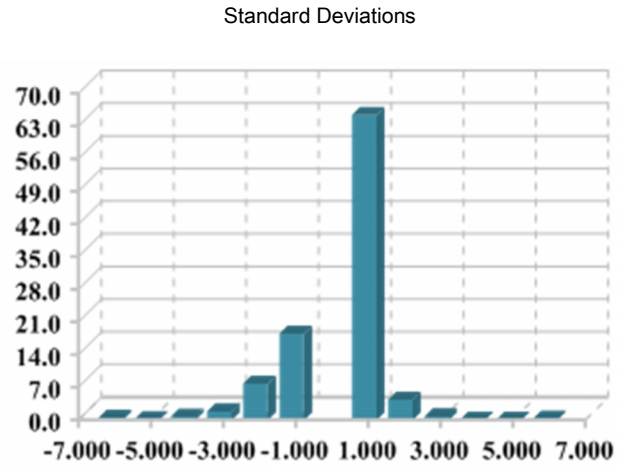

Appendix 2: B

Geomagic Control Report

Date Inspected: 7/7/2015

Date Generated: 7/7/2015, 12:05 pm

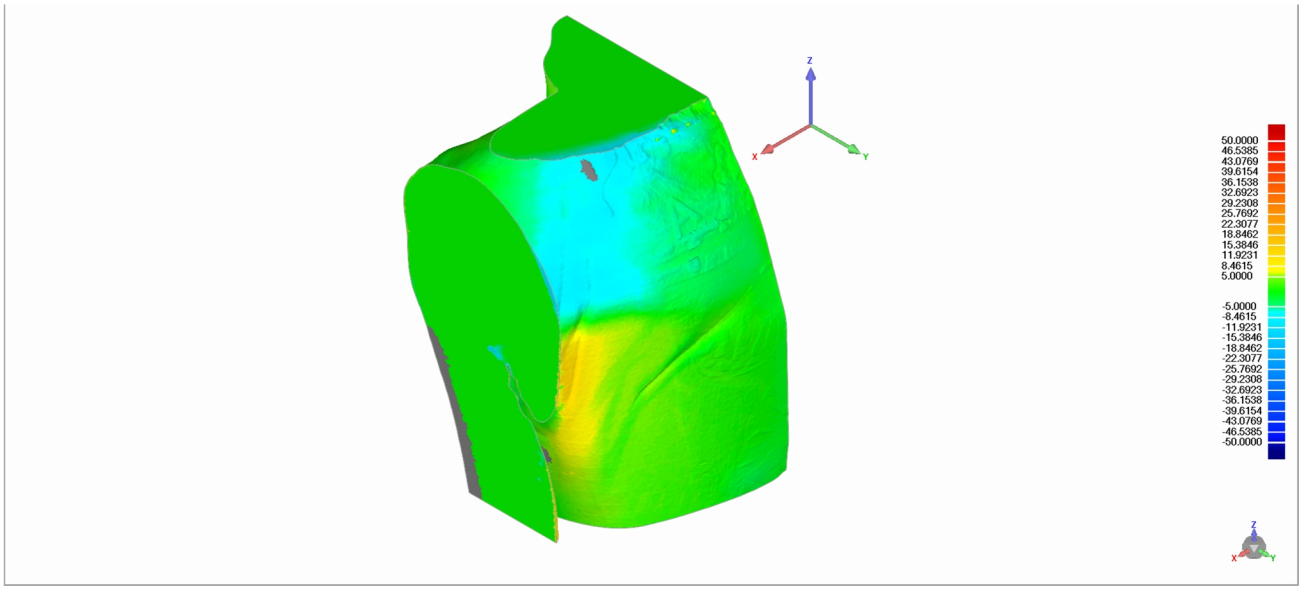

Author: cpotgiet:CPOTGIETPC2

Client Name: 3D Systems, Inc.

Reference Model: MPI

Test Model: MPI_Mirror

3D Comparison Results

Reference Model	MPI
Test Model	MPI_Mirror
No. of Data Points	47804
# Outliers	1794

Tolerance Type	3D Deviation
Units	mm
Max. Critical	50.0000
Max. Nominal	5.0000
Min. Nominal	-5.0000
Min. Critical	-50.0000

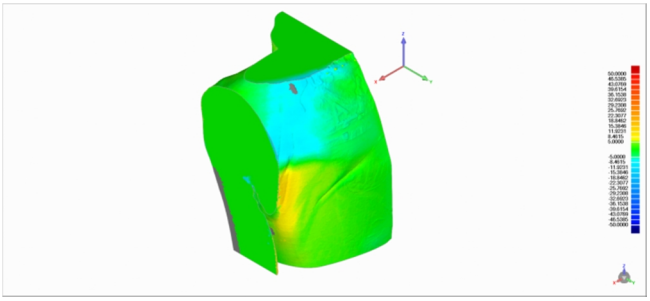

Deviation	
Max. Upper Deviation	49.2197
Max. Lower Deviation	-49.3656
Average Deviation	1.6269 / -4.8029
Standard Deviation	5.2847

Deviation Distribution

>=Min	<Max	# Points	%
-50 0000	-46 5385	14	0 0293
-46 5385	-43 0769	19	0 0397
-43 0769	-39 6154	23	0 0481
-39 6154	-36.1538	26	0 0544
-36.1538	-32 6923	39	0 0816
-32 6923	-29 2308	51	0.1067
-29 2308	-25.7692	81	0.1694
-25.7692	-22 3077	58	0.1213
-22 3077	-18 8462	81	0.1694
-18 8462	-15 3846	158	0 3305
-15 3846	-11 9231	601	1 2572
-11 9231	-8.4615	1362	2 8491
-8.4615	-5.0000	4581	9 5829
-5.0000	5.0000	38367	80.2590
5.0000	8.4615	1494	3.1253
8.4615	11 9231	430	0 8995
11 9231	15 3846	167	0 3493
15 3846	18 8462	22	0 0460
18 8462	22 3077	38	0 0795
22 3077	25.7692	45	0 0941

Deviation Distribution

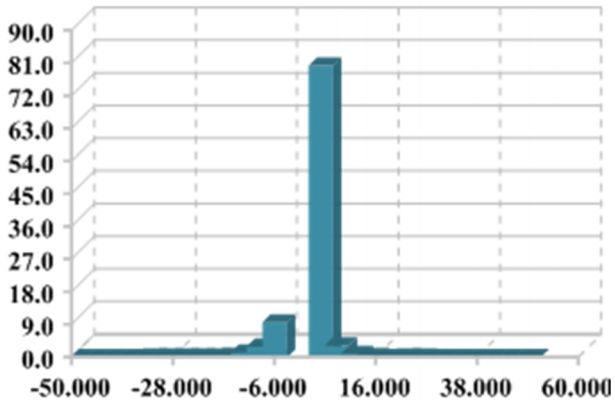

25.7692	29 2308	26	0 0544
29 2308	32 6923	32	0 0669
32 6923	36.1538	28	0 0586
36.1538	39 6154	25	0 0523
39 6154	43 0769	15	0 0314
43 0769	46 5385	12	0 0251
46 5385	50 0000	9	0 0188

Out of Upper Critical	0	0 0000
Out of Lower Critical	0	0 0000

Standard Deviations

Distribution (+/-)	# Points	%
-6 * Std. Dev.	223	0.4665
-5 * Std. Dev.	95	0.1987
-4 * Std. Dev.	128	0.2678
-3 * Std. Dev.	873	1.8262
-2 * Std. Dev.	4203	8.7922
-1 * Std. Dev.	10050	21.0233
1 * Std. Dev.	29378	61.4551
2 * Std. Dev.	2229	4.6628
3 * Std. Dev.	365	0.7635
4 * Std. Dev.	41	0.0858
5 * Std. Dev.	72	0.1506
6 * Std. Dev.	147	0.3075

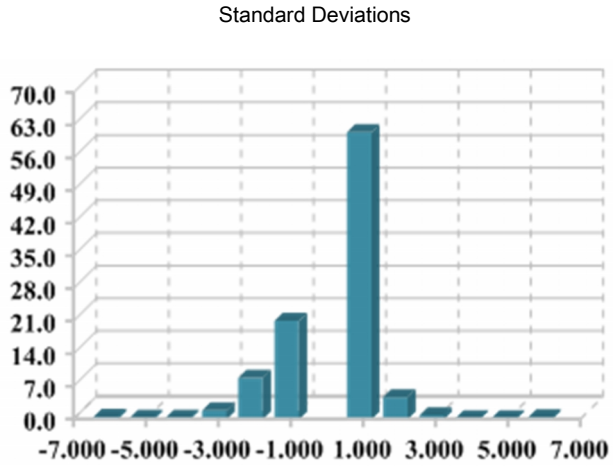

Appendix 2: C

Geomagic Control Report

Date Inspected: 7/7/2015

Date Generated: 7/7/2015, 11:20 am

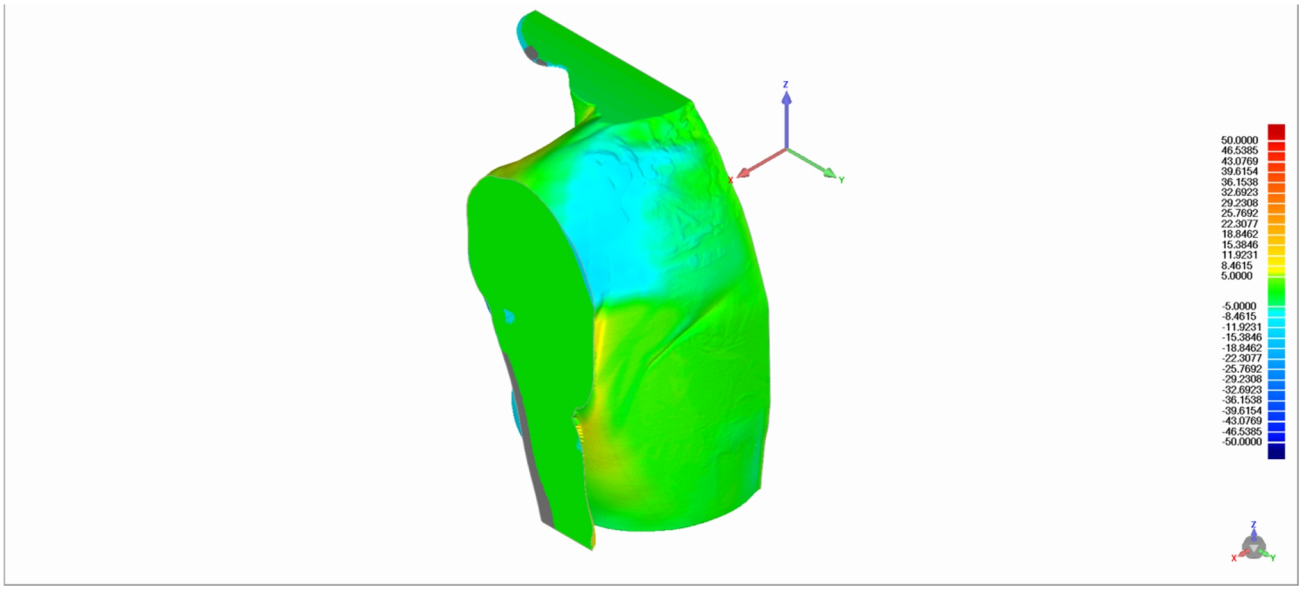

Author: cpotgiet:CPOTGIETPC2

Client Name: 3D Systems, Inc.

Reference Model: MWTPI 2_Fix

Test Model: MWTPI 2_Fix_Mirror

3D Comparison Results

Reference Model	MWTPI 2_Fix
Test Model	MWTPI 2_Fix_Mirror
No. of Data Points	396627
# Outliers	2787

Tolerance Type	3D Deviation
Units	mm
Max. Critical	50.0000
Max. Nominal	5.0000
Min. Nominal	-5.0000
Min. Critical	-50.0000

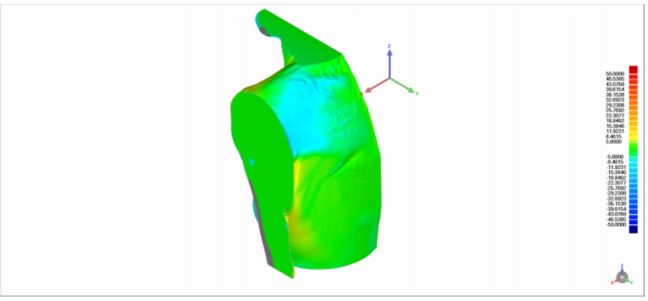

Deviation	
Max. Upper Deviation	49.8759
Max. Lower Deviation	-49.9565
Average Deviation	1.5345 / -4.0180
Standard Deviation	4.2624

Deviation Distribution

>=Min	<Max	# Points	%
-50 0000	-46 5385	42	0 0106
-46 5385	-43 0769	52	0 0131
-43 0769	-39 6154	46	0 0116
-39 6154	-36.1538	67	0 0169
-36.1538	-32 6923	34	0 0086
-32 6923	-29 2308	65	0 0164
-29 2308	-25.7692	56	0 0141
-25.7692	-22 3077	309	0 0779
-22 3077	-18 8462	1156	0 2915
-18 8462	-15 3846	1462	0 3686
-15 3846	-11 9231	2606	0 6570
-11 9231	-8.4615	8999	2 2689
-8.4615	-5.0000	27248	6 8699
-5.0000	5.0000	326766	82.3862
5.0000	8.4615	24305	6.1279
8.4615	11 9231	2673	0 6739
11 9231	15 3846	74	0 0187
15 3846	18 8462	66	0 0166
18 8462	22 3077	70	0 0176
22 3077	25.7692	79	0 0199
25.7692	29 2308	60	0 0151

Deviation Distribution

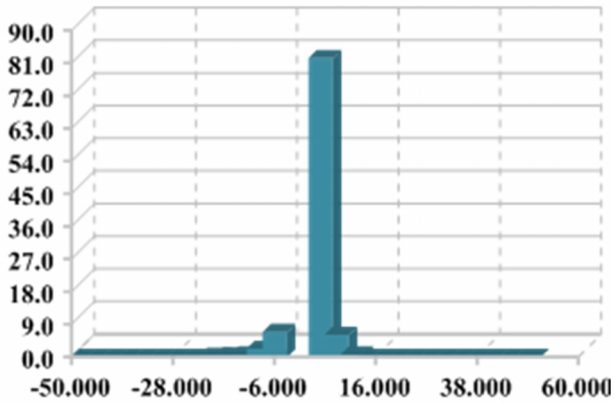

29 2308	32 6923	79	0 0199
32 6923	36.1538	82	0 0207
36.1538	39 6154	62	0 0156
39 6154	43 0769	61	0 0154
43 0769	46 5385	56	0 0141
46 5385	50 0000	52	0 0131

Out of Upper Critical	0	0 0000
Out of Lower Critical	0	0 0000

Standard Deviations

Distribution (+/-)	# Points	%
-6 * Std. Dev.	864	0.2178
-5 * Std. Dev.	1539	0.3880
-4 * Std. Dev.	2135	0.5383
-3 * Std. Dev.	8033	2.0253
-2 * Std. Dev.	32927	8.3018
-1 * Std. Dev.	75628	19.0678
1 * Std. Dev.	234662	59.1644
2 * Std. Dev.	36628	9.2349
3 * Std. Dev.	3502	0.8829
4 * Std. Dev.	61	0.0154
5 * Std. Dev.	82	0.0207
6 * Std. Dev.	566	0.1427

Standard Deviations

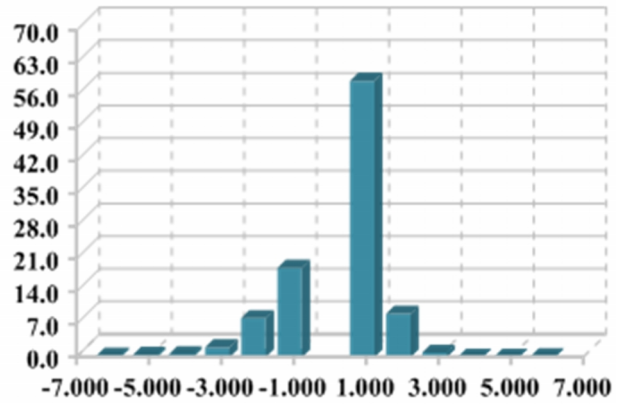

Appendix 2: D

Geomagic Control Report

Date Inspected: 7/7/2015

Date Generated: 7/7/2015, 10:55 am

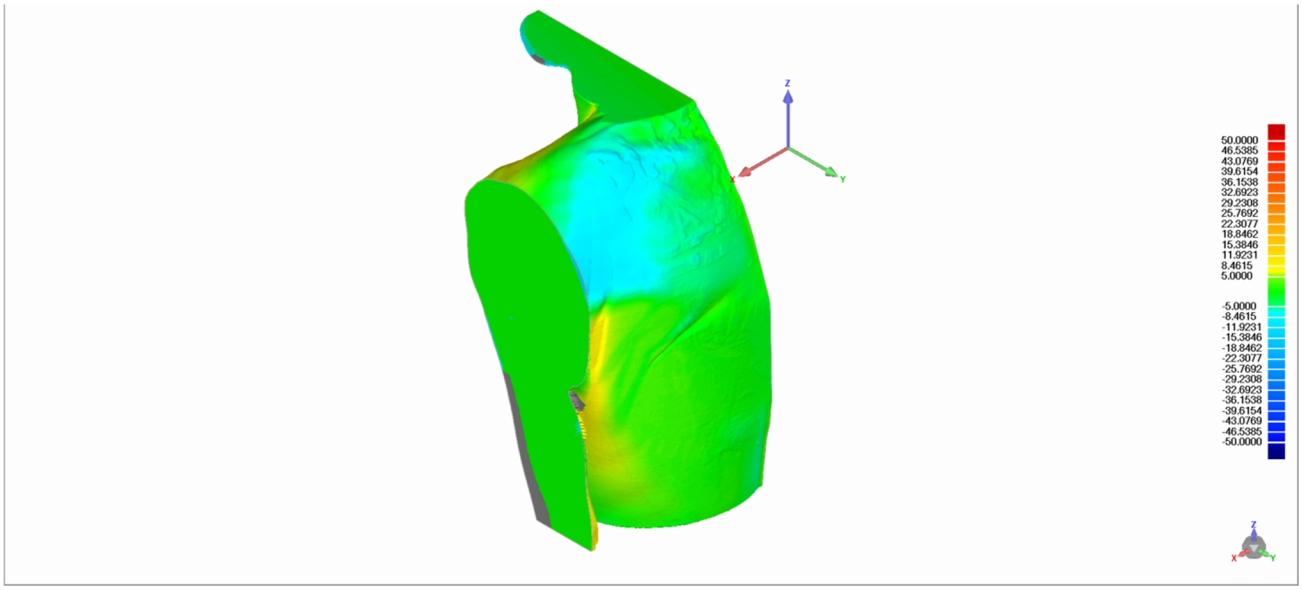

Author: cpotgiet:CPOTGIETPC2

Client Name: 3D Systems, Inc.

Reference Model: MPI 2_Fix

Test Model: MPI 2_Fix_Mirror

3D Comparison Results

Reference Model	MPI 2_Fix
Test Model	MPI 2_Fix_Mirror
No. of Data Points	525131
# Outliers	316

Tolerance Type	3D Deviation
Units	mm
Max. Critical	50.0000
Max. Nominal	5.0000
Min. Nominal	-5.0000
Min. Critical	-50.0000

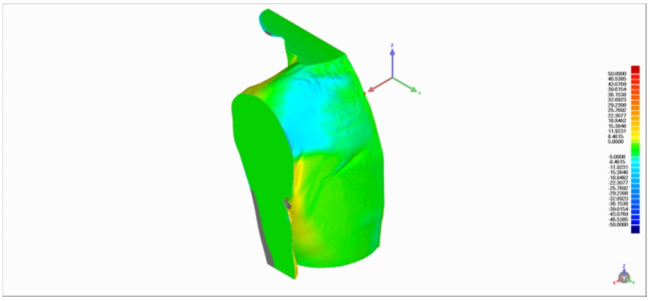

Deviation	
Max. Upper Deviation	49.9264
Max. Lower Deviation	-33.5562
Average Deviation	1.4797 / -3.7393
Standard Deviation	3.7579

Deviation Distribution

>=Min	<Max	# Points	%
-50 0000	-46 5385	0	0 0000
-46 5385	-43 0769	0	0 0000
-43 0769	-39 6154	0	0 0000
-39 6154	-36.1538	0	0 0000
-36.1538	-32 6923	5	0 0010
-32 6923	-29 2308	11	0 0021
-29 2308	-25.7692	18	0 0034
-25.7692	-22 3077	142	0 0270
-22 3077	-18 8462	173	0 0329
-18 8462	-15 3846	882	0.1680
-15 3846	-11 9231	2592	0.4936
-11 9231	-8.4615	13092	2.4931
-8.4615	-5.0000	37920	7 2211
-5.0000	5.0000	433001	82.4558
5.0000	8.4615	30565	5 8205
8.4615	11 9231	6505	1 2387
11 9231	15 3846	13	0 0025
15 3846	18 8462	7	0 0013
18 8462	22 3077	0	0 0000
22 3077	25.7692	0	0 0000

Deviation Distribution

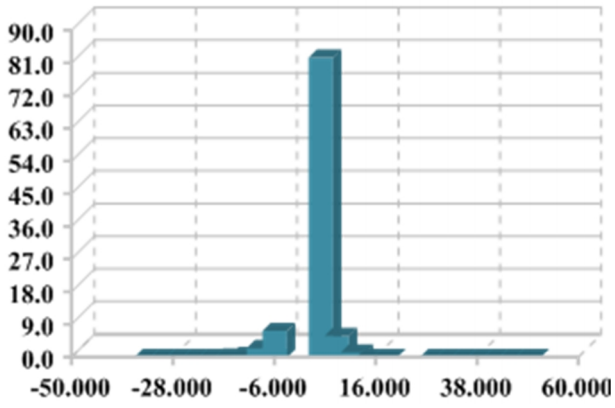

25.7692	29 2308	4	0 0008
29 2308	32 6923	10	0 0019
32 6923	36.1538	26	0 0050
36.1538	39 6154	38	0 0072
39 6154	43 0769	35	0 0067
43 0769	46 5385	43	0 0082
46 5385	50 0000	49	0 0093

Out of Upper Critical	0	0 0000
Out of Lower Critical	0	0 0000

Standard Deviations

Distribution (+/-)	# Points	%
-6 * Std. Dev.	339	0.0646
-5 * Std. Dev.	916	0.1744
-4 * Std. Dev.	3122	0.5945
-3 * Std. Dev.	18998	3.6178
-2 * Std. Dev.	43048	8.1976
-1 * Std. Dev.	91181	17.3635
1 * Std. Dev.	310081	59.0483
2 * Std. Dev.	43522	8.2878
3 * Std. Dev.	13467	2.5645
4 * Std. Dev.	243	0.0463
5 * Std. Dev.	9	0.0017
6 * Std. Dev.	205	0.0390